Technological applications of luminescent, colorimetric and absorption based sensors.

Ricketts, Stephen Robert

Technological applications of luminescent, colorimetric and absorption based sensors

by

Stephen Robert Ricketts

174970

A thesis submitted to Swansea University in partial fulfilment of the requirements for the degree of Doctor of Philosophy in Chemistry

Department of Chemistry
School of Engineering
Swansea University
July 2009

Declaration

This work has not previously been accepted in substance for any degree and is not being concurrently submitted in candidature for any degree.

.....

(Signature of candidate)

.....

(Date)

Statement 1

This thesis is the result of my own investigations, except where otherwise stated. Other sources are acknowledged by footnotes giving explicit references. A bibliography is appended.

.....

(Signature of candidate)

.....

(Date)

Statement 2

I hereby give my consent for my thesis, if accepted, to be available for copying and for inter-library loan, and for the title and summary to be made available to outside organisations.

.....

(Signature of candidate)

.....

(Date)

Acknowledgements

I would like to acknowledge a number of people who have helped make this thesis a reality particularly my parents who have supported me all the way through and are now hoping for a return on their financial investment. I would like to thank Jo for putting up with me all the time.

I would especially like to thank Dr Peter Douglas who has helped me with all the technical problems throughout this thesis, but more importantly been an inexhaustible source of tea. I like to thank all the members of the research group Dr Vic, Dr Hans, Dr Rachel, Dr Jeremie, Matt, Souad and Kaz and Dr Mike Garley.

I would also like to thank Stan who is probably the most important member of the chemistry department, John Tregembo for helping to make some of the equipment in the thesis, Paul Tregembo for helping with ordering of chemicals Professor Bill Johns and all the people at Haemair who are all strangely called skip who have helped out with the blood gas sensors.

I would also like to thank all the other people who I have know throughout my time at Swansea in particular Dr Dez, Rhys, Gareth, Angela, Ruth, and all the other people who have accidentally gone to pub on the pond on a nice day just for the one.

Summary

This thesis deals with the development of luminescent, absorbance based, and colorimetric sensors for a variety of technological applications including pressure sensitive paints, sensors for the preservation of artefacts for the British museum and sensors for the measurement of dissolved carbon dioxide and oxygen in blood. Throughout this thesis it can be seen that these sensors have significant advantages over traditional sensors.

Chapter 3 describes the development of colorimetric oxygen sensors for the detection of leaks in display cases specifically developed for the British Museum. The technological challenges facing the development of these sensors such as means of illumination and photodegradation are assessed and solutions to these problems are sought.

Chapter 4 sees the development of a novel temperature corrected pressure sensitive paint. Utilising a luminescent colorimetric oxygen sensor and an absorption based temperature sensor together in the same sensor. The colour response of the absorption based temperature layer viewed under white light enables temperature corrections to be made to the response of the luminescent colorimetric oxygen sensor which can be viewed under UV light.

Chapter 5 describes the development of a new type of colorimetric oxygen sensor, which uses a green LED as a source of both excitation and emission, replacing the green lumophores used in two lumophore colorimetric sensors.

The work discussed in Chapter 6 describes the design of luminescent based sensors for the measurement of oxygen and carbon dioxide in blood, such as might be required to monitor the performance of an artificial lung. The development and design of a combined complete compact sensor, comprising: excitation source, sensor element, and detector. The sensors measure oxygen and carbon dioxide in blood and water with an inline response to changing concentrations of these gases from partial pressures of 0-100 kPa for oxygen and 0-40 kPa for carbon dioxide within the range of clinical interest.

Publications and Presentations

Published papers

Ricketts, S.R.; Douglas, P.; *Sensors and Actuators B*, 135, **2008**, 46-51.

Technical reports

A technical report was produced for Haemair Ltd entitled "Technical information for dissolved oxygen and carbon dioxide sensors" in January 2009.

Oral Presentations

An oral presentation was given from this thesis to the Welsh Printing and Coating technical conference entitled "Luminescent colorimetric sensors" in November 2007.

Poster Presentations

A first poster was presented at the Analytical Research Conference in Cork entitled "Photodegradation of colorimetric luminescent materials" in July 2006.

A second poster was presented at the IUPAC International Photochemistry Conference in Cologne entitled "Preparation and photostabilisation of colorimetric and luminescent oxygen sensors" in July 2007.

Abbreviations and symbols

BHT - butylated hydroxytoluene

BM – British Museum sensor

k_b – bimolecular rate constant

CIE – Commission Internationale de l'Eclairge

CPSP – colorimetric pressure sensitive paint

DABCO – diazobicyclo[2.2.2]octane

EC – ethyl cellulose

f – fractional contribution of each site

HPTS - 8-hydoxypyrene-1,3,6-trisulfonic acid trisodium salt

I – intensity

F(R) – Kubelka Munk function

τ – lifetime

MTEOS – methyltriethyloxysilane

NPD - nickel (II) N-phenyl dithiocarbamate

k_{obs} – observed rate constant

PdOEP – palladum (II) octaethyl propyrin

pCO_2 – partial pressure of carbon dioxide

pO_2 – partial pressure of oxygen

PtOEP – platinum (II) octaethylporphyrin

PtPYR – platinum(II) N^C^N 1,3,6-tri-(2-pyridyl)benzene

PS – polystyrene

PSP – pressure sensitive paint

PVA – polyvinylalcohol

k_q – quenching rate constant

k_{sv} - Stern-Volmer constant

TSL – temperature sensitive layer

PSPSENS – the combined TSL and CPSP in the same sensor

TBPP - tris(2,4-ditert-butyl-phenyl)phosphate

η – viscosity

VITE - vitamin E

VOC's – Volatile Organic Compouds

Contents

Contents *page(s)*

Chapter 1 - Introduction 1-59

1.1. Sensors..... 1-2

1.2. Luminescent sensors..... 2-9

1.3. Luminescent oxygen sensors..... 10-15

1.4. Measurement of luminescent sensors..... 15-18

1.5. Problems associated with luminescent sensors..... 18-21

1.6. Multi-lumophore sensing.....21

1.7. Colour..... 21-32

1.8. Specific applications of luminescent sensors..... 32-39

1.9. Temperature sensors..... 40-44

1.10. Carbon dioxide sensors.....44-48

1.11. Thesis overview..... 49-50

1.12. References..... 51-59

Chapter 2 - Experimental details 60-89

2.1. Materials..... 60-61

2.2. Experimental methods..... 61-73

2.3. Polymer matrices..... 74-76

2.4. Colorimetric oxygen sensors..... 76-77

2.5. UV-Vis spectrometry and film thicknesses..... 77-78

2.6. Diffuse reflectance.....78

2.7. Emission measurements.....79-83

2.8. Gas mixing.....83-84

2.9. Irradiation suite.....84-86

2.10. Lifetime measurements..... 86-88

2.11. Errors and statistical handling of data.....88

2.12. References.....89

Chapter 3 - Development and stabilisation of colorimetric dual lumophore oxygen sensors 90-145

3.1. Summary..... 90-91

3.2. Introduction..... 91-95

3.3. Methods and materials..... 95-106

3.4. Choice of lumophore..... 106-108

3.5. Choice of matrix..... 108-112

3.6. Source of illuminations..... 112-114

3.7. Sensor response characteristics..... 115-121

3.8. Photostability..... 121-139

3.9. Conclusions..... 139-141

3.10. References..... 142-145

Chapter 4 - A novel colorimetric pressure sensitive Paint..... 146-182

4.1. Summary.....146

4.2. Introduction..... 147-149

4.3. Materials..... 149-150

4.4. Methods..... 150-151

4.5. Results and discussion..... 151-176

4.6. Versatility of PSPSENS..... 176-177

4.7. Future work..... 177-178

4.8. Conclusions..... 178-179

4.9. References..... 180-182

Chapter 5 - A simple colorimetric luminescent oxygen sensor using a green LED with Pt octaethylporphyrin in ethyl cellulose as the oxygen responsive element..... 183-214

5.1. Summary..... 183

5.2. Introduction..... 184-185

5.3. Materials..... 185

5.4. Experimental..... 185-187

5.5. Optical arrangement..... 187-192

5.6. Emission characteristics for sensors of varying formulation..... 192-195

5.7. Stability..... 195-210

5.8. Conclusions..... 211-212

5.9. References..... 213-214

Chapter 6 - Sensors for detecting partial pressures of oxygen and carbon dioxide in blood..... 215-261

6.1. Summary..... 215

6.2. Introduction..... 216-218

6.3. Materials and methods..... 218-222

6.4. Sensor design..... 222-250

6.5. Responses in blood and water..... 250-255

6.6. Conclusions..... 255-257

6.7. Future work..... 257-258

6.8. References..... 259-261

Chapter 7 - Conclusions 262-269

7.1. Conclusions..... 262-268

7.2. Future work..... 268-269

"Deep into that Darkness,

Long I stood there,

Wondering,

Fearing,

Doubting..."

Edgar Alan Poe

"...and then I remembered to open the shutter"

Stephen Ricketts

Introduction

1.1 Sensors

The field of sensorics[1] is a vast and interesting field covering many scientific disciplines. Sensors can be found in chemistry, physics, biology, engineering and geography. A sensor is defined as "a device giving a signal for the detection or the measurement of a physical property to which it responds."[2] Everyday examples include: thermometers, where the density of mercury, or ethanol, changes with temperature; barometers, where the height of a column of mercury is used to measure air pressure[3]; and breathalysers where a chemical reaction is used to determine the alcohol levels in breath.[4,5] Sensors are of vital importance in medicine, where devices for measuring levels of glucose[6] , uric acid[7], oxygen and carbon dioxide in blood[8], are regularly used. Sensors have been developed which allow the detection of: nerve agents[9] and landmines on the battlefield[10]; explosives and drugs at airports[11]; harmful levels of volatile organic compounds (VOCs) in a laboratory or factory.[12]; or trace VOCs in breath, blood or urine which might be possible markers for cancers.[4,5]

Some sensors are purely qualitative and only allow the analyst to determine whether a substance is present of not. Other sensors are quantitative and allow the analyst to determine the quantity of analyte present. If quantitative measurements can be made to give a time resolved response it is possible to increase our understanding of phenomena. A classic example is the use of a pH meter in reactions, where the pH is monitored as a base is added to acid or vice versa over time, and a neutralisation curve is generated.[13] Monitoring the change in pH associated with changes in reaction conditions over time allows the determination of a number of different

parameters such as equilibrium constants, rate constants and pKa values, and have helped to develop our understanding of chemistry.[14]

1.2 Luminescent sensors

Recent research has centred on the development of luminescent gas sensors for the detection of particular gases of biological interest such as carbon dioxide and oxygen,[14-19] Luminescent sensors have received a great deal of attention because they are versatile and can be applied to a wide variety of technological applications. They may provide cheap, accurate, precise, and fast alternatives to the electrochemical[20] and spectroscopic methods[21] currently used.[22] It is for these reasons that this thesis is concerned with the further development and applications of luminescent and optical sensors.

1.2.1 Construction of luminescent sensors

Before discussing the detail of the physicochemical principles involved in the operation of this type of sensors it may be useful to provide an outline of their construction and mode of operation. The basis of luminescent sensors is an analyte responsive luminescent dye, usually encapsulated,[23] or adsorbed[24], in a matrix (fig1.1). The choice of luminescent dye controls the type of parameter that can be measured because there has to be a measurable change in luminescence with changing analyte concentration or physical parameter. The way in which the dye is adsorbed/encapsulated in the matrix is also important. If encapsulated, the analyte must enter the polymer matrix to interact with the dye, and therefore only analytes

that can penetrate the matrix can influence the dye, thus the matrix can affect the selectivity and sensitivity of the sensor.

Selectivity is maximised by encapsulating a dye within a polymer and therefore all luminescent sensors made in this thesis involve the encapsulation of the dye within a polymer matrix. Furthermore there are problems which arise from the difficulties of reproducing sensors that involve adsorbing dyes on to surfaces.[24]

Because all of the sensors that are going to be used in this thesis are going to be encapsulated in a polymeric matrix it is important to clarify the processes that occur when an analyte enters the polymer. The permeability is defined as the transmission of molecules through a polymer film of which the permeability coefficient (P) is a measure. Permeation occurs via a two step process: the first is the dissolution of the permeant into the polymer, and the second is the diffusion of the permeant within the polymer. The product of these two processes gives the permeability coefficient (equation 1.1):[25]

$$P = D \times S \qquad [1.1]$$

Where P is the permeability coefficient, D is the diffusion coefficient, and S is the solubility coefficient.

The polymer can also influence the sensitivity of the sensor; a highly permeably polymer will generally produce a sensor with a higher sensitivity than one that posses a lower permeability because more analyte will be able to reach the dye. The

response time is also affected by the choice of polymer.[26,27] For example in temperature sensitive luminescent sensors, the response time will be dependent on the thermal properties of the polymer; the faster that heat can penetrate the polymer the faster the response. The polymer can also affect the optical properties of the sensor. A cloudy matrix will have a lower transmittance than a glassy one, and this will generally reduce the magnitude of the signal from the sensor.[26,28]

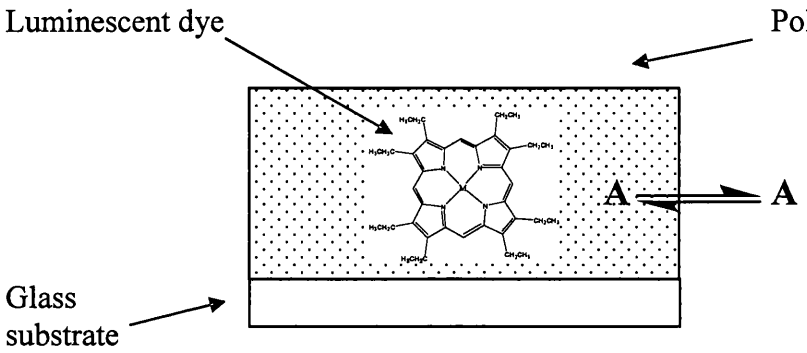

Fig.1.1. The structure of a polymer encapsulated luminescent sensor (A = analyte)

1.2.2 The origin of luminescence

Luminescence is an umbrella term which is generally used to describe emission from a "cold" emitting source. (Emission from a hot source is often referred to as incandescence). The type of luminescence is usually indicated by a prefix often indicating the energy source, e.g. electroluminescence from LEDs, bioluminescence from living organisms, chemiluminescence from chemical reactions, or photoluminescence from excitation with

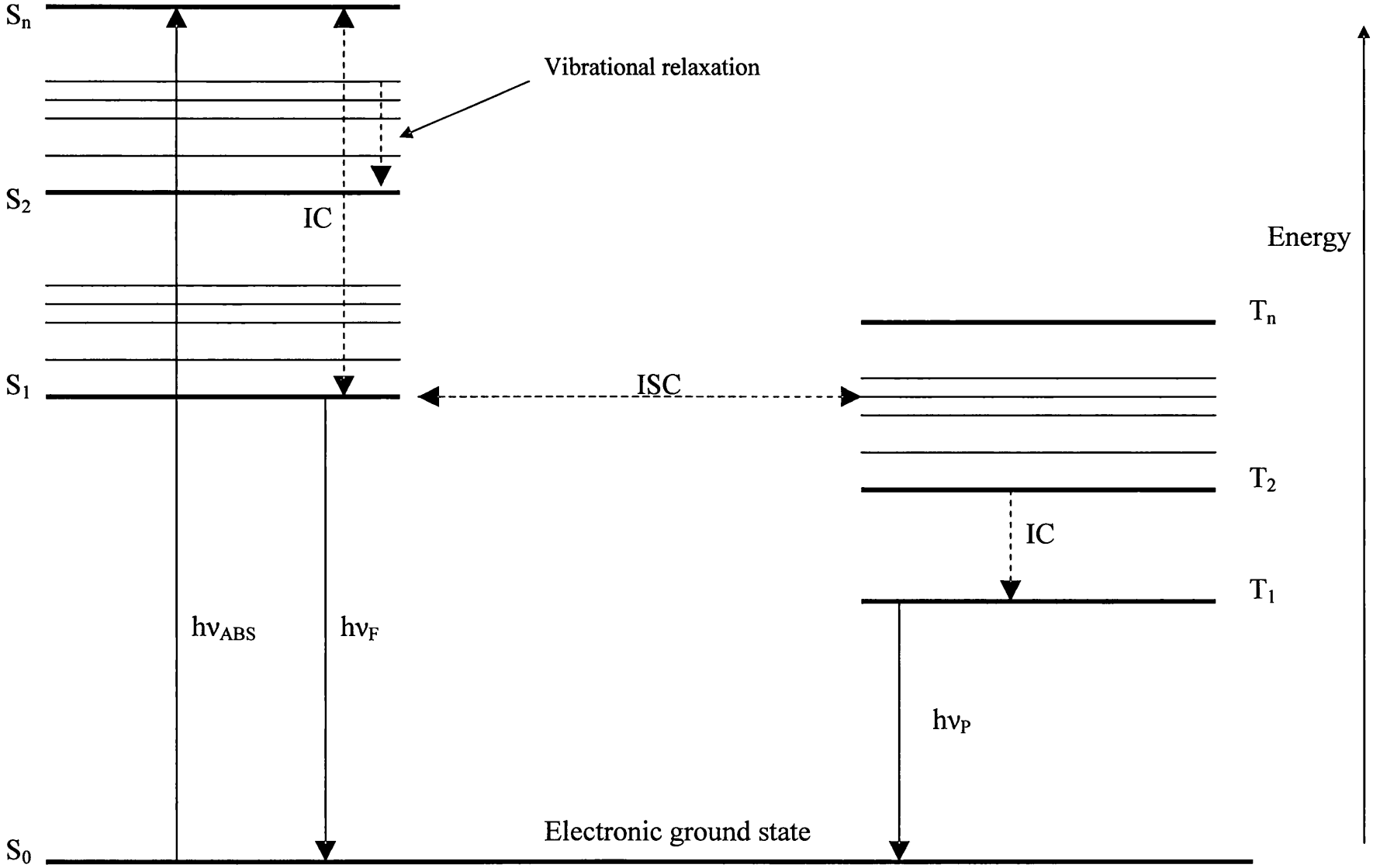

Fig.1.2. The Jablonski diagram describing the processes that can occur in a typical luminescent organic dye. A full description of the processes can be found in section 1.22

When considering photoluminescence from molecular species it is useful to refer to the Jablonski diagram (fig.1.2) which shows the molecular states involved and the various processes that can occur. The first process which must occur for photoluminescence is absorption of a photon from an excitation source, shown as $h\upsilon_{ABS}$ on the Jablonski diagram (fig.1.2). This excites the molecule from the ground state, which for organic molecules is usually the singlet ground state S_0, to an excited singlet state shown as S_n on the diagram (the origin of the terms for the states is explained in section 1.2.2.4). Once promoted to the S_n state the dye is said to be in an excited state. The excess energy is then lost as the dye returns to the thermodynamically most stable state, the ground state. In general there are two possible pathways to return to the ground state. The first possibility is that the dye returns to the ground state via emission of a photon; all processes which result in emission of a photon are termed radiative processes. The second group of processes return the molecule to the ground state without luminescence; these are termed radiationless processes.[29]

1.2.2.1 Radiative processes

There are two types of radiative processes that can occur. The first process is known as fluorescence, labelled as $h\nu_F$ on the Jablonski diagram. Here the dye returns to the ground state via emission of a photon from an excited singlet state. Generally fluorescence occurs from the S_1 state, however it is also possible, in some rare cases, for fluorescence to occur from higher singlets such as the S_2.[29] Fluorescence can therefore be defined as a process where the molecule returns from an excited state to

the ground state via the emission of a photon where both the ground state and the excited state have the same spin multiplicity.

The second radiative process is that of phosphorescence, labelled $h\nu_P$ on the Jablonski diagram. For this to occur a radiationless process must first occur, whereby the dye changes from the S_1 state to a T_n state by a process known as intersystem crossing (ISC). Intersystem crossing is enhanced by the presence of a heavy metal atom and this effect is explained in section 1.2.2.5. Once in the T_n state a second radiationless process can occur which is that of internal conversion to the T_1 state. Relaxation from the T_1 state to the singlet ground state via emission of a photon in a spin forbidden process termed phosphorescence. Phosphorescence can therefore be defined as the process by which a molecule returns to the ground state from an excited state which has a different spin multiplicity to the ground state via emission of a photon. The spin forbidden nature of the process means that the radiative lifetime (τ) of the T_1 state is generally much longer than that of the S_1 state, and therefore the lifetime of phosphorescence is generally much longer than observed for fluorescence.[29]

1.2.2.2 Radiationless Processes

A number of radiationless processes can occur within the molecule, two of which have already been encountered namely those of intersystem crossing from the S_1 to the T_2 state, and internal conversion (IC) which is the radiationless relaxation between two states with the same spin multiplicity, shown as IC on the Jablonski diagram. ISC crossing has already been encountered and can be thought of as a non radiative process between states of different spin multiplicities. It is also possible for

the process of reverse ISC to occur, and this can lead to the phenomenon of delayed fluorescence which will be discussed in chapter 4. One further radiationless transition can occur, and that is of vibrational relaxation whereby the molecule changes from a higher to a lower vibrational state within the same electronic state.[29]

1.2.2.3 Quantum Yield

The ratio of the number of photons emitted to those absorbed is known as the emission quantum yield (Φ_{lum}). There are usually some radiationless processes and therefore the luminescence quantum yield is almost never 1.[29]

1.2.2.4 Classification of electronic states

On the Jablonski diagram the different energy levels are labelled as triplets and singlets and it is important to explain the origin of these terms before continuing. Electronic states can be classified as singlet, doublet, triplet, etc, where these terms define the multiplicity of the molecular spin state. The multiplicity of a state is given by (2S+1), where S is the total electronic spin of the state. In the singlet state, shown in the Jablonski diagram as S, the electron spins are paired (often represented as opposing arrows i.e.↑↓) and there is no resultant spin magnetic moment and therefore S = 0, and there is only one state. A doublet state which is not encountered in this thesis would have an unpaired electron in the highest occupied molecular orbital (i.e ↑) with a resultant spin of S = ½ and therefore spin multiplicity is given by 2S + 1 = 2 therefore there are two states which is termed a doublet. In the triplet state, T, there are two unpaired electrons (i.e ↑↑) with a resultant spin of S = 1. The spin multiplicity of the state is given by 2S+1 = 3 and this state is therefore given the name triplet because there are three degenerate spin states.[14]

1.2.2.5 Selection rules for optical transitions

The excitation and relaxation of electronic states are governed by selection rules that indicate the feasibility of a transition of one state to another. These selection rules arise because angular momentum has to be conserved during a transition and a photon has a single unit of angular momentum.

The most important selection rule is the spin selection rule, which states that all radiative transitions are forbidden between states possessing different multiplicity (i.e. $\Delta S = 0$).

The major breakdown of the selection rules for the lumophores described in this thesis is that of the heavy atom effect. This occurs because of spin orbit coupling which mixes the singlet and triplet states so that transitions become allowed to an extent which depends on the relative orientations of the spin and the orbital magnetic moments, and the nuclear charge on the atoms involved. The greater the nuclear charge the greater the current generated by the electron orbital angular momentum, and thus the stronger the magnetic field. The electron spin magnetic moment interacts with this orbital magnetic field, it therefore follows that heavy atoms which have a high effective nuclear charge will promote a high degree of spin orbit coupling and lead to a break down in the selection rules.[29]

1.3 Luminescent oxygen sensors

Oxygen sensors have received a great deal of attention of late due to the wide range of technologies in which oxygen plays an important role such as: modified atmosphere packaging, pressure sensitive paints, medicine, and the preservation of artefacts in anaerobic atmospheres. Traditional detection of oxygen is by the Clark electrode in which oxygen is reduced at a catalytic platinum electrode leading to a change in current which can be detected.[20] However this can be expensive and not always ideal for applications such as pressure sensitive paints where the pressure needs to measured over a whole surface or modified atmosphere packaging, where a sensors needs to be placed into a sealed container. Both of these applications are described in more detail in section 1.8.

In 1984 a new method of detecting oxygen was proposed by Peterson and co-workers who developed a blood oxygen optical probe,[31] which used a luminescent molecule which could be quenched by oxygen and the change in luminescence could be related to the changing concentration of blood oxygen. Since then a number of different molecules have been used in luminescent oxygen sensors, such as pyrene[32,33], which possess a long lived singlet state. Later research has centred on triplet emitters such as ruthenium tris bypyridyl[22], platinum and palladium porphyrins[34] and cyclometallated platinum complexes[35] because they posses longer lived, and potentially more sensitive, excited states,

1.3.1 Stern-Volmer quenching

As previously mentioned the luminescence from an oxygen sensitive complex is reduced as the partial pressure of oxygen increases. The partial pressure of a gas is defined as the pressure that it would exert if it alone occupied the container.[14] The quenching process can be summarised by the process shown in fig.1.3. Process 1.3a describes the process of absorption whereby the lumophore (D) is excited via the absorption of a photon producing an excited state (D^*). Once in the excited state a number of different possibilities can occur. In the absence of a quencher molecule process 1.3b can occur and the molecule returns to the ground state (D) with either emission of a photon emission or via emission of heat (process 1.3b). However in the presence of a quencher molecule the excited state of the lumophore can be deactivated by energy transfer to the quencher molecule (process 1.3c). If this occurs no emission from the molecule can be observed; this is the basis of luminescent sensing. Processes 1.3d to 1.3f summarise the possible bimolecular processes that can occur for the quencher molecule. Process 1.1d shows the possible catalytic deactivation of the lumophore without energy transfer to the quencher. Processes 1.3e and 1.3f shown the possible excited state redox processes of electron transfer.[36]

$$D + h\nu \longrightarrow D^* \qquad [1.3a]$$

$$D^* \longrightarrow D + h\nu \text{ or } \Delta \qquad k_1 \qquad [1.3b]$$

$$D^* + Q \longrightarrow D + Q^* \qquad k_2 \qquad [1.3c]$$

$$\longrightarrow D + Q + \Delta \qquad [1.3d]$$

$$\longrightarrow D^+ + Q^- \qquad [1.3e]$$

$$\longrightarrow D^- + Q^+ \qquad [1.3f]$$

Fig.1.3. The Stern-Volmer bimolecular kinetic quenching scheme, D is a lumophore, Q is a quencher molecule (generally oxygen), k_1 is the rate constant for the unperturbed decay of the excited state, k_2 is the bimolecular rate constant for the sum of all bimolecular quenching processes that can deactivate the excited state

The relationship between the partial pressure of oxygen and the decrease in luminescence can often be described by the Stern-Volmer relationship eq 1.2.

$$Io/I = \tau o/\tau = 1 + kq\tau o pO_2 \qquad [1.2]$$

where Io and I are emission intensities in the absence and presence of oxygen at pO_2 respectively, τo and τ are the corresponding lifetimes, and kq is the bimolecular quenching rate constant for oxygen quenching. The Stern-Volmer plot of Io/I, or $\tau o/\tau$, against pO_2 has a slope of $kq\tau o$, which is often referred to as the Stern-Volmer constant, K_{sv}.[37]

1.3.2 Non linear Stern-Volmer plots

For simple homogeneous systems, such as fluid solutions, Stern-Volmer plots are straight lines. However for lumophores adsorbed on or encapsulated in other matrices it is common to obtain non linear plots (fig.1.4). The general approach to such non linear Stern –Volmer plots is to assume that the lumophore occupies different sites in the polymer. If the plot is linear it is assumed that the lumophore occupies a single site and the quenching of this site is referred to as homogenous quenching,[38] However more commonly it is thought that the lumophore will occupy more than one site where each site differs in one or more relevant property, e.g. lumophore lifetime, diffusion of oxygen, or solubility of oxygen at the site. In order to model this generally undesirable behaviour a number of different approaches have been adopted.[38] The most common approach is the dual site approach which uses the sum of fractional components of two distinct sites which gives the factional contribution of each site to the total decay (equation 1.3).

$$Io/I = [(f_1 /1 + K_{sv1}pO_2) + (f_2 /1 + K_{sv2}pO_2)] \quad [1.3]$$

Here f_1 and f_2 represent the fraction contribution of each of the sites, $f_1 + f_2 = 1$, and K_{sv1} and K_{sv2} describe the oxygen sensitivities at each of the sites.[39-41] While this only describes a dual site model it is possible to expand this model to as many sites as desired.[38]

A less common method that is used for modelling non linear Stern-Volmer plots uses a Gaussian model to explain the non linear behaviour of sensors. Here it is assumed

that there is a Gaussian distribution of sites throughout the sensor. In the Gaussian model Stern-Volmer quenching is described by equation 1.4.

$$I_{0,i}/I_i = 1 + K_i \,.\, pO_2 \qquad [1.4]$$

For a site type i with a Stern-Volmer quenching constant K_i, the intensity of luminescence in the absence of quencher $I_{0.i}$, will be proportional to the number of sites n_i, and it follows that n is related to the average number of sites n_{av} by equation 1.5.

$$n_i/ n_{av} = \exp(- x^2) \qquad [1.5]$$

where x is related to the value of K_i associated with the average number of sites from equation 1.6.

$$x = ((k_i/k_{av}) - 1)/ p \qquad [1.6]$$

where *p* is a measure of the distribution of sites.[42,43]

The Freudlich isotherm is another approach which has been used. The simplest approach takes the form of equation 1.7.

$$(I/I_o)-1 = \alpha(pO_2)^{\beta} \qquad [1.7]$$

α and β are considered to be empirical constants with no physical significance.[44]

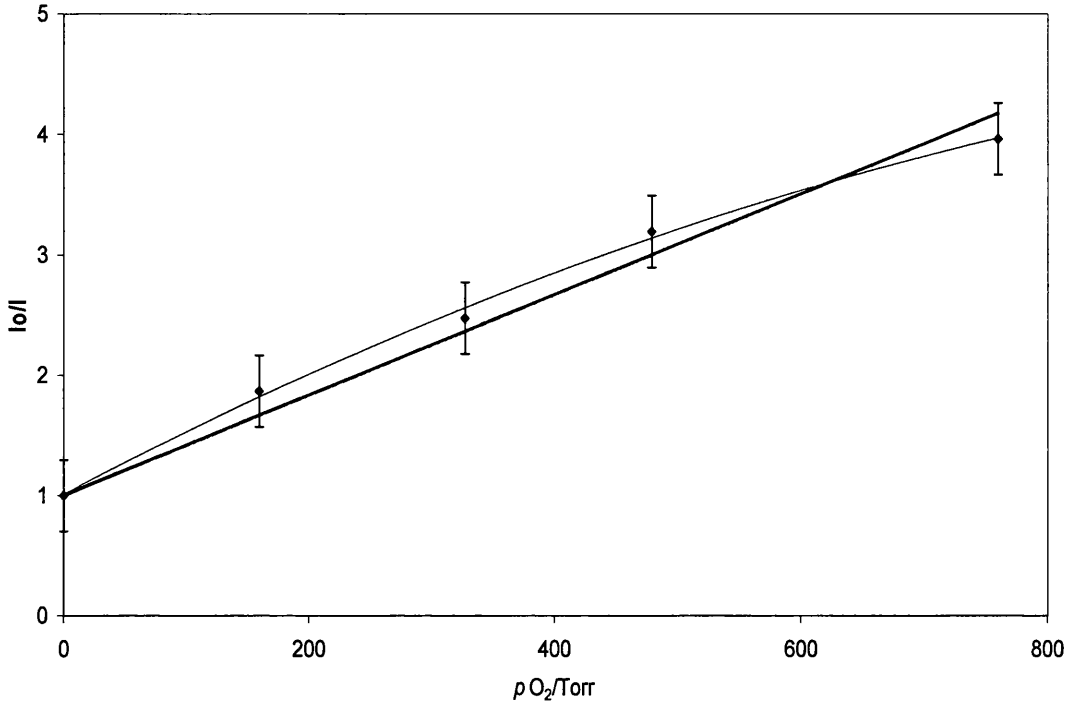

Fig.1.4. A Stern-Volmer plot for PtPYR in an EC matrix, if all the quenching was homogeneous the data would fit to the straight trendline ($R^2 = 0.974$), however the curved line ($R^2 = 0.998$) shows a better fit to the data demonstrating the downward curving nature of the Stern-Volmer plot suggesting heterogeneous quenching

1.4 Measurement of luminescent sensors

Measurement of luminescent sensors is generally performed using a fluorimeter of appropriate sophistication. The operation of the sensor can be broken down into three distinct processes: excitation, the luminescent sensing component, and detection of emission. The sensing part of the apparatus is the luminescent sensor which has been previously described, excitation and detection will be described here in sections 1.4.1 and 1.4.2.

1.4.1 Excitation

Excitation is required to excite the luminescent sensor so that luminescence can occur.[29] In a standard fluorimeter the excitation source will often be a Xe arc lamp, and this is the case in our laboratory. A monochromator is used to select the desired wavelength and produce monochromatic emission.[30] However other types of excitation may also be used such as lasers which may be employed for lifetime measurements[45], and LEDs which have the advantages that they are cheap, stable, intense and small, (LEDs are used for the sensors described in chapters 3 and 6). Desirable properties of the excitation source generally include: high intensity, high stability, monochromaticity, small size and low cost.[46]

1.4.2 Detection of emission from luminescent sensors

Detection of emission from luminescent sensors can be made using a number of different devices. The most common laboratory device for the detection of light is the photomultiplier.[13] In order to measure emission lifetimes emission intensity needs to be measured in a time resolved fashion, and to do this in our laboratory an oscilloscope is used coupled to a fast response photomultiplier. Using these methods excellent results can be obtained, however these systems can be bulky and difficult to make portable, therefore in practical sensor design other light detectors such as photodiodes and phototransistors may be preferable.[47] Many of the sensors described in this thesis are colorimetric and uses the human eye for detection, this has the advantage that a person can detect colour over a much larger area.

1.4.3 Measurement using phase angles

Phase angle, also called phase shift fluorimetry, (shown in fig.1.5) is sometimes used instead of lifetime or intensity measurements as a method of collecting the signal from a luminescent sensor (fig.1.5). The sensor is excited by a sinusoidally modulated excitation source at a known frequency, and, because of the lifetime of the oxygen sensor, a phase shift is observed between the frequency of excitation and emission. As the lumophore is quenched a change occurs in the phase shift and this can be used to measure the lumophore lifetime using equation 1.8.[48-50]

$$\tan \Delta\Phi = 2\pi\nu\tau \qquad [1.8]$$

Here Φ is the phase shift, ν the modulation frequency, and τ the lifetime of the luminescent species.

This relationship can be used for single exponential decays from single sites, however it is less good for more complicated decay kinetics such as double exponential decays. The advantages of phase shift measurement is that it is more or less independent of degradation and it reduces degradation of the lumophore because having a pulsed source means it is excited for less time per measurement. However it is complicated and more expensive than other methods of detection.[51,52] It was therefore not used in the work presented in this thesis.

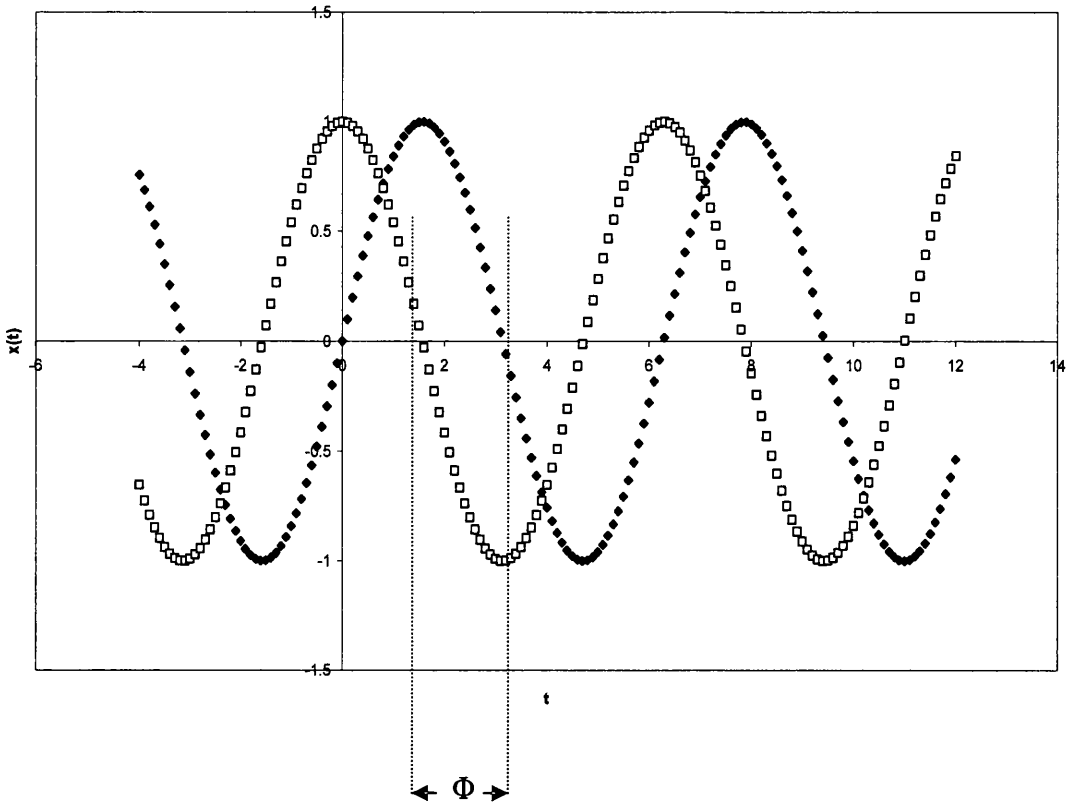

Fig.1.5. The phase shift (Φ) between two different frequencies

1.5 Problems associated with luminescent sensors

1.5.1 *Degradation*

Degradation is a common problem with luminescent sensors. This results in a reduction of the emission intensity from the lumophore as the lumophore is degraded over time shown in fig.1.6.[53-56] This alters the Stern-Volmer relationship and gives false values as the sensor degrades. This problem may be particularly important in colorimetric sensors where degradation alters the colour change of the sensors (section 1.8) if one of the lumophore layers is degraded faster than the other. The effect of degradation can be mitigated by regular calibration of the sensor, but this is

inconvenient and the sensor is constantly losing sensitivity as it degrades. The mechanism of degradation is examined in chapter 3 and the approaches used to prevent degradation are also discussed.

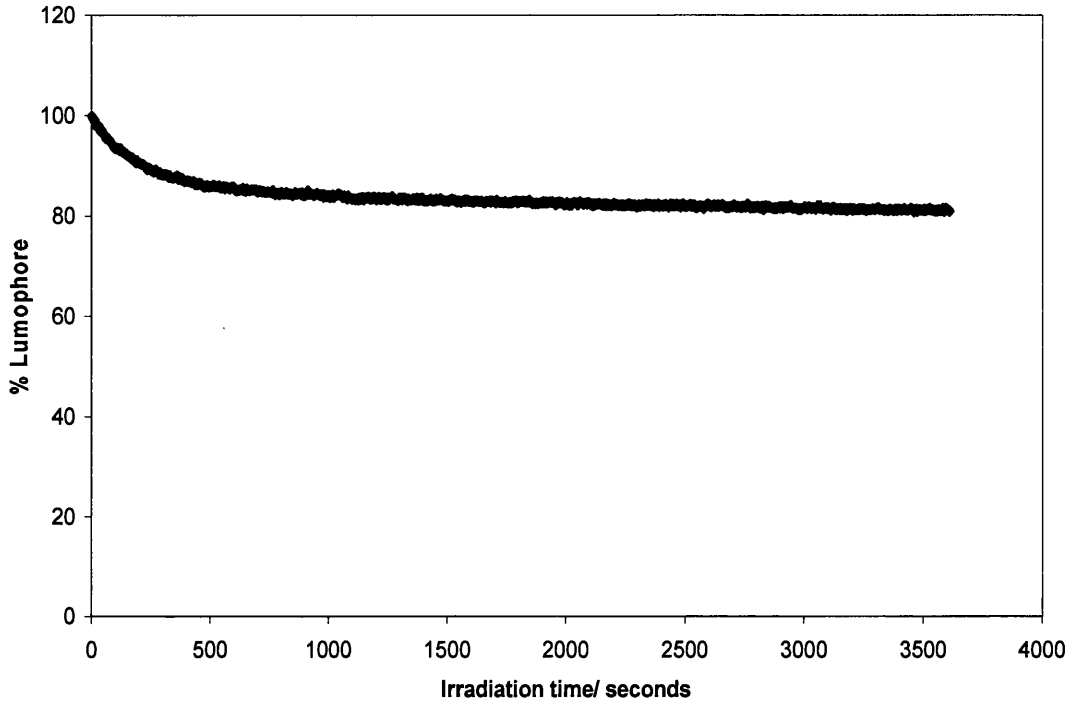

Fig.1.6. Loss of intensity due to photodegradation observed in an oxygen sensor described in chapter 3

1.5.2 Temperature dependence

Like the Clark electrode and many other sensors luminescent sensors are temperature dependent.[57] They become more sensitive as temperature is increased as described in chapter 4.

This can be attributed to the increase in permeability of the polymer matrices with temperature.[25] A decrease in the emission many also be observed in the absence of the analyte, and this can be attributed to an intrinsic temperature dependent non radiative decay route.[25,58] Temperature dependence also effects phase angle and

lifetime measurements. It is normally necessary to use an analyte independent but temperature sensitive second lumophore to monitor the sensor temperature. This response can be used to apply a correction factor to calibrate for temperature .[59]

1.5.3 Changes in excitation intensity

If there are changes in excitation intensity there will be a corresponding change in the emission intensity, and therefore a false reading.[60] This can be compensated for by using a ratiometric sensor in which one layer has an analyte independent lumophore. Since changes in excitation intensity are registered in both layers the analyte independent response can be used to correct for variations in excitation intensity.

1.5.4 The ideal oxygen lumophore

The ideal lumophore would have a single sharp well defined absorption band in an easily accessible part of the UV so that it can be efficiently excited and absorption does not interfere with the emission from any other lumophores. It would have a single sharp emission band with a large Stokes shift so that interference from the excitation source would not be a problem. The emission quantum yield would be 1 to give the best signal to noise ratio. A long lived triplet state would be the most desirable because this would make the most sensitive lumophore for interaction with oxygen. Oxygen quenching would follow the simple homogenous Stern–Volmer relationship at all concentrations. The lumophore would be photostable and insensitive to changes in temperature.

In reality such a lumophore does not exist. However platinum (II) octaethylporphyrin, which is used throughout this thesis, possesses many of the desired characteristics. It has a large Stokes shift with a sharp absorption band at 382 nm and emission maximum of 645 nm. Emission originates from a long lived triplet which has a lifetimes of around 0.091 ms[26] making it very sensitive, and it has a high quantum yield of 0.6.[26] However it does form aggregates in solution and it is usual to observe a non homogenous behaviour in polymers. It is also sensitive to temperature and degradation.

1.6 Multilumophore sensing

1.6.1 Ratiometric sensing

Ratiometric sensing uses either an additional lumophore which is unaffected by the analyte, or direct photoelectric measurement of the excitation intensity, either of which can therefore can be used as a reference for the sensing lumophore.[62-63] This approach is used in the blood sensors described chapter 6, where the non absorbed light from the LED is used as a reference for any change in excitation intensity. Dual lumophore ratiometric measurement can also be less sensitive to changes in temperature.[62]

1.7 Colour

In 1666 Isaac Newton was the first to show that white light could be separated into its constituent colours: red, orange, yellow, green, blue, indigo and violet. Further experimentation by Newton showed that it is not possible to separate these colours

further. Newton had assigned seven primary colours, however, in (1801) the trichromacy theory of Young and Helmholtz postulated that there are only three perceptible primary colours: blue, green and red, and that all other colours are derived from combinations of the primary colours.[64]

Humans detect colour with their eyes, and the brain processes the signal from the eyes to produce an image. There are two different types of cell in the retina which is that part of the eye that responds to light. The rods respond to changes in monochromatic light and are the most sensitive, the cones respond to colour and are less sensitive particularly at low light levels. There are three types of cone which have peak sensitivities corresponding to the primary colours of Young and Helmholz although the peak sensitivity of the red cone is closer to yellow than red.[65]

While it is easy to believe that rods and cones are separate entities when it comes to colour vision, it would be an over simplification to think of this as the case. This is demonstrated by the Purkinje phenomenon whereby red flowers in a garden appear brighter than blue flowers in daylight, but as the sun goes down, this is reversed and the blue flowers appear brighter. It therefore clear that the rods also contribute to colour perception and that light intensity is an important factor. [64]

The perception of colour in highly photopic (high intensity) conditions can be thought of in the following fashion. Light enters the eye and falls on the retina, and selectively stimulates each of the cones. For each wavelength there is a specific response and three different signals are generated in the brain to produce three opponent signals which are sent to the brain for interpretation, one of these signals is

achromic i.e is not related to colour but to light intensity, and the other two are chromic corresponding to the red-green and yellow-blue colour balances. The chromatic components allow the hue to be determined with the addition of the achromatic part determining the colour saturation. [64]

It is therefore important to develop a system of measurement for colour which accounts for both the chromatic and achromatic sections of vision. In this thesis the Commission Internationale de L'Eclairge (CIE) colour system is used.

1.7.1 Commission Internationale de L'Eclairge (CIE) colour

In order to develop a numerical system to quantify colours the idea of colour matching functions was introduced, whereby a set of functions are developed such as those shown in fig.1.7 which are related to the responses of a standard observer (i.e the average human eye). These functions can be applied to spectral data by equation 1.9 to gain numerical values known as tristimulus values, denoted X,Y and Z. Using equation 1.10 produces the x and y coordinates that can be plotted on a two dimensional colour space such as the one in fig.1.8. Using the CIE system, two colours with the same x and y values should appear the same provided that they are viewed under the same photopic conditions and that they are viewed at the same angles.[65]

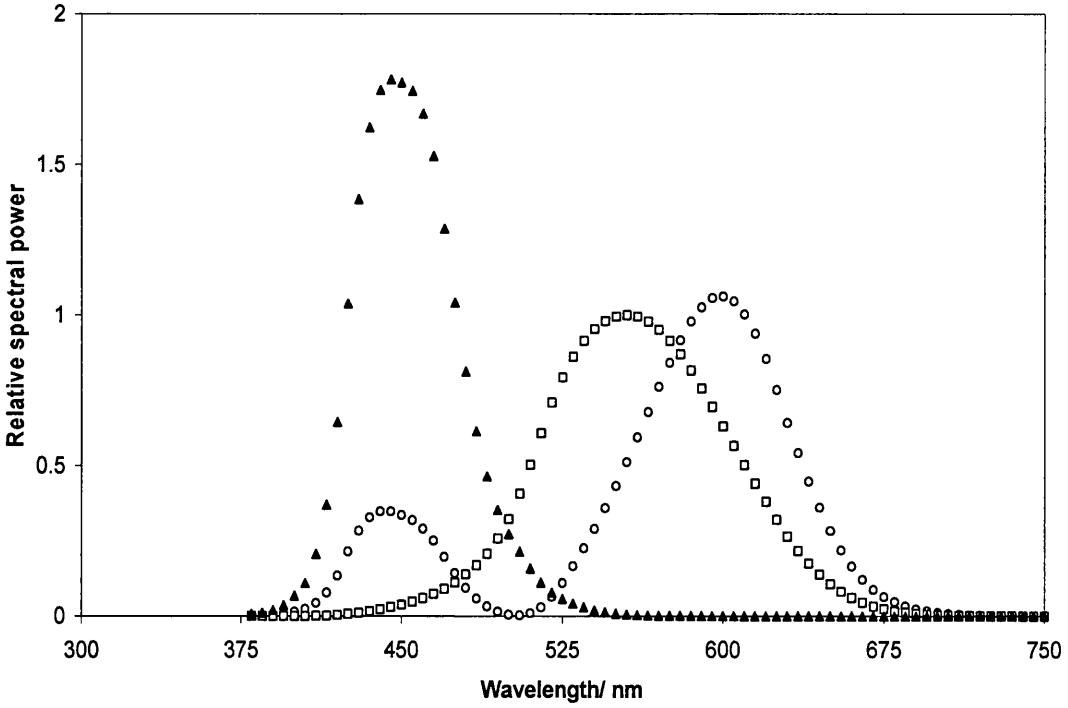

Fig.1.7. The 1931 CIE colour matching functions: $\bar{x}_\lambda$ (diamonds), $\bar{y}_\lambda$ (squares) , $\bar{z}_\lambda$ (triangles) from reference 65

Initial experiments of the additive mixing of light proved that there are no three colours which when additively mixed can duplicate all spectral colours. While this does produce the correct hue it does not produce the desired saturation as illustrated by the Purkinje phenomenon. In order to obtain a perfect match the idea of a negative colour has to be introduced in order to desaturate the spectral hue. This lead to the first colour matching functions known as the RGB colour matching system. A mathematical formula was later applied transforming the RGB colour matching functions into the CIE colour matching functions eradicating the idea of negative light as the idea of negative light was thought to be misleading. As previously mentioned human vision involves the use of achromatic vision to desaturate colours, and it would appear from fig.1.7 that only the responses of the cones are taken into

account, however the curve shown as $\bar{y}_\lambda$ in fig.1.7 is the same as the response of the rods in photopic vision and this therefore accounts for achromatic contribution to colour vision as well as the response of the green cone. The Y tristimulus value therefore represents the luminance of the colour and accounts for the brightness of the colour. This system therefore encompasses the ideas of achromic and chromic vision and it is possible to plot all colours on the CIE chromaticity diagram.[65]

The curve of the CIE chromaticity diagram is made of the pure colours from the blue to the red, covering the entire visible spectrum (380 nm – 770 nm) and this is known as the spectral locus. The two extremes of the spectral locus (red and blue) are connected by a straight line called the purple boundary. Therefore the colours at the purple boundary can not be denoted as pure colours. The centre of the diagram is known as the white point. The area of diagram enclosed by the spectral locus and the purple boundary encloses ten million estimated hues.[65]

Later additions have been made to the colour matching functions, with the 1976 CIE colour matching functions. This alteration was to make changes in the CIE diagram more equal i.e colour changes of the same magnitude would appear the same when plotted on the diagram; the problem is similar to that seen in many atlas projections where India appears smaller and Greenland much larger that they really are. However in the thesis the 1931 CIE colour matching functions are used for all of the colour coordinates because the CIE 1931 colour matching system is the one most commonly encountered.[65]

Colour can be divided into two classes; that of substances that are coloured because they emit light such as lamps and LEDs known as emissive colour, and that of substances that are coloured because they absorb light, such as paints, this is known as non-emissive colour. The next sections deal with the two types of light and shows how spectral data can used to generate the tristimulus values.

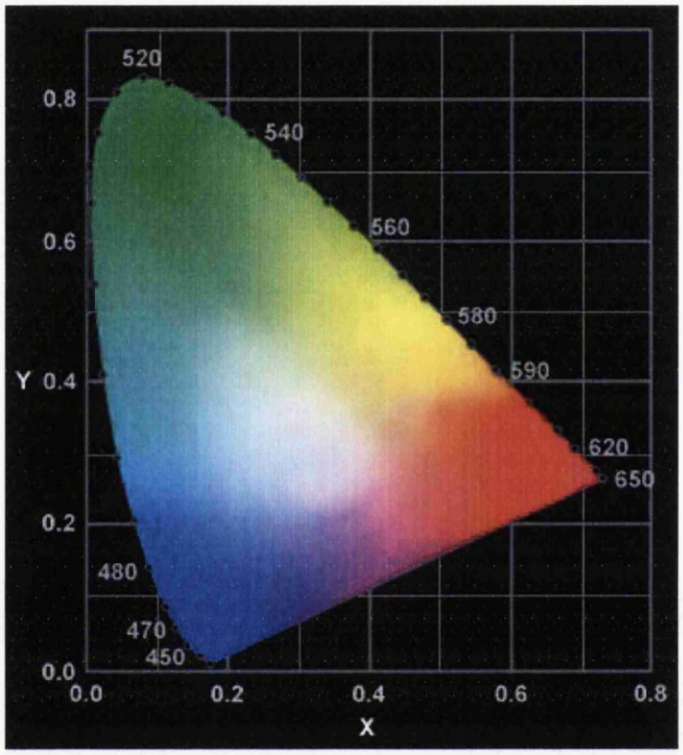

Fig.1.8. The 1931 CIE chromaticity diagram

1.7.2 *Emissive colour*

For the work described in this thesis emission spectra were recorded using the fluorimeter described in chapter 2, normalised, corrected for the sensitivity of the photomultiplier, and converted from photon intensity to energy intensity. The whole of the spectrum was then multiplied by each of the spectral weighting functions producing three values corresponding to the relative energy multiplied by each of the three spectral weighting functions $\bar{x}_\lambda$, $\bar{y}_\lambda$ and $\bar{z}_\lambda$ at each wavelength (E_λ (eq.1.9)

summing the product of each of these values produces the tristimulus values X, Y and Z.[69]

$$\left\{\begin{aligned} X &= \sum_{\lambda=380}^{700} \bar{x}_\lambda \cdot E_\lambda(\Delta\lambda) \\ Y &= \sum_{\lambda=380}^{700} \bar{y}_\lambda \cdot E_\lambda(\Delta\lambda) \\ Z &= \sum_{\lambda=380}^{700} \bar{z}_\lambda \cdot E_\lambda(\Delta\lambda) \end{aligned}\right\} \qquad [1.9]$$

The Y tristimulus value is known as luminance and is related to the brightness of a colour. The X and Z tristimulus correspond to no perceptible attribute. From the tristimulus values the two dimensional x and y coordinates can be calculated from eq.1.10, and can then be plotted on the CIE chromaticity diagram fig.1.8.

$$x = X/(X+Y+Z)$$

$$y = Y/(X+Y+Z) \qquad [1.10]$$

The CIE colour matching functions tabulated for every 5 nm were used for all of the CIE co-ordinates shown in this thesis.[66]

1.7.3 Non emissive colour

Non emissive colour is observed when light is passed through, or reflected from, an object, and a fraction of visible light is absorbed; the colour of the object is the non absorbed visible light. This effect is observed in paints or coloured band pass filters. (In this thesis the Co salts used for the pressure sensitive paint, described in chapter 4, displays non emissive colour.)

It therefore follows that the colour of non emissive substances is dependent on the light that is used to illuminate them. For the CIE system a number of different standard illuminants are used. Standard illuminant A is based on the spectral power distribution from a tungsten lamp. The definition of A is an illuminant having the same relative spectral power distribution as a Planckian radiator at temperature of 2856 K which follows the Planck distribution equation 1.11.[65]

$$dE = pd\lambda$$

$$p = 8\pi hc/\lambda^5 \, (1/e^{hc/\lambda kT}-1) \qquad [1.11]$$

h = Planck's constant, c = speed of light in a vacuum, λ = wavelength of emitted light, k = Boltzmann's constant, T = temperature, p = proportionality constant, E = energy[14]

The other standard illuminants are used to reproduce daylight. Daylight is a very difficult light to reproduce, because it varies considerably from latitude to latitude it is not the same on a dreary day in Swansea as it is on a glorious day in Hawaii, and therefore it is necessary to use averaged values. The second problem is that like Planckian radiators the light from the sun is dependent on the temperature at the surface of the sun. The centre of the sun is many millions of degrees, however the surface of the sun is around 5800 K, and because the radiation of the sun has to pass through its own and the earth's atmosphere the colour temperature of the sun seen

from earth is approximately 5500 K, which alters depending on which time of day that it is seen. The colour temperature will appear cooler as the sun goes down.

The sky plays an important part in determining the intensity of sunlight. On a clear sunlit day about 90 % of the colour comes from the sun while 10 % comes from the sky. However on an overcast day the sunlight will be dispersed by the clouds and the colour is similar to the sunlight plus skylight on a clear day which is also estimated to be around 5500 K. (Sky light refers to the colour of the sky i.e blue on a sunny day).

Indoor daylight is different again, and it is even more variable than the outside light since it depends on the outside sunlight, the geometry and transmission of the windows, and even the décor inside the room. An average value of 6500 K surface temperature is used to approximate this.

The first two standard illuminants to replicated daylight were standard illuminants B and C. Standard illuminant B is representative of sunlight at a surface temperature at about 4879 K and is meant to represent average daylight, while C is meant to represent average daylight indoors and has a correlated temperature of 6500 K.

These first two standard illuminants are reasonable approximations of daylight but do not posses the adequate amount of UV light that is present in sunlight, which becomes an issue with fluorescent colours. Therefore the D illuminates are used. A number of different D illuminates are available with the number that is assigned to each D illuminant corresponding to different surface temperatures of a black body

radiator. Throughout this thesis the standard illuminant of choice is standard illuminant D^{65} (fig.1.10) which is a close approximation to average daylight indoors.[65]

Once the standard illuminant has been chosen it is then possible to calculate the CIE co-ordinates using the transmission or reflectance spectrum of a sample. For the pressure sensitive paint described in chapter 4 reflectance spectra were used because the light is scattered by a white background in the sensor in a similar way to a paint.

For calculation of the CIE coordinates the standard illuminant D^{65} was chosen (fig.1.9). The illuminant spectrum was then multiplied wavelength by wavelength by the reflectance spectrum (fig.1.10) obtained using the Lambda 9 spectrometer described in chapter 2, to obtain a spectrum corresponding to the non absorbed light (fig.1.11). This was then treated in the same way as the emissive colour to obtain colour coordinates.[65]

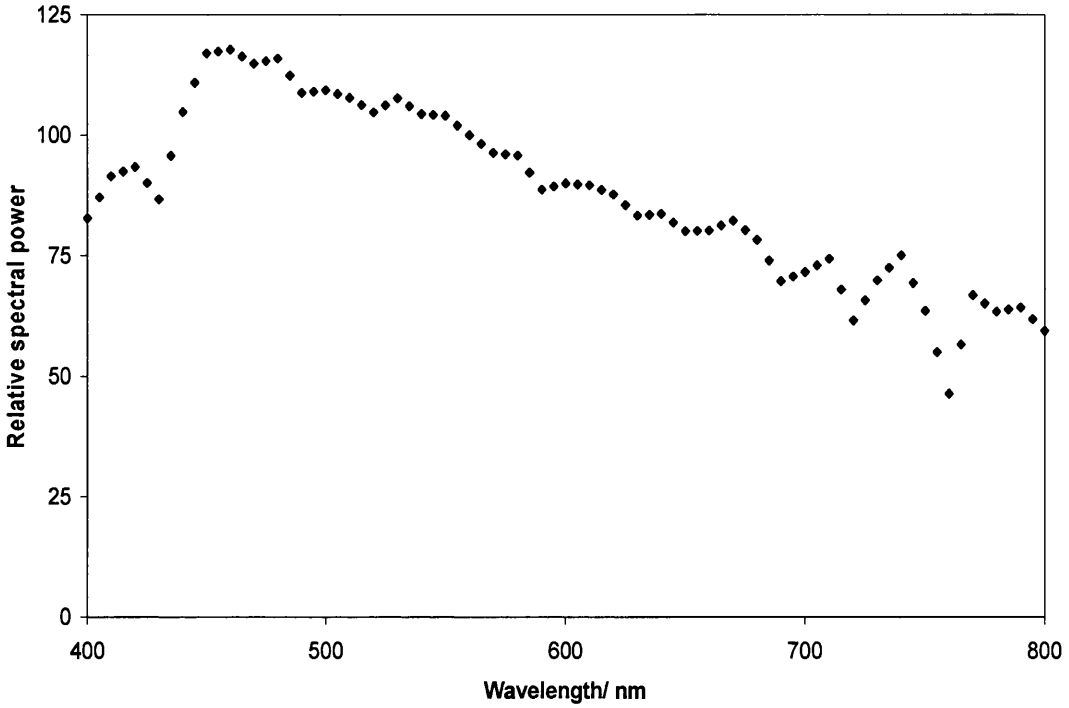

Fig.1.9. Spectral power distribution for standard illuminant D^{65} from reference 60

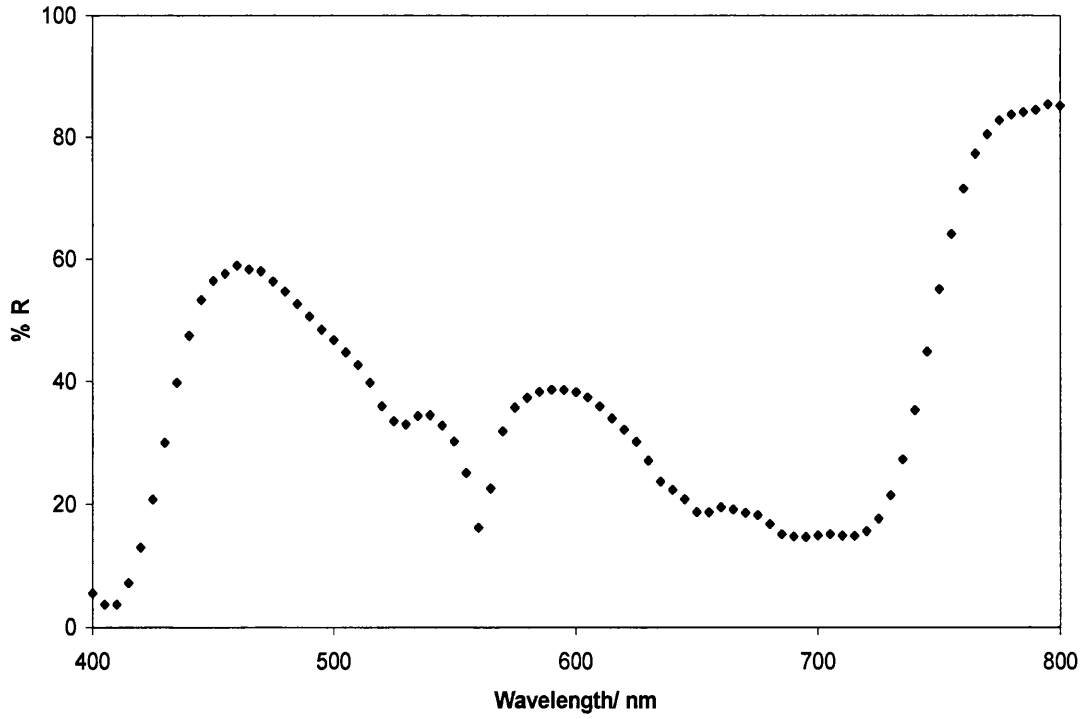

Fig.1.10. Reflectance spectra of the $CoCl_2$ in polyvinyl alcohol used for the PSP sensor described in chapter 4

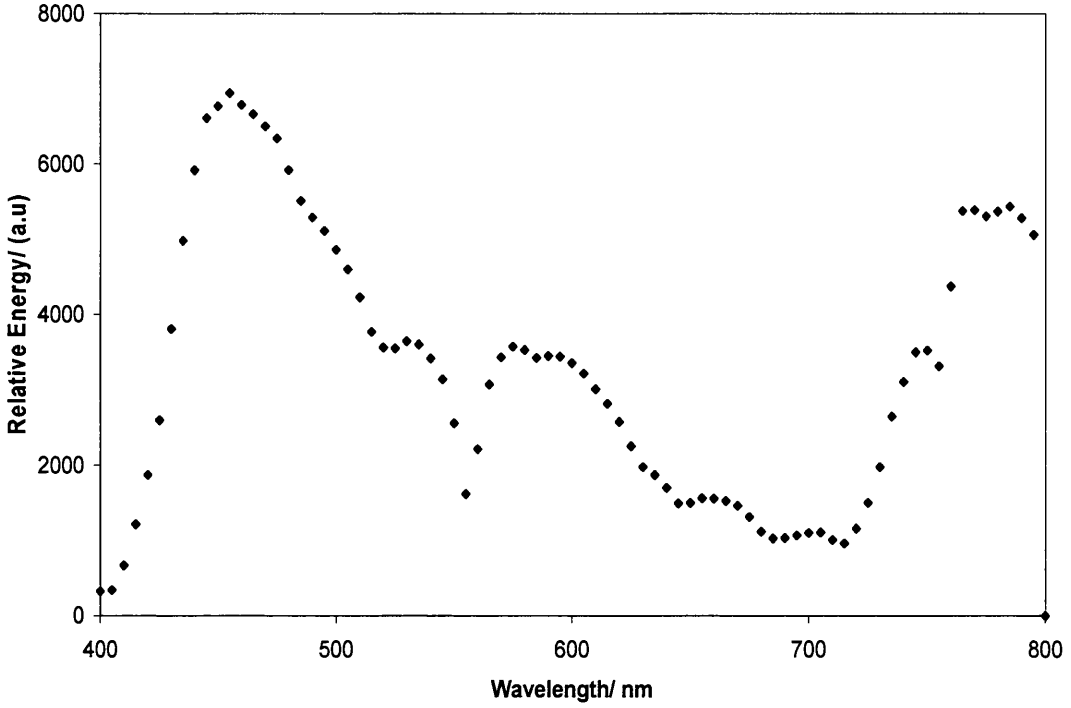

Fig.1.11. The result of multiplying D^{65} by the reflectance values in fig.1.10

Because the angle at which a colour is viewed alters the perception of colour all the luminescent colours were recorded at the same angle on the modified sensor holder described in chapter 2. The non emissive colours were recorded on the diffuse reflectance.

1.8 Specific applications of luminescent sensors

1.8.1 Colorimetric oxygen sensors

Colorimetric oxygen sensors are sensors that change colour in response to changing oxygen partial pressures.[67,68] The sensors that give red to green colour changes sensors are constructed by using two or more lumophore layers with different oxygen sensitivities (fig.1.12),[69, 70] the upper layer being the most sensitive to oxygen partial

pressure. For example in the sensor made to meet the requirements of the British Museum for monitoring anaerobic storage (described in chapter 3), the upper layer is PtOEP in an EC matrix, while the bottom layer is rhodamine 110 encapsulated in a gelatin matrix. The lower layer is insensitive to changes in oxygen partial pressure and remains unchanged while the upper layer is readily quenched as the oxygen partial pressure is increased.

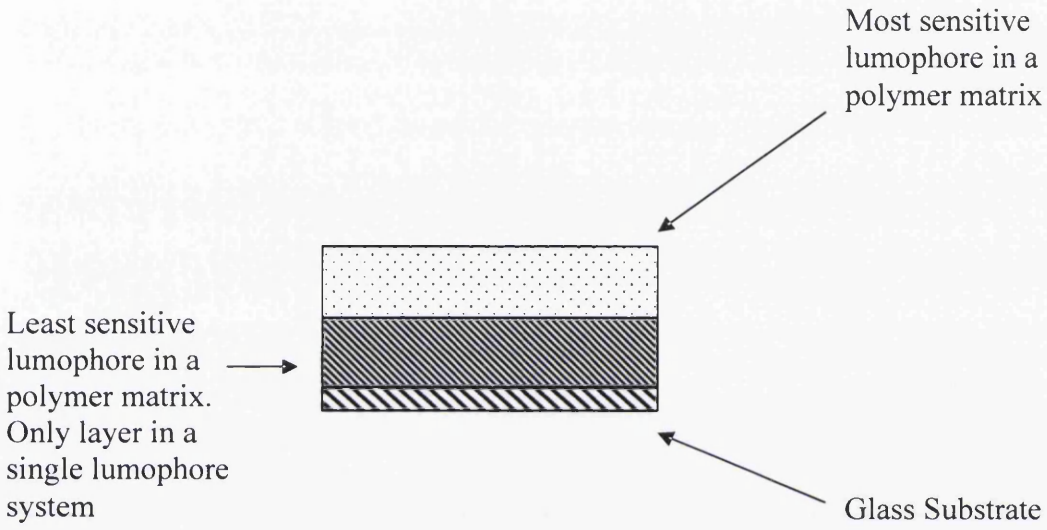

Fig.1.12. The construction of a typical dual lumophore colorimetric oxygen sensor

In the absence of oxygen the red emission from PtOEP is unquenched and is the prominent emission from the sensor, and the sensor emission appears as red. As the partial pressure of oxygen increases the emission from the PtOEP decreases and the green emission from the rhodamine 110 comes to prominence, this changes the emission from red to yellow and finally to green. This colour change is known as the "traffic light" colour change shown in fig.1.13, and is the most desirable colour change because it is the most easy to detect with the eye.[66]

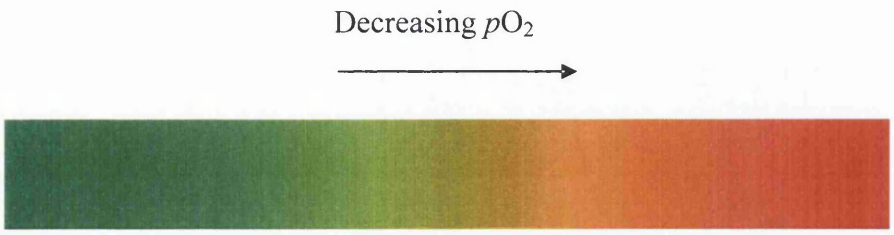

Fig.1.13. The range of colours in a traffic light response that can occur in a colorimetric oxygen sensor

In colorimetric sensors only one excitation wavelength is used and it is therefore necessary that both lumophores can be excited by the same wavelength as shown in fig.1.14 with both lumophores used for the PtPYR sensor. If only one is excited no colour change will be observed.

While red to green is the most desirable colour change it is not the only colour change that can be obtained, e.g. in chapter 4 a red to blue colour changed is used. It is possible to make most colour changes by choice of appropriate lumophores.[66]

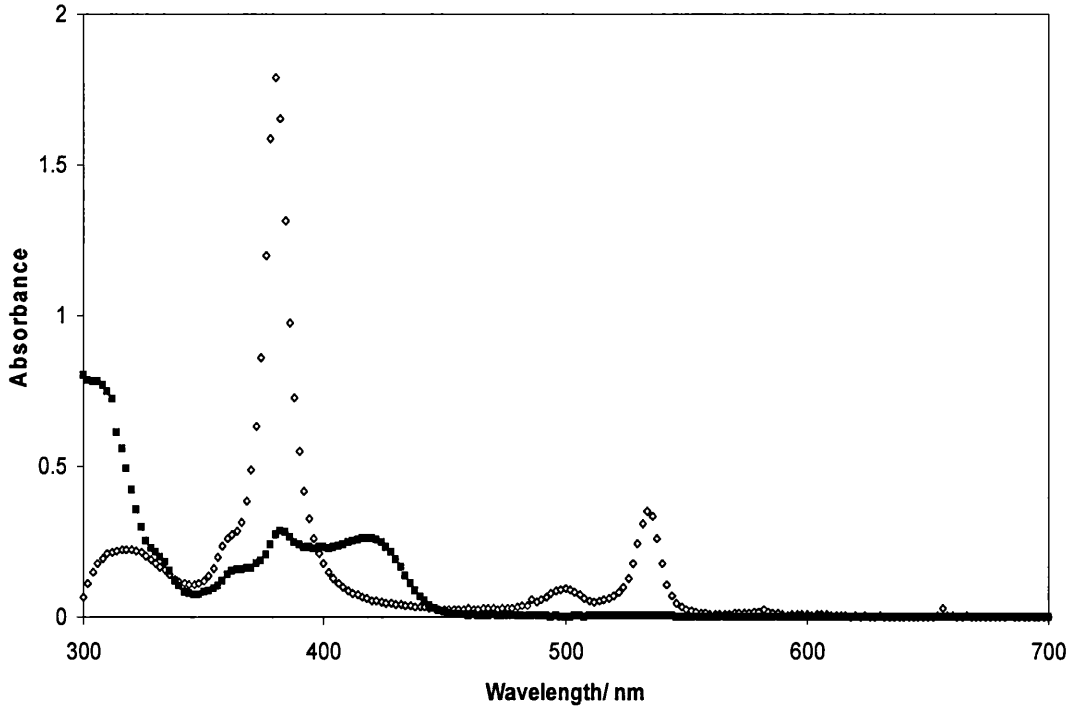

Fig.1.14. The absorption spectra in THF of the two lumophores used in the PtPYR colorimetric oxygen sensor described in chapter 3: PtOEP (open), PtPYR (closed) recorded on the UV-Vis spectrometer described in chapter 2

1.8.2 *Modified Atmosphere packaging*

One of the major applications for colorimetric sensors is in modified atmosphere packaging (MAP).[71,72] Modified atmosphere packaging uses an atmosphere which is unsuitable for biological growth such as 0.5 – 2 % oxygen[73] or a high carbon dioxide concentration.[74] This retards bacteriological growth and increases shelf life. However if there is any leak in the packaging bacterial growth can occur and the product becomes spoiled and potentially harmful to the consumer. By placing colorimetric sensors in the packaging any leak can be detected instantly. While this would be a useful gimmick for shoppers to see how fresh products are, it is of much more value to manufacturers who can only batch test products at the moment. Using colorimetric sensors it is possible to test every product for leakage without affecting

the production process very substantially, and this is therefore one of the major potential applications for colorimetric sensors.

1.8.3 Preservation of artefacts

Artefacts and works of art can be also be preserved by using modified atmospheres, although generally they use a reduced pressure environment to preserve art works and artefacts.[75-77] Leaks in the containers in which they are contained are not immediately obvious and an easy indicator of the partial pressure of oxygen would be very beneficial. A colorimetric sensor would be ideal for this, and this is demonstrated in chapter 3 where a sensor has been developed for the type of requirements suggested in discussion with staff from the laboratories of the British Museum.

1.8.4 Pressure sensitive paints (PSPs)

PSPs are used to monitor the flow of air over a surface in a wind tunnel, such as a car or an aeroplane (fig.1.15). PSPs are the focus of much attention of late because they offer many advantages over conventional methods.[78,79] The conventional methods used are pressure taps placed at discreet points on the surface of a vehicle. The information is then extrapolated to gain the flow over the whole vehicle.[80] This process is extremely expensive since for example, it costs around $ 0.5-1 M to create a model of the air flow over a plane.[59] Pressure sensitive paints offer a real alternative to pressure taps as they can be placed over the whole vehicle and the pressure at all points can be monitored simultaneously. PSPs consist of a luminescent sensor embedded in a polymeric matrix or paint, and when they are

excited by UV light the air flow over the surface can be monitored by measuring emission intensity over the surface.[81,82]

In a wind tunnel gas mixtures are not used, however changes in intensity still arise in the PSP. As air flows over a flat surface it will create a pressure differential in the same way that a vacuum can be created by using flowing water. This creates areas of low pressure with a low partial pressure of oxygen, which leads to an increase in emission intensity from the PSP. It is important to keep consistent lighting conditions when using PSPs generally a vehicle will be imaged in sections to overcome this.

The behaviour of PSP's are often described using the modified Stern-Volmer equation 1.12.[61]

$$I_0/I = A(T) + B(T)\, P/P_0 \qquad [1.12]$$

T = temperature, I = intensity with air flow, I_0 = intensity in the absence of air flow, P = pressure, P_0 = pressure in the absence of air flow, P = pressure with air flow, A(T) and B(T) are coating sensitivities which are determined experimentally at different temperatures and so are temperature dependent.

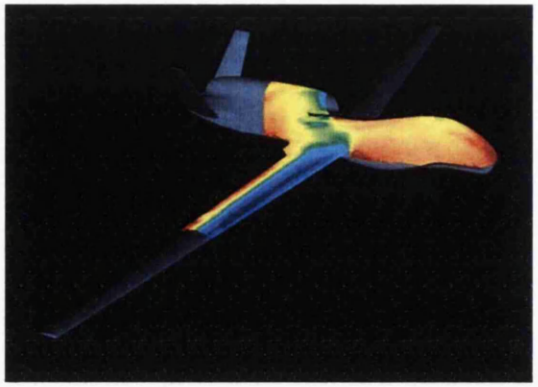

Fig.1.15. Imaging airflow over an aeroplane using PSPs[83]

1.8.5 Medical applications of luminescent sensors

Medical applications is an area in which there is keen interest for these sensors, in particular the measurement of dissolved oxygen and carbon dioxide in the blood.[8] Present methods utilise either pulse oximetry[84,85] or electrochemical methods to detect the concentration of gases in blood, both of which have drawbacks.[86] Pulse oximetry has limited accuracy, and the electrochemical methods available have tended to not be in line, and this means that samples have to be taken.[87-89]

Luminescent sensors have offered an alternative to these methods and a number of different ways of measuring changes in gas concentration have been described.[8] For most applications both the carbon dioxide and oxygen are measured together. Blood is not transparent to UV and most visible wavelengths, therefore a non contact method is used.[90,91] A gas permeable barrier is placed between the blood and the sensor. One such example involved microdialysis. Water was flowed through dialysis tubing, in the opposite direction to the blood flow, to cuvettes that contained optical sensors. The gas diffuses out of the blood into the water until equilibrium is obtained, the luminescent sensors determine the concentration of dissolved analyte in

the water and correspondingly the dissolved concentration in the blood.[15] In chapter 6 sensors are described for the measurement of gases in blood in which luminescent sensors are covered with gas permeable membranes of polyethersulfone and polypropylene.

An interesting question is, where does the oxygen that diffuses out of the blood come from? Oxygen is bound to the haemoglobin in blood and could be released from this, however most of blood is water and some oxygen is present in this, it is therefore possible that the diffused oxygen comes from here. The answer to this is not known,[92] however the concentration of oxygen in the plasma will be proportional to the saturation of the haemoglobin and therefore can still be used as an accurate measure of oxygen saturation.

Wolfbeis and co workers created a sensor which used the skin as a barrier and a luminescent oxygen sensor was place on the skin. The skin had to be warmed to 40 °C in order to facilitate vasodilatation and allow efficient diffusion of gases through the skin.[16]

1.8.6 Advantages of colorimetric sensors

Colorimetric sensors have all of the same general advantages of luminescent sensors described earlier. However they have an additional advantage in that they give an obvious colour change to the changing partial pressures of the analyte. Therefore they do not require any specialist knowledge, and there is no need for a spectrometer or similar expensive equipment for analysis.[69, 66]

1.9 Temperature sensors

Optical temperature sensors fall into the two different categories of luminescent and absorption sensors. Many different types of compounds can be utilised as optical thermometers because almost all reactions can be influenced by temperature.[93]

1.9.1 Luminescent temperature sensors

Luminescent temperature sensors are based on changes in luminescence in response to temperature. Compounds such as PtOEP can be utilised to detect changes in temperature because the lifetime is temperature dependent and this gives a decrease in phosphorescence with temperature (fig.1.16).

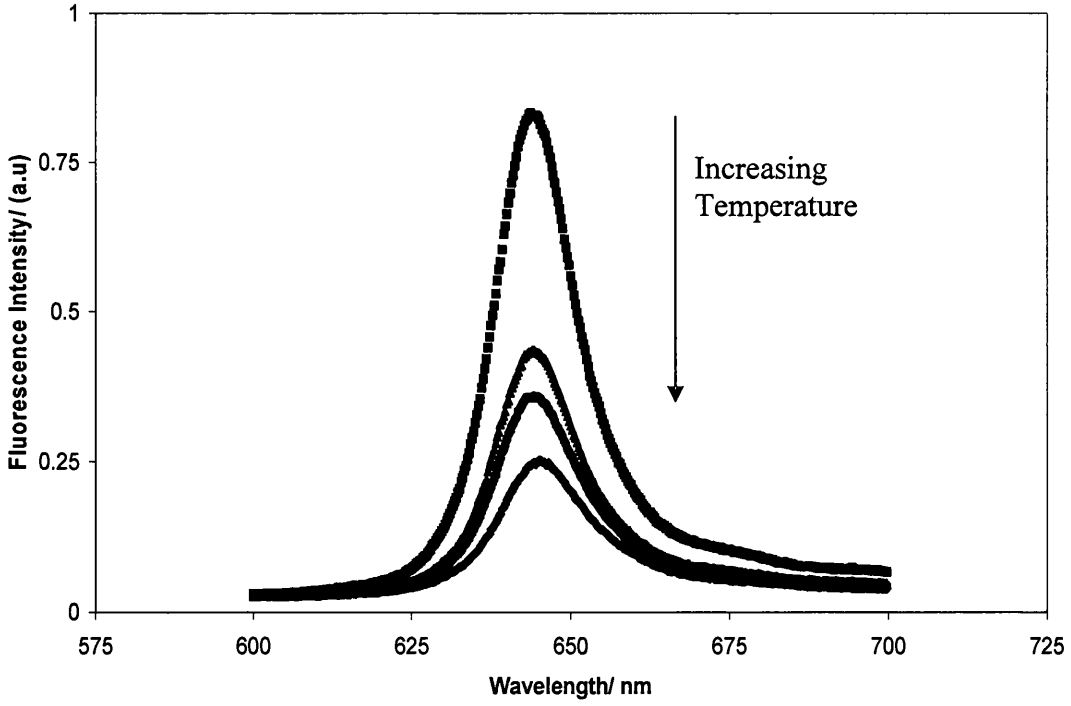

Fig.1.16. The decrease in PtOEP emission under nitrogen from 24 °C to 52 °C

Phosphors doped with trace elements are also used as temperature sensitive paints. In such phosphors Y_2O_3 luminescence intensity increases with temperature. They will

operate at quite high temperatures, e.g. Eu doped phosphors will operate between room temperature and 400 °C, and they can also be incorporated into commercially available paints.[95]

Further examples of luminescent temperature sensors include CdSe quantum dots which give an appreciable decrease in emission from around 20 °C to 50 °C. The advantage of this type of sensor is that the sensor element is so small that it is possible to measure temperature in very small volumes such as cells, which may be advantageous in biological measurements.[96]

1.9.2 Absorption based temperature sensors

Absorption based temperature sensors give a change in absorption with changes in temperature (fig.1.17). The temperature sensor used in chapter 4 is based on the dehydration and hydration of cobalt chloride from the octahedral $[Co(H_2O)_6]^{2+}$ (pink) complex to a tetrahedral $[Co(H_2O)_4]^{2+}$ (blue) complex.[97-100]

Fig.1.17. A thermochromic toy at room temperature (left) and approximately 50 °C (right)

A variety of inorganic compounds are available that display thermochromic behaviour and which could be used a temperature sensors. Vanadium dioxide is known to show thermochromic changes in the IR region by inter conversion between polymeric forms.[101] Cu_2HgI_4 is a commonly known thermochromic compound which is known to give a red to black colour change from 25-85 °C which is related to a change in the lattice structure.[102]

A variety of organic compounds are also available which are thermochromic. Crystal violet lactone undergoes a reversible ring opening reaction on heating to produce a tautomer and an associated blue to colourless colour change, fig.1.18.[104,105] Others compounds which exhibit this type of behaviour are lophine[106] and spiropyrans.[107] A drawback of using this type of compound is that a melting solvent is often required to allow the colour change to occur. The compound is encapsulated in a waxy solvent with an acid, as the solvent melts the compound is protonatated and a colour change is observed.[108,109]

Other absorption based sensors utilised other types of sensor and rely on temperature to change the reaction condition such as the acid base equilibrium equation 1.13 used in carbon dioxide sensors. This is shown in the work by Mills and Lepre whereby the temperature sensitivity of the buffer system is exploited to produce a temperature dependent colour change.

$$Q^{*}HCO_3^{-} . (x\text{-}1)H_2O.DH \overset{K_t}{\rightleftharpoons} Q^{+}D^{-} . xH_2O + CO_2 \qquad [1.13]$$

As the temperature of the environment increases the equilibrium is shifted to the right and the deprontonated form of the dye becomes more prominent,[103] and, for example using phenolphthalein a colourless to purple colour change is observed. It becomes necessary to maintain a constant partial pressure of carbon dioxide for this sensor to work.[103]

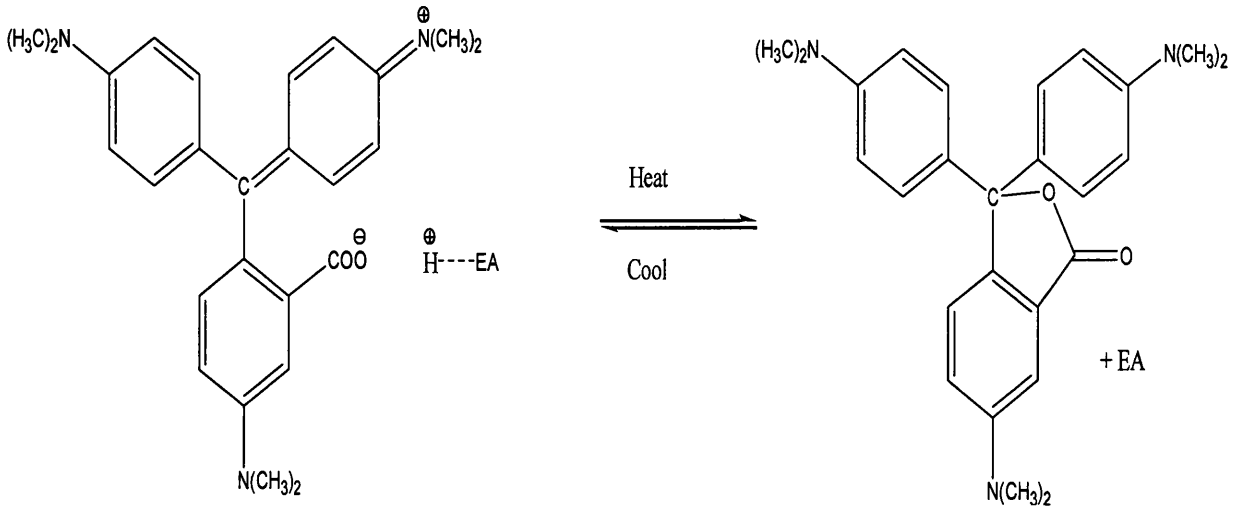

Fig.1.18. Reversible thermochromic reaction of crystal violet lactone from violet (left) to colourless (right) EA = electron acceptor

1.9.3 liquid crystal thermometers

Thermochromic liquid crystals are crystals that exhibit a selective reflectance of light as a function of temperature. The internal structure of the crystal changes across a known temperature range. As the temperature changes the wavelength of the reflected light is altered, and therefore a colour change, can be observed. Liquid crystals can be very accurate, and also have the advantage that they can be used to measure the temperature over the whole surface.[110] However they can be

complicated to make.[111] Cholesterol derivatives are a typical example of liquid crystals.[112]

1.9.4 Uses and advantages of optical temperature sensors

The major use of optical temperature sensors is as temperature sensitive paint to give the temperature of surfaces. They are also used in conjunction with pressure sensitive paints to provide temperature correction factors. The major advantage of this is that a whole surface can be measured at once. They are also of use when analysing high temperature surfaces which are maybe difficult to get close to or are dangerous.

The other uses of temperature sensors is as temperature sensitive inks used for security inks and food labelling, and also as novelty items such as clothing which changes colour, and children's toys (fig.1.17).[113,93]

1.10 Carbon dioxide sensors

1.10.1 The operation of carbon dioxide sensors

The conventional methods of detecting carbon dioxide is either by infra red spectroscopy, which is expensive and is very sensitive to the presence of water[114], or by an electrochemical method which is essentially a pH meter [115,116] where the drop in pH is caused by the reactions outlined in equations 1.14 to 1.17. In the first of these reactions carbon dioxide dissolves in water to form a neutral aqueous species, (equation 1.14).[117]

$$CO_{2(g)} \rightleftharpoons CO_{2(aq)} \qquad [1.14]$$

Once dissolved carbon dioxide can react with the solvent to form carbonic acid, equation 1.15.

$$CO_{2(aq)} + H_2O \rightleftharpoons H_2CO_3 \qquad [1.15]$$

The acid will then dissociate and thus lower the pH, equation1.16.

$$H_2CO_3 \rightleftharpoons H_3O^+ + HCO_3^- \qquad [1.16]$$

While this is the major reaction responsible for the changes in pH carbonic acid contains a second proton that can also dissociate.

$$HCO_3^- \rightleftharpoons H_3O^+ + CO_3^{2-} \qquad [1.17]$$

The reaction in equation 1.17 is a further possibility, however is very rarely observed due to the high pKa value.

Part of the work discussed in this thesis is concerned with optical detectors of carbon dioxide which utilises the changes in pH associated with changes in carbon dioxide partial pressures. Optical carbon dioxide sensors are based on pH indicating dyes such as phenolphthalein[103], bromothymol blue, and cresol red[117,118], which will give a change in absorption with a change in partial pressures of carbon dioxide. The

earliest examples of these sensors used a pH indicating dye in a hydrophobic matrix with a bicarbonate buffer.[119]

In later work the idea of an ion pair (fig.1.19) was developed whereby the pH indicating dye is bound to the ion pair first thus making it more soluble in hydrophobic polymer matrices, such as ethyl cellulose[120] which has a high permeability to carbon dioxide. The most common ion pair is tetraoctyl ammonium hydroxide.[121] One of the advantages associated with the ion pair is that the ion pair is believed to have some water associated with it and so water does not have to be added to the sensor for activation, whereas it does for bicarbonate based sensors. The general mode of activity of these sensors is given in eq 1.18.

$$[Q^+D^-.\ xH_2O] + CO_{2(g)} \rightleftharpoons [Q^+D^-.xH_2O.CO_{2(aq)}]$$

$$[Q^+D^-.xH_2O.CO_{2(aq)}] \rightleftharpoons [Q^+D^-.(x-1)H_2O.H_2CO_3]$$

$$[Q^+D^-.(x-1)H_2O.H_2CO_3] \rightleftharpoons [Q^+HCO_3^-.(x-1)H_2O.HD]$$

Eq.1.18. Q is the ion pair agent, D is the dye

While this approach produces sensitive sensors that are accurate, they are often unstable, sometimes lasting only hours.[122] The degradation is thought to arise from leeching of the ion pair and the permeation of trace gases such as NO_2 and sulphur containing gases. These produce nitric and sulphuric acid which are much stronger

acids and have lower pKa values than carbonic acid.[114,122] These strong acids protonate the indicators permanently and destroy the sensor.

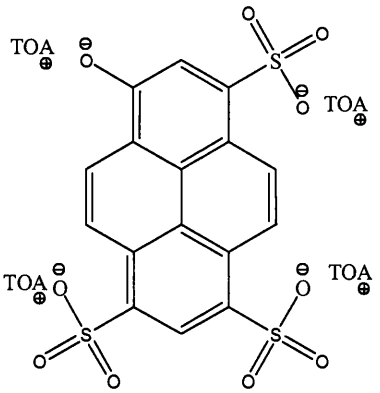

Fig.1.19. Ion pairing of HPTS with tetraoctylammonium ion (TOA)

To combat this, different approaches have been developed. The first involved placing hydrophobic films such as teflon over the sensor or by covering it with silicon rubber.[123] Other workers have created reservoirs so that the dye is constantly replenished thus extending the operational lifetime of the sensor.[124] Later developments have been to start using different polymer matrices, most notably sol gel polymers, and it is now possible to get carbon dioxide sensors that are so stable they are steam sterilisable.[125,126]

While the earliest sensors were all absorption based later sensors tend to be fluorescence based because of the higher degree of stability of these sensors[123]. The choice of sensing molecule is almost exclusively 1-hydroxy-3-6-8-pyrenetrisulfonic acid (HPTS) sometimes referred to as pyranine.[127,128] Further developments used with this types of sensor is the use of the ion pair cetyltrimethyl ammonium hydroxide[129], which creates a less sensitive sensor than using a tetraoctyl ammonium hydroxide ion pair. Although this is less sensitive it may be more desirable because the sensor can operate over a higher carbon dioxide concentration range.[51]

1.10.2 Applications of carbon dioxide sensors

Carbon dioxide is a biologically active gas and detected the levels of carbon dioxide is very important to clinicians, it is exchanged with oxygen in alveoli in the lungs and is produced as a by product of respiration. The level of carbon dioxide in the body gives a key indication about the health of an individual. If an individual has poor respiration then carbon dioxide builds up in the blood, because blood is mainly water it forms methanoic acid. This in turn lowers the blood pH to give a condition known as acidosis[130,131] which can lead to serious problems such as cardiac arrhythmia (irregular heart beat).[132, 133] Another medical application is the placement of nasoenteric feed tubes in patients that can not feed themselves. Complications can arise if the tube is placed into the airway rather than the oesophagus. In a recent study the use of a luminescent carbon dioxide sensor was compared to the current method of radiography. The cost of the carbon dioxide sensor was $ 23 and the cost of the radiographs was $ 795, so a simple luminescent sensor could be a potential replacement for expensive radiography techniques.[134] It is also possible to used carbon dioxide sensors in modified atmosphere packaging since many modified atmospheres often used carbon dioxide atmospheres.[74]

1.11 Thesis Overview

In chapter 2 the general experimental procedures used in this work are described, along with the properties of the lumophores and the polymer matrices used.

Chapter 3 deals with the development of a dual lumophore colorimetric oxygen sensors for use in vacuum storage artefact preservation as discussed with staff at the British Museum. Polymer matrices, choices of lumophores, methods for making dual lumophore sensors, and methods for illuminating the sensors are all discussed. The problem of degradation of the lumophores is examined in detail and a method is established for stabilising multilumophore systems.

Chapter 4 presents results from studies on a proof of concept sensor for a novel pressure sensitive paint. This utilises a dual lumophore colorimetric luminescent oxygen sensor with an absorption based temperature sensor. The emission colour of the dual lumophore sensor under UV excitation gives an easy indication of the changes in air flow, while the absorption colour of the temperature sensing layer under visible light allows temperature correction of the oxygen sensor response to be made.

Chapter 5 describes a different approach to constructing a dual lumophore sensor with a traffic light response, whereby a green LED is used for both emission and excitation in place of a the green lumophore and UV excitation source described previously.[69] The red lumophore is once again PtOEP. The problems with using this approach are examined in detail.

Chapter 6 describes the construction of two sensors for the detection of dissolved carbon dioxide and oxygen in blood, using two optical sensors based on HPTS and PtOEP. These sensors were developed for Haemair Ltd to help with the development of an artificial lung. LEDs were used for excitation, while two methods of detection were assessed; photodiodes and phototransistors coupled to picolog picoscopes. Bandpass filters were used to help improve the signal to noise ratio.

Chapter 7 gives general conclusions and suggestions for future work.

1.12. References

1) Hezinger, A.F.E.; Tebar, J.; Gopferich, A. *Eur. J. Pharm. Biopharm.,* 68, **2008,** 138-152.

2) *The Concise Oxford Dictionary, 8th ed.,* Oxford, (1990), p1103.

3) Jones, L.; Atkins, P. *Molecules Matter and Change, 4th 2ed.,* Freeman, (2000), pp 177-197.

4) Rizvi, N.; Hayes, D.F. *Lancet,* 353, **1999,** 1897-1898.

5) Di Francesco, F.; Fuoco, R.; Trivella, M.G.; Ceccarini. A. *Microchem. J.,* 79, **2005,** 405-410.

6) Choudhury, B.; Shinar, R.; Shinar, J. *J. Appl. Phys.,* 5, **2004,** 2949-2954.

7) Schrenkhammer, P.; Wolfbeis, O.S. *Biosens. Bioelectron.,* 24, **2008,** 1000-1005.

8) Liener, M.J.P. *Anal. Chim. Acta,* 255, **1991,** 209-222.

9) Lee, S.C.; Choi, H.Y.; Lee, S.J.; Lee, W.S.; Huh, J.S.; Lee, D.D.; Kim, J.C. *Sens. Actuators B,* 137, **2009,** 239-245.

10) Albert, K.J.; Walt, D.R. *Anal. Chem.,* 72, **2000,** 1947-1955.

11) Ercag, E.; Uzer, A.; Apak, R. *Talanta,* 78, **2009,** 772-780.

12) Arotiounian, V. *Int. J. Hydrogen. Energ.,* 32, **2007,** 1145-1158.

13) Christian, G.D. *Analytical Chemistry, 5th ed.,* Wiley, (1994), pp172-233.

14) Atkins P.W. *Physical Chemistry, 6th ed.,* Oxford, (2001).

15) Conney, C.G.; Towe, B.C.; Eyster, C.R. *Sens. Actuators B,* 69, **2000,** 183-188.

16) Babilas, P.; Lamby, P.; Prantl, L.; Schreml, S.; Jung, E.M.; Leibsch, G.; Wolfbeis, O.S.; Landthlaler, M.; Szeimies, R-M.; Abels, C. *Skin. Res. Technol.,* 14, **2008,** 304-311.

17) Shinar, R.; Zhou, Z.; Choudhury, B.; Shinar, J. *Anal. Chim. Acta,* 568, **2006,** 190-199.

18) Wolfbeis, O.S. *Anal. Chem.,* 72, **2006,** 81R-89R.

19) Wolfbeis, O.S. *J. Mater. Chem.,* 15, **2005,** 2657-2669.

20) Hahn, C.E.W. *Analyst,* 123, **1998,** 57R-86R.

21) Vargas-Rodriguez, E.; Rutt, H.N. *Sens. Actuators B,* 137, **2009,** 410-419.

22) Bacon, J.R.; DeGraff, B.A.; Carraway, E.R.; Demas, J.N. *Anal. Chem.,* 63, **1991,** 337-342.

23) Aposotolidos, A.; Klimant, I.; Andrezjewski, D.; Wolfbeis, O.S. *J. Comb. Chem.,* 6, **2004,** 325-331.

24) Carraway, E.R.; Demas, J.N. *Langmuir,* 7, **1991,** 2991-2998.

25) Bandrup, J.; Immergut, E.H.; Grulke, E.A. *Polymer Handbook, 4th ed.*, Wiley, (1999).

26) Mills, A.; Lepre, A. *Anal. Chem.,* 69, **1997,** 4653-4659.

27) Hearn, R.; Brocas, J.; Vander Donckt, E. *Anal. Chim. Acta,* 364, **1998,** 131-141.

28) Hartman, P.; Trettnak, W. *Anal. Chem.,* 68, **1996,** 2615-2620.

29) N.J. *Modern Molecular photochemistry, 1st ed.,* University Science Books, (1989).

30) Lacowicz, J.R. *Principles of Fluorescence Spectroscopy, 2nd ed.,* Springer, (1999).

31) Peterson, J.I.; Fitzgerald, R.V.; Buckhold, D.K. *Anal. Chem.,* 56, **1984,** 62-67.

32) Xu, W.; Schmidt, R.; Whaley, M.; Demas, J.N.; DeGraff, B.A.; Karlkari, E.K.; Fanner, B.L. *Anal. Chem.,* 67, **1995,** 3172-3180.

33) Amao, Y.; Asai, K.; Ichiro, O. *Analchim. Acta,* 407, **2000,** 41-44.

34) Douglas, P.; Eaton, K. *Sens. Actuators B,* 82, **2002,** 200-208.

35) Farley, S.J.; Rochester, D.L.; Thompson, A.L.; Howard, J.A.K.; Williams, J.A.G. *Inorg. Chem.,* 44, **2005**, 9690-9703.

36) Demas, J.N.; DeGraff, B.A.; Xu, W. *Anal. Chem.,* 67, **1995,** 1377-1380.

37) Mills, A, *Analyst,* 124, **1999,** 1301-1307.

38) Chaung, H.; Arnold, M.A. *Anal. Chim. Acta,* 368, **1998,** 83-89.

39) Yu-Long, L.; Chen-Shane, C., Jiahn-Piring, Yur., Yuan-Che, C. *Sens. Actuators B,*13, **2008**, 479-488.

40) Hartmann, P.; Trettnak, W. *Anal. Chem.,* 68, **1996,** 2615-2620.

41) Hartman, P.; Leiner, M.J.; Lippitsch, M.E. *Sens. Actuators B,* 29, **1995,** 251-257.

42) Mills, A. *Sens. Actuators B,* 51, **1998,** 60-78.

43) Mills, A, *Analyst,* 124, **1999,** 1301-1307.

44) Douglas, P.; Eaton, K. *Sens Actuators B,* 82, **2002,** 200-208.

45) Hughes, V.A.; Douglas, P. *J. Fluoresc.*, 16, **2006**, 403-409.

46) Standish, B. *Biophotonics Int.,* 14, **2007,** 37-40.

47) Di Natale, C.; Samilbeni, D.; Paolesse, R.; Macagnano, A.; D'Amico, A. *Sens. Actuators B,* 65, **2000,** 220-226.

48) Stubenrauch, K.; Sandholzer, M.; Niedermair, F.; Waich, K.; Mayr, T.; Klimant, K.; Trimmel, G.; Slugovc, C. *Euro. Poly. J.,* 22, **2008,** 2558-2566.

49) Craith, B.D.M.; Donagh, C.M.; McEvoy, A.K. *Sens. Actuators B,* 29, **1995,** 226-230.

50) Holst, G.A.; Koster, T.; Voges, E.; Lubbers, D.W. *Sens. Actuators B,* 29, **1995,** 231-239.

51) Bultzingslowen, C.; McEnvoy, A.K.; McDonagh, C.; MacCraith, B.D.; Klimant, I.; Kause, C.; Wolfbeis, O.S. *Analyst,* 127, **2002,** 1478-1483.

52) Burke, C.S.; Markey, A.; Nooney, R.I.; Byrne, P.; McDonagh, C. *Sens. Actuator B,* 199, **2006,** 288-294.

53) Hartmann, P.; Leiner, M.J.P.; Kohlbacher, P. *Sens. Actuators B,* 51, **1998,** 196-202.

54) Fuller, Z.J.; Bare, W.D.; Kneas, K.A.; Xu, X-Y.; Demas, J.N.; DeGraff, B.A. *Anal. Chem.,* 75, **2003,** 2670-2677.

55) Captitan-Vallvey, L.F; Asensio, L.J; Lopez-Gonzalez, J; M.D. Fernandez-Ramos, M.D; Palma, A.J, *Anal. Chim. Acta.,* **2007,** 583, 166-173.

56) Palma, A.J; Lopez-Gonzalez, J; Asensio, L.J; Fernandez-Ramos, M.D; Captan-Vallvey, L.J., *Sens. Actuators B,*121, **2007**, 629-638.

57) Yu-Long, L.; Chen-Shane, C., Jiahn-Piring, Yur., Yuan-Che, C. *Sens. Actuators B,* 131, **2008**, 479-488.

58) Schanze, K.S.; Carroll, B.F.; Korotkevitch, S.; Morris, M.J. *A.I.A.A. Journal,* 35, **1997,** 306-310.

59) Wolfbeis, O.S.; Kovacs, B.; Goswani, K.; Klainer, S.M. *Michrochim. Acta,* 129, **1998,** 181-188.

60) Trettnak, W.; Reininger, F.; Dolezal, C.; O'Leary, P.; Binot, R.A. *Adv. Space Res.*, 22, **1998,** 1465-1474.

61) Khalil, G.E.; Costin, C.; Crafton, J.; Jones, G.; Grenoble, S.; Gouterman, M.; Callis, J.B.; Dalton, L.R. *Sens. Actuators B,* 97, **2004,** 13-21.

62) Zelelow, B.; Khalil, G.E.; Phelan, G.; Carlson, B.; Gouterman, M.; Callis, J.B.; Dalton, L.R. *Sens. Actuators B,* 96, **2003,** 304-314.

63) Parker, J.W.; Laksin, O.; Yu, C.; Lau, M-L.; Klima, S.; Fisher, R.; Scott, I.; Atwater, B.W. *Anal. Chem.,* 65, **1993,** 2329-2334.

64) Nassau, K. *The Physics and Chemistry of Colour, 2nd ed.,* Willey, (2001), pp 3-31.

65) Hunt, R.W.G., *Measuring Colour, 3rd ed.,* Fountain Press, (1998).

66) Evans, R.C; Douglas, P., *Anal. Chem.,* 78, **2006,** 5645-5652.

67) Ricketts, S.R.; Douglas, P.; *Sens. Actuators B,* 135 **2008**, 46-51.

68) Katoh, R.; Nakamura, M.; Sasaki, Y.; Furube, A.; Yokoyama, T.; Nanjo, H., *Chem. Lett.,* **2007,** 36, 1310-1311.

69) Evans, R.C.; Douglas, D.;Williams, J.A.G.; Rochester, D.L. *J. Fluores.,* **2006,** 16, 201-206.

70) Wang, X.; Chen, X.; Zhao-xiong; X.; Wang, X., *Angew. Chem. Int. Ed.,* 47, **2008**, 7450-7453.

71) Smolander, M.; Hurme, E.; Ahvenainen, R. *Trend. Food Sci. Technol.,* 8, **1997,** 101-106.

72) Crowley, K.; Pacquit, A.; Hayes, J.; Lau, K,T.; Diamond, D. *I.E.E.E.* **2005,** 754-757.

73) Mills, A. *Chem. Soc. Rev.,* 34, **2005,** 1003-1011.

74) Del-Valle, V.; Munoz-Hernandez, P.; Catala, R.; Gavara, R. *J. Food Eng.,* 91, **2009,** 474-481.

75) Maekawa, S., *Oxygen-Free Museum Cases, 1st ed.*, The Getty Conservation Institute, (1998), pp 1-15.

76) Daniel, V.; Lambert, F.L. *W.A.A.C. Newsletter,* 15, **1993,** 12-14.

77) Daniel, V.; Hanlon, G.; Maekawa, S. *W.A.A.C. Newsletter,* 15, **1993,** 15-19.

78) Zelelow, B.; Khalil, G.E.; Phelan, G.; Carlson, B.; Goutermann, M.; Callis, J.B.; Dalton, L.R. *Sens. Actuators B,* 96, **2003,** 304-314.

79) Hradil, J.; Davis, C.; Mongey, K.; McDonagh, C.; MacCraith, B.D. *Meas. Sci. Technol.,* 13, **2002,** 1552-1557.

80) Kose, M.E.; Carroll, B.F.; Schanze, K.S. *Langmuir,* 21, **2005,** 9121-9129.

81) Castaldo, A.; Massera, E.; Quercia, L.; Di Francia, G. *Sens. Actuators B,* 118, **2006,** 328-332.

82) Grenoble, S.; Goutermann, M.; Khalil.; Callis, J.; Dalton, L.*J. Lumin.,* 113, **2005,** 33-35.

83) http://www.aerospaceweb.org

84) Jubran, A. *Crit. Care,* 3, **1999,** 11-17.

85) Meinke, M.; Ott. E.; Gersonde. I.; Helfmann, J.; Albrecht, H.; Muller, G.; Hahn, A; Kopitz, M.; Hetzer, R. *Med. Laser Appl.,* 22, **2007,** 248-255.

86) Lauks, I.R. *Acc. Chem. Res.,* 31, **1998,** 317-324.

87) Jubran, A. *Crit. Care,* 3, **1999,** 11-17.

88) Meinke, M.; Ott. E.; Gersonde. I.; Helfmann, J.; Albrecht, H.; Muller, G.; Hahn, A; Kopitz, M.; Hetzer, R. *Med. Laser Appl.,* 22, **2007,** 248-255.

89) Weiwei, Y.; Aiyu, Z.; Baoshan, H.; Xinxia, C. *Sensors and Actuators B,* 130, **2008,** 21-24.

90) Horecker, B.L. *J. Biol. Chem.,* 148, **1943,** 173-174.

91) Stenstrom, W.; Reinhard, M. *J. Biol. Chem.,* 66, **1925,** 819-827.

92) Des Jardins, T.J.; Burton, G.G. *Clinical Manifestations and Assessment of Respiratory Disease, 5th ed.,* Elsevier Health Sciences, (2005), pp 81-82.

93) Miodiwnik, M, *Materials Today,* 11, **2006,** 6-7.

94) Lupton, J.M. *Appl. Phys. Lett.* 81, **2002,** 2478-2480.

95) Syed Azim, S.; Solaiyan, C.; Venkatachari, G. *J. P. Org. Coat.,* 62, **2008,** 28-31.

96) Li, S.; Zhang, K.; Yang, J-M.; Lin, L.; Yang, H. *Nano Lett.,* 7, **2007,** 3102-3105.

97) Greenwood, N.N.; Earnshaw, A., *Chemistry of the Elements,* 2nd ed, Butterworth Heinemann, 2001, p1129.

98) Srivastava, J.; Srivastava, J.N.; Alam, S.; Mathur, G.N., *App. Poly. Sci.,* 100, **2006,** 4832-4834.

99) Lazareva, T.G.; Kabisheva, I.V.; Il'yushchenko, I.A., *Proc. S. P. I. E.,* 3324, **1998**, 308-317.

100) Dybo, A.; Wroblewski, W.; Rozniecka, E.; Maciejewski, J.; Brozozka, Z. *Sens. Actuators B,* 76, **1999,** 203-207.

101) Manning, T.D.; Parkin, I.P.; Pemble, M.E.; Sheel, D.; Vernardou, D. *Chem. Mater.,* 16, **2004,** 744-749.

102) Day, J.H. *Chem. Rev.,* 68, **1968,** 649-657.

103) Mills, A.; Lepre, A. *Analyst,* 124, **1999,** 685-689.

104) Zhu, C.F.; Wu, A.B. *Thermochim. Acta,* 425, **2005,** 7-12.

105) MacLaren, D.C; White, M.A. *Materials.,* 13, **2003,** 1695-1700.

106) Fernandez-Valdivielso, C.; Egozkue, E.; Matias, I.R.; Arregui, F.J.; Baraiain, C. *Sens. Actuators B,* 91, **2003,** 231-240.

107) Day, J.H. *Chem. Rev.,* 63, **1963,** 65-80.

108) Nelson, G. *I. J. Pharm.,* 242, **2002,** 55-62.

109) Monllor, P.; Bonet, M.A.; Cases, F. *Euro. Poly. J.,* 43, **2007,** 2481-2490.

110) Grassi, W.; Testi, D.; Della Vista, D.; Torelli, G. *Measurement,* 40, **2007,** 898-903.

111) Abdullah, N.; Talib, A.R.A.; Saiah, H.R.M.; Jaafar, A.A.; Salleh, M.A.M. *Exp. Therm. Fluid. Sci.,* **2009,** doi:10.1016/j.expthermflusci.2008.12.002.

112) Majumdar, K.C.; Mondal, S.; Pal, N.; Sinha, R.K. *Tetrahedron, Lett.,* **2009,** doi: 10.1016/j.tetlet.2009.02.065.

113) *Plastics Additives and Compounding,* 5, **2003,** 26-30.

114) Amao, Y.; Nakamura, N. *Sens. Actuators B,* 100, **2004,** 347-351.

115) Anjos, T.G.; Hahn, C.E.W. *Sens. Actuators B,* 125, **2008,** 224-229.

116) McMurray, N.H. *J. Mater. Chem.,* 2, **1992,** 401-406.

117) Mills, A.; Chang, Q.; McMurray, N. *Anal. Chem.,* 64, **1992,** 1383-1389.

118) Mills, A.; Lepre, A.; Wild, L., *Sens. Actuators B,* 38, **1997,** 419-425.

119) Parker, J.W.; Laksin, O.; Yu, C.; Lau, M-L.; Klima, S.; Fischer, R.; Scott, I.; Atwater, B.W. *Anal. Chem.,* 65, **1993,** 2329-2334.

120) Geddes, C.D.; Lacowitz, J.R. *Advanced Concepts in Fluorescence Sensing Part A, 1st ed.,* Springer, (2005), pp138.

121) Weigl, B.H.; Wolfbeis, O.S. *Sens. Actuators B,* 28, **1995,** 151-156.

122) Oter, O.; Ertekin, K.; Topkaya, D.; Alp, S. *Sens. Actuators B,* 117, **2006,** 295-301.

123) Wolfbeis, O.S.; Kavacs, B.; Goswami, K.; Klainer, S.M. *Mikrochim. Acta.,* 129, **1998,** 181-188.

124) Ertkin, K.; Klimant, I.; Neurauter, G.; Wolfbeis, O.S. *Talanta,* 59, **2003,** 261-267.

125) Chang, Q.; Randers-Eichhorn, L.; Lakowicz, J.R.; Rao, G. *Biotechnolo. Prog.,* 14, **1998**, 326-331.

126) Bultzigslowen, C.; McEnvoy, A.K.; McDonagh, C.; MacCraith, B.D. *Anal. Chem. Acta.,* 480, **2003,** 275-283.

127) Chu, C-S.; Lo, Y-L. *Sens. Actuators B,* 129, **2008,** 120-125.

128) Kocincova, A.S.; Borisov, S.M.; Krause, C.; Wolfbeis, O.S. *Anal. Chem.,* 79, **2007,** 8486-8493.

129) Ge, X.; Kostov, Y.; Rao, G. *Biotechnol. Bioeng.,* 89, **2005,** 329-334.

130) Sood, M.M.; Pauly, R.P. *Crit. Care,* 23, **2008,** 431-433.

131) Cheng, H.; Smith, G.L.; Orchard, C.H.; Hancox, J.C. *Mol. Cell. Cardiol.,* 46, **2009,** 75-85.

132) Williams, D.T.; Smith, R.S.; Mallon, K. *J. Emer. Med.,* **2008,** doi:10.1016/j.jemermed.2008.05.001.

133) Becerril-Herrera, M.; Alonso-Spilsbury, M.; Lemus-Flores, C.; Guerrero-Legarreta, I.; Olmos-Hernandez, A.; Ramerirez-Necoachea, R.; Mota-Rojas, D. *Meat Sci.,* 81, **2009,** 233-237.

134) Munera-Seeley, V.; Ochoa, J.B.; Brown, N.; Bayless, A.; Correia, M.I.T.D.; Bryk, J.; Zenati, M. *Clin. Res.,* 23, **2008,** 318-321.

2. Experimental section

2.1 Materials

Table 2.1 list all the materials used in this thesis.

Material	Source	Grade
tris(2,4-ditertbutylphenyl)phosphate (TBPP)	Aldrich	98 %
Polystyrene	Aldrich	100,000 Mw
8-hydoxy-1,3,6-trisulfonic acid trisodium salt methyltriethyloxysilane (MTEOS)	Aldrich	97 %
hydrochloric acid	Aldrich	98 %
Ethyl cellulose (EC)	Aldrich	(46 % ethoxyl content)
Cetyltrimetylammonium hydroxide	Fischer	98 %
Diazobicyclo[2.2.2]octane (DABCO)	Aldrich	98 %
Cobalt chloride	Aldrich	98 %
Coumarin 110	Aldrich	99 %
orthophosphoric acid	Aldrich	85 wt % in H_2O
polyvinylalcohol (PVA)	Aldrich	78,000 Mw
Gelatin	Aldrich	From bovine skin
(1'3'-dihydro-8-methoxy-1'3'3'-trimethyl-6-nitrospiro[2H-1-benzopyran-2,2'(2H)-indole])	Aldrich	97 %
Rhodamine 110	Aldrich	99 %
5(6)carboxfluorescein	Aldrich	95 %
Vitamin E (VITE)	Aldrich	97 %
2,4-di-tert-butyl-4-methylphenol (BHT)	Aldrich	99 %
Silicon rubber	Techsil Ltd	RTV 118

Platinum(II) N^C^N 1,3,6-tri-(2-pyridyl)benzene (PtPYR)	Gareth Williams' Inorganic synthesis group Durham University	-
Zinc oxide	Aldrich	99 %
Tris-2-(ethylhexyl)phosphate	Aldrich	97 %
Titanium dioxide	Aldrich	Degussa P-25
Dupont tripure TiO_2	Welsh printing and Coating	-
Silver oxide	Aldrich	99 %
Crystal violet lactone	Aldrich	97 %
Platinum (II) octaethylporphyrin (PtOEP)	Frontier scientific	98 %
Palladium octaethylporphyrin (PdOEP)	Aldrich	85 %

Table.2.1. A list of all the materials used in this thesis, their sources and grades

2.2 Experimental methods

2.1.1 Preparation of sensors

Generally a common method was used for making the sensors discussed in this thesis. The exceptions being the oxygen sensors described in chapter 5 which used an LED as both a source of emission and excitation, and the carbon dioxide sensor described in chapter 6.

The sensors films are made by spin coating one or more layers of lumophores dissolved in polymers onto a substrate. Typically each layer is prepared by

dissolving a small volume of a concentrated solution of the desired lumophore, e.g 1 mg in 1 ml of solvent, in a solution of the polymer matrix. Once mixed, other additives e.g. a stabiliser, such as DABCO, may be added. The resulting solution is then spin coated onto a substrate to create the sensor layer. Depending upon the application the full sensor may be made up of between one and seven layers, each layer having a specific function in that particular sensor. Table 2.2 shows the function of each of the sensors and the layers that make them up.

Chapter	Sensor type	Layer 1	Layer 2	Layer 3	Layer 4	Layer 5	Layer 6	Layer 7	Number of layers
3	Colorimetric O_2 sensor	PtPYR in EC	gelatin	PtOEP in EC	-	-	-	-	3
3	Colorimetric O_2 sensor	Rhodamine 110 in gelatin	PtOEP in EC with DABCO	-	-	-	-	-	2
4	Temperature corrected PSP	Acrylic paint	EC	$CoCl_2$ in PVA with phosphoric acid	EC	Coumarin 110 in EC	Gelatin	PtOEP in EC	7
5	Oxygen sensor	Green LED	PtOEP in EC with ZnO and DABCO	-	-	-	-	-	2
6	Oxygen sensor	PtOEP in EC with DABCO	-	-	-	-	-	-	1
6	CO_2 sensor	EC	HPTS in a sol gel with cetyltrimethyl ammonium hydroxide	HPTS in a sol gel with cetyltrimethyl ammonium hydroxide	polystyrene	-	-	-	4

Table.2.2 Description of the sensors constructed in this thesis.

2.2.2 Lumophores

A number of different lumophores have been used; each has various characteristics which make them desirable for particular applications. Important characteristics are: absorption and emission wavelengths, emission quantum yields, and excited-state lifetimes. Table 2.3 collects data for the lumophores used in this work.

Lumophore	Φ_{Lum}	τ_O
5,(6)-Carboxyfluorescein	0.30 [1]	-
PtOEP	0.5 [2]	0.091 ms [2]
PdOEP	0.2 [2]	0.99 ms [2]
PtPYR	0.57 [3]	9.2 μs [3]
Rhodamine 110	0.31 [4]	-
Coumarin 110	-	3.34 ns [5]
Coumarin 153	0.76 [6]	5.0 ns [5]
HPTS	>0.9 [7]	5.2-6 ns [8]

Table 2.3. Photochemical parameters for the lumophores used in this work, Φ_{Lum} = luminescence quantum yield, τ_O = lifetime in the absence of oxygen quenching, for HPTS this is the lifetime in the protonated form

2.2.3 Oxygen Sensitive Lumophores

Oxygen sensitive lumophores are lumophores which possess a long lived emissive state, generally a triplet state with a lifetime in the order of microseconds in duration. This allows sufficient time for deactivation by oxygen to occur. The oxygen

sensitive lumophores used in this thesis emit in either the green (PtPYR) or red (PtOEP and PdOEP, figs.2.1-2.5).

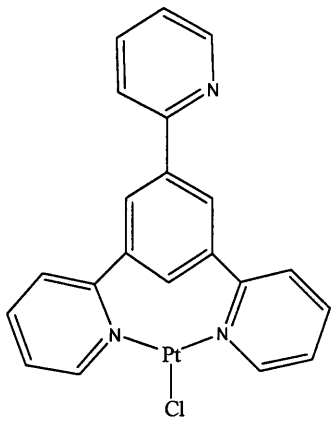

Fig.2.1. The structure of PtPYR

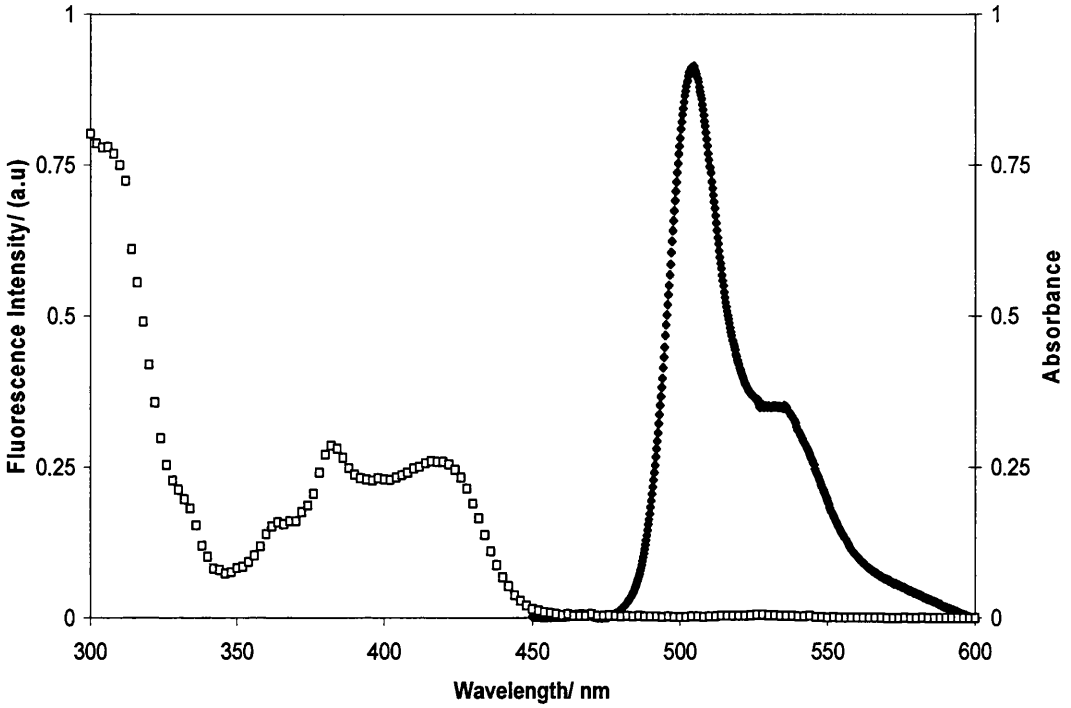

Fig.2.2. Absorption spectrum of PtPYR in THF 7.24 x 10^{-5} mol dm^{-3} (open squares) and emission spectrum (closed diamonds) for PtPYR in EC, from 1 mg of PtPYR dissolved in 1 ml THF and 0.4 ml of this solution dissolved in 1 g of 10 % EC toluene:ethanol 80:20 (w:v) which is spin coated onto a glass substrate

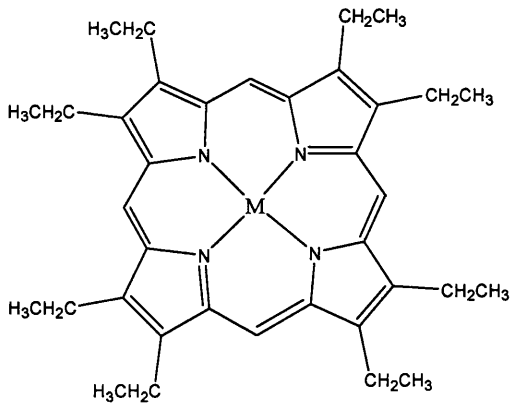

Fig.2.3. The structure of PdOEP (M = Pd) and PtOEP (M = Pt)

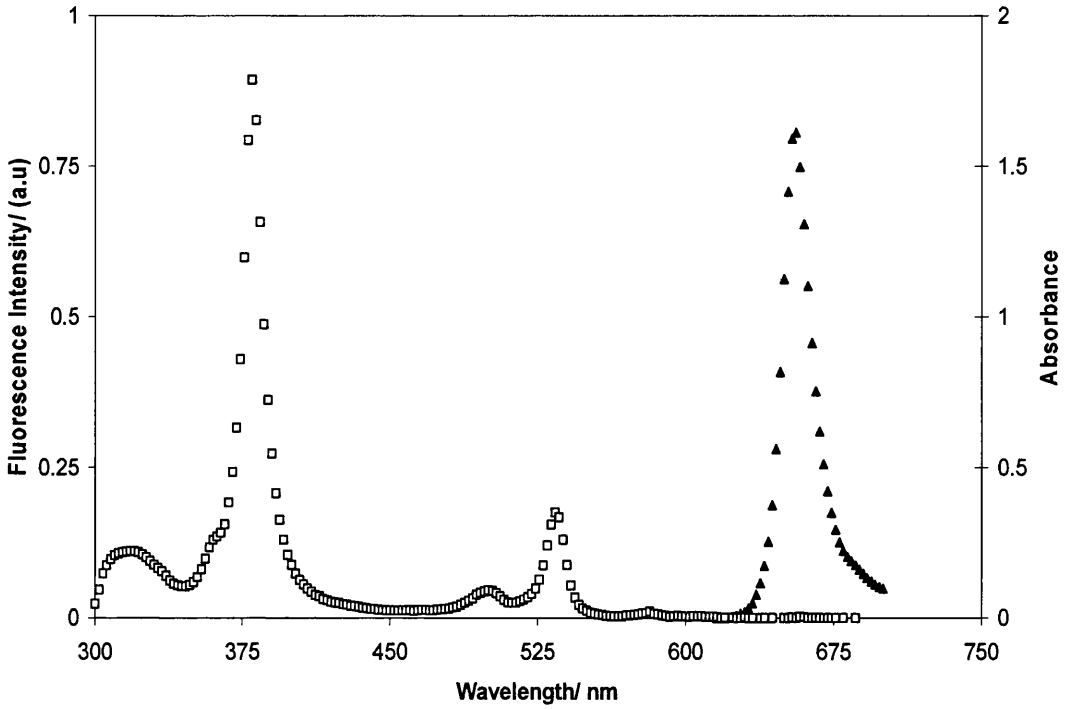

Fig.2.4. Absorption spectra of PtOEP in THF 6.24 x 10^{-5} mol dm^{-3} (open squares) and emission spectra (closed diamonds) for PtOEP in EC from 13.5 mg of PtOEP dissolved in 10 ml THF and 0.4 ml of this solution dissolved in 1 g of 10 % EC toluene:ethanol 80:20 (w:v) spin coated onto a glass substrate

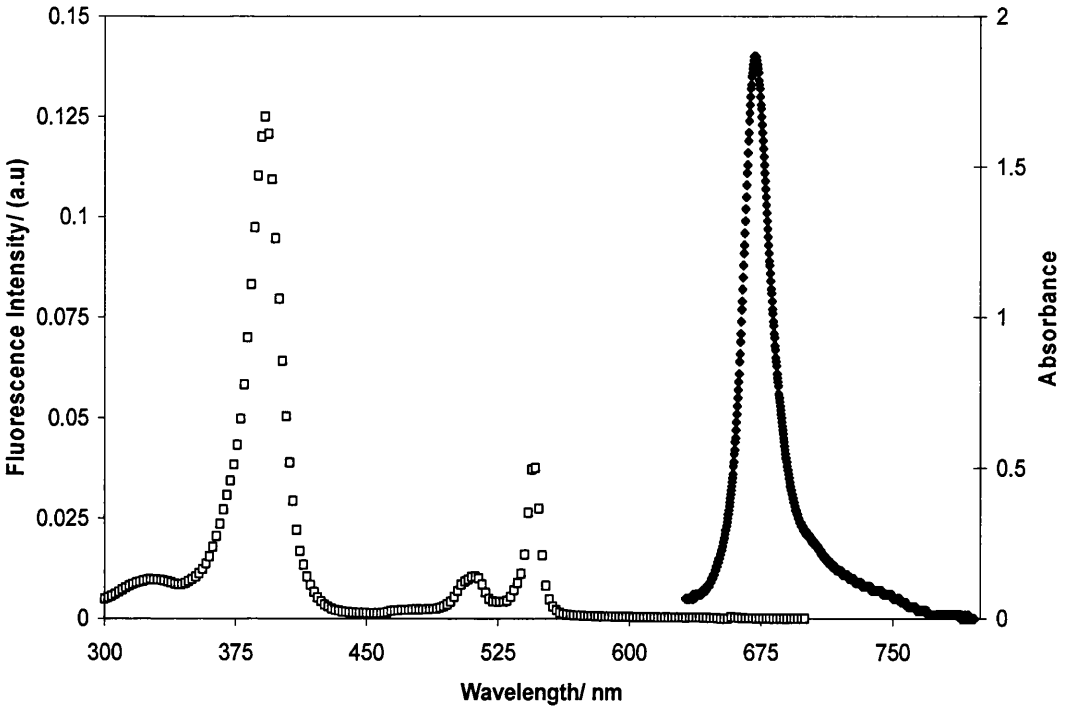

Fig.2.5. Absorption spectra (open squares) and emission spectra (closed diamonds) for PdOEP both in EC from 13.5 mg of PdOEP dissolved in 10 ml THF and 0.4 ml of this solution dissolved in 1 g of 10 % EC toluene:ethanol 80:20 (w:v) spin coated onto a glass substrate

2.2.4 Oxygen insensitive lumophores

These lumophores are not sensitive to changes in the partial pressure of oxygen. They are all singlet state emitters, with the lifetime of the S_1 state being in the order of nanoseconds (table 2.3), much too short for any significant oxygen quenching of emission. These lumophores are used to provide colour "anchor points" for colorimetric sensors. Structures and spectra are shown in figs. 2.6-2.12.

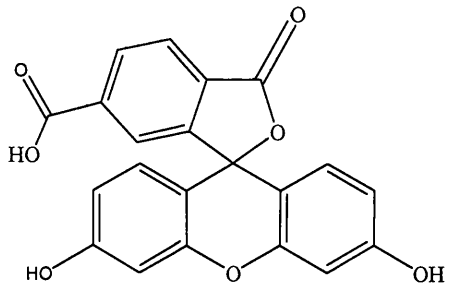

Fig.2.6. The structure of rhodamine 110

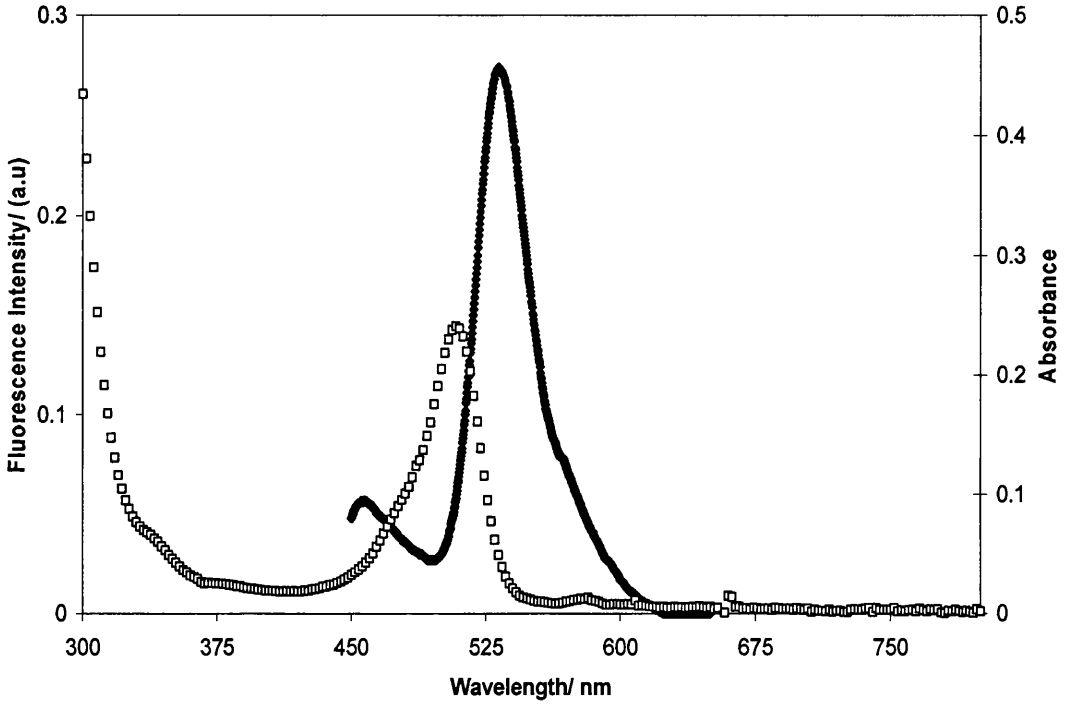

Fig.2.7. Absorption spectrum (open squares) in gelatin from a solution of 2 mg rhodamine 110 dissolved in 1 ml methanol and 0.4 ml of this solution dissolved in 1 g of 10 % aqueous gelatin spin coated on a glass substrate and emission spectrum of rhodamine 110 in methanol 2.73 x 10^{-3} mol dm^{-3}(closed diamonds)

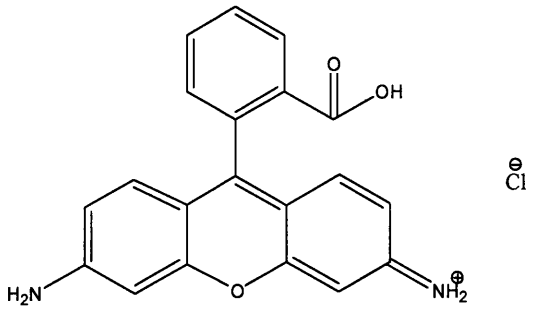

Fig.2.8. The structure of 5,(6)-carboxyfluorescein

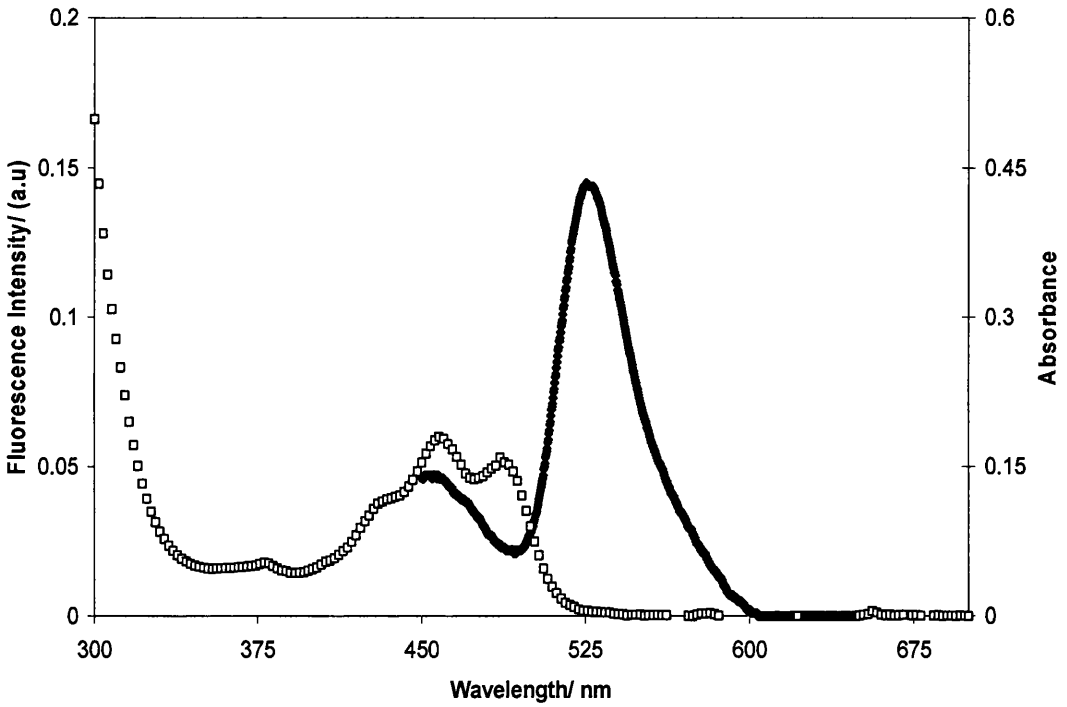

Fig.2.9. Absorption spectra (open squares) and emission spectra of 5,(6)-carboxyfluorescein (closed diamonds) Absorption spectrum (open squares) in gelatin from a solution of 1 mg 5,(6)-carboxyfluorescein dissolved in 1 ml methanol and 0.4 ml of this solution dissolved in 1 g of 10 % aqueous gelatin spin coated onto a glass substrate and the emission spectrum of 5,(6)-carboxfluorescein in methanol 2.66 x 10^{-3} mol dm^{-3}(closed diamonds)

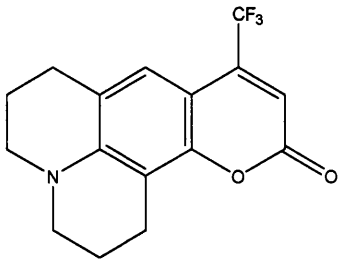

Fig.2.10. The structure of Coumarin 153

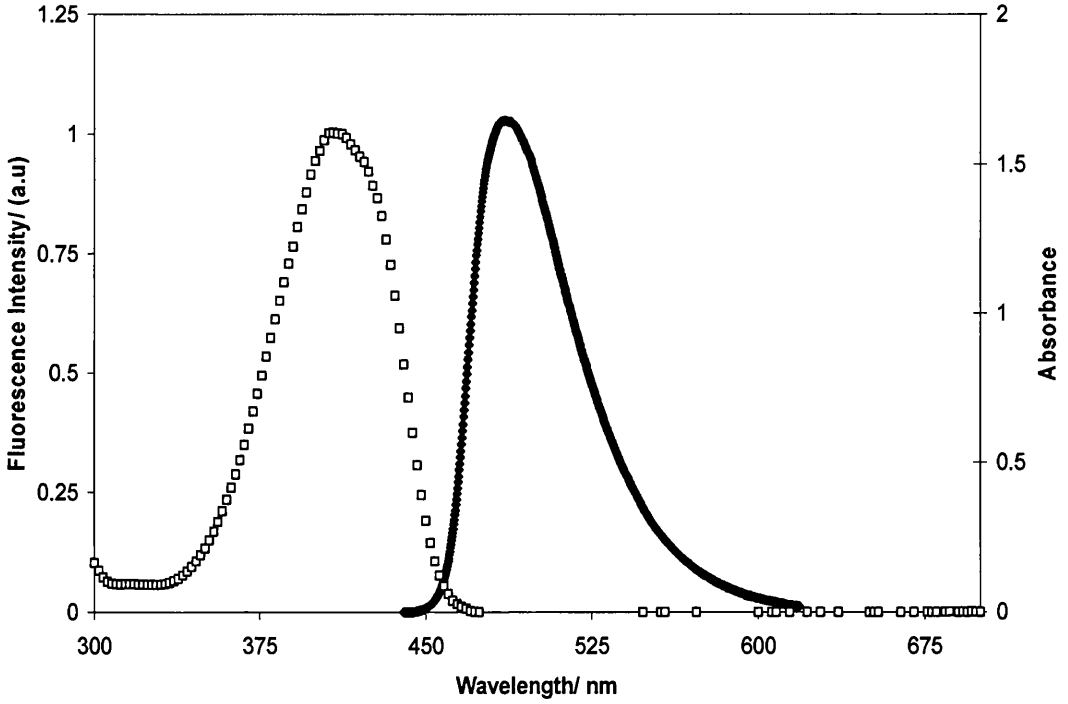

Fig.2.11. Absorption spectrum (open squares) and emission spectrum (closed diamonds) of coumarin 153 in THF 2.7 x 10^{-5} mol dm^{-3} for both absorption and emission measurements

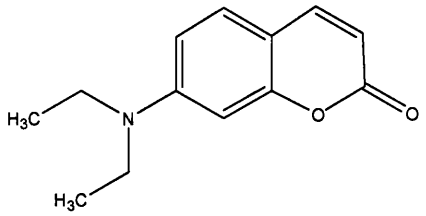

Fig.2.12. The structure of coumarin 110

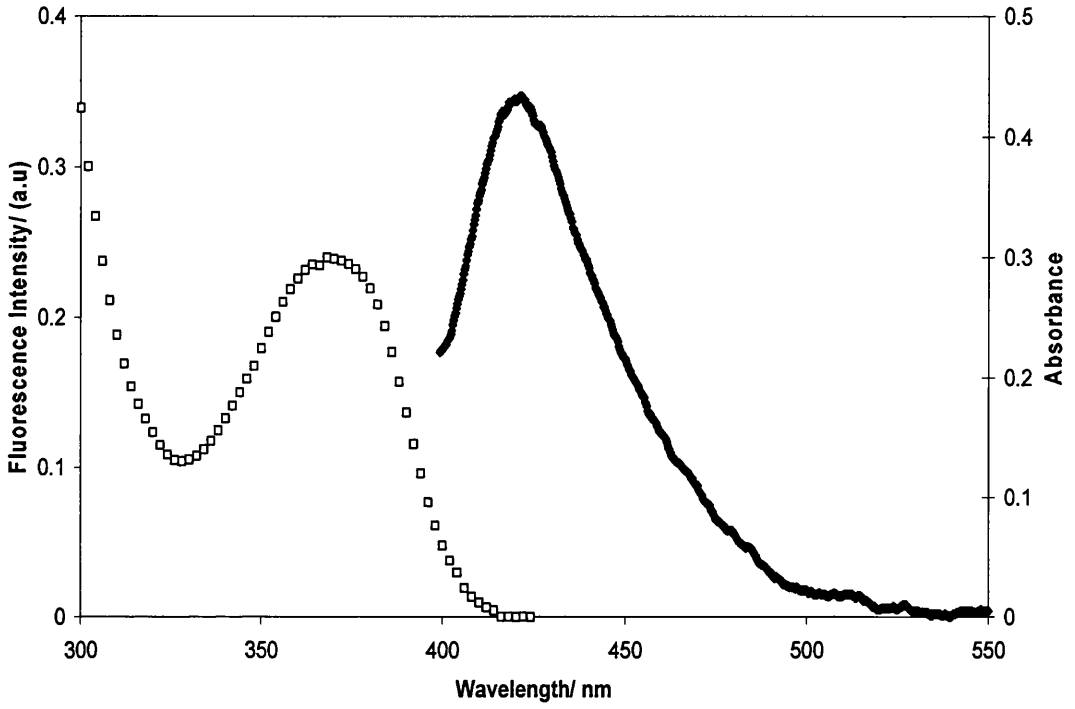

Fig.2.13. Absorption spectra (open squares) of coumarin 110 in THF 1.74 x 10^{-5} mol dm^{-3} emission spectra (closed diamonds) of coumarin 110 in EC from a solution of 2 mg of coumarin 110 dissolved in 1 ml THF and 0.4 ml of this solution dissolved in 1 g of 10 % 80:20 toluene:ethanol (w:v) spin coated on to a glass substrate

2.2.5 Carbon dioxide sensor lumophores

Only one carbon dioxide sensitive lumophore was used in this work, 8-hydroxy-1,3,6-trisulfonic acid (HPTS). This lumophore is responsive to changes in pH which arises as carbon dioxide reacts with residual water in the polymer matrix forming

carbonic acid. The detailed method of operation of these sensors is described in full in the introduction and chapter six.[9]

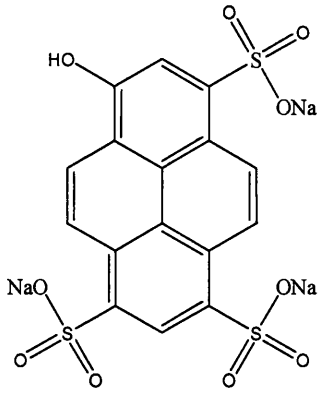

Fig.2.14 The structure of HPTS

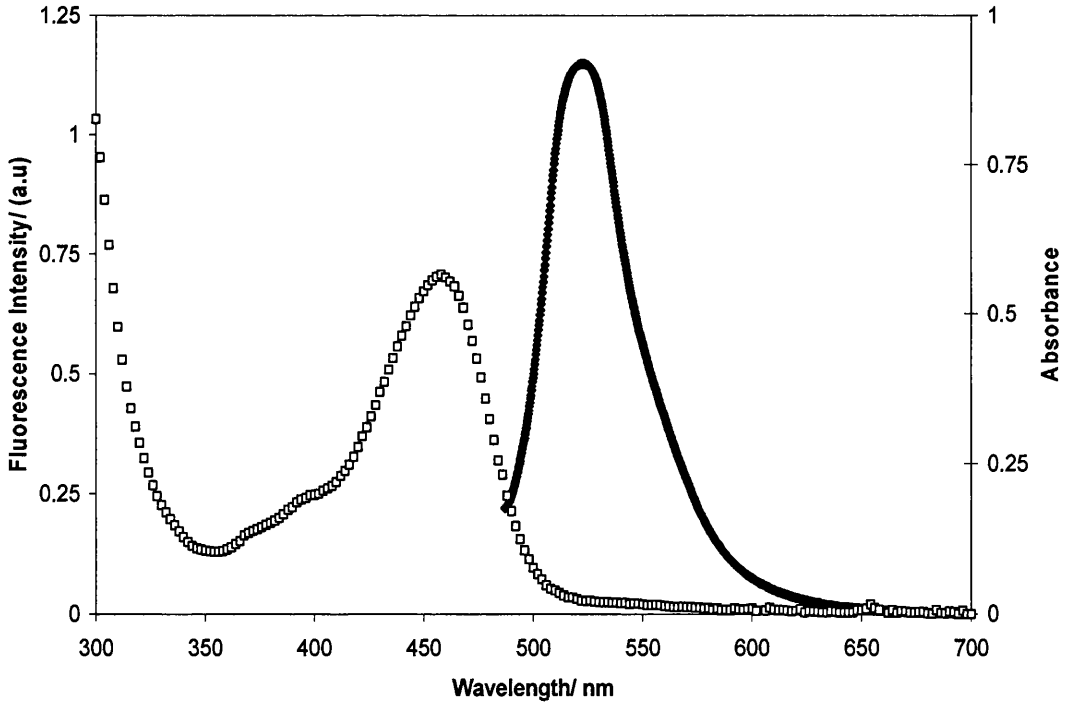

Fig.2.15. Absorption spectra (open squares) and emission spectra (closed diamonds) for HPTS ion paired with cetyltrimethylammonium hydroxide from the sensor described in chapter 6

2.3 *Polymer matrices*

The choice of polymer matrix affects many facets of sensor behaviour, such as response, response time, sensitivity, stability, and the optical properties of the sensor. The polymers used were: ethyl cellulose (EC), gelatin, polystyrene (PS), polyvinylalcohol (PVA), silicon rubber RTV-118 and a sol gel based on methyltriethyloxy silicate (sol gel) (fig.2.15). The relevant properties of these polymers are summarised in table 2.4.

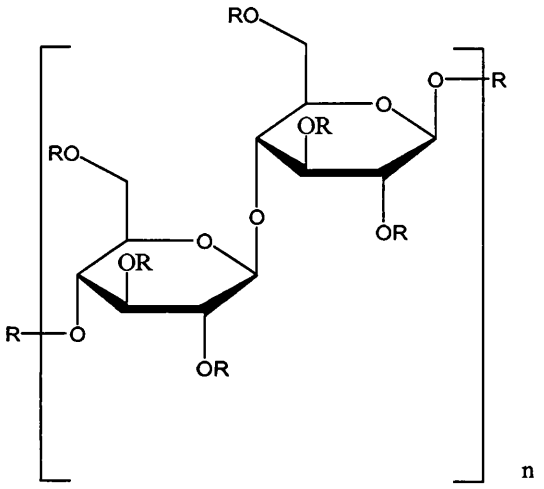

ethyl cellulose

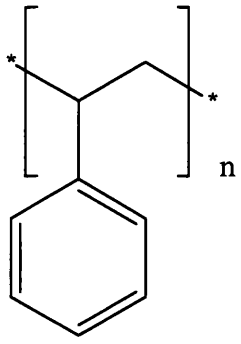

polystyrene

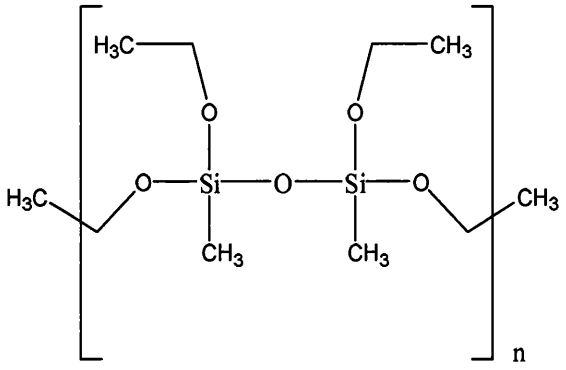

sol gel based on MTEOS

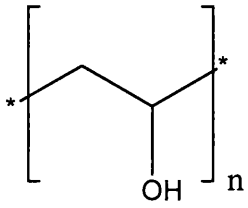

Polyvinyl alcohol

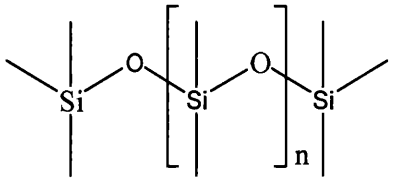

basic structure of silicon rubber

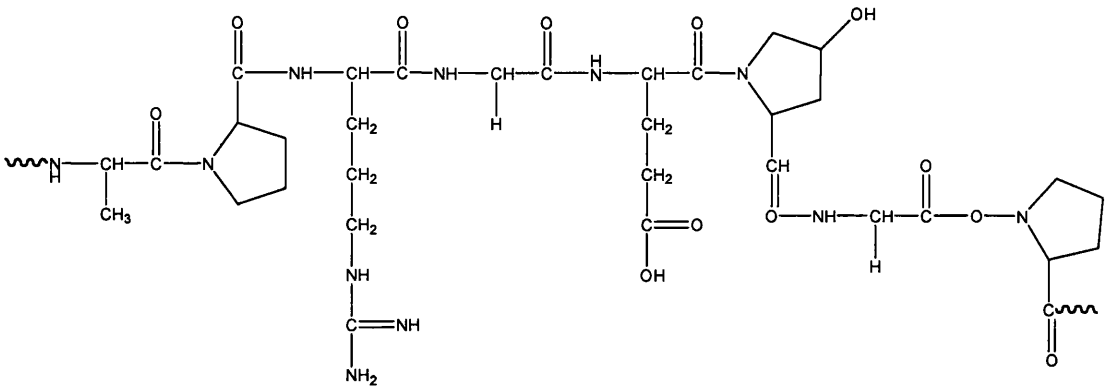

Typical structure of gelatin comprising of -Gly-Pro-Arg-Gly-Glu-4Hyp-Gly-Pro-

Fig.2.15. Structures of the polymer matrices used in this work

Polymer	Oxygen permeability ($P \times 10^{13}$)	Carbon dioxide permeability ($P \times 10^{13}$)	Refractive index (n)
Silicon rubber	367	2430	-
Ethyl cellulose	11	84.8	1.479
polystyrene	1.9	7.9	1.59
Polyvinyl alcohol	0.00665	65.0	1.5214

Permeability P/ cm^3 (273.15 K; 1.135×10^5 Pa) x cm/(cm^2 x s x Pa) for both oxygen and carbon dioxide, all data from reference 10

Table.2.4. Relevant properties of the polymers used in this work

The refractive index (n) is defined as the speed of light in the medium over the speed of light in vacuum. Generally, for sensors a higher refractive index is desired because this means that the critical angle required for total internal reflection is lower, thus decreasing the amount of light internally reflected, and therefore increasing the amount of light transmitted through the polymer.[10]

2.4 Colorimetric oxygen sensors

Colorimetric oxygen sensors were prepared by spin coating the least oxygen sensitive layer down first (fig.2.7). For example for the British Museum sensor described in chapter 3 the first layer is the green emitting rhodamine 110 in gelatin which is not quenched by oxygen. After the less sensitive layer it is often necessary to add a barrier layer which prevents removal of the lumophore in the lower layer when subsequent layers are added (fig.2.7). In general a hydrophobic layer will not

strip out a hydrophilic layer. This is evident in the PtPYR sensor described in chapter 3 whereby a gelatin barrier layer is placed between the two slides. Once a barrier layer has been applied the most sensitive layer is added, this is normally PtOEP in an EC matrix.

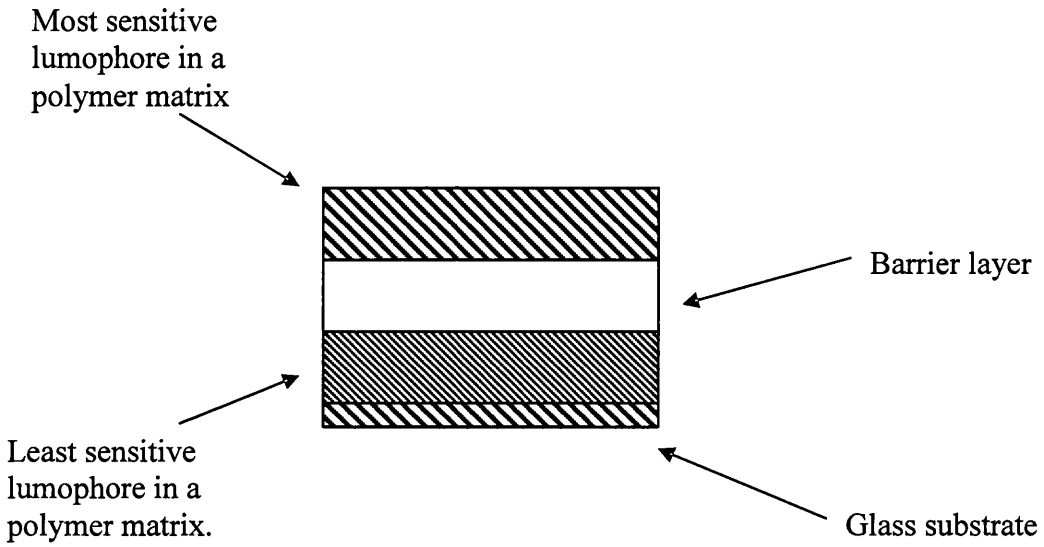

Fig.2.7. The construction of a typical dual lumophore colorimetric oxygen sensor

2.5 UV-VIS Spectrometry and film thicknesses

UV-vis spectrometry was performed using a Hewlett Packard 825A diode array spectrometer at room temperature against an appropriate blank, normally a glass slide. For temperature dependent spectra a water circulator was coupled to the sample holder to allow temperature control.

Using the Beer Lambert law equation 2.1 it is possible to estimate the thickness of thin films.

$$A = \varepsilon cl \qquad [2.1]^{11}$$

Where A is absorbance, ε is the lumophore extinction coefficient, c the concentration of the lumophore in the sample, and l the pathlength i.e. film thickness.
For a spin coated layer made using a solution of PtOEP in 10 % EC 80:20 toulene: ethanol (w:v) the thickness of the film is calculated to be approximately 10 microns by recording the absorption of a sensor film and then applying the Beer Lambert equation the concentration is known and the extinction coefficient is the calculated from PtOEP in THF. By substituting these values into the equation it is possible to calculate the film thickness.

2.6 Diffuse Reflectance

Diffuse reflectance spectra were recorded using a Perkin Elmer Lamda 9 UV-vis-NIR spectrometer with a diffuse reflectance attachment added. Barium oxide was used as reflectance standard. Spectra were measured in % R and converted into Kubelka-Munk function using equation 2.2.

$$F(R) = (1 - R)^2 / 2R \qquad [2.2]^{12}$$

F(R) = Kubelka Munk Function

R = % Reflectance

2.7 Emission Measurements

Steady state emission measurements were recorded on a Perkin-Elmer MPF44-E with a 150 W Xe arc lamp as the excitation source and a Hammamatsu R928 photomultiplier. Excitiation and emission monochromators can be set to allow 0.4 to 20 nm bandpass. All experiments were conducted at room temperature unless otherwise stated.

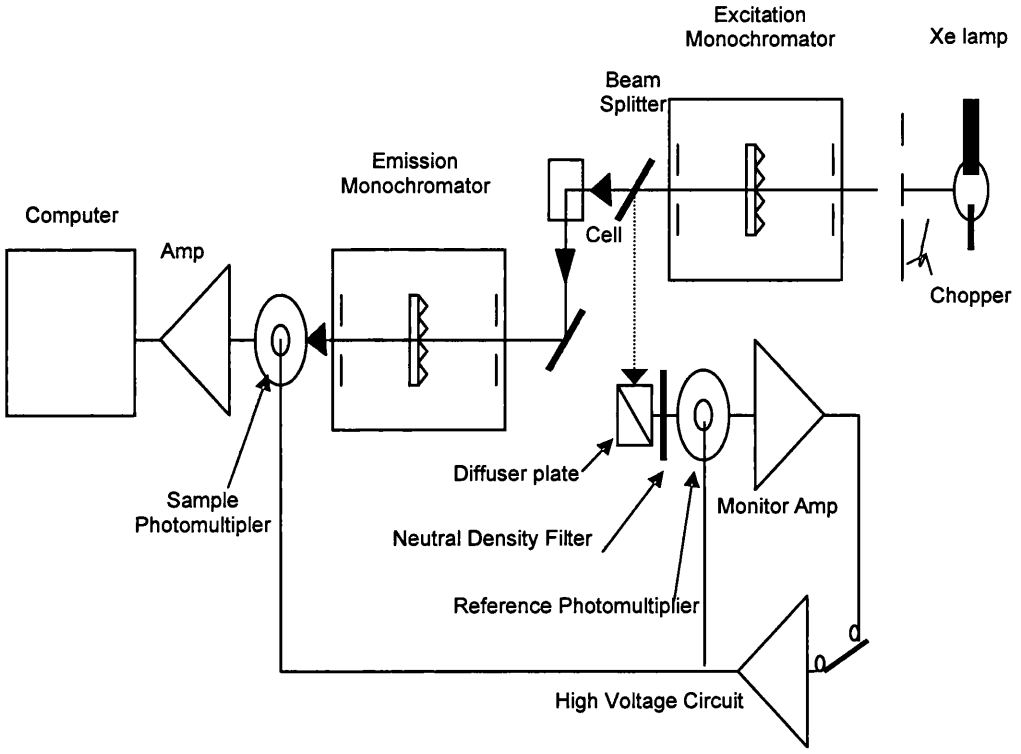

Fig.2.18. Schematic of the Perkin-Elmer MPF44-E fluorimeter

The emission spectra of samples in solution were recorded by placing the solution in a 1 cm^3 fluorescence cuvette and placing the cuvette in the sample holder supplied with the fluorimeter. However, in order to record the spectra of the luminescent

sensors a custom made sample holder had to be constructed; this is shown in fig.2.19. The sample holder was screwed to a brass plate and could be held in the sample compartment of the fluorimeter. The sample sensor is held at an angle of 24.5 ° to the excitation beam, which was discovered to be the optimum angle to obtain the maximum emission from the sensors.

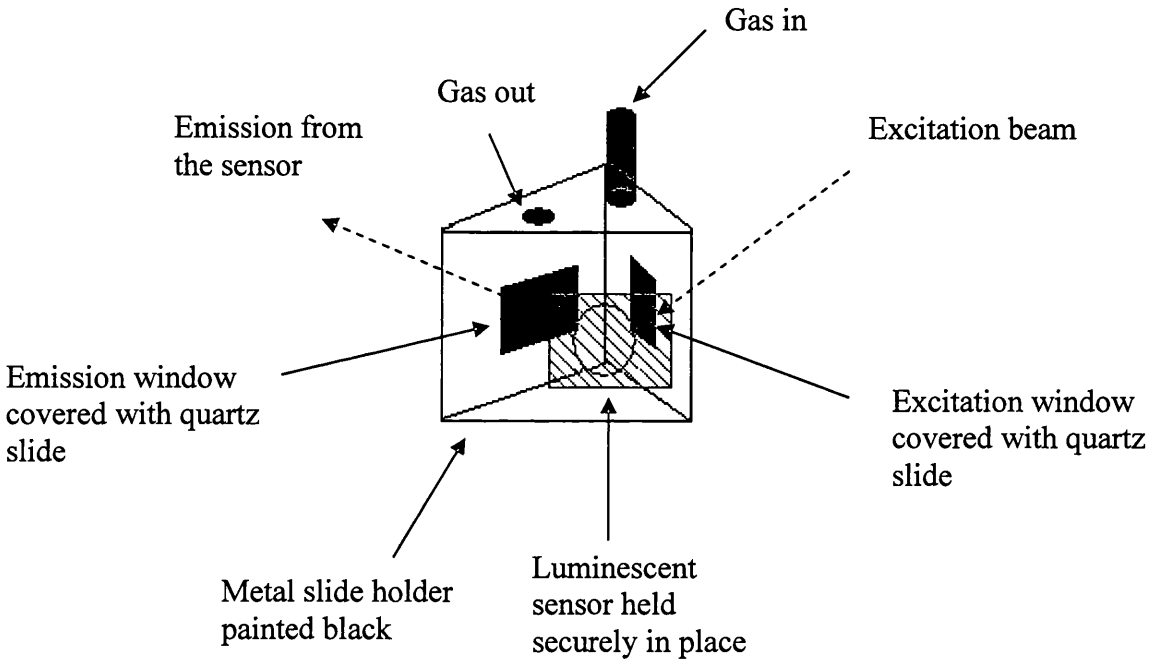

Fig.2.19. The configuration of the slide holder used for luminescent sensors, the path of the excitation and emission beams are shown with dashed arrows

2.7.1 Correction factors for colorimetric measurement

The emission spectra generated by the fluorimeter does not compensate for the sensitivity of the detector, and therefore it was necessary to measure the sensitivity of the instrument to calculate the CIE co-ordinates. Excitation spectra were corrected for the wavelength dependence of the intensity of the exciting light using methylene

blue and rhodamine B quantum counters in ethylene glycol using the method described by Demas and Crosby.[13] Emission spectra were corrected for the emission monochromators and the photomultiplier tube by calibrating the xenon lamp source for its spectral output using rhodamine B as a quantum counter and barium sulphate as a diffuse reflectance standard. The excitation monochromator is first scanned with the quantum counter in place to determine the relative photon output, $L(\lambda)$. The diffuse reflectance standard is then placed in the sample holder and the excitation and emission monochromators are then scanned in unison. The observed spectrum is described by $L(\lambda)\cdot S(\lambda)$, where $S(\lambda)$ is the sensitivity of the detection system and the required correction factor ($S(\lambda)$) is obtained by division of $L(\lambda)\cdot S(\lambda)$ by $L(\lambda)$. Correction factors were used to correct all emission spectra used to calculate CIE co-ordinates.

2.7.2 Wavelength calibration of the fluorimeter

The emission and excitation monochromators were calibrated as follows. The excitation monochromator was set to 0 nm therefore allowing all of the light from the arc lamp to pass through the excitation monchromator. The setting at which the light was brightest was set at 0 nm. Once this setting was found the emission monochromator could be calibrated by scattering the light from the excitation monochromator using 0.1 g of milk diluted with distilled water in a 1 cm^3 cuvette. The emission from the arc lamp was then used to calibrate the emission monochromator by matching it with the sharp emission line 468 nm (fig.2.20).

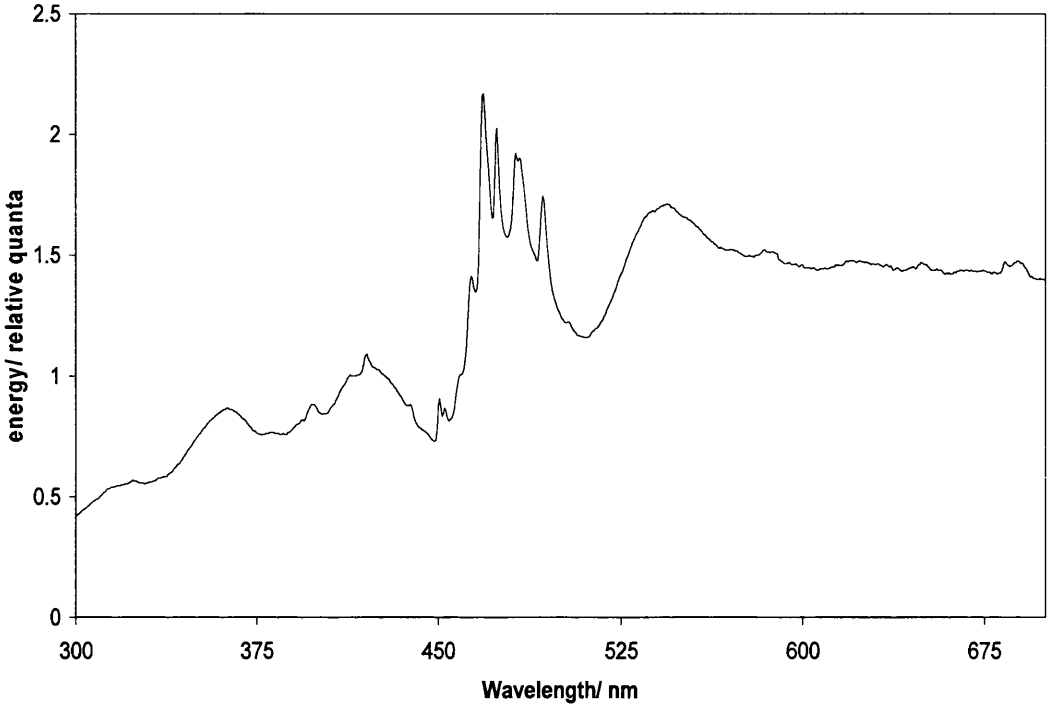

Fig.2.20. The emission spectrum for the 150w Xe arc lamp

2.7.3 CIE xy colour coordinates

The XYZ tristimulus values were calculated for emissive colour by taking the corrected emission spectra at 5 nm intervals using expression 2.3:

$$\left\{\begin{aligned} X &= \sum_{\lambda=380}^{700} \bar{x}_\lambda \cdot E_\lambda(\Delta\lambda) \\ Y &= \sum_{\lambda=380}^{700} \bar{y}_\lambda \cdot E_\lambda(\Delta\lambda) \\ Z &= \sum_{\lambda=380}^{700} \bar{z}_\lambda \cdot E_\lambda(\Delta\lambda) \end{aligned}\right\} \qquad [2.3]$$

where E_λ is the emission intensity and $\bar{x}_\lambda$, $\bar{y}_\lambda$ and $\bar{z}_\lambda$ are the corresponding colour-matching functions at each wavelength (the colour matching functions are described

in the introduction), λ. The XYZ tristimulus values were converted to corresponding *xy* colour coordinates using equations 2.4 and 2.5:

$$x = X/ (X+Y+Z) \qquad [2.4]$$

$$y = Y/(X+Y+Z) \qquad [2.5]$$

Non emissive colour spectra do not need any correction. The diffuse reflectance spectrum is then multiplied by the relative spectral power of the standard illuminant D^{65} (fig.1.9) at every 5 nm. The product of this can then be treated in the same way as the emissive colour.

2.8 Gas Mixing

Oxygen and nitrogen were mixed using an 852 V1-B gas blender from Signal Instruments Co. UK. The gas blender was calibrated using oxygen probe which was a Handy Polaris using the Henry's law (equation 2.6) to determine oxygen concentrations (fig. 2.21). For most applications the output from the gas blender was always checked against the probe. The probe was sensitive to ± 1.5 % saturation, and was internally temperature corrected.

$$P = Kc \qquad [2.6]$$

P = partial pressure, K = Henry's law constant, c = concentration [8]

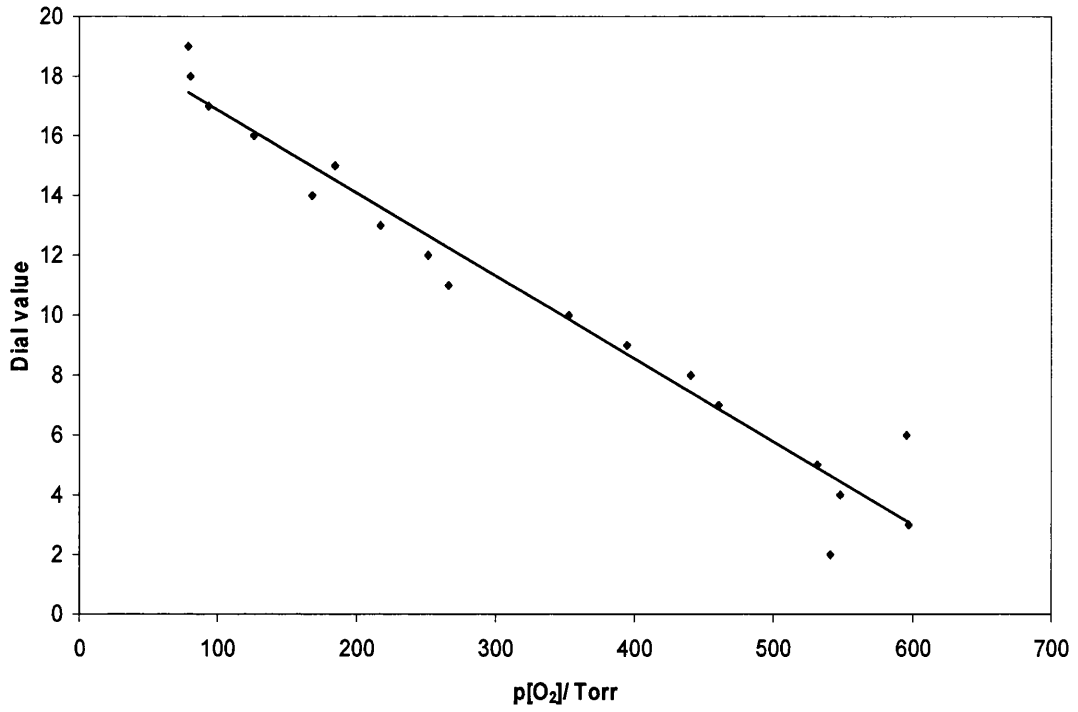

Fig.2.21. The partial pressures of oxygen in the oxygen: nitrogen gas mixtures produced by the gas blender, at the various dial values

2.9 Irradiation Suite

Irradiations were carried out using an irradiation suite comprising of a 150 W Hg arc lamp with a water filter and UV bandpass filter (fig.2.24). A Hg arc lamp was preferred to a Xe arc lamp, because it emits a higher UV content (fig.2.23). A water filter was used to remove the IR emission and prevent the bandpass filter from becoming too hot and cracking during irradiations. The UV bandpass filter (fig.2.24) allows the transmission of wavelengths from 300 nm to 400 nm. The total output was measured to be 2 mW/cm^2 using a light intensity meter, which was covered with a piece of card with a 1 cm^2 hole cut into it. The card was positioned in a variety of different positions so that an average power output could be obtained. The sample

holder was held 30 cm from the lamp, and could be removed from the irradiation suite and placed in the fluorimeter without disturbing the sample. Degradations were measured as a change in emission intensity as a function of time.

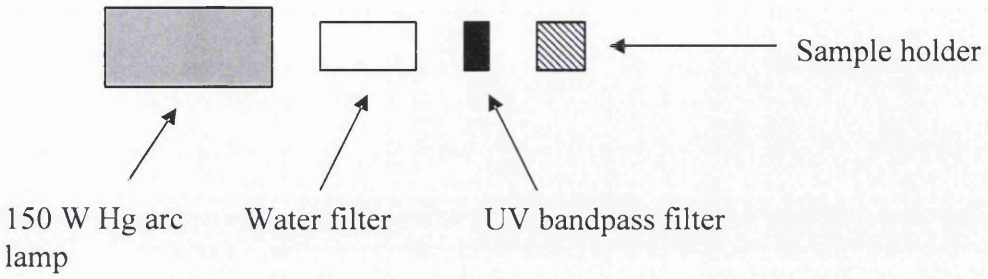

Fig.2.22. Schematic of the Irradiation suite

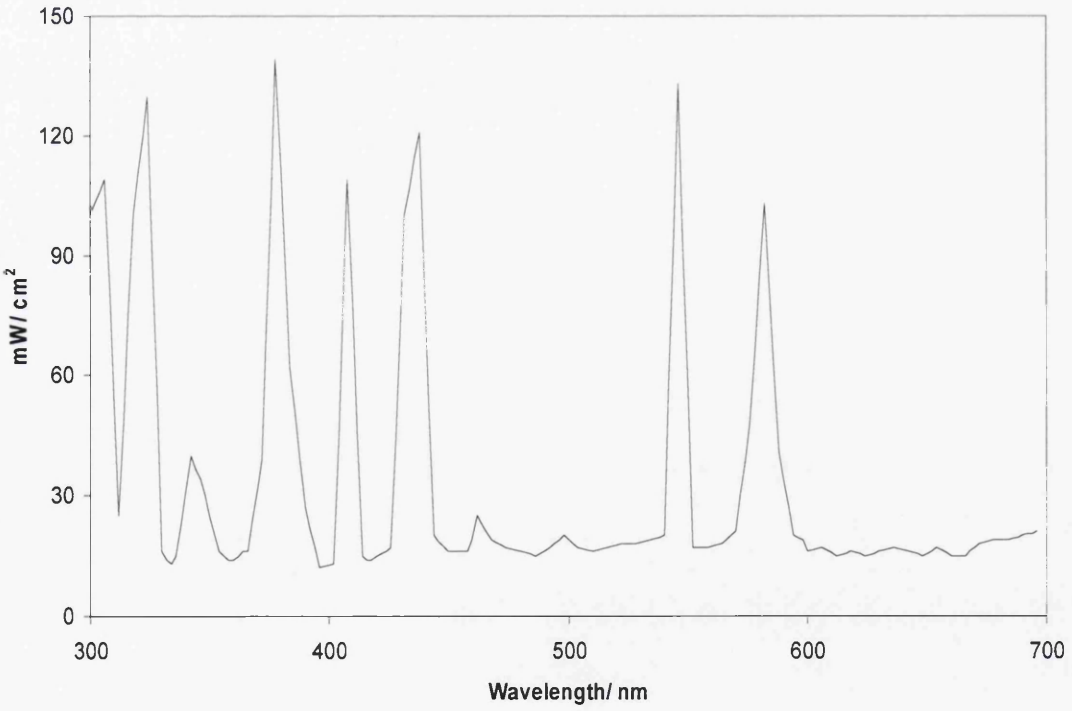

Fig.2.23. The spectral output from a 150 W Hg arc amp obtained from reference 14

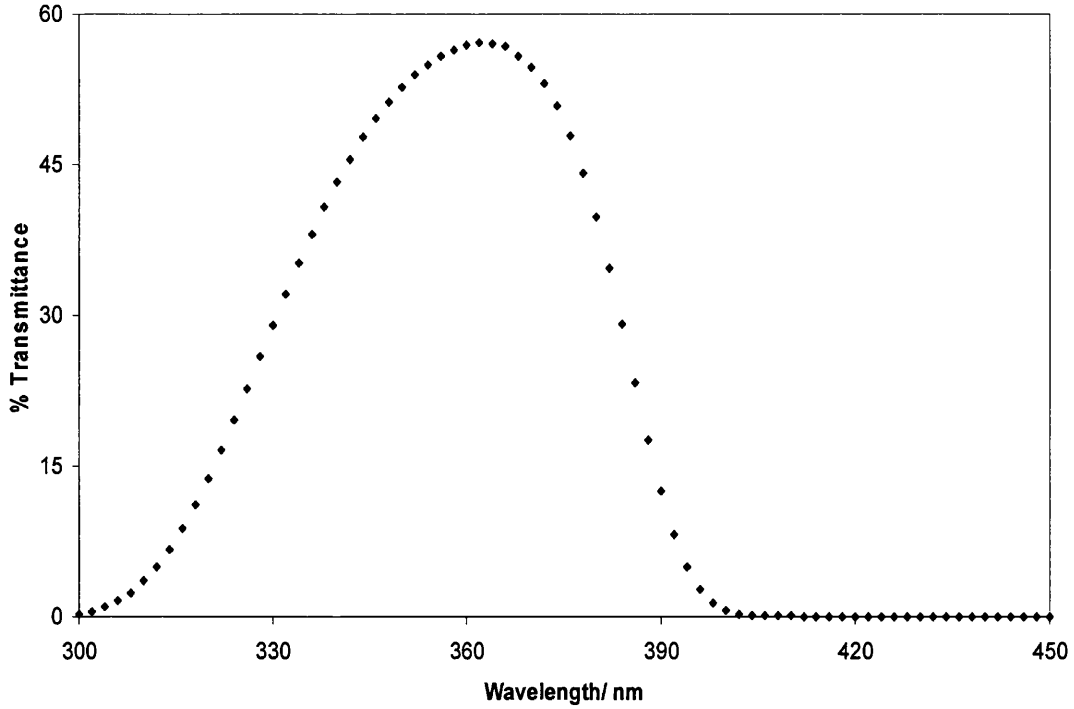

Fig.2.24. Transmission spectrum of the bandpass filter used in the irradiation suite

2.10 Lifetime measurements

Lifetime data was obtained by exciting samples with the third harmonic, 355 nm, pulse from a ns Nd/YAG laser. The emission data was recorded using an Applied Photophysics laser kinetic spectrometer, and a Lecroy oscilloscope before being transferred to a PC for data analysis. Curve fits for the data were obtained using the 2D curve fitting program by Jandel with least means squares optimisation.

Singlet exponential decays are usually only observed if emission is from a single emitting site. Both PtPYR and PtOEP can form aggregates which can lead to more complex decay kinetics.[3,15] The formation of aggregates is concentration dependent and can be monitored by the decay kinetics. It can be shown that at low

concentrations of approximately 1 x 10^{-6} mol dm^{-3} for both PtOEP (fig.2.25) and PtPYR virtually no aggregate is present and therefore equation. 2.7 can be used to obtained lifetime data.

A single exponential decay follows equation 2.7.

$$y = a + b \exp(-cx) \qquad [2.7]$$

where y is the emission intensity, x is time, a is a small zero offset fitting constant, b the amplitude of the exponential and c is the rate constant

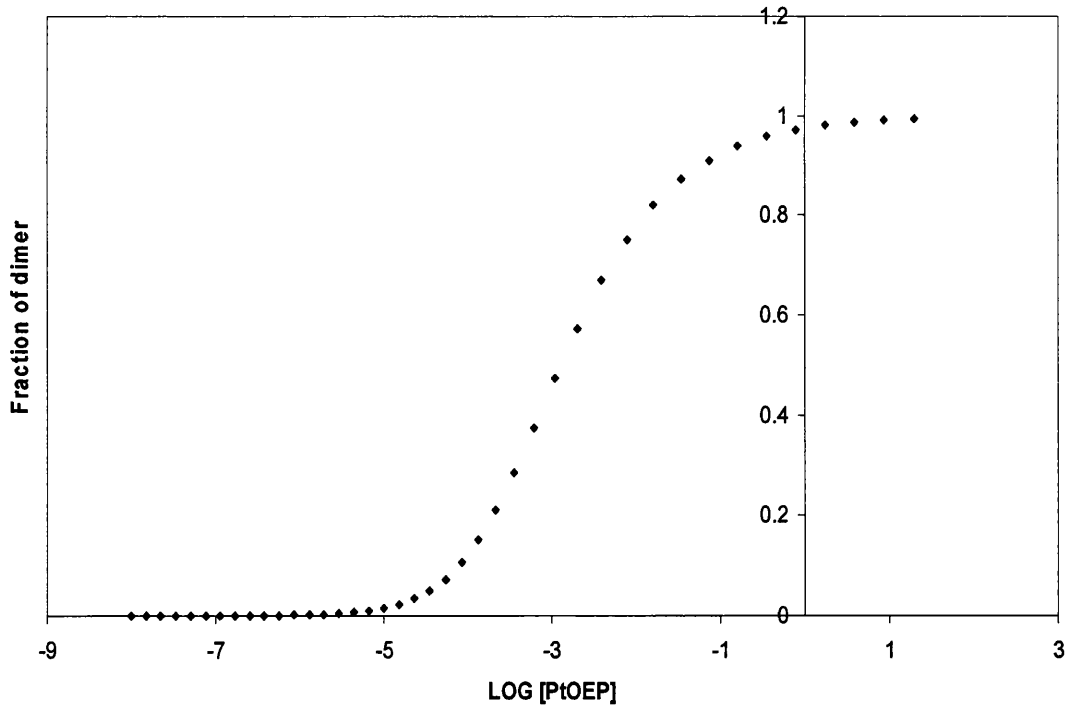

Fig.2.25. The fraction of dimer vs log [PtOEP] for PtOEP using equilibrium constant data from reference 15

2.10.1 Temperature effects on decay kinetics

Some temperature effects were observed when comparing recorded data to the literature values, which was attributed to the temperature dependence of k_{obs}. All decay kinetics in this thesis were recorded at a room temperature of ca. 287 K.

2.11 Errors and statistical handling of data

For straight line fits the lines of best fit were obtained from excel using the least means square approximation. All errors are given to 2 standard deviations unless stated otherwise. [16]

2.12 References

1) Massou, S.; Albigot, R.; Prats, M. *Biochem. Educ.,* 28, **2000,** 171-173.

2) Mills, A; Lepre, A. *Anal. Chem.,* 69, **1997,** 4653-4659.

3) Farley, S.J.; Rochester, D.L.; Thompson, A.L.; Howard, J.A.K.; Williams, J.A.G. *Inorg. Chem.,* 44, **2005**, 9690-9703.

4) Petracci, A.; Delfos, R.; Westerweel, J. 13th *Int. Symp. on Applications of Laser Techniques to Fluid Mechanics*, **2006,** paper 1221.

5) Gustavsson, V.; Cassara, L.; Gulbinas, V.; Gurzadyan, G.; Mialocq, J.C.; Pommeret, S.; Sorgius, M.; van der Meulen, P. *J. Phys. Chem. A,* 102, **1998,** 4229-4245.

6) Lewis, J.E.; Maroncelli, M. *Chem. Phys. Lett.,* 282, **1998,** 197-200.

7) Schulman, S.G.; Chen, S.; Bai, F.; Leiner, M.J.P.; Weis, L.; Wolfbeis, O.S. *Anal. Chim. Acta,* 304, **1995,** 165-170.

8) Barnadas-Rodriguez, R.; Estelrich, J. *Photochem. Photobiol. A,* 198, **2008,** 262-267.

9) Ertkin, K.; Klimant, I.; Neurauter, G.; Wolfbeis, O.S. *Talanta,* 59, **2003,** 261-267.

10) Bandrup, J.; Immergut, E.H.; Grulke, E.A. *Polymer Handbook, 4th ed.*, Wiley, (1999).

11) Atkins P.W. *Physical Chemsitry, 6th ed.,* Oxford, (2001).

12) Hunt, R.W.G. *Measuring Colour,* 3rd ed., Fountain Press, (1998).

13) Demas, J.N; Crosby, G.A., *J. Phys. Chem.,* 75, **1971,** 991-1024.

14) http://www.lot-oriel.com/site/site_down/ls_radiance_unken06.pdf

15) Hughs, V.E.; Douglas, P. *J. Fluoresce.,* 16, **2006,** 403-409.

16) Miller, J.C.; Miller, J.N. *Statistics for Analytical Chemistry, 3rd ed.,* Ellis Horwood Ltd, (1993).

Development and stabilisation of colorimetric dual lumophore oxygen sensors

3.1 Summary

This chapter investigates the technological difficulties associated with the development of luminescent dual lumophore oxygen sensors which give green-yellow-red "traffic light" responses to decreasing partial pressures of oxygen (described in chapter 1). A sensor designed for a specific application of these sensors, i.e. their use as an aid to preservation of artefacts in the British Museum stored under low oxygen environments such as a vacuum, is described; such a dual lumophore colorimetric sensor is an ideal indicator for any leak in the containment vessel.

Two main types of sensors are examined in this chapter: the first is based on the combination of rhodamine 110 with PtOEP which was chosen as the best candidate for the British Museum (referred to in the following discussion as BM sensors), and the second is based on PtPYR and PtOEP (referred to in the following discussion as PtPYR sensors). The use of different coating methods for the construction of these sensors has been examined i.e. spin coating, inkjet printing and Meyer bar coating. The photostability of the sensors was studied and photodegradation was observed in the PtPYR and PtOEP lumophores. The mechanism of photodegradation has been briefly studied, and it is thought to be most likely via singlet oxygen. A number of different additives and singlet oxygen quenchers were assessed as to their suitability

to stabilise the sensors. Ultimately placing DABCO in the PtOEP layer was found to stabilise both the PtPYR and BM sensors. The response of the sensors was also analysed and found to be very fast. Finally, methods of excitation for the sensors were considered and a hand held LED torch was developed for the easy excitation of the dual lumophore sensors.

3.2 Introduction

This chapter deals with the development of sensors which change colour in response to changing partial pressures of oxygen, such sensors are also discussed in chapters 1, 4 and 5.[1,2]

3.2.1 Principle of operation

The colorimetric sensors described in this chapter consist of two different lumophores with different emission wavelengths and excited state lifetimes. The emission from each lumophore is quenched by oxygen, as the partial pressure of oxygen increases, as described by the Stern-Volmer relationship eq. 3.1.

$$Io/I = \tau o/\tau = 1 + kq\tau o p O_2 \qquad [3.1]$$

Where Io and I are emission intensities in the absence and presence of oxygen at pO_2 respectively, τo and τ are the corresponding lifetimes, and kq is the bimolecular quenching rate constant for oxygen quenching. The Stern-Volmer plot of Io/I, or $\tau o/\tau$, against pO_2 has a slope of $kq\tau o$, which is often referred to as the Stern-Volmer

constant K_{sv}.[2] Generally the longer the lifetime the more sensitive the lumophore is to quenching by oxygen.[3-5]

Each lumophore is encapsulated in a polymer matrix[6]. The polymer matrices used possess different permeabilities to oxygen and sometimes different optical characteristics.[7] Each lumophore layer is laid down on a glass substrate, generally with the most sensitive lumophore as the upper layer (fig.3.1).

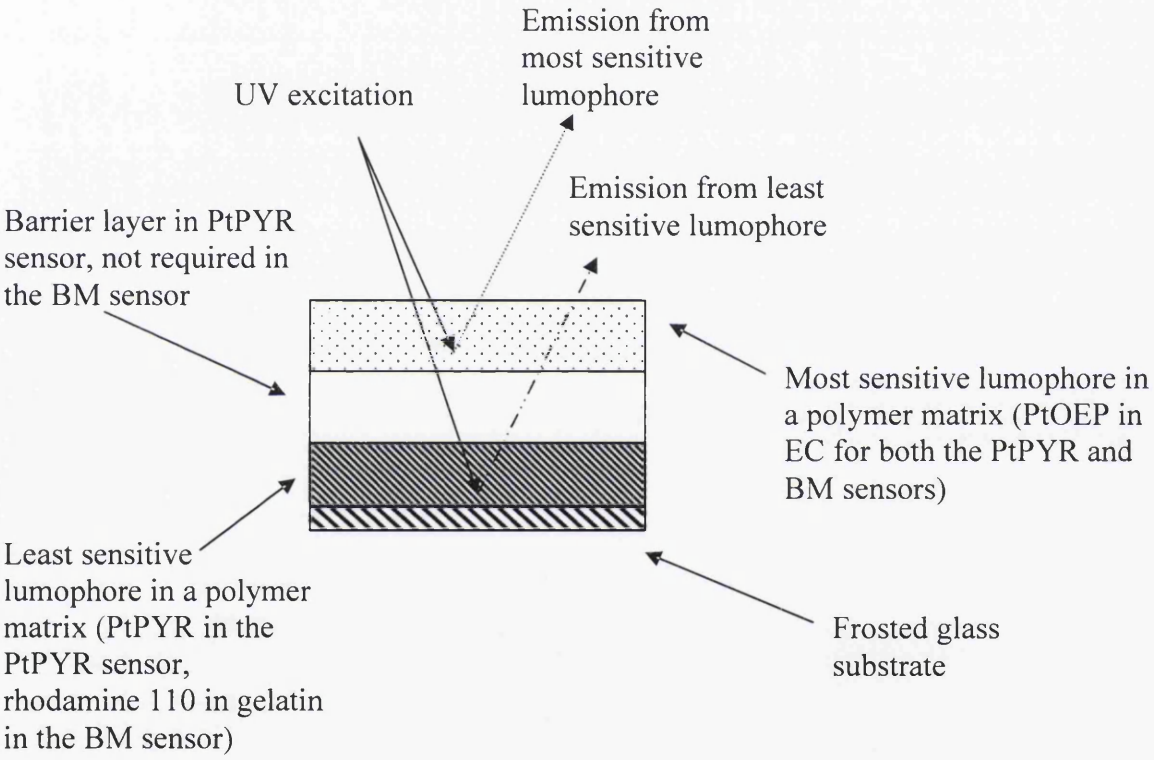

Fig.3.1. The construction of a typical dual lumophore colorimetric oxygen sensor

A colour change is effected because the lumophores have different sensitivies to oxygen, for example if we consider the sensor using a combination of the red emitting PtOEP ($\tau_0 = 0.091$ ms)[7] and green emitting PtPYR ($\tau_0 = 9.2$ μs) [8] (fig.3.1). In the absence of oxygen neither lumophore will be quenched and both emission

intensities are at maximum. The sensor is constructed so that the most sensitive lumophore, in this case PtOEP is the most intense emitter in the absence of oxygen, much more intense than the less sensitive lumophore, PtPYR. Therefore, under nitrogen, emission from PtOEP predominates and the sensor appears red. As the partial pressure of oxygen increases emission from PtOEP is quenched much more effectively than that from PtPYR, and therefore the emission colour from PtPYR becomes more apparent, and a colour change is seen, from red through to firstly yellow, and then finally green as PtOEP emission is completely quenched. Such a red-yellow-green traffic light response (fig.3.2) is the most desirable colour change, because the human eye can easily separate the various colours.[9]

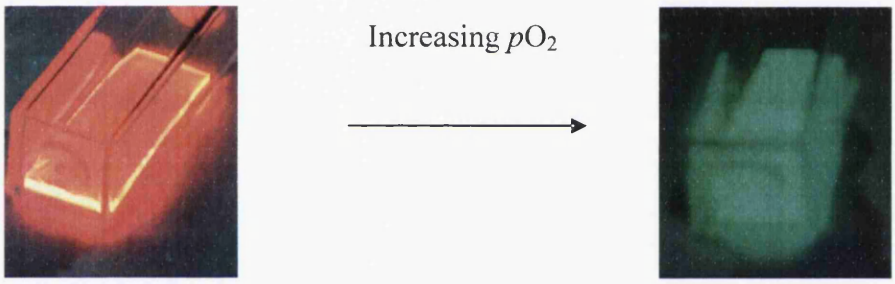

Fig.3.2. Changes in emission colour of a PtPYR based sensors under O_2 (right) and N_2 (left)

3.2.2 A sensor for monitoring oxygen pressure in artefact preservation

Following the initial work on colorimetric oxygen sensors in the group[3,10] contact was made with the science division of the British Museum who were interested in a simple device to monitor oxygen pressures in containers for artefacts. In the work presented here we have taken this to proof of principle stage with the design of both a colorimetric sensor and an associated hand held illumination torch. These British

Museum (BM) sensors have been designed for a specific purpose. They are designed to be placed inside transparent cases with artefacts inside. In order to preserve artefacts, particularly iron and organic artefacts, they are kept under vacuum or low oxygen environments to prevent chemical degradation, decomposition by bacteria, fungus and air pollutants. Notable examples of artefacts conserved using this method are the royal mummies of Egypt and the original documents of the constitution of India.[11-13] This low pressure environment means that there is a low partial pressure of oxygen and therefore it is possible to use oxygen sensitive lumophores to monitor changes in the pressure. Under vacuum, the sensor will appear red when illuminated with UV light, however if a leak occurs there will be a rise in partial pressure of oxygen and the sensor will change colour to green under UV light, thus making any leak very easy to detect.

The advantages of this approach to more traditional approaches are that the sealing of the container does not have to be breeched and no power need be supplied to the sensor device, as would be required with traditional methods such a Clark electrode, and it is much cheaper than a pressure meter. It is also very easy to use, and requires no additional scientific training.[10] While this chapter is mainly concerned with the development of sensors for the preservation of museum artefacts these types of sensors can be applied to a wide variety of areas, notably modified atmosphere packaging[14] and pressure sensitive paints[15-17] as described in chapter 4.

In this chapter the critical choices for the various parts of the sensors are discussed; the effects of using different lumophore systems, different polymer matrices, and also the method of illumination used are examined. The stability of the lumophore

systems are examined in detail. The thermal, chemical and photochemical stability of the lumophore is critical in that they must be stable for as long a time as is possibly.[18,19] If the lumophores degrade this will substantially alter the colour change of the sensor and render it useless. Since their mode of operation requires use of UV excitation, the generation of long lived excited states, and the generation of singlet oxygen in the oxygen quenching process, photochemical stability is particularly important, and various stabilisers have been examined in ways to improve photochemical stability.

3.3 Methods and Materials

3.3.1 Materials

Rhodamine 110, 5,(6)-carboxy fluorescein, ethyl cellulose (46% ethyloxy content) (EC), gelatin, diazobicyclo[2.2.2]octane (DABCO), vitamin E (VIT E), butylatedhydroxytoluene (BHT), and tris(2,4-ditert-butylphenyl)phosphate (TBPP) were all purchased from Aldrich Chemicals and used as supplied (fig.3.3). PtOEP was obtained from Frontier Scientific. Optical filters were obtained from Schott optical filters. Silicon rubber RTV 118 was from Techsil Ltd. UV LEDs were purchased from Roitner Laser Technik. Platinum(II) N^C^N 1,3,6-tri-(2-pyridyl)benzene (PtPYR) was a gift from Gareth Williams, Durham University, and nickel (II) N-phenyl dithiocarbamate (NPD) was synthesised according to a literature method (fig.3.3).[20]

3.3.2 Methods

BM low pressure sensors were made by spin coating solutions of sensors, polymers and other components at 1500 rpm. The first layer was spin coated from a solution made up of 0.4 ml of rhodamine 110 in methanol (1 mg to 1 ml methanol) and 1 g of 10 % gelatin in water (w:v). This rhodamine 110 layer was repeatedly coated between three and five times to investigate the effect this had on the colour change of the sensor, thereby making three different sensors with differing numbers of rhodamine 110 layers. On top of this layer a PtOEP layer was spin coated from a solution made up of 0.2 ml PtOEP in THF (0.74 mg PtOEP to 1 ml THF) and 1 g of 10 % ethyl cellulose 80:20 toluene:ethanol (w:v). This layer was identical for each of the sensors. It was determined that it was not necessary to incorporate a barrier layer into this sensor.

PtPYR sensors were made by spin coating a layer from a solution made up of 0.4 ml PtPYR in THF (1 mg to 1 ml THF) and 1 g of 10 % EC 80:20 toluene:ethanol (w:v) spin coated onto a frosted glass substrate at 700 rpm. On top of this a barrier layer of 10 % gelatin in water (w:v) at 50 °C was spin coated at 700 rpm. Finally a PtOEP layer was spin coated over the barrier layer at 1250 rpm using a solution made up of 0.4 ml of PtOEP in THF (135 mg to 10 ml THF) and 1 g of 10 % ethyl cellulose 80:20 toluene:ethanol (w:v). Stabilising additives were dissolved in the appropriate solutions just before they were spin coated.

Absorption spectra were recorded on a Hewlett Packard 825A diode array spectrometer.

Inkjet printing was performed on a dimatrix x-y inkjet printer where prepared solutions could be placed into separate inkjet cartridges and inkjet printed.

Emission spectra and the colorimetric measurements were obtained using a Perkin Elmer MPF 44-E fluorimeter with a 150 W Xe arc lamp. For emission spectra obtained directly from the BM sensor/torch combination, and subsequent CIE co ordinates, excitation was from the head of the torch (described in the illumination section 3.6) taped securely to the side of a custom built holder for the sensor shown in chapter 2. The emission correction factors for the fluorimeter were obtained using the method of Demas and Crosby as described in the experimental section.[21] CIE colour coordinates were calculated using the colour matching functions given in reference 9.[21]

Degradations were performed by using the degradation suite described in chapter 2, and the emission spectra were recorded using the fluorimeter under air.

Sensor response times were recorded by attaching a water suction pump to the sensor holder and allowing the sensor to reach equilibrium, and then releasing the vacuum. The change was monitored on the fluorimeter at an emission wavelength of 645 nm.

Time resolved (ns) laser studies were made using a Nd/YAG spectron laser with an applied photophysics laser kinetic spectrometer. The third harmonic pulse (355 nm) was used for excitation and the average trace from 32 kinetic decays was collected on a Lecroy 9504 AM quad 200 MHZ oscilloscope and transferred to PC for analysis. Analysis was performed using the 2D curve fitting program by JANDEL.

The data for PtOEP was obtained from PtPYR sensors containing low concentrations of the lumophores under nitrogen which generate decay curves which fit well to a single exponential decay. At high concentrations aggregation products are formed which produce double exponential decays.[22] The concentration of dye solutions used were: 0.1 mg lumophore to 1 ml of THF for both layers (this concentration was used for the sensors used in lifetime studies only to produce single exponential decays), and the dye/polymer solutions for spin coating were the prepared as previously described when required stabiliser (fig.3.3) was also added to solutions prior to spin coating. The amount of each stabiliser added is shown in table 3.3.

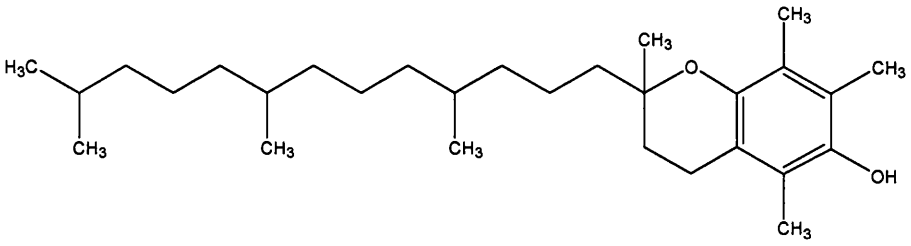

Vitamin E

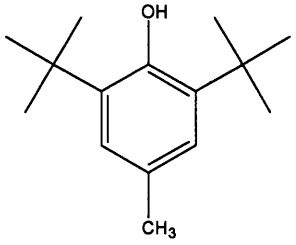

BHT

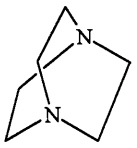

DABCO

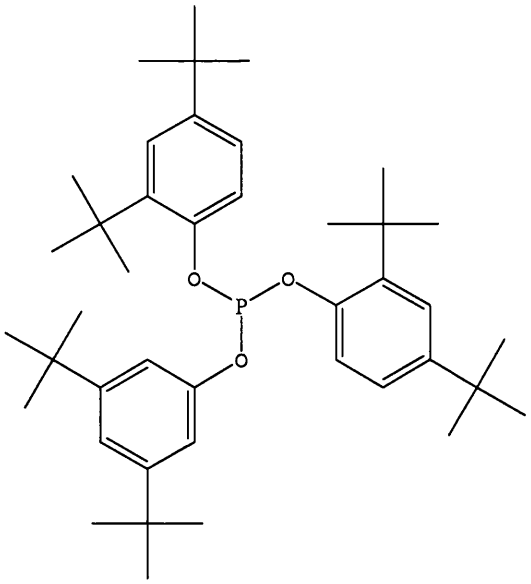

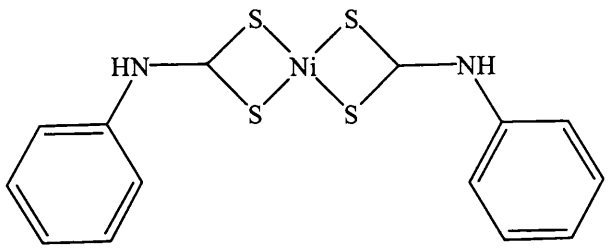

TBPP NPD

Fig.3.3. The structures of the additives examined as possible photostabilisers

Decay curves in solution were obtained under nitrogen using a concentration of 1.78×10^{-5} mol dm^{-3} PtPYR in THF. Small quantities of solutions of known concentrations of the different additives in THF were then added to this solution and the decay curves were recorded after each addition, therefore allowing the bimolecular rate constants to be calculated. The addition of the additives each time slightly increased the volume in the cuvette, so excess solvent was allowed to evaporate to the initial volume before the data was collected.

3.3.3 Spin coating

Traditionally luminescent oxygen sensors have been made by depositing the sensor layers from a spin coated solution onto a substrate, typically glass.[23, 3] The substrate is held securely on a rotating central column, and the sensor solution is placed on the substrate. The substrate is then spun at high speeds typically around 1500 rpm and the solution is coated in a continuous uniform layer by centrepedial acceleration, and

evaporation of the solvent leaves a dry film. The thickness of the layer can be controlled by a number of factors; such as the viscosity of the solution, and spin speed. The higher the viscosity the thicker the film produced. However, if the solution viscosity is too high the film will not cover the substrate uniformly, and if it is too low the film will break resulting in a patchy covering of the substrate.[24]

Both the speed and the length of time the substrate is spun for can be altered during the coating process. A high spin speed over a long period will produce a thinner film but a more uniform coating, while a slower speed produces a thicker coating. In the preparation of all of the different sensor layers a two stage spin process was used. The duration of the first stage was fixed at 20 s duration, but different spin speeds were examined, while for the second stage the duration was 25 s, at 285 rpm. The second stage was kept constant for all sensor layers. All spin coating was carried out at room temperature.

3.3.4 *Inkjet printing of dual lumophore sensors*

Inkjet printing was explored as a possible way of producing the dual lumophore sensors since there are a number of examples in the literature where this process has been used for the printing of polymers and sensors.[25-28] Inkjet printing works by having a low viscosity ink, typically 20 mPas,[29] in a nozzle that has a high enough surface tension so the ink is not ejected from the nozzle spontaneously. Ink ejection, and hence printing, occurs when the ink is ejected from the nozzle by a crystal that expands when an electric current is applied to it due to the pizo-electric effect. This is known as "drop on demand" printing, and it was this type that was used for printing of the sensors.[30]

Different formulations of inks were used. The first inks used polystyrene in toluene for the polymer matrix. Polystyrene was chosen as the first polymer matrix to be used for the sensor because it has been shown that it can be inkjet printed and used as a matrix for oxygen sensors.[6,30] A 2 % polymer solution was used initially [30] However this had to be diluted in a 6:1 ratio with toluene before the solution became printable on the dimatrix printer. Each lumophore was loaded into a separate cartridge. The coumarin 153 formulation was printed first, followed by PtOEP as only one cartridge could be printed at a time. However, for both layers it was found that it was necessary to print each layer up to ca 20 times to gain a sensor that could be easily viewed (fig.3.4).

The second inks which were tried used higher concentrations of lumophores with EC as polymer matrix since EC has higher oxygen permeability than polystyrene.[7] The use of higher concentrations of lumophores meant that fewer coatings were required to produce visible emission: ten layers for the coumarin 153 lumophore and six for the PtOEP lumophore gave a sensor where colour changes could be observed. The solvent for the ink was a 50:50 (v/v) mixture of γ butyrol lactone: toluene. γ butyrol was suggested as a possible solvent for inkjet printing of ethyl cellulose in reference 31. A mixture was required because EC has low solubility in γ butyrol lactone. The best inks for printing were obtained by adding either 0.4 ml of coumarin in THF (1 mg coumarin 153 to 1ml THF) or 0.4 ml of PtOEP in THF (1.35 mg PtOEP to 1 ml THF) to 1 g of 0.286% EC in 50:50 toluene: γ butyrol lactone (v/v).

Unfortunately inkjet printing was never found to be successful. Ultimately the problem is that the polymers required for the sensor are not ideal for printing,

because they are too viscous and have too high surface tensions. Although their have been reports of 2 % polymer solutions being inkjet printed[30] this could never be achieved with the apparatus available for this project. Therefore low polymer concentrations had to be used. This caused problems in drying the large amounts of excess solvent which need to be evaporated, and also because of the need for numerous layers before an adequate sensor colour could be obtained.

One solution to this problem would be to use a monomer that could be printed and then polymerised on the substrates such as a sol gel [32]. Although this may allow the printing of single layers that would be visible, inkjet printing is slow compared to other printing systems such as screen printing. Because of the problems with inkjet printing it was decided to examine the Meyer bar method of printing.

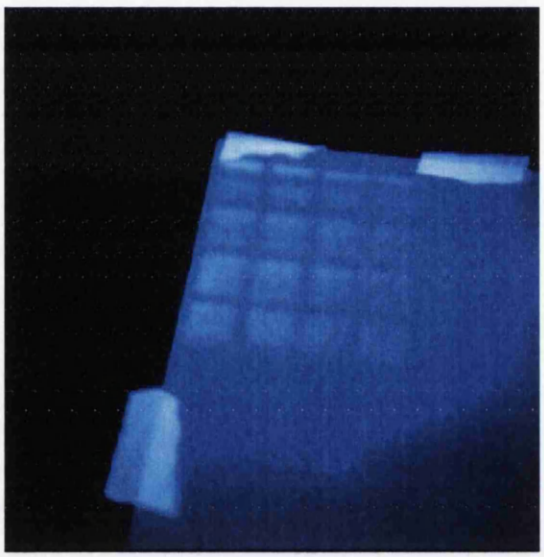

Fig.3.4. Photograph of a dual lumophore inkjet printed sensor on paper, in air therefore only the green/blue emission is visible. The two lumophores are coumarin 153 and PtOEP, both in polystyrene matrices. The dominant blue colour is produced from the optical brightener present in the paper substrate.

3.3.4 Meyer bar coating

The Meyer bar coating technique[23] is also known as a smoothing bar[33] method of printing. In this process the sensor solution is first pipetted onto a substrate, and then the Meyer bar is passed over the solution on the substrate pushing the solution in front of it and coating the substrate. The Meyer bar is a stainless steel bar with thin wire wrapped around it, (fig.3.5). The wire wrapped around the bar is graded and can be changed, generally the higher the grading the thicker the wire and the thicker the coating.

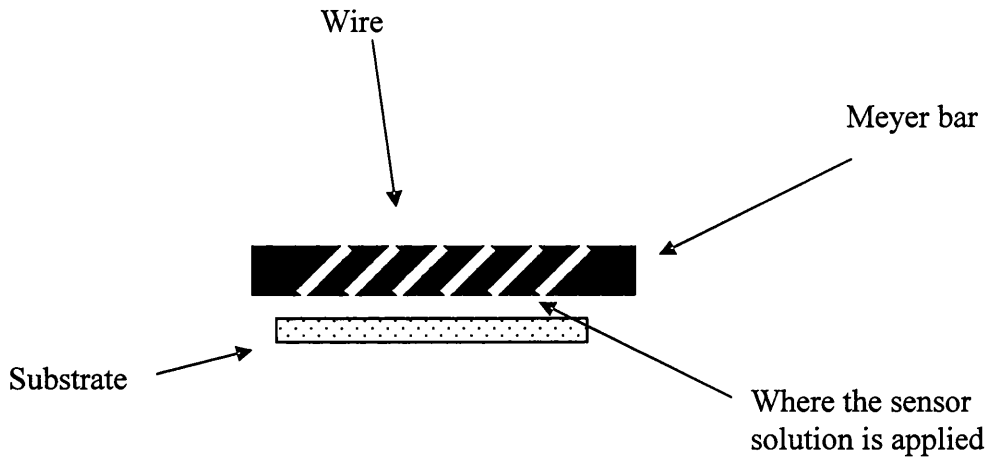

Fig.3.5. Schematic of the Meyer bar coating apparatus

The advantages of Meyer bar coating is that the same sensor solutions as used for spin coating can also be used with this technique. The results collected in table 3.1, whereby single layers of POEP in EC were coated, demonstrates that it is possible to make single layers of approximately 20 microns in thickness using Meyer bar coating, which is thicker than any of the other techniques examined. The drawbacks of this technique are that, once again, stripping out, where the applications of subsequent layers leads to the removal of lumophore from the lower layers, could be

observed (exp.6 in tab.3.1), and it was not possible to coat gelatin easily by this method. This method was not further investigated because it did not seem to have many advantages over spin coating.

Coating	Speed of bar (m/min)	Solution	Gauge of bar (USD)	Slide thickness (Microns)
1	1	1	3	1.5
2	1	2	3	1.6
3	1	2	1	2.5
4	1	2	0	22.5
5	1	1	0	18.9
6	1	1 + 2	0	17.1

Table.3.1. Table of coating experiments for PtOEP in EC using the Meyer bar apparatus (Solution 1 = the ethyl cellulose solution described in the experimental, solution 2 = the ethyl cellulose solution described in the experimental but using 12.5% EC instead of 10%). Grade 0 was the thickest gauge of wire used.

3.3.6 Substrates

When coating or printing these sensors the choice of substrate becomes critical because it can have a profound effect on the emission from the sensors. A significant problem with using ordinary printing paper as a substrate arises because optical brighteners are often added to make the paper appear "blue whiter". The addition of optical brighteners produces blue emission under UV light, which can mix with the emission from the lumophore resulting in a different hue to the one required e.g. the red emission from PtOEP appears purple on a substrate with optical brighteners. A

simple way of preventing this is to coat a new layer over the paper containing a UV absorbing non luminescent substrate. For the inkjet printing of sensors this was solved by dip coating strips of paper in solution of ethyl cellulose containing a TiO_2 based paint pigment.

Another important property of the substrate is the ability to scatter light, and the effect that the scattering has on emission from the sensor layer that is above it. If the substrate is transparent then all but a small part of the excitation light and emitted light reflected at the sensor film/substrate interface passes straight through the substrate. If the substrate scatters the excitation beam and there is an air gap between the sensor membrane and the substrate, then the effect is such that the excitation beam will be reflected; therefore the sensor layer is excited twice and also some of the lumophore emission emitted in the backwards direction is scattered into the forward direction; both effects increase the intensity of the forward emission. However if the sensor layer is coated directly onto a scattering substrate the excitation beam is scattered by the substrate directly into the sensor membrane, thus increasing the excitation substantially and therefore the emission intensity is significantly increased (fig.3.6).[9] For this reason both the BM sensors and the PtPYR sensors are spin coated on frosted glass substrates. (It was found to be difficult to spin coat on paper due to the lack of rigidity of the paper).

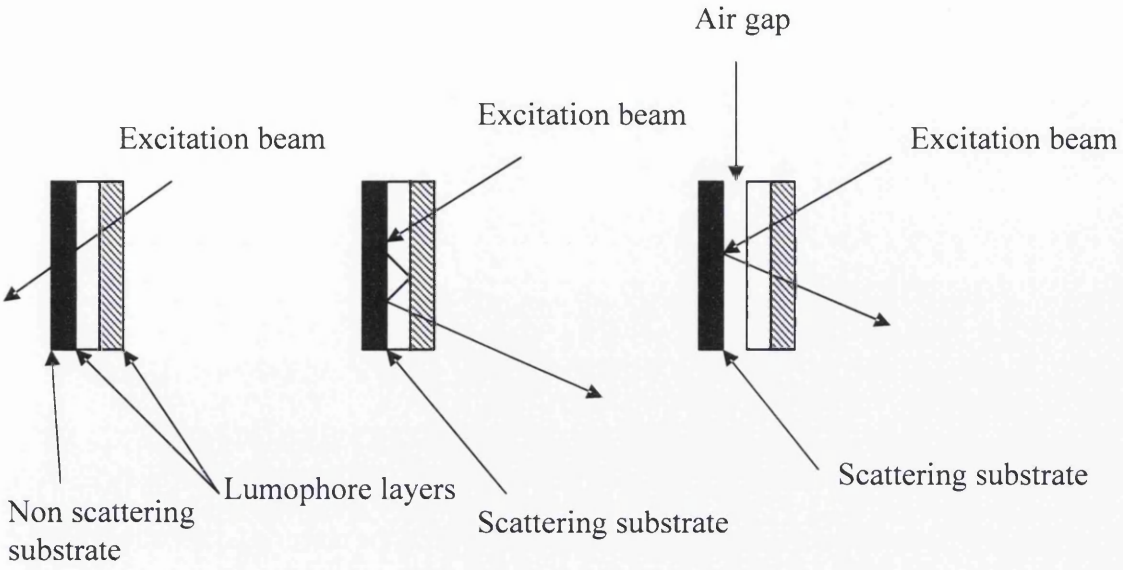

Fig.3.6. The effects of using a non scattering (left), scattering substrate (middle) and a scattering substrate with an air gap (right) on the excitation beam

3.4 Choice of Lumophores

The choice of lumophore and matrix give the sensor its response characteristics. The types of lumophore chosen can alter the colour change and sensitivity, while the choice of matrix affects the response and optical properties of the sensors.

The BM sensor was designed so as to give an easily seen colour change at low partial pressures. As previously discussed the easiest colour change for most people to observe is the "traffic light" red-yellow-green colour change, therefore a green and a red lumophore were required.[3] The lumophores must also be capable of excitation using UV light since any visible light will affect the colour change, and excitation by IR is not possible due to the relative photon energies. Both lumophores need to be

able to absorb across the same excitation band as only one excitation source is used to excite both lumophores in the sensor.[4]

As with previous sensors the oxygen sensitive lumophore used in the BM sensor was PtOEP. This has a sufficiently long lived triplet state to be readily quenched by molecular oxygen, a high quantum yield, good stability, and the desired "cherry red" emission colour (fig.3.2).[4] The palladium analogue was also tried as the red lumophore because it also has a good red colour and, because of a significantly longer lifetime (PtOEP τ_0 = 0.091 ms, PdOEP τ_0 = 0.99 ms),[34] it is more readily quenched by oxygen than PtOEP in the same polymer matrix. However the quantum yield for PdOEP is only 0.2, compared to 0.5 for PtOEP, and this gives a poor emission intensity.[35] Therefore PtOEP was chosen for the red lumophore.

To produce a colour change at the lowest partial pressure, the most desirable green lumophore is one that is insensitive to quenching by oxygen. PtPYR was used in the first dual lumophore sensor, however it is not the best choice because the emission lifetime (τ_0 = 9.2 μs) is long enough for it to be quenched at moderate/high oxygen pressures.[8], and, an important practical consideration, is that it is not a commercially available dye.

Coumarin 153 was used to provide green emission for inkjet printing, however this is quite a blue green and in combination with PtOEP yields a green-pink-red colour change, which is not ideal (fig.3.4).

Two suitable candidates were found for the green lumophore of the BM sensor: 5-(6)- carboxfluorescein and rhodamine110. In both cases emission is fluorescence, and thus emission intensity is not sensitive to changes in oxygen partial pressure up to a few atmospheres. Both can be excited by UV light at around 382 nm. Both are reasonably chemically and photochemically stable, and no degradation in emission intensity was observed for either lumophore. Ultimately rhodamine 110 was chosen because it has a higher absorbance at 382 nm which is the wavelength that is used to excite PtOEP.

3.5 Choice of matrix

The choice of matrix is almost as important in determining the response characteristics as the choice of lumophore. The oxygen permeability and diffusion coefficient of the matrix affect the speed of response and the sensitivity of the sensor.[34,36]

One of the first polymer matrices chosen for use in oxygen sensors was polystyrene which has a high refractive index and which has moderate permeability to oxygen. Later examples have tended to use ethyl cellulose because it has higher oxygen permeability and also a high refractive index. In turn EC is not as permeable as many of the silicon rubber matrices. The first BM sensors were made using a silicon rubber, RTV 118, chosen because of its high oxygen permeability,[37,7] and this gave a good colour change initially. However once the silicone matrix dried the sensor response times became very long, and the colour change was no longer observed. An additional problem was that RTV 118 contains a white pigment which makes the

polymer translucent. Therefore work with RTV 118 was abandoned and EC was used for all subsequent sensors as the preferred polymer matrix for the oxygen sensitive lumophore.

EC could not be used for the green lumophore layer because rhodamine 110 is not soluble in a solvent that could expand the EC polymer and thus dissolve it. Gelatin was used instead, however a single spin coated layer of aqueous gelatin was insufficient to produce an intense green colour, and therefore multiple layers were spin coated on top of each other. No stripping out of the lumophore from the lower layer was observed during spin coating numerous layers (fig.3.9).

Barrier layers were found to be required for the PtPYR sensor because the application of the upper layer of EC containing PtOEP was shown to remove some of the PtPYR from the lower layer (fig.3.7). The application of a gelatin interlayer prevents this from occurring (fig.3.8). For the BM sensor no stripping of lower layers was observed upon the addition of subsequent layers, because the lower gelatin layer is insoluble in the solvents used for the subsequent layer (fig.3.9).

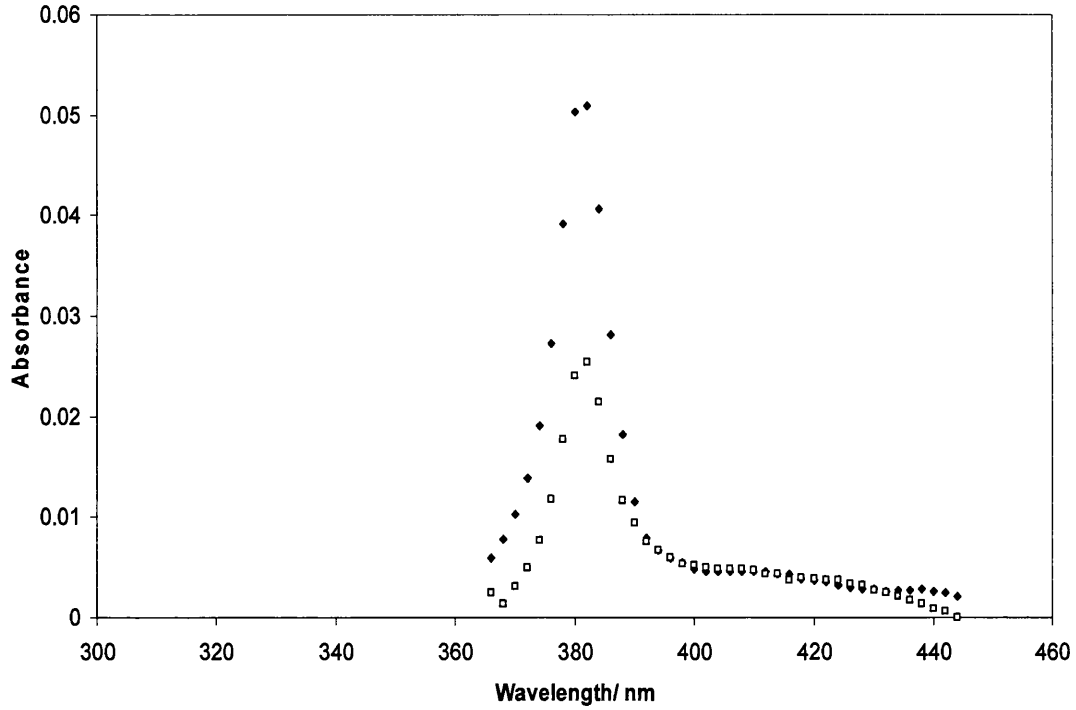

Fig. 3.7. Absorption spectra of lumophore layers in a dual lumophore sensor after they have been spin coated, 1st layer is PtOEP in EC (closed squares, absorbance at 382 nm = 0.05), 2nd layer is coumarin 153 in EC (open squares, absorbance at 382 nm = 0.05), demonstrating the loss lumophore from the 1st layer due to spin coating

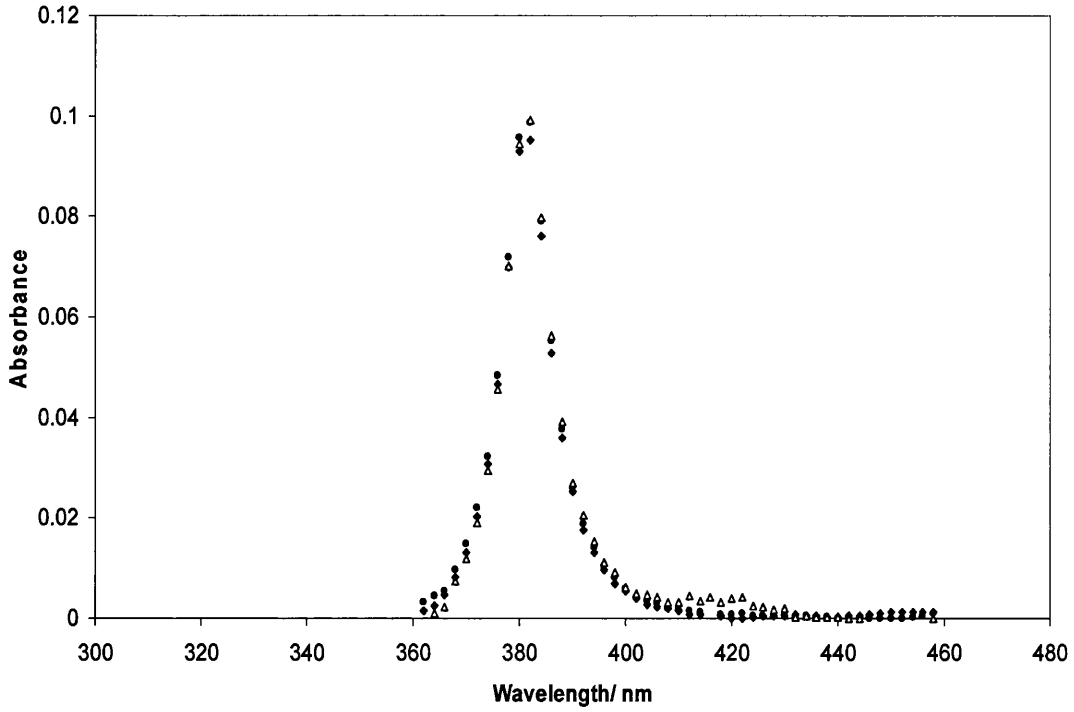

Fig.3.8. Absorption spectra during the building up of a dual lumophore sensor with a barrier layer; 1st layer is PtOEP in EC (diamonds), then a 2nd gelatin barrier layer is over coated to give the spectrum shown by circles, and then the 3rd coumarin 153 in EC layer is added to give the final spectrum shown by triangles. The fact that the PtOEP absorption band at 382 nm is not reduces as subsequent layers are coated over it demonstrates the effectiveness of the gelatin barrier layer.

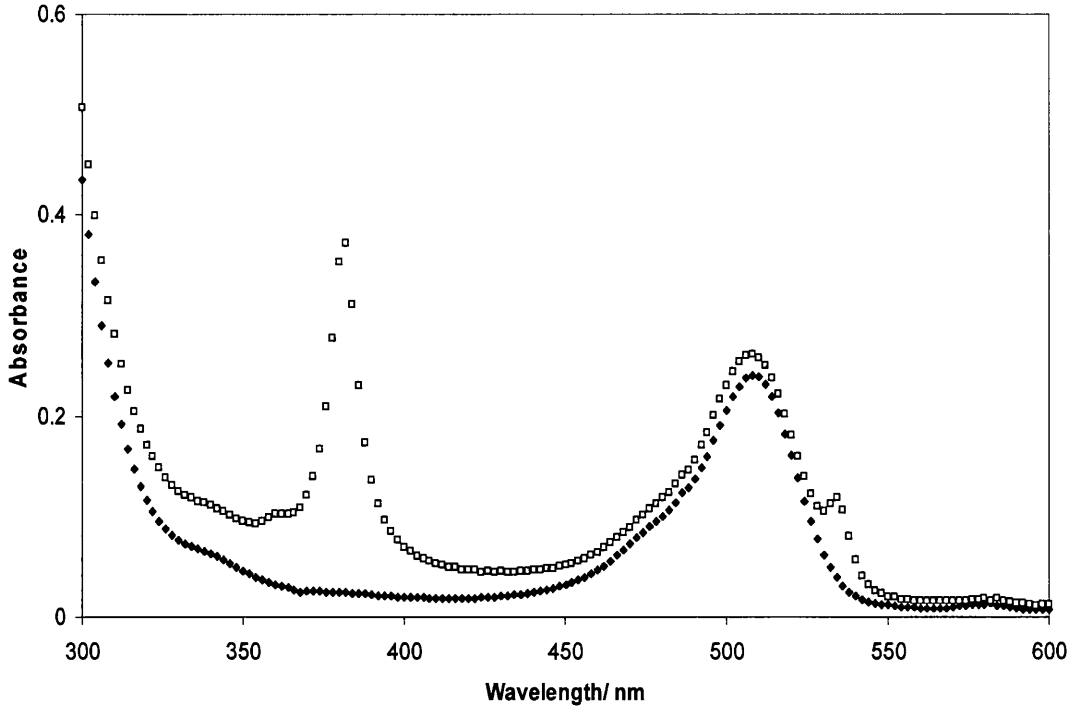

Fig.3.9. Absorption spectra showing the build up of the BM sensor: the 1st layer is rhodamine 110 in gelatin (diamonds), and the spectrum after the 2nd layer of PtOEP in EC has been spin coated on top is shown by squares.

3.6 Source of illumination

The source of illumination for the BM sensors was a hand held device, i.e. a UV torch. This can be shone into a display case to excite the sensor and from the sensor colour any changes in partial pressure can be identified immediately. A torch was considered the best way to illuminate the sample, because constant illumination could possibly damage the artefact, and a device that could be triggered remotely would be difficult to make, and probably much more expensive. Although there are a number of "UV" torches on the market (http://www.maplin.co.uk 4/5/2009) many of these have their peak wavelength at 400 nm and thus show a blue emission colour.

Therefore a new device had to be constructed for our application Three UV LEDs were used and powered by a 6 V battery (fig.3.10). Three LED's were required to provide an adequate level of illumination.

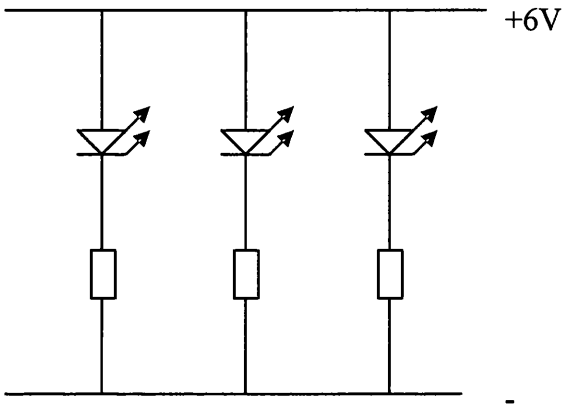

Fig.3.10. The schematic of the circuits for the LED torch, all resistors are 100Ω

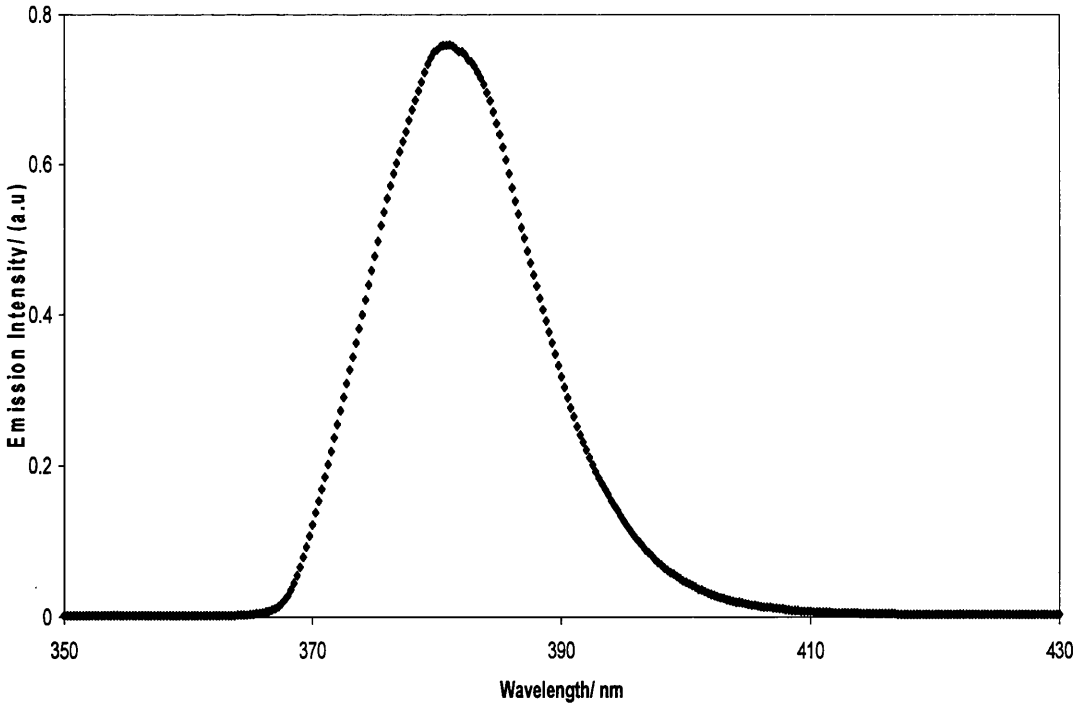

Fig.3.11. Emission spectrum of the LED torch with the Schott filter in fig.3.13

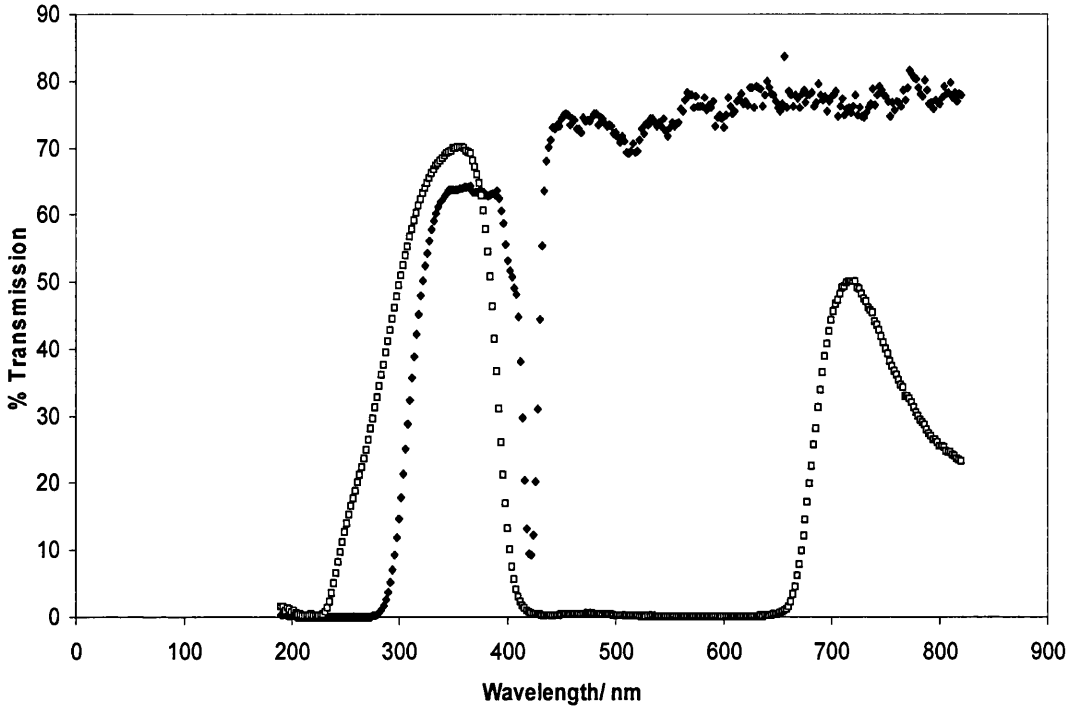

Fig.3.12. Transmission spectra of the two filters examined as possible filters for the LED torch: Schott filter (open shapes), tetraphenyl porphyrin in EC (closed shapes)

The LED's used for the torches have a small amount of visible blue emission. This will alter the colour of the sensors by mixing with the emission from the lumophores thus producing a slightly different hue. This is undesirable and has to be prevented by the addition of bandpass filters. Two filters were assessed for use with the torch. The first was a Schott 11 glass UV and IR bandpass filter. The second was a home made filter comprising of tetraphenyl porphyrin in EC. From fig.3.12 it can be seen that the porphyrin filter is less desirable than the Schott filter, because more transmittance is observed for the Schott filter. Red emission can also be observed from the home made filter that would have to be quenched to make the filter effective. The emission from the torch can be seen in fig.3.11.

3.7 Sensor response characteristics

With the lumophores and polymer matrices chosen for the BM sensor as rhodamine 110 in gelatin for the oxygen insensitive bottom layer, and PtOEP in EC for the oxygen sensitive upper layer, the optimum formulation could be determined. Firstly a starting point was established by using a PtOEP coating which gave an intense red colour under nitrogen when excited by the torch. This was made by spin coating from a solution of 0.4 ml of PtOEP in THF (0.75 mg PtOEP in 1 ml THF) and 1 g of 10 % ethyl cellulose (w:v) in 80:20 toluene:ethanol. With this layer established, the effect of the thickness of the rhodamine 110 layer could then be investigated. Figs 3.14 to 3.16 demonstrate the effect of increasing the number of rhodamine 110 layers. Fig 3.13 shows Stern-Volmer plots for PtOEP and rhodamine 110 in a sensor made with three layers of rhodamine 110 in gelatin. There is no change in the rhodamine 110 emission peak as the oxygen partial pressure is increased. A Stern-Volmer constant of 0.0737 ± 0.00937 $Torr^{-1}$ was obtained for the red, 645 nm, emission from the PtOEP in the sensor (fig.3.13).

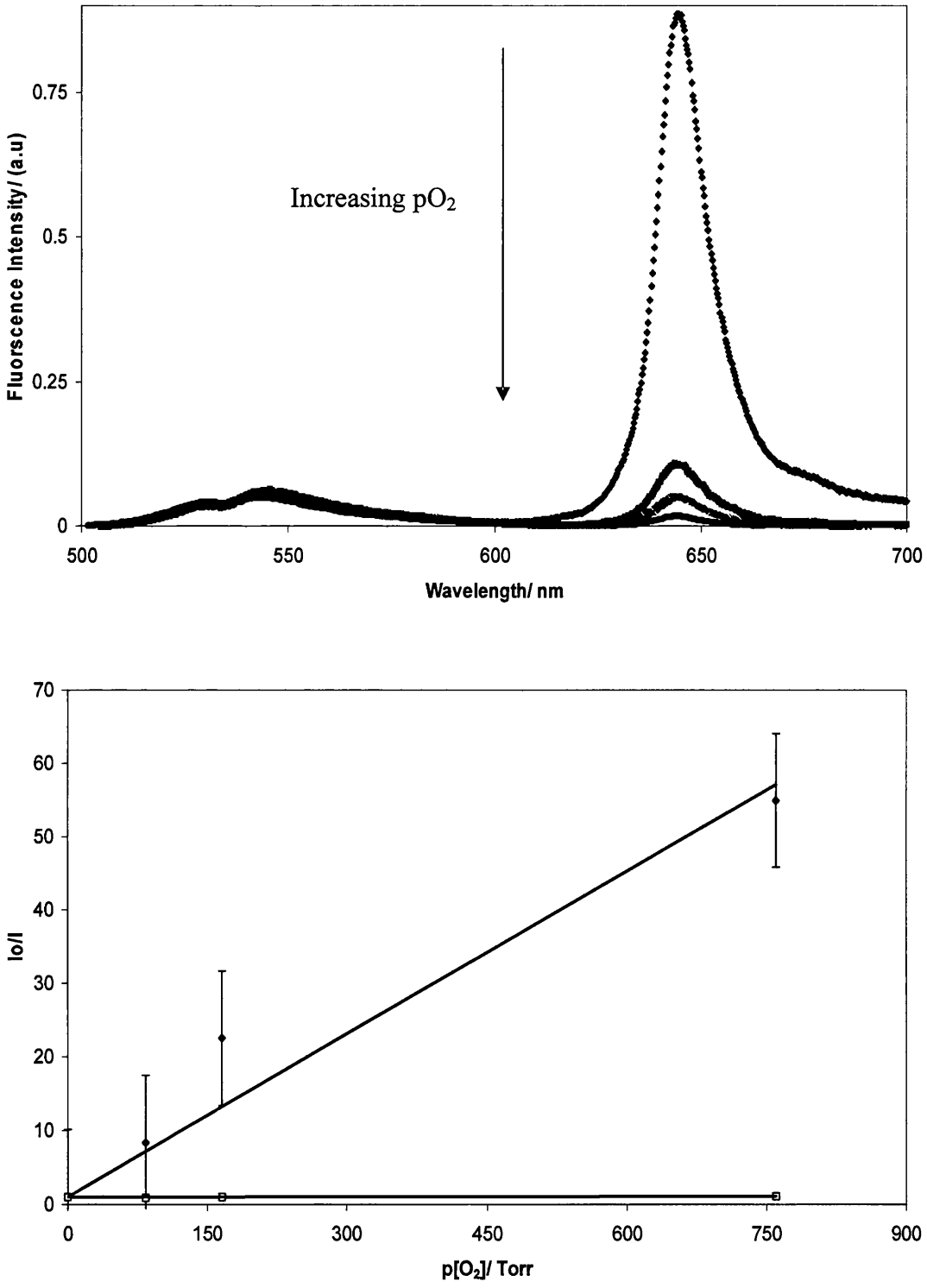

Fig.3.13. The changes in emission spectrum with increasing pO_2 for the BM sensor with three rhodamine 110 in gelatin layers (top), below is the Stern-Volmer plots for the PtOEP emission peak at 645 nm (closed shapes) $K_{sv} = 0.0737 \pm 0.0094$

$Torr^{-1}$,R^2 = 0.946, and Rh110 emission peak at 544 nm (open shapes) $K_{sv} = 8 \times 10^{-5} \pm 1.12 \times 10^{-4}$ $Torr^{-1}$ $R^2 = 0.162$

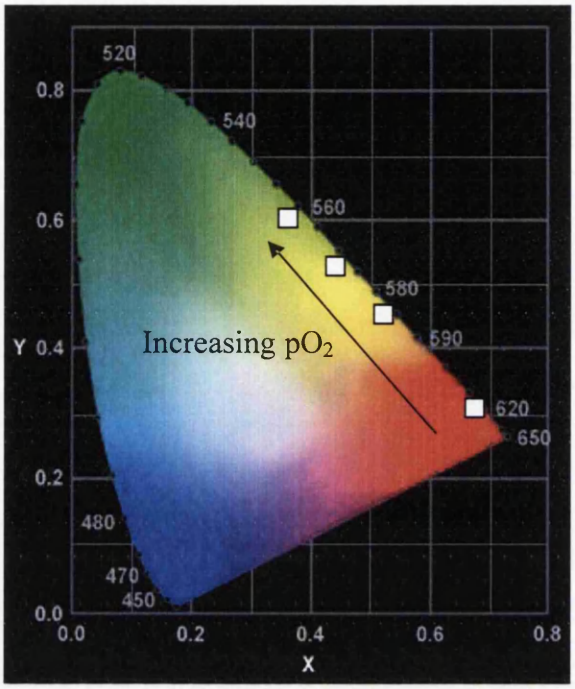

Fig.3.14. CIE coordinates for the BM sensor with PtOEP in EC and three layers of Rh110 in gelatin; pO_2 values: 0, 84, 166 and 760 Torr

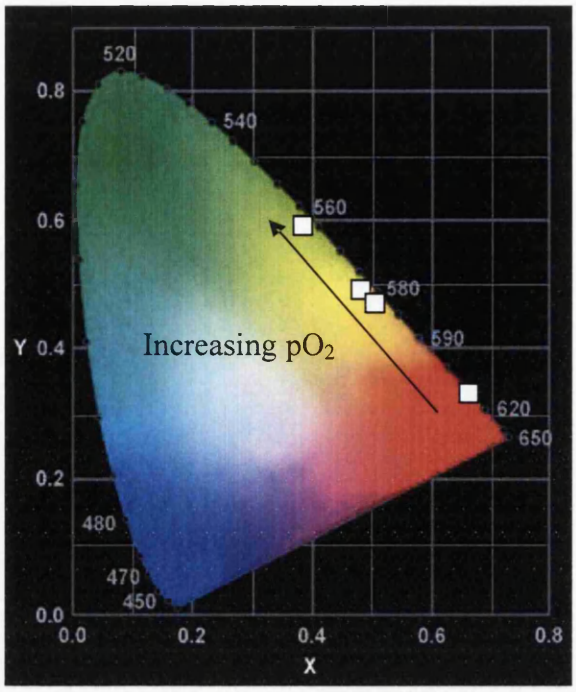

Fig.3.15. CIE coordinates for the BM sensor with PtOEP in EC and four layers of Rh110 in gelatin; pO_2 values: 0, 84, 166 and 760 Torr

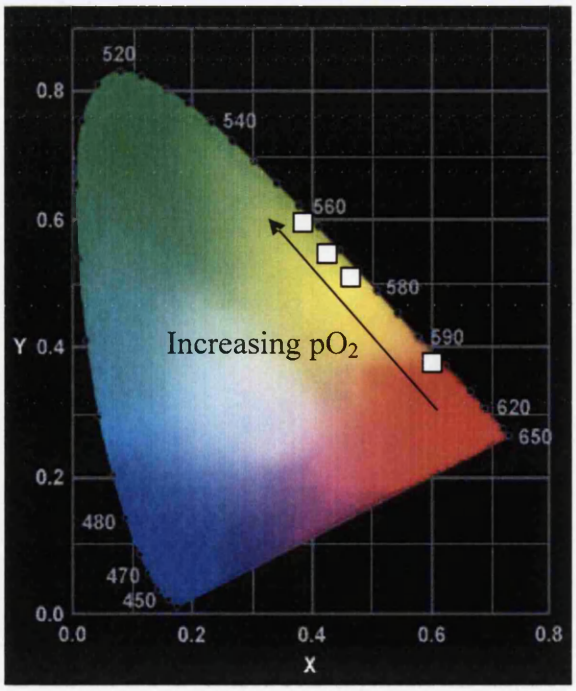

Fig.3.16. CIE coordinates for the BM sensor with PtOEP in EC and five layer of Rh110 in gelatin; pO_2 values: 0, 84, 166 and 760 Torr

pO_2/ Torr	BM 3 layers rhodamine 110	BM 4 layers rhodamine 110	BM 5 layers rhodamine 110
0	x = 0.68, y = 0.32	x = 0.67, y = 0.33	x = 0.60, y = 0.39
84	x = 0.52, y = 0.48	x = 0.50, y = 0.49	x = 0.47, y = 0.52
166	x = 0.44, y = 0.55	x = 0.49, y = 0.50	x = 0.43, y = 0.56
760	x = 0.39, y = 0.60	x = 0.40, y = 0.59	x = 0.40, y = 0.59

Table.3.2. Effect of the number of layers of rhodamine 110 on the CIE coordinates for the various BM sensors at different partial pressures of oxygen.

Increasing the number of layers moves the colour change of the sensor, as the number of layers increases the sensor appears green at a much lower partial pressure of oxygen (table 3.2). At 84 Torr the CIE co-ordinates that are closest to green belong to the sensor containing five layers, while the sensor containing three layers is closest to the red area of the chromaticity diagram (fig.3.14). However, the more rhodamine 110 layers the more orange the colour of the sensor is in the absence of oxygen therefore making the colour changes more difficult to identify.

From figures 3.14 to 3.16 it can be seen that the sensor made from three rhodamine 110 layers gives the best colour change. This has the best red colour with the least number of rhodamine 110 layers. Therefore this is the most identifiable colour change. Fig 3.17 shows this sensor under vacuum and in air. The colour change is obvious even though the colour in vacuum is more orange than the cherry red of PtOEP emission alone.

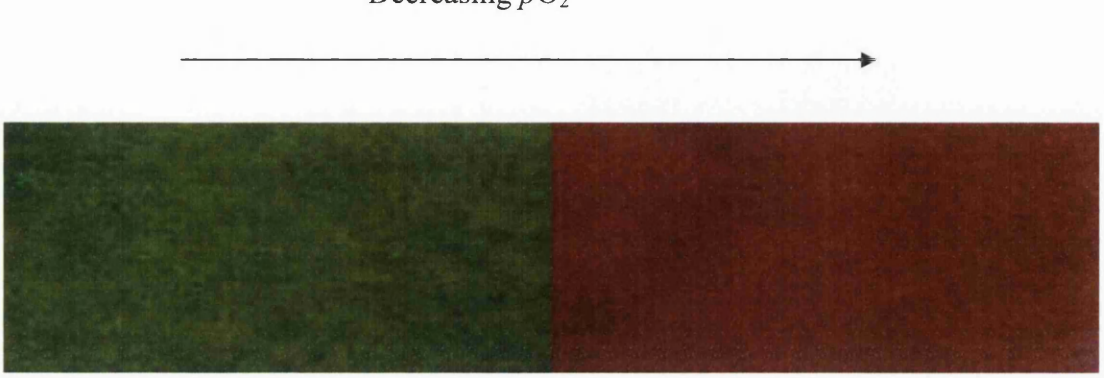

Fig.3.17. A BM sensor with three layers of Rh110 in gelatin illuminated with the LED torch under atmospheric conditions (left), and under vacuum (right)

3.7.1 Response times

The response times for the BM sensors are shown in fig..3.18. This data was obtained by reducing the pressure of the slide holder with a rotary evaporator pump and then releasing the rotary evaporator tap to simulate a leak. This was a simple way to roughly mirror the conditions that the sensors maybe working under, particularly the release of pressure if a leak is caused in a display case.

As fig 3.18 shows the sensors have response times in the region of 1 s for both pressuring and depressurising the cell holder. This very fast response (fig.3.18) is a generally a desirable property of thin film optical sensors.

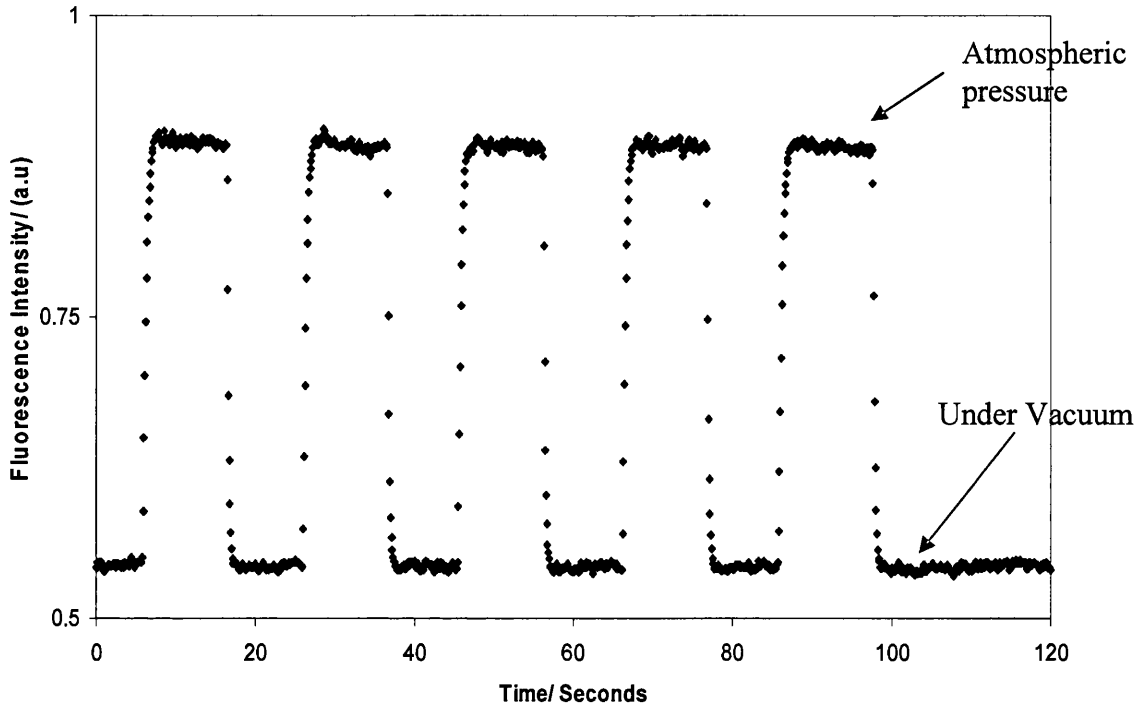

Fig.3.18. Responses under atmospheric pressure and under partial vacuum of a BM sensor at 645 nm, partial vacuum is obtained by attaching the sample holder to the vacuum pump from a rotary evaporator

3.8 Photostability

The photostability of the sensors is a very important factor in a dual lumophore colorimetric sensor. If the layers degrade at different rates then the colour response is altered significantly (Tab.3.6 models this effect on a PtPYR sensor). Ideally a sensor should not degrade, however if this does occur then a strategy needs to be found in order to reduce it.

The problem of degradation was analysed in detail with PtPYR sensors, and the information from these experiments was later used to stabilise the other multilumophore sensors described in this thesis. The first step was to ascertain

whether the lumophore films degraded when spin coated on their own, and if they did at what rates.

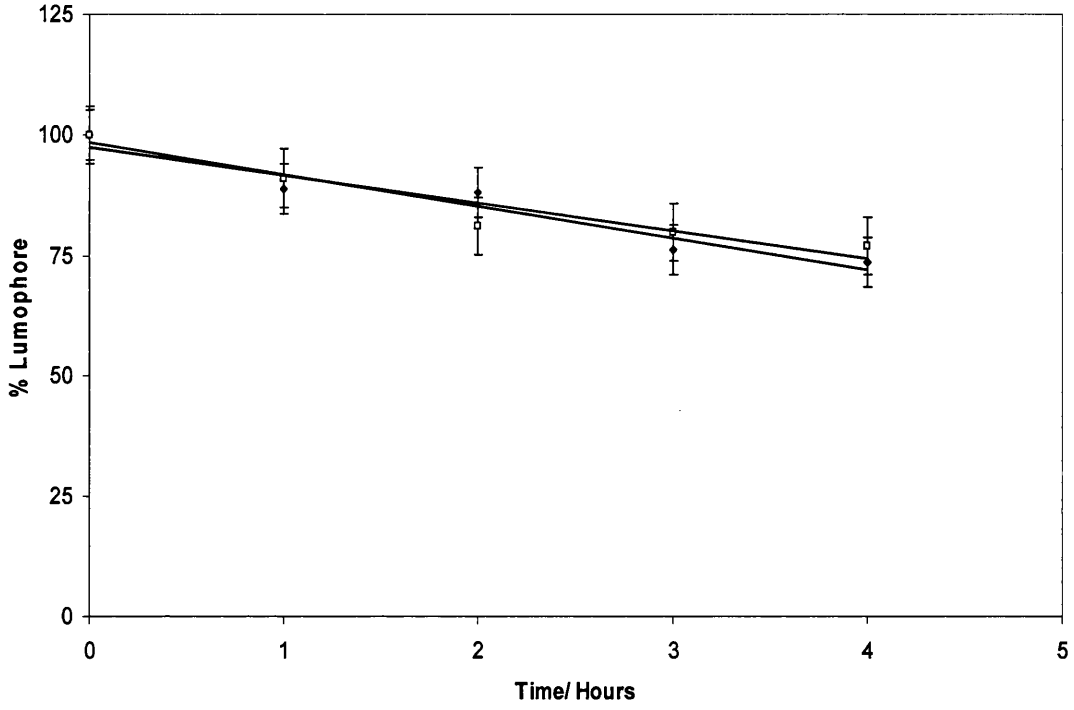

Fig.3.19. Degradation of single layers: PtPYR (circles, 1 mg of PtPYR to 1 ml THF and 0.4 ml of this solution in 1 g of 10 % EC), degradation rate = 6.57 ± 0.95 $\%hr^{-1}$, $R^2 = 0.94$; and PtOEP (squares 1 mg of PtOEP to 1 ml THF and 0.4 ml of this solution in 1 g of 10 % EC) degradation rate = 5.74 ± 1.09 $\%hr^{-1}$, $R^2 = 0.94$ using the degradation suite described in chapter 2

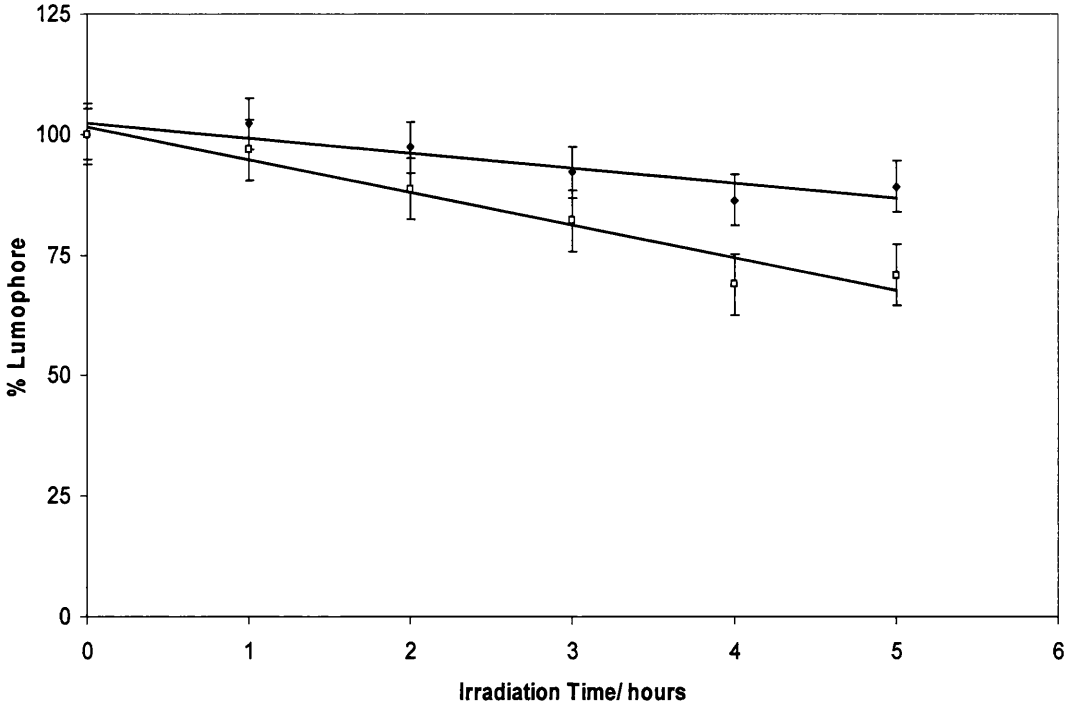

Fig.3.20. Degradation in the mulitlumophore unstabilised sensor: PtOEP (squares) degradation rate = 6.75 ± 0.84 $\%hr^{-1}$, $R^2 = 0.82$; PtPYR (diamonds) degradation rate = 3.07 ± 0.84 hr^{-1}, $R^2 = 0.94$. Using the degradation suite describe in chapter 2

From fig.3.19 it is clear that both lumophores degrade at similar rates in single layers. However when they are placed in a dual lumophore sensor (fig.3.20), they can be seen to degrade at different rates, and this will affect the colour change of the sensor, because the colour change is dependent on the ratio of emission from the two lumophores.

3.8.1 Singlet oxygen

In order to develop a strategy to minimise the effect of the degradation it was necessary to establish the mechanism of degradation. One of the possibilities was a reactive oxygen species, most likely singlet oxygen because porphyrins are known to act as sensitizers for singlet oxygen.[38]

The ground state of oxygen is the $O_2(^3\Sigma_g^-)$ species which exists in the triplet state with two unpaired electrons, one in each of the two highest molecular orbitals. Therefore the spin multiplicity is a triplet and consequently this allows for preferred interaction with sufficiently long lived triplet or partial triplet states of an excited state lumophore, such as PtOEP or PtPYR, by a spin allowed energy transfer process (fig.3.21).

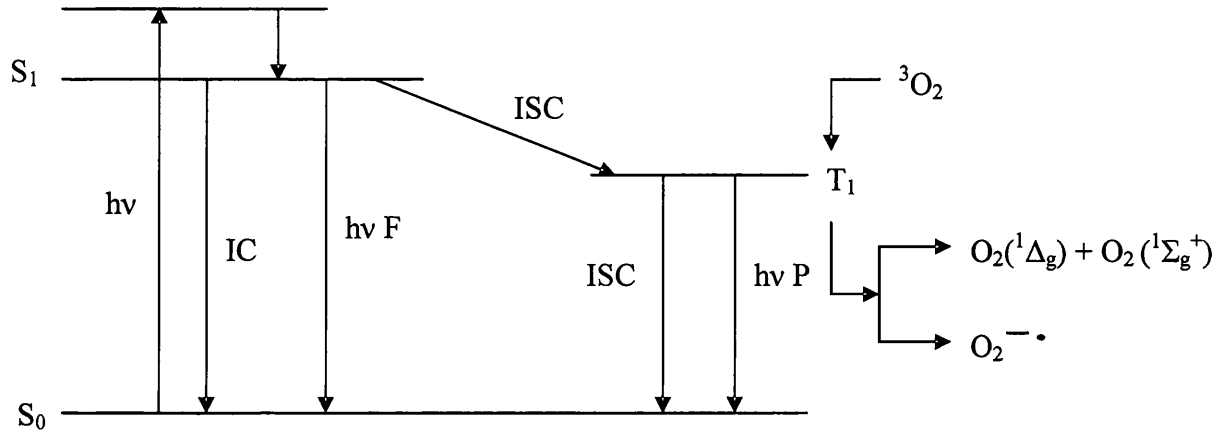

Oxygen	Configuration of spins in highest occupied MO	Relative energy kJ mol^{-1}	eV
$O_2(^3\Sigma_g^-)$	↑ ↑	0	0
$O_2(^1\Delta_g)$	↑↓	94.2	0.98
$O_2(^1\Sigma_g^+)$	↑ ↓	157.1	1.63
$O_2^{-\bullet}$	↑↓ ↑	-	-

Fig.3.21. Scheme of formation of $^1O_2$ by sensitised photooxidation with a table of the spin configuration in the highest occupied molecular orbitals in oxygen species and relative positions of the corresponding energy levels relative to $^3O_2$.[39]

Energy transfer from a (π,π^*) molecular orbital on the sensitizer can lead to the formation of two excited singlet species; $O_2(^1\Delta_g)$ and $O_2(^1\Sigma_g^+)$. The formation of the second species $O_2(^1\Sigma_g^+)$ is a high energy process creating a thermodynamically unstable species, and this is rapidly converted to the lower energy singlet species in a spin allowed process.

The spin flip process of activating oxygen during quenching is believed to occur by a variety of different mechanisms: either a dipole-dipole interaction characteristic of a Forster energy transfer reaction or an electron exchange reaction by collision energy transfer. The later is believed to be far more likely for a triplet state.[39]

From fig.3.21 it can be seen a further species can be formed from the interaction of $^3O_2$ and the sensitizer, and that is the superoxide anion. This can be generated because some of the lumophore may be present in a lower energy (n, π^*) molecular orbital characteristic of low lying triplet states. This can form the superoxide anion by electron exchange.[39]

From this scheme it can be shown that at least two very reactive species can be generated by the interaction of excited-state lumophore and molecular oxygen both of which could be potentially responsible for the degradation of the sensor. (The higher energy singlet species, $O_2(^1\Sigma_g^+)$ may be discounted due to its short lifetime). To confirm which species was responsible for lumophore degradation in the sensors, slides were prepared which contained diphenylisobenzofuran, DPBF, which is known to react very rapidly with singlet oxygen; these slides were then irradiated, and the loss of DPBF followed spectrophotometrically (fig.3.22).[40] It is worth noting

that singlet oxygen can not be generated directly from irradiation of oxygen with UV light because it is a spin forbidden process and therefore a sensitizer is required. The degradation of DPBF in sensor layers containing either PtOEP or PtPYR both reacted faster than that containing only DPBF, which suggests that the reactive species is most likely singlet oxygen.

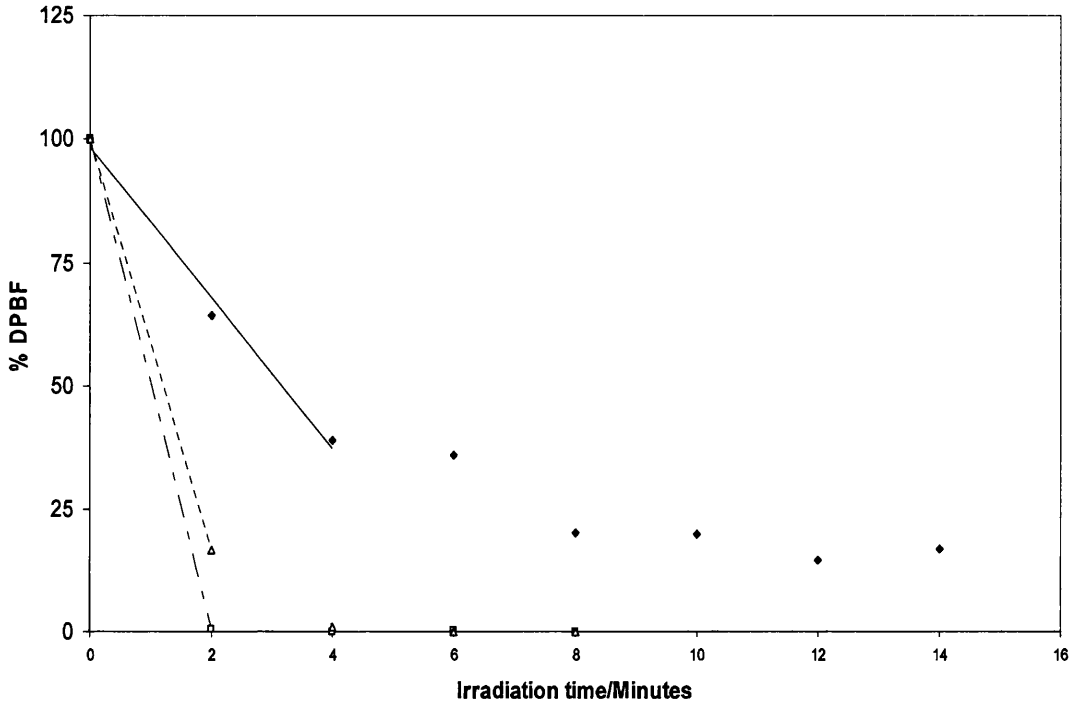

Fig.3.22. Degradation of DPBF in single lumophore EC layers containing DPBF and irradiated using the irradiation suite described in chapter 2. DPBF alone in EC (filled diamonds), DPBF with PtPYR in EC (triangles), DPBF with PtOEP in EC (circles).

3.8.2 Deactivation of singlet oxygen

From the data obtained from the reaction with DPBF it was assumed that degradation occurred via singlet oxygen and therefore one stabilisation mechanism would be to deactivate the singlet oxygen. Deactivation of singlet oxygen can occur by either a physical or chemical pathway. A physical pathway is preferred as a stabilising

mechanism as this preserves the quencher, allowing it to continue deactivating singlet oxygen. Diazobicyclo[2.2.2]octane (DABCO) is an example of a physical quencher, and the method of deactivation is believed to be by the formation of a charge transfer exciplex[41,42] as in the reaction scheme fig 3.23.

$$Q + {}^1O_2\Delta_g \underset{-k_{diff}}{\overset{k_{diff}}{\rightleftharpoons}} {}^1(Q^1O_2\Delta_g)_{EC} \underset{-k_{ex}}{\overset{k_{ex}}{\rightleftharpoons}} {}^1(Q^1O_2\Delta_g)_{CT} \xrightarrow{k_p} {}^3(Q^3O_2\Sigma_g^-)_{CT} \longrightarrow Q + O_2{}^3\Sigma_g^-$$

Fig.3.23. Process for the deactivation of singlet oxygen by the formation of a charge transfer complex

In this process an encounter complex is formed when the quencher (Q) and singlet oxygen ($O_2{}^1\Delta_g$) collide in a diffusion controlled process. This is stabilised by the transfer of electronic charge from the oxygen molecule to the quencher in a charge transfer exciplex ${}^1(Q^1O_2\Delta_g)_{EC}$. This decays mainly by ISC to a triplet ground state ${}^3(Q^3O_2\Sigma_g^-)_{CT}$, which dissociates to the products (Q and $O_2{}^3\Sigma_g^-$) without charge separation in most cases.[39]

The second physical method for the deactivation of the singlet oxygen is by electronic to vibrational energy transfer, whereby the electronic energy of the oxygen is converted into vibrational energy of the oxygen and the quencher. This occurs in quenchers that have a sufficiently high triplet state energy that the charge transfer mechanism could not occur, and this is believed to be the case for quenching by nickel (II) N-phenyl dithiocarbamate (NPD).[45]

The final method for the deactivation of singlet oxygen is chemical, i.e. by the reaction of the singlet oxygen with a quencher. This partially occurs in quenching by vitamin E (VIT E) and butylated hydroxytoluene (BHT).[44] VIT E is a mostly physical quencher, with up to 93-99% physical in character,[45] however there is some chemical reaction. BHT follows a similar pathway and the scheme in fig.3.24 demonstrates this process. The result of this behaviour is that while the most of the singlet oxygen is deactivated physically some of the quencher is destroyed, and eventually all of the quencher is consumed. The chemical reaction involves hydrogen abstraction however this is believed to produce only the ground state products shown in the scheme and does not lead to a variety of different products in the same way that a radical reaction scheme would.

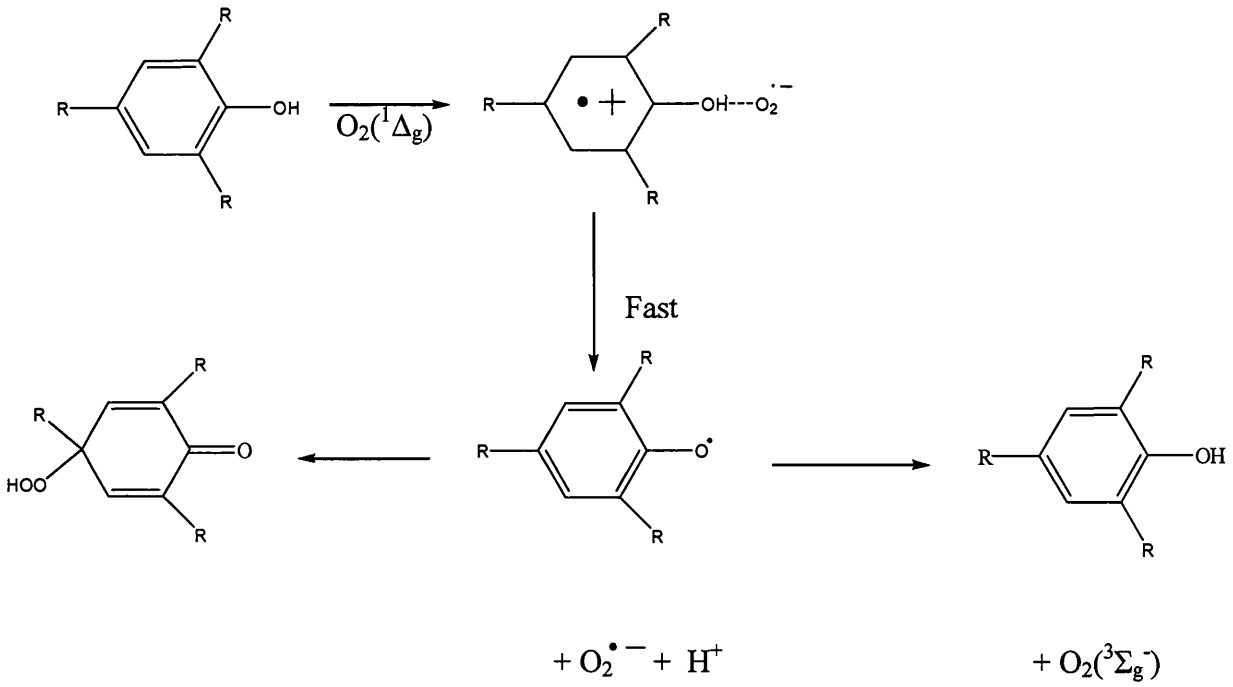

Fig.3.24. Reaction scheme for quenching of singlet oxygen by BHT showing both a physical quenching route and route involving chemical reaction; R = C_4H_9

Although tris(2,4-ditert-butyl-phenyl)phosphate TBPP is a commonly known stabiliser for polymers[46] its reaction with singlet oxygen is not well known. Popisil and co workers suggested that it would react chemically in a similar fashion to that of aryl phosphines,[47] While Bolduc and Goe suggested that phosphites are converted to phosphates.[48] Our own work showed that it did not stabilise PtOEP, possibly because of oxidation in the solvent used to make up the sensor solutions,[49] and so it was not investigated further.

3.8.4 Stabilising additives

In the past work by other groups has shown that putting additives into the polymer matrix can have a stabilising affect on the lumophore.[50,51] For this study a group of additives were chosen which were either widely used as stabilisers by the polymer industry or they were known singlet oxygen quenchers. The additives examined were: (DABCO), (VIT E), (BHT), (NPD), and (TBPP). The lifetimes of the sensors with and without the additives were investigated to see if they quenched the lumophore emission, and once the suitability of a sensor was established their ability to stabilise the sensor was then examined.

Once the various different additives were tested the first impressions were that the addition of some additives to the lumophores were quenching the emission from the lumophores in solution especially PtPYR (table.3.5). Lifetime studies were carried out on sensors containing the different additives. The amounts of additives used in these studies are given in table 3.3.

Additive	Amount added to PtPYR Layer (phr)*	Amount added to PtOEP layer (phr)*
Nickel (II) N-phenyl dithiocarbamate (NPD)	0.23	0.30
Vitamin E (VIT E)	2.98	2.72
tris(2,4-ditert-butyl-phenyl)phosphate (TBPP)	0.34	0.22
butylated hydroxytoluene (BHT)	0.45	0.26
Diazobicyclo[2.2.2]octane DABCO	0.16	0.45

Table 3.3. List of additives to the lumophore layers of the PtPYR sensors used for lifetime analysis, the amount of VITE used is much higher than the amount used for the other additives because it was not convenient to handle smaller amounts that this

*__phr__ parts per hundred resin

Firstly the effect on PtOEP was analysed by measuring the decay curves from dual lumophore sensors and fitting these to single exponential decays in order to calculate the observed rate constant k_{obs}. The analysis of the decay curves (fig.3.25), showed that none of the additives acted as quenchers for PtOEP in EC films with the possible exception of NPD (table 3.4). (But NPD was not the best candidate as a stabiliser in any case because it is coloured (fig 3.26)).

Additive	k_{obs} $s^{-1}/10^3$
NPD	12.6 ± 1.1
DABCO	10.4 ± 0.9
VIT E	10.1± 0.9
TBPP	10.3 ± 0.9
BHT	10.4 ± 0.9
No Stabiliser	10.4 ± 0.9

Table.3.4. k_{obs} for Pt-OEP in PtPYR sensors with the various additives at 293 K

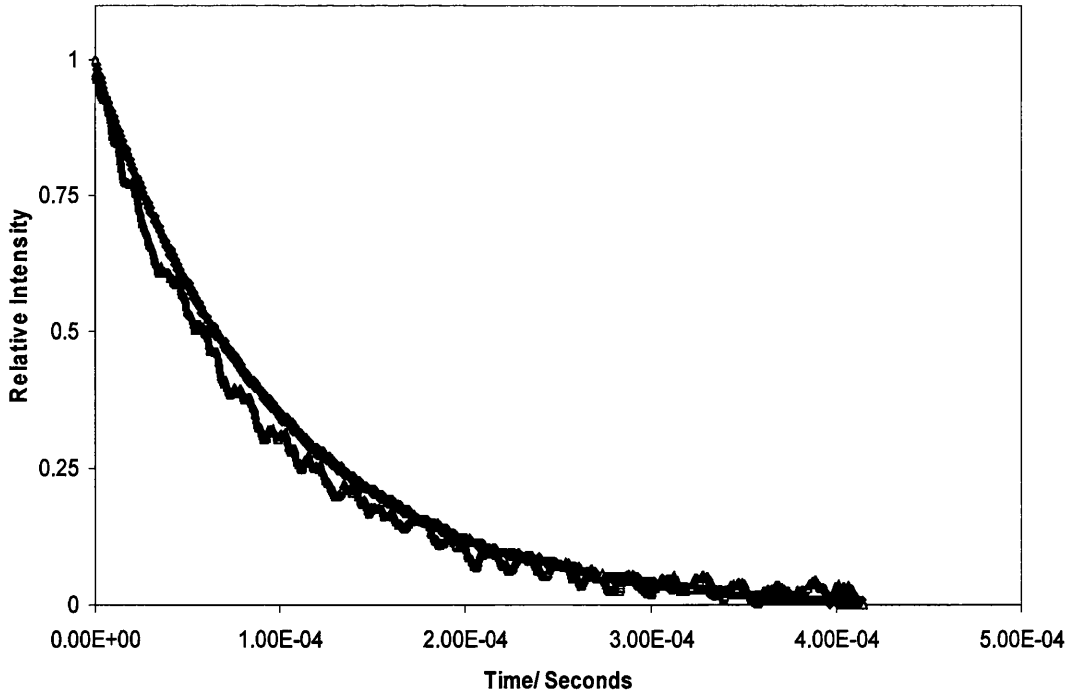

Fig.3.25. Decay curves under nitrogen for PtOEP in EC with no additive (top), and PtOEP in EC with NPD added (bottom) (the noise in the NPD trace can be attributed to a reduced signal because of absorption of the laser pulse by NPD fig.3.22)

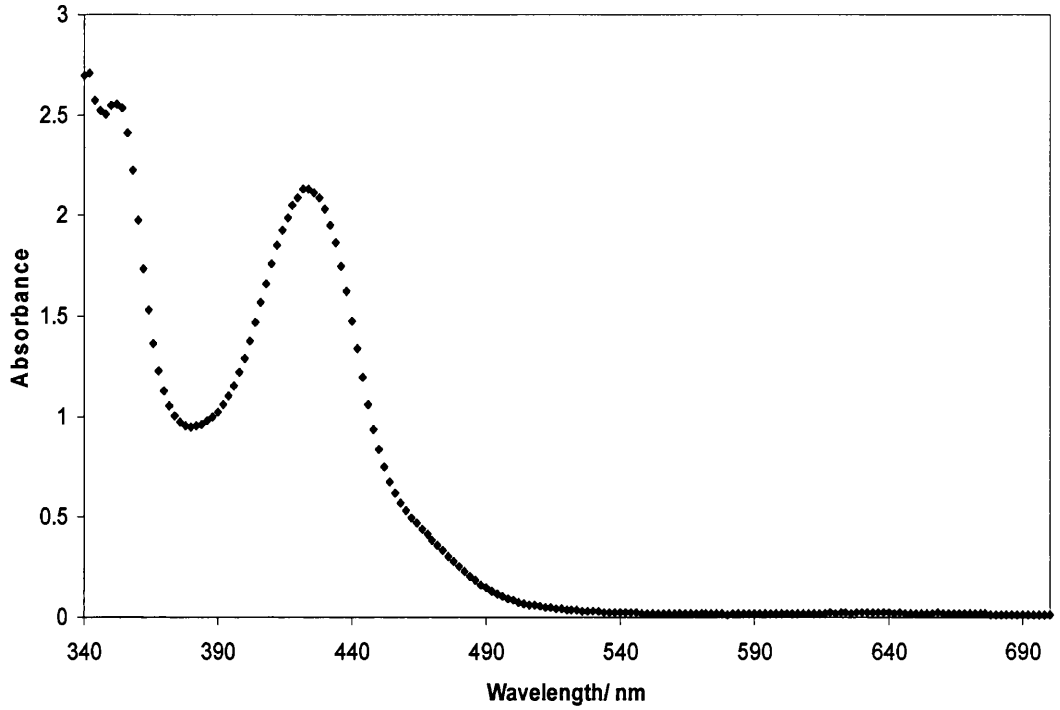

Fig.3.26. Absorption spectrum of NPD in THF

3.8.5 PtPYR solution phase studies

Solution phase studies show that all of the additives are quite efficient quenchers of PtPYR in solution (fig.3.27 and table 3.5). However, because of the restricted mobility in the EC polymer films bimolecular quenching can be ignored for all but the most mobile of molecules i.e oxygen.

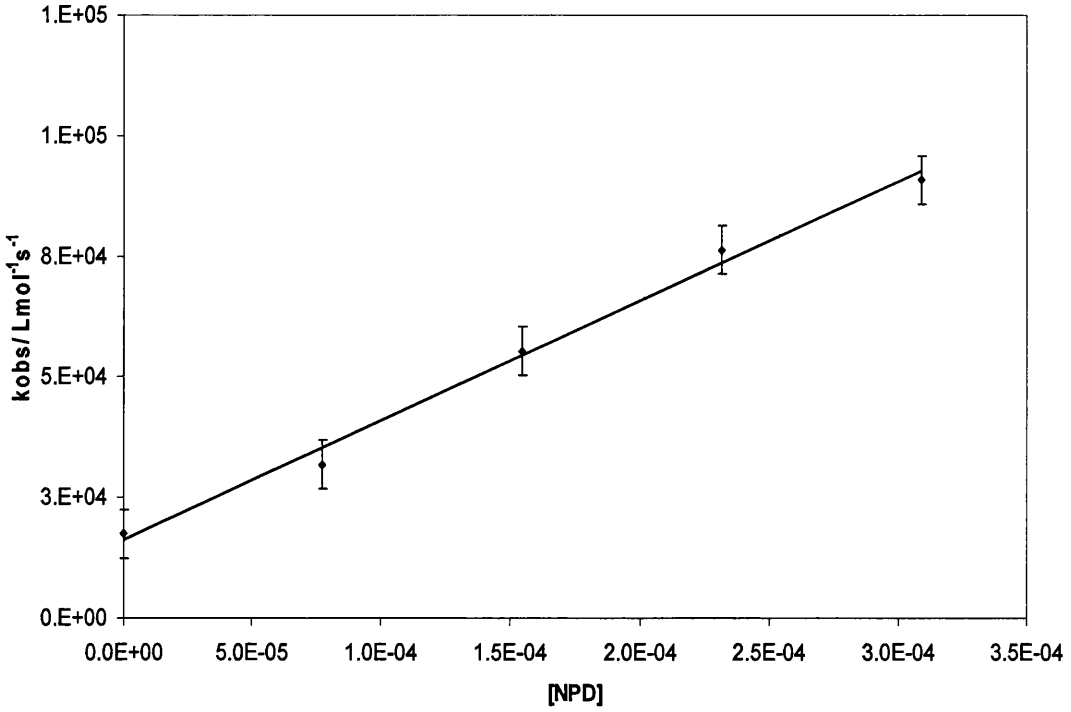

Fig.3.27. A plot of k_{obs} against NPD concentration for the luminescence decay of PtPYR in THF; the slope gives k_q.

Additive	**Bimolecular rate constant (k_q) L $mol^{-1}s^{-1}$**
DABCO	4.37 (±0.46) x 10^9
NPD	2.80(±0.28) x 10^8
VIT E	2.47(±0.33) x 10^8
TBPP	4.79(±0.44) x 10^7
BHT	3.21(±1.46) x 10^7

Table 3.5. Bimolecular rate constants for quenching of Pt-PYR luminescence in THF at 287 K.

However since the lowest k_q was for BHT, it seemed like a likely candidate as a stabiliser.

Figure 3.28 demonstrates the effect of adding BHT to both layers lumophore layers in a dual lumophore sensor. Unfortunately the addition of the BHT had the opposite effect to the desired one, and the addition of the BHT sped up the degradation of the lumophores rapidly. Although this has not been studied further it would be reasonable to postulate that the addition of BHT may lead to an increase in the mobility of the singlet oxygen throughout the matrix, thus accounting for the rapid degradation. It is also not clear as to why the addition of BHT speeds up degradation of the sensor and this does not occur with other stabilisers such as DABCO. It maybe that this occurs because the additions of the other stabilisers increases the mobility of species in the polymeric matrix, but the quenching nature of these species negates this effect. It is therefore an area that would require further work to determine.

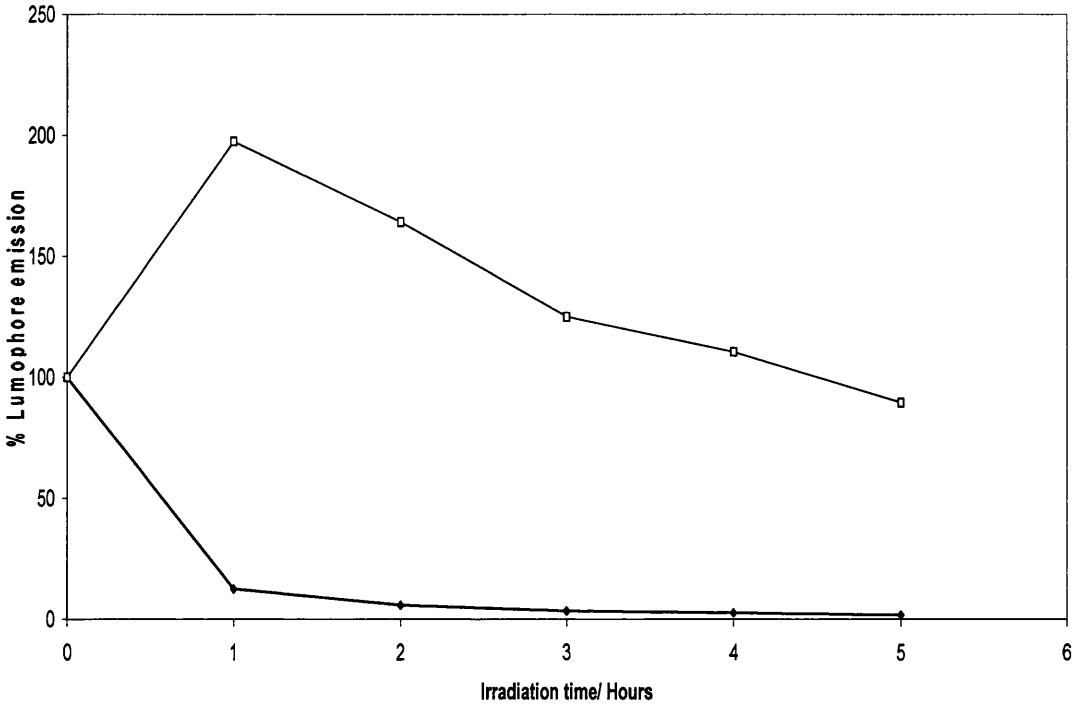

Fig.3.28. Degradation of a dual lumophore sensor with BHT added to both lumophore layers and irradiated using the irradiation suite described in chapter 2; PtPYR (squares) PtOEP (diamonds)

Since it was already known that the addition of DABCO could be used to stabilise PtOEP,[50,51] and that the long lifetime of PtOEP meant that this was most likely the origin of any singlet oxygen generated, it was decided to add DABCO to the PtOEP layer and evaluate this formulation for photostability. As fig.3.29 and table 3.6 shows this approach was successful and it is this approach to stabilisation which has been adopted through the rest of this work.

This method of stability was extended to the BM sensor, and in fig.3.30 the BM sensor is shown to be very stable with the addition of DABCO. It would be expected that this maybe more stable due to the lower concentration of the PtOEP, and also the

rhodamine 110 is probably more stable than PtPYR, because it is unlikely to sensitize the production of singlet oxygen.

No thermal degradation was evident, and no spoilage of the gelatin has been observed even in samples that have been kept up to a year.

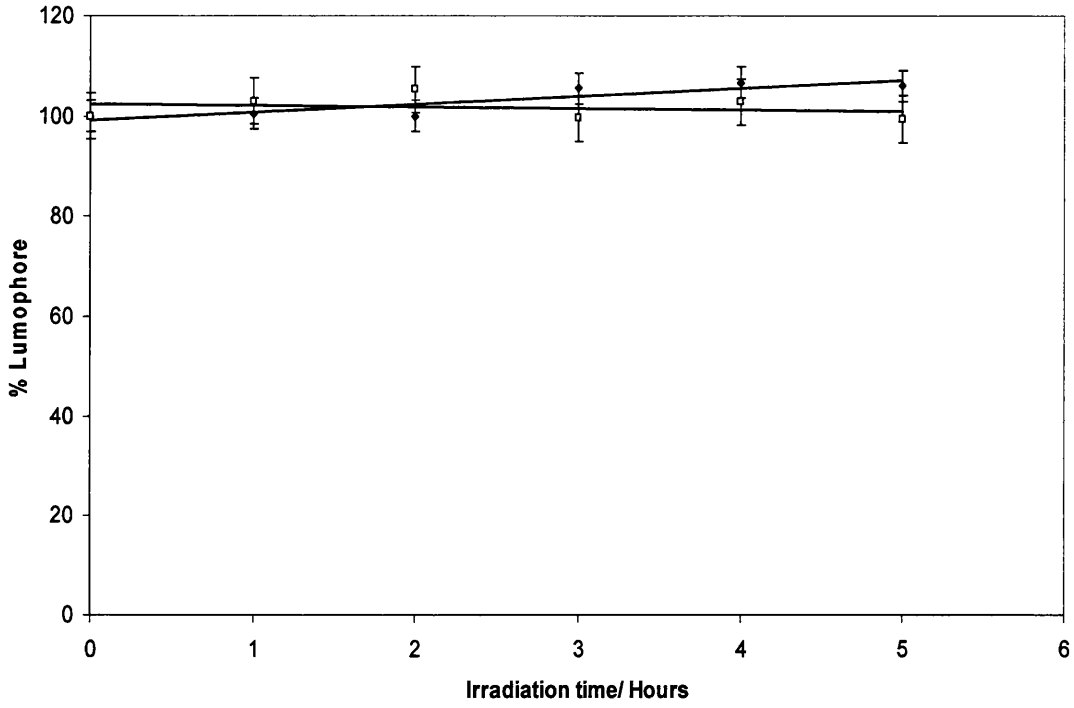

Fig.3.29. The PtPYR sensor with DABCO added to the PtOEP layer degraded using the irradiation using the irradiation suite described in chapter 2 degradation rates; PtPYR (open) = 1.56 ± 0.40 $\%hr^{-1}$, $R^2 = 0.79$, PtOEP (closed) = 0.269 ± 0.62 $\%hr^{-1}$ $R^2 = 0.04$

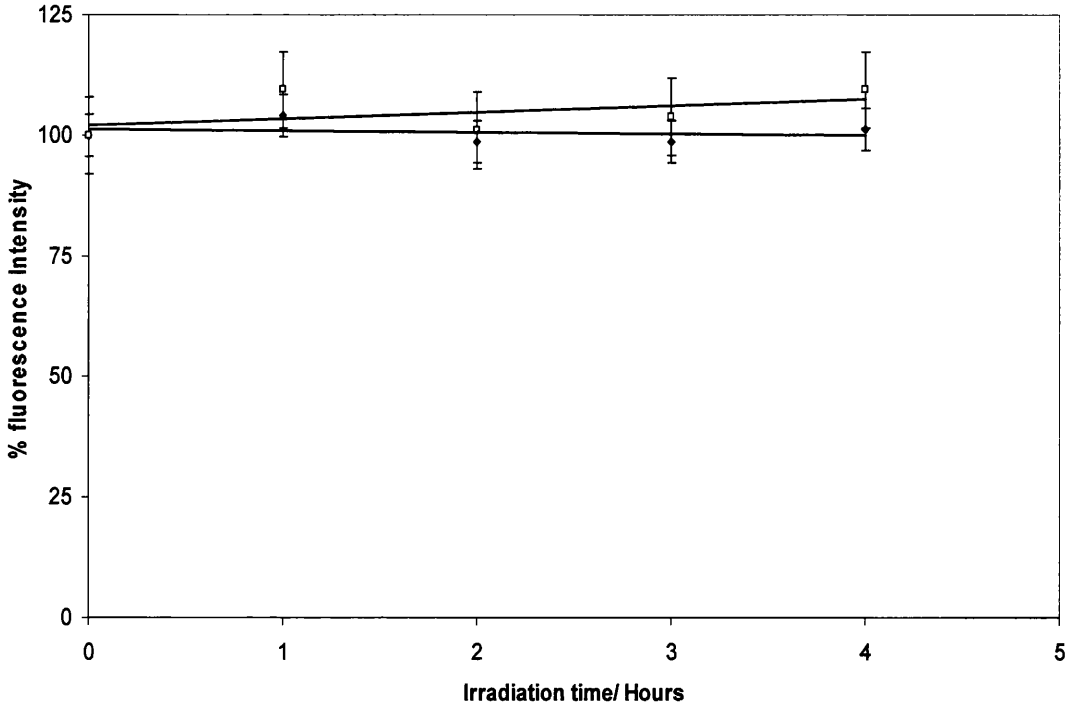

Fig.3.30. Degradation plot (BM sensor) at 645 nm (squares) degradation rate = 1.32 ± 1.45 %hr^{-1} R^2 = 0.22, degradation rate at 535 nm = 0.295 ± 0.808 % hr^{-1} R^2 = 0.043

3.8.3 Modelling the colour change of unstabilised and stabilised PtPYR sensor

Modelling of the effect of degradation on the colour change of the PtPYR sensor was achieved by taking the emission spectra for both the unstabilised and stabilised PtPYR sensors under nitrogen and normalising them. All wavelengths up to 600 nm in the spectra were multiplied by the change in peak height due to changing pO_2 from the Stern-Volmer for PtPYR fig 3.31. Wavelengths above 600 nm were multiplied by the change in peak height from the second Stern-Volmer for PtOEP fig.3.32. Using this technique predicted spectra prior to any degradation could be obtained for the various oxygen partial pressures (table 3.6). Once the predicted spectra were calculated the spectral weighting functions could be applied and CIE coordinates could be calculated for the different partial pressures.

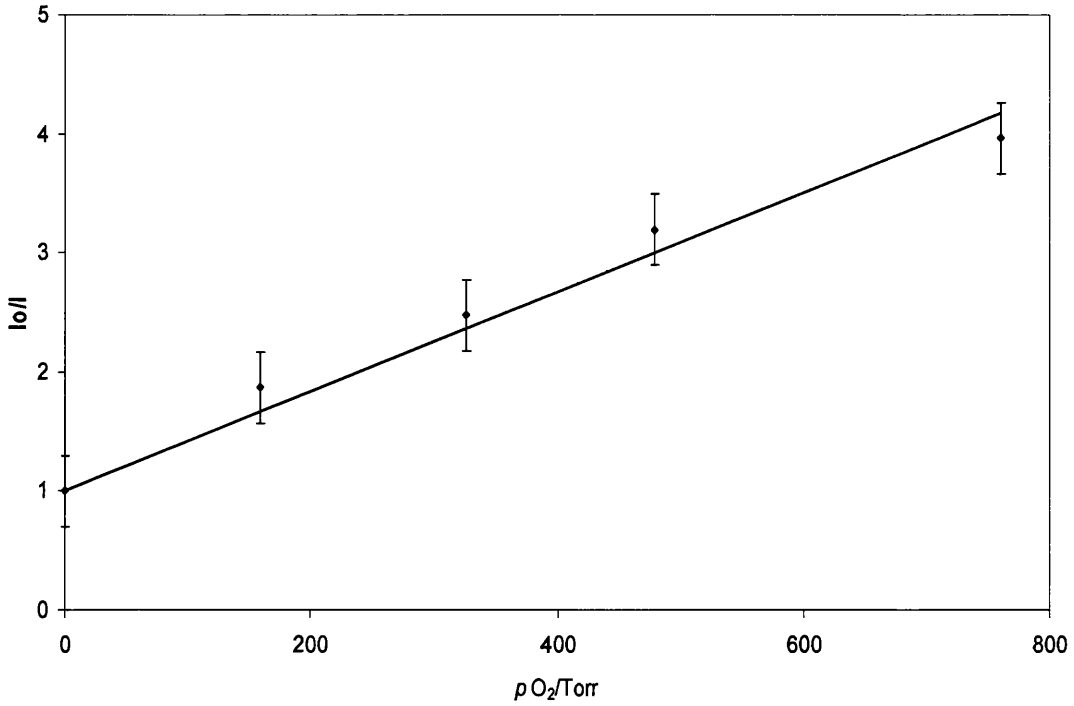

Fig.3.31. Stern-Volmer plot for the PtPYR in the PtPYR sensor: $K_{sv} = 0.0042 \pm 0.0003$ Torr^{-1}, $R^2 = 0.9741$

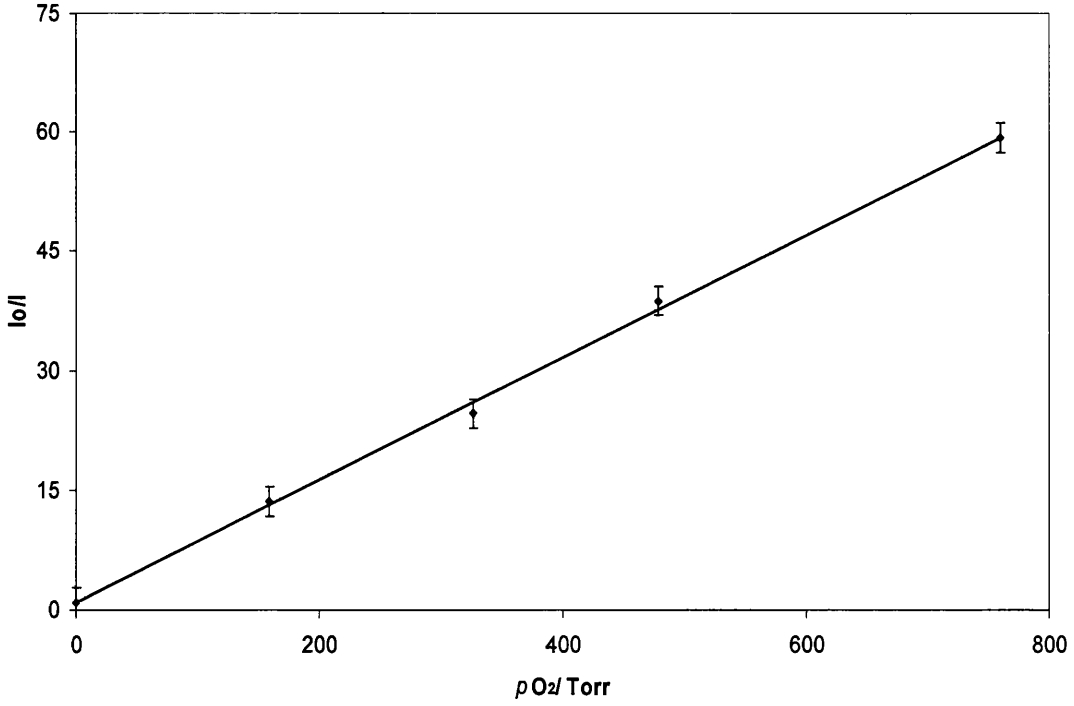

Fig.3.32. Stern-Volmer of the PtOEP in a PtPYR sensor: $K_{sv} = 0.077 \pm 0.002$ Torr^{-1}, $R^2 = 0.998$

To predict the changes due to degradation the same process as described previously was repeated, but after the peak heights had been reduced due to partial pressure, they were reduced again inline with peaks after the five hours of degradation, using the values given in fig.3.20 for the unstabilised PtPYR sensor, and fig.3.29 for the stabilised PtPYR sensor. This produced predicted spectra after degradation from which the CIE coordinates could be calculated. The results from the modelling can be seen in table 3.6.

pO_2/Torr	Unstabilised before degradation	Unstabilised slide after degradation	Sensor stabilised with DABCO before degradation	Sensor stabilised with DABCO after degradation
0	x = 0.67, y = 0.32	x = 0.66, y = 0.33	x = 0.67, y = 0.32	x = 0.67, y = 0.32
159.6	x = 0.50, y = 0.46	x = 0.46, y = 0.48	x = 0.51, y = 0.45	x = 0.50, y = 0.46
326.8	x = 0.46, y = 0.46	x = 0.43, y = 0.51	x = 0.47, y = 0.48	x = 0.46, y = 0.48
478.8	x = 0.43, y = 0.51	x = 0.41, y = 0.53	x = 0.45, y = 0.50	x = 0.44, y = 0.50
760	x = 0.40, y = 0.53	x = 0.37, y = 0.55	x = 0.42, y = 0.52	x = 0.41, y = 0.53

Table.3.6. The CIE coordinates for the unstabilised and stabilised sensors at different oxygen pressures, before and after irradiation for five hours

3.9 Conclusions

A sensor has been designed which gives a tuneable response to increasing oxygen partial pressures. The desirable colour change of red-yellow-green was obtained by using green and red lumophores with different oxygen sensitivities.

The lumophores chosen were PtOEP and rhodamine 110. PtOEP is very sensitive to oxygen partial pressure with a high quantum yield and a good red emission. Rhodamine 110 was chosen because it produces a desirable green colour and is not responsive to oxygen partial pressure. A PtPYR sensor was shown to also produce a highly visible green to red colour change but PtPYR is not commercially available and is subject to some degree of quenching by oxygen, and was therefore considered a less desirable green lumophore than rhodamine 110.

EC was chosen as the matrix for the PtOEP, because it is highly oxygen permeable, has good optical properties and is easy to spin coat. The rhodamine 110 was encapsulated in gelatin, which is highly oxygen impermeable. It was found necessary to use multilayers of this lumophore layer to produce a good colour change.

Inkjet printing of the sensors was investigated but found to be slow and less useful than spin coating, because it only made very thin layers which required many layers printed on top of each other to produce a visible colour. Meyer bar coating was also assessed. It produce thick films up to 20 microns in thickness, but was found to have few advantages over spin coating, and so was not investigated further, although we note that it could be used to produce these sensors.

A small efficient handheld illumination source was made from a modified torch using three LEDs and a UV bandpass filter. With this as an illumination source it would be a simple operation to check the colour of the sensor in any cabinet provided

there was a window transparent to near UV e.g. one made of glass or plastic, and it also means that no complicated equipment is required to be kept inside the cabinet.

Different sensor compositions can be made so that the optimum response can be obtained depending on how complete the vacuum is. If storage was in the total absence of oxygen (i.e 0 Torr and not the partial vacuum created using the vacuum pump) the best sensor composition is one that has three layers of rhodamine 110 in gelatin.

The sensors can be stabilised with the addition of DABCO to the PtOEP layer of the sensor. No degradation in either lumophore was observed as a consequence of thermal reactions at room temperature or bacteriological growth.

Response of the sensors was very rapid, ca. 1 s from vacuum to air.

In conclusion, it has been demonstrated that it is possible to build a tuneable, fast response, sensor with good clarity that can be illuminated by a hand held device, ideal for use as an aid for preservation of artefacts via storage in a low oxygen environment.

3.10 References

1) Katoh, R.; Nakamura, M.; Sasaki, Y.; Furube, A.; Yokoyama, T.; Nanjo, H. *Chem. Lett.*,36, **2007**, 1310-1311.

2) Ricketts, S.R.; Douglas, P.; *Sens. Actuators B*, 135, **2008,** 46-51.

3) Evans, R.C; Douglas, P., *Anal. Chem.*, 78, **2006,** 5645-5652.

4) Evans, R.C.; Douglas, D.;Williams, J.A.G.; Rochester, D.L. *J. Fluores.*,16, **2006,** 201-206.

5) Wang, X.; Chen, X.; Zhao-xiong; X.; Wang, X., *Angew. Chem. Int. Ed.*,47, **2008,** 7450-7453.

6) Mills, A, *Analyst,* 124, **1999,** 1301-1307.

7) Bandrup, J.; Immergut, E.H.; Grulke, E.A., *Polymer Handbook, 4th ed.,* Wiley.

8) Farley, S.J.; Rochester, D.L.; Thompson, A.L.; Howard, J.A.K.; Williams, J.A.G. *Inorg. Chem.,* 44, **2005**, 9690-9703.

9) Hunt, R.W.G., *Measuring Colour, 3rd ed.,* Fountain Press, (1998).

10) Evans, R.C.; Douglas, D.; Williams, J.A.G.; Rochester, D.L. *J. Fluores.*,16, **2006**, 201-206.

11) Maekawa, S., *Oxygen-Free Museum Cases, 1st ed.*, The Getty Conservation Institute, (1998), pp 1-15.

12) Daniel, V.; Lambert, F.L. *W.A.A.C. Newsletter,* 15, **1993,** 12-14.

13) Daniel, V.; Hanlon, G.; Maekawa, S. *W.A.A.C. Newsletter,* 15, **1993,** 15-19.

14) Mills, A. *Chem. Soc. Rev.,* 34, **2005,** 1003-1011.

15) Castlado, A.; Massera, E.; Quercia, L.; Di Francia, G. *Sens. Actuators B,* 118, **2006,** 328-332.

16) McLachlan, B.G.; Bell, J.H. *Exp. Therm. Fluid Sci.,* 10, **1995,** 470-485.

17) Hradil, J.; Davis, C.; Mongey, K.; McDonagh, C.; MacCraith, B.D. *Meas. Sci. Technol.,* 13, **2002,** 1552-1557.

18) Hartmann, P.; Leiner, M.J.P.; Kohlbacher, P. *Sens. Actuators B,* 51, **1998,** 196-202.

19) Fuller, Z.J.; Bare, W.D.; Kneas, K.A.; Xu, W-Y.; Demas, J.N.; DeGraff, B.A. *Anal. Chem.,* 75, **2003,** 2670-2677.

20) Coucouvanis, D; Fackler, J.F., *Inorg. Chem.,* 6, **1967,** 2047-2053.

21) Demas, J.N; Crosby, G.A., *J. Phys. Chem.,* 75, **1971,** 991-1024.

22) Hughes, V.A.; Douglas, P. *J. Fluoresce.*, 16, **2006,** 403-409.

23) Norman, K.; Ghanbari-Siankali, A.; Larson, N.B. *Annu. Rep. Prog. Chem. Sect. C,* 101, **2005,** 174-201.

24) Li, Bo.; Santhanam, S.; Schultz.; Jeffries-EL, M.; Iovu, M.C.; Sauve, G.; Cooper, J.; Zhang. R.; Revelli, J.C.; Kusne, A.G.; Synder, J.L.; Kowalewski, T.; Weiss, L.E.; McCullough.; R.D.; Fedder, G.K.; Lamberth, D.N. *Sens. Actuators B,* 123, **2007,** 651-660.

25) deGans, B.; Schubert, U.S. *Langmuir,* 20, **2004,** 7789-7793.

26) Yoldas, B.E. *Sol-gel Sci. Tech.,* 13, **1998,** 147-152.

27) Horng-Show, K.; Mi, C.; Po-Chaun, P. *Thin Solid Films,* 515, **2006,** 896-901.

28) Tuladhar, T.R.; Mackley, M.R. *J. Non-Newtonian Fluid Mech.,* 148, **2007,** 97-108.

29) Calvert, C. *Chem. Mater.,* 13, **2001,** 3299-3305.

30) Tekin, E.; deGANS, B.; Schubert, U.S. *Chem. Mater.* 14, **2001,** 2627-2632.

31) European Patent application EP 1 783 179 A1.

32) Yoldas, B.E. *Sol-gel Sci. Tech.,* 13, **1998,** 147-152.

33) Briston, J.H; Katan, L.L, *Plastic Films, 1st ed.,* London Lliffe Books, (1974), 220-232.

34) Mills, A; Lepre, A., *Anal. Chem.,* 69, **1997,** 4653-4659.

35) Mills, A, *Platinum Metals Rev.,* 41, **1995,** 115-127.

36) Hartman, P; Trettnak, W. *Anal. Chem.,* 68, **1996,** 2615-2620.

371) Mills, A, *Sens. Actuators B,* 51, **1998,** 60-68.

38) Kreitner, M.; Ebermann, R.; Alth, G. *J. Photochem. Photobiol. B,* 36, **1996,** 109-111.

39) Popsil, J.; Nespurek, S.; Pilar, J. *Polym. Degrad. Stab.,* 93, **2008,** 1681-1688.

40) Wilkinson, F.; Helman, W.P.; Ross, A.D, *Chem. Ref. Data,* 24, **1995,** 663-677.

41) Schweitzer, C; Schmidt, *Chem. Rev.,* 103, **2003,** 1685-1757.

42) Quannes, C.; Wilson, T. *J. Am. Chem. Soc.,* 90, **1968,** 6527-6528.

43) Monroe, B.M.; Mrowca, J.J, *J. Phys. Chem.,* 83, **1979,** 591-595.

44) Velioglu, Y.S.; Mazza, G.; Gao, L.; Oomah, B.D. *J. Agric. Food Chem.,* 46, **1998,** 4113-4117.

45) Gorman, A.A.; Gould, I.R.; Hamblett, I.; Standen, M.C. *J. Am. Chem. Soc.,* 106, **1984,** 9656-6959.

46) Fearon, P.K.; Phease, T.L.; Billingham, N.C.; Bigger, S.W. *Polymer,* 43, **2002,** 4611-4618.

47) Gao, R.; Ho, D.G.; Dong, T.; Khuu, D.; Franco, N.; Oemer, S.; Selke, M. *Org. Lett.,* 3, **2001**, 3719-3722.

48) Bolduc, P.R.; Goe, G.L. *J. Org. Chem.,* 39, **1974,** 3178-3179.

49) Garrido-Lopez, A.; Sancet, I.; Montano, P.; Gonzalez, R.; Tena, M. *J. Chromatogr. A,* 1175, **2007,** 154-161.

50) Captitan-Vallvey, L.F; Asensio, L.J; Lopez-Gonzalez, J; M.D. Fernandez-Ramos, M.D; Palma, A.J, *Anal. Chim. Acta.,* 583, **2007,** 166-173.

51) A.J; Lopez-Gonzalez, J; Asensio, L.J; Fernandez-Ramos, M.D; Captan-Vallvey, L.J., *Sens. Actuators B,* 121, **2007,** 629-638.

A novel colorimetric pressure sensitive paint

4.1 Summary

One of the most significant limitations in the application of luminescence oxygen sensors is the temperature dependent response they show. This temperature dependence arises from a combination of the temperature dependence of both the solubility and diffusion of oxygen in the polymer matrix support. The most common approach to dealing with this problem is the use of a dual lumophore sensor in which one lumophore is temperature sensitive only, while the other is sensitive to both temperature and pO_2 .[1-5]

The aim of this chapter was to develop a "proof of concept" colorimetric pressure sensitive paint in which the temperature is measured colorimetrically under visible light, while pO_2 is measure colorimetrically by emission under UV light. Thus producing a pressure sensitive paint that shows the air flow over the surface under UV light, and the temperature of the surface under visible light. The two lumophores chosen for the colorimetric oxygen sensors are coumarin 110 and PtOEP which give a blue to red colour change on decreasing oxygen partial pressure. The temperature sensitive layer is based on $CoCl_2$ in polyvinyl alcohol with H_3PO_4, which gives a pink to blue colour change with increasing temperature over the range 0 °C to 50 °C. Throughout the text the full pressure sensitive paint sensor is referred to as PSPSENS.

4.2 Introduction

Pressure Sensitive Paints (PSPs) are paints that are applied to cars and aeroplanes[6-8] so that when they are placed in a wind tunnel the flow of air around the object can be seen and the aerodynamics of the vehicle visualised. They are of considerable interest because they are cheaper and provide a more accurate picture of the air flow over a surface than the use of discreet pressure taps. Prior to the development of PSPs pressure taps were placed at key points over the surface and the data collected was extrapolated to predict the flow over the whole surface. It is estimated that the cost of using pressure taps could be between $ 1 million and $ 500,000 to develop a complete aerodynamic model for an aeroplane.[9]

PSP's are essentially oxygen sensors, such as those described in this thesis in chapter 3, which are used to measure the partial pressure of oxygen and hence the total gas pressure at any point on the surface under examination. It is possible to monitor the flow of air over a large area and gain an accurate picture of the flow over a whole object.[1,9] The earliest examples of PSPs consisted of an oxygen quenchable lumophore, either PtOEP [10,11] or ruthenium tris(bipyridyl),[12-14] in a polymeric binder, which gives concomitant change in luminescent intensity with increasing oxygen partial pressure. In studies of oxygen sensors that have been discussed in this thesis so far, the change in luminescence has been obtained by using different mixtures of oxygen and nitrogen at one atmosphere total pressure. In a wind tunnel the atmospheric composition remains the same and changes in luminescence occur because as air flows around an object areas of higher and lower pressures are created, which manifest themselves as differing partial pressures of oxygen.

For the purposes of aerodynamic testing the Stern-Volmer equation is used in the form given in equation 4.1. Here A(T) and B(T) are temperature dependent coating parameters, which are determined by experimental calibration at different temperatures.[9]

$$I_0/I = A(T) + B(T)\, P/P_0 \qquad [4.1]$$

I is the emission intensity with air flow, I_0 is the emission intensity in the absence of air flow (the so called wind off measurement), P_0 is pressure in the absence of air flow, and P is pressure with air flow.

There are, however, a number of problems with the development of PSPs. The most significant is that emission from these sensors is temperature dependent. As the temperature increases the sensitivity of the sensor increases, and a higher degree of quenching is observed. [1-5] (In a colorimetric oxygen sensor, such as the one developed here, this means that the colour change is observed at a lower oxygen partial pressure than would be observed at room temperature.)

To compensate for this effect two lumophores can be integrated into the same sensor: one of which is a temperature sensor, and is calibrated for temperature changes and is independent of changes in oxygen partial pressure, which is used as a reference to correct the response of the other lumophore which is sensitive to both pO_2 and temperature.[13-14]

Another problem is that luminescence response is dependent on the intensity of the excitation source, and so any change in excitation intensity manifests itself as change in intensity of the sensor.[16] A possible solution to this is to measure the lifetime of the lumophore since this is independent of the excitation intensity. However this has the added problem that sophisticated optical arrangements are needed to analyse lifetimes, which considerably increases the cost of the technique.[10]

In this chapter a sensor is described, and developed to the proof of concept stage, which has the potential to overcome all of these problems. The sensor consists of a colorimetric oxygen sensor that has two lumophores making it ratiometric and therefore independent of variation in excitation intensity. To correct the changes that occur in emission due to temperature an absorption based temperature sensitive layer, (this part of the full PSPSENS will be referred to as the TSL), is used to indicate any changes in temperature so that the response of the colorimetric pressure sensitive paint, (this part of the full PSPSENS will be referred as the CPSP), can be calibrated accordingly. When both the TSL and the CPSP are together in one sensor the sensor is referred to as PSPSENS. Under visible light the TSL can be observed, while under UV irradiation the CPSP is seen, thus the partial pressure of oxygen across the whole of an object can be obtained simply by imaging firstly in visible light and then under UV light with the same camera.

4.3 Materials

Anhydrous cobalt chloride, coumarin 110, ethyl cellulose (46 % ethoxyl content), 80 % ortho phosphoric acid in water, polyvinyl alcohol M.W. 72,000, and gelatin were

all purchased from Sigma-Aldrich. PtOEP was purchased from Frontier Scientific. White acrylic paint was Decoart Crafter's Acrylic purchased from Harrison Stationers Ltd, Swansea. Premixed gases (40 % oxygen in nitrogen, and 63 % oxygen in nitrogen), nitrogen, air and oxygen were all obtained from BOC gases.

4.4 Methods

Temperature controlled emission spectra were obtained using a Perkin Elmer MPF 44-E fluorimeter. The sensor was placed on a modified sample holder, and the premixed gases were passed through a 2 m coil of copper tubing in a column heater (Anachem PE 442266). A thermocouple was placed in the sample holder to determine the temperature of the gases at the sensor. The emission correction factors for the fluorimeter were obtained using the method of Demas and Crosby as described in the experimental section.[18] CIE colour coordinates were calculated using the colour matching functions given in ref. 19.

Diffuse reflectance measurements were obtained using a Perkin-Elmer Lambda 9 UV/VIS/NIR spectrophotometer with a diffuse reflectance attachment. Measurements at different temperatures were obtained by preheating the slides to a known temperature and rapidly recording the spectra, (the rate of cooling of the sensor slides is slow enough to allow the recording of spectra without a significant temperature loss, see fig.4.7). CIE coordinates were calculated for the absorption curves using the colour matching function for emission curves under the standard daylight illuminant D^{65}.[19]

Responses of the temperature sensitive layer were recorded using a Hewlett Packard 825A diode array spectrometer in kinetic mode with the cell holder cycled between 18°C and 55 °C using a Tecam C-400 Circulator.

Temperatures below 0 °C were obtained by placing the sensor in a freezer.

4.5 Results and Discussion

4.5.1 Preparation of the sensor (PSPSENS)

The sensors are produced by spin coating layers one on top of one another on a glass slide (Fig. 4.1). The layers, in order of deposition, are as follows:

1 - The first layer is white acrylic paint, which acts as a diffuse reflective surface.

2 – The second layer is ethyl cellulose, which acts as a protective barrier layer to prevent destruction of the first acrylic layer when the third layer is applied. The ethyl cellulose is laid-down from a 10 % solution (w:v) in 80:20 toluene:ethanol.

3 - The third layer is the temperature sensitive layer (TSL). The solution used is prepared as follows. 0.74 g of cobalt chloride is dissolved in 4 g of aqueous 10 % PVA and then 1.4 g of phosphoric acid is added. Once this layer is spin coated the slide is heated to 50 °C on a hot plate for 45 minutes and then while hot the fourth layer is rapidly applied.

4 – The fourth layer is identical to the second and has the same function.

5- The fifth layer is the colour anchor layer. It also is applied while the slide is still hot, and the solution used to lay it down is made as follows. 2 mg of dye, either coumarin 110 or coumarin 153, is dissolved in 1 ml tetrahydrofuran (THF), and 0.4

ml of this solution is added to 1 g 10 % ethyl cellulose (w:v) in 80:20 toluene:ethanol.

6- Layer six is deposited from a 10% gelatin-in-water barrier layer, applied after the slide has cooled.

7 - The seventh and final layer is the oxygen sensitive layer. The solution used to lay this down is prepared as follows. 1 mg of PtOEP is dissolved in 1 ml THF and 0.4 ml of this solution is added to 1 g 10% ethyl cellulose in 80:20 (v/v) toluene:ethanol.

All layers were spin coated with a spin coated at a spin speed of 1500 rpm.

As Figure 4.2 shows, the addition of each of the layers does not affect the previous layers.

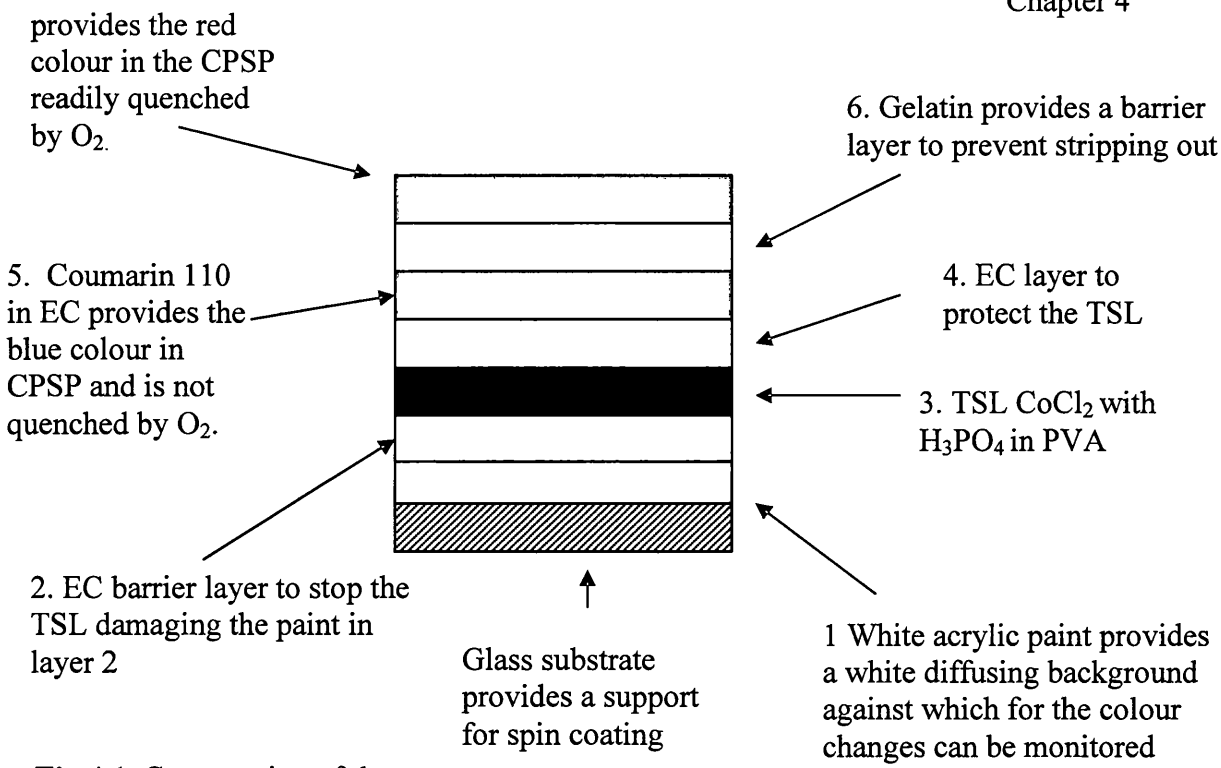

Fig.4.1. Construction of the sensor

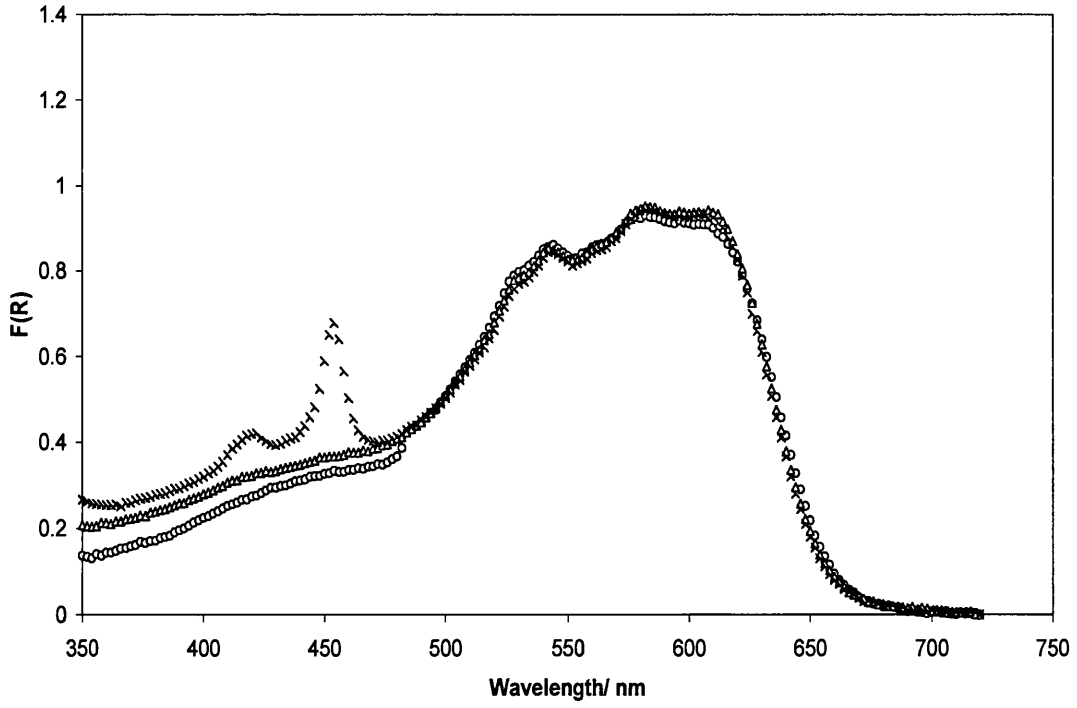

Fig.4.2. The changes in the diffuse reflectance spectrum of the sensor as different layers are spin coated on top of each other. The three spectra are: after layers 1-3 including the TSL (circles); layers 1-5 including the coumarin 110 layer (triangles), and layers 1-7 including the PtOEP layer (crosses).

4.5.2 Development of the Temperature Sensitive Layer, TSL

A number of different sensors were evaluated for the TSL. The first sensor examined was a carbon dioxide sensor that was based on the pH indicator phenolphthalein with a tetraoctylammonium hydroxide buffer encapsulated in an EC polymer matrix.[20] The equilibrium between the dye and the buffer is temperature dependent, and with an increase in temperature, as the deprotonated form of the dye becomes more prevalent, a purple colour develops. However, despite the fact carbon dioxide makes up approximately 0.03 % of the atmosphere, once the sensor was covered with non permeable layers the sensor response was severely reduced and so this was not chosen for the TSL.

The spiropyran (1'3'-dihydro-8-methoxy-1'3'3'-trimethyl-6-nitrospiro[2H-1-benzopyran-2,2'(2H)-indole]) was assesses as a possible TSL as spiropyrans are reportedly thermochromic as well as photochromic[21], however this compound only displayed photochromic behaviour and the spiropyrans as a class were not investigated further.

Crystal violet lactone[22] has been used as a temperature sensitive indicator in thermal printing and this was considered as another promising candidate for the TSL. However the thermal head printing uses microencapsulation whereby the deprotonated dye is encapsulated in wax in an acidic polymer layer. On heating the wax microspheres melt, the crystal violet lactone is protonated and a colour change can be observed. This approach was not followed further due to the difficulty in producing the microencapsulation, and obvious lack of reversibility.

Eventually, for our proof of principle application, $CoCl_2$ was chosen as the TSL layer, because it had already been demonstrated that it could be placed in polymeric matrices[25], and it gave a clear colour change at low temperatures that could be easily created in the laboratory. Other inorganic thermochromic complexes such a $Cu_2Hg_2I_4$[23] and VO_2 [24] also look to be promising candidates for the TSL, and could be utilised as such in future applications because they have different temperature ranges to $CoCl_2$.

4.5.3. Cobalt Chloride TSL

The TSL of the sensor makes use of the thermochromic behaviour of cobalt chloride. This gives a pink to blue colour change (fig.4.3) when the complex changes from an octahedral $[Co(H_2O)_6]^{2+}$ complex to a tetrahedral $[Co(H_2O)_4]^{2+}$ complex,[26]

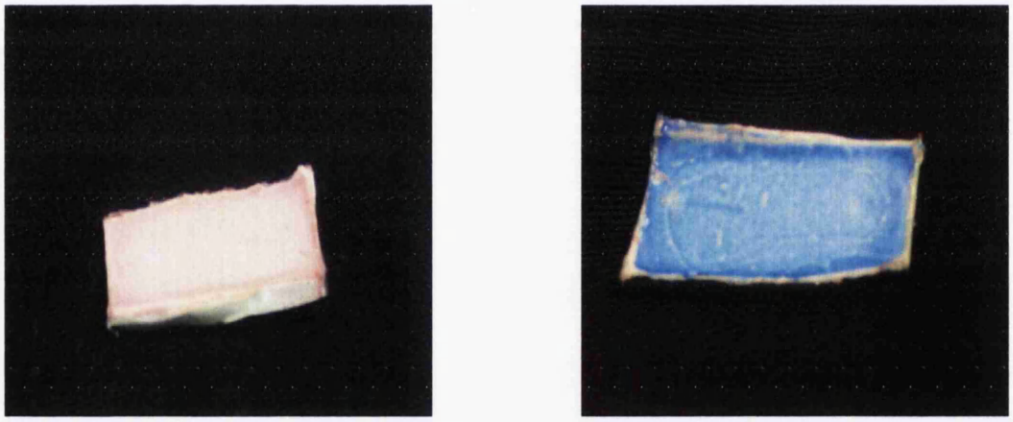

Fig.4.3. PSPSENS at room temperature (left) and at 50 °C (right)

Due to this easily identifiable colour change and its ability to be easily incorporated in a polymer matrix it is an ideal candidate for the TSL. We have followed the practise of previous workers in using phosphoric acid as a complexing agent additive

to modify the film (fig.4.4). The addition of phosphoric acid results is the development of linkage between the polymer chain and the cobalt cation, which gives a sensor with a more gradual colour change (fig.4.5) due to a higher enthalpy required to hydrate and dehydrate the cobalt cations in these chains.[27,28]

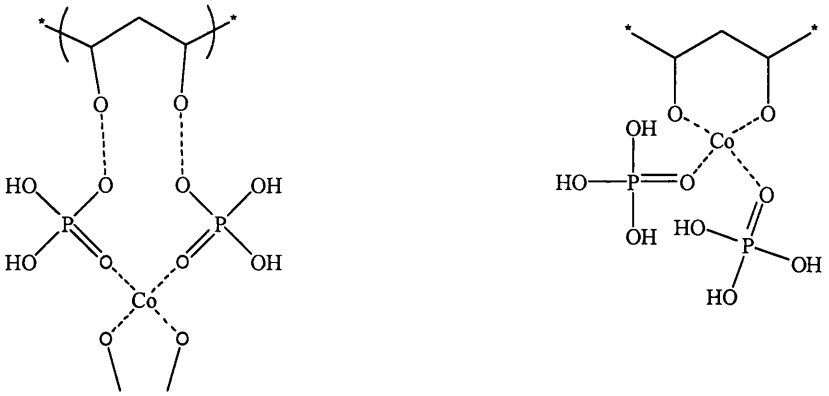

Fig.4.4. Complexes formed between the cobalt cation, phosphoric acid and PVA in the TSL.[24,25] The two possible complexes which can be formed between the cobalt cation and the phosphoric acid and PVA are shown here.

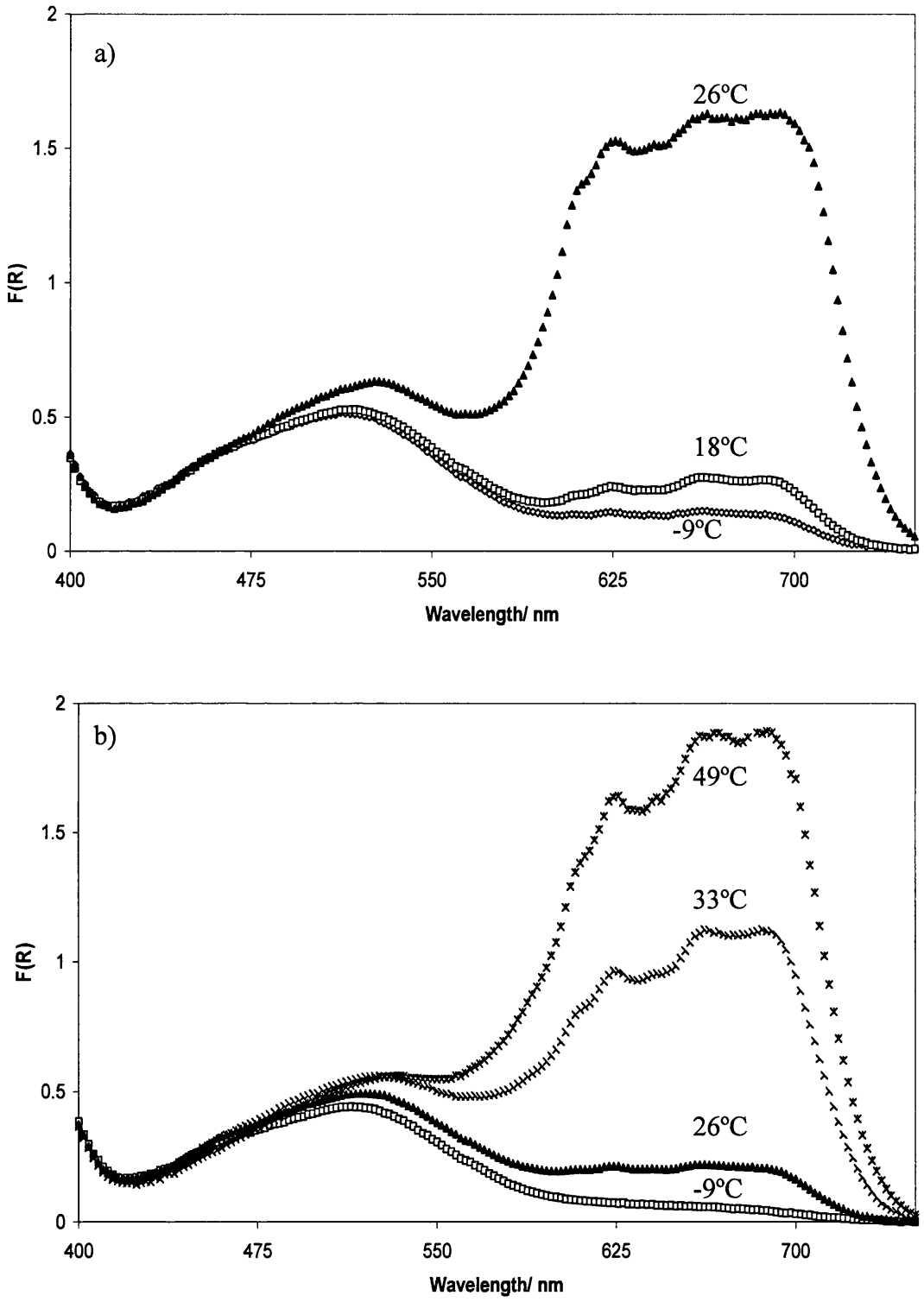

Fig.4.5. Absorption spectra of the cobalt chloride TSL a) TSL with no phosphoric acid present at: -9 °C, 18 °C and 26 °C and b) TSL with phosphoric acid at -9 °C, 26 °C, 33 °C and 49 °C.

The response time for changes in the TSL is relatively slow (fig.4.6), which can be used beneficially. The diffuse reflectance instrument was not temperature controlled, and therefore it was not possible to make internally controlled temperature dependent diffuse reflectance measurements. However, because the temperature response is so slow very little change occurs even over the few minutes or so required to measure a spectrum (fig.4.7.).

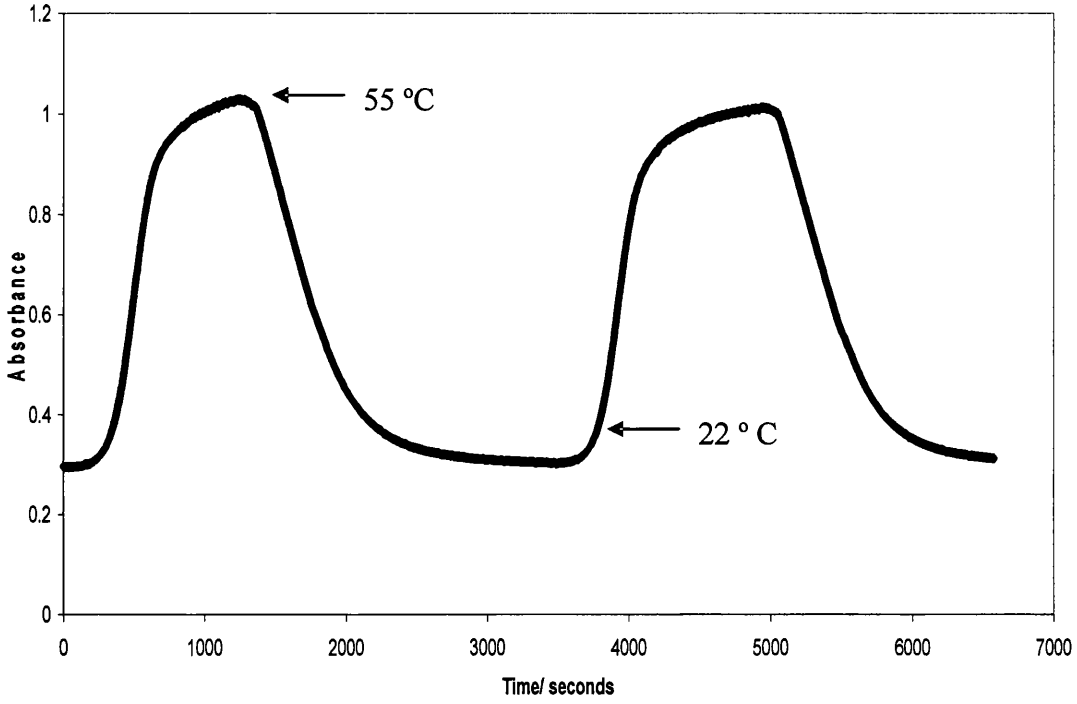

Fig.4.6. The reversible response of the TSL where the temperature is switched between 22 °C and 55 °C, absorbance measured at 664 nm

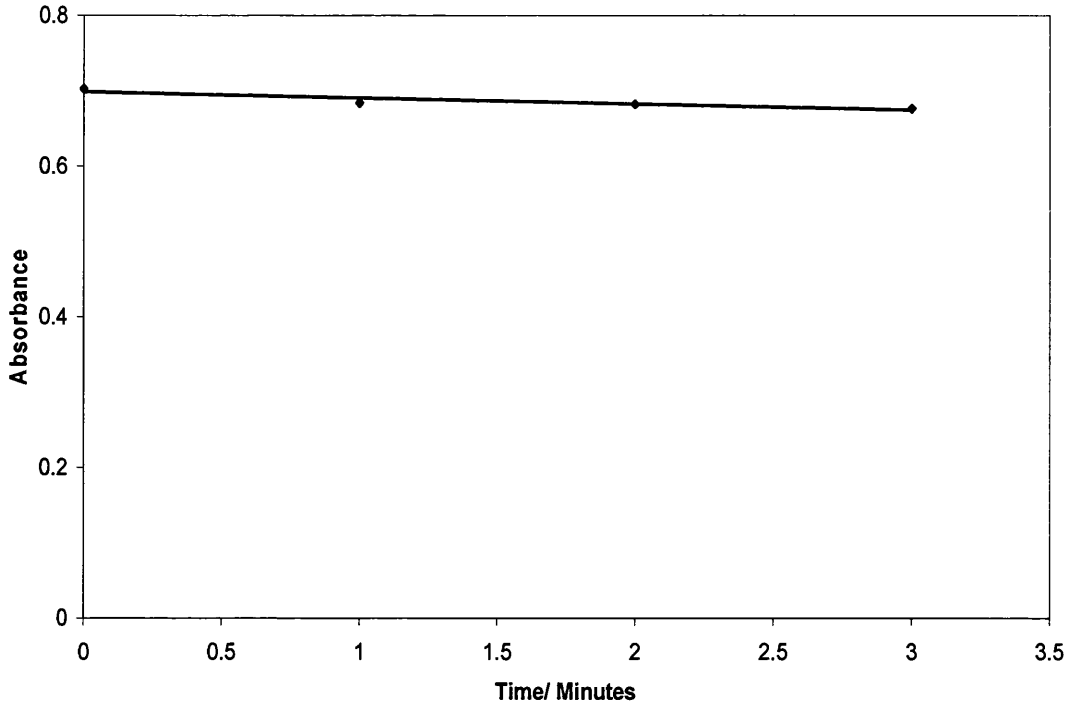

Fig.4.7. The absorption of the TSL at 664 nm after being heated to 50°C, and then being allowed to cool at room temperature, slope = -0.0079 A/ min

The technique of using pseudo temperature controlled diffuse reflectance was used to measure the temperature dependent spectra of the TSL shown in fig.4.8. These were recorded as reflectance, which was needed to calculate the CIE co-ordinates of the TSL, shown in table 4.1, and which could be used to obtain the Kubelka Munk function F(R) by equation 4.2.

$$F(R) = (1-R)^2 / 2R \qquad [4.2]$$

F(R) is the Kubelka Munk function, while R is reflectance[19]

The colour change of the TSL can be seen to be non linear (fig.4.9) with temperature. There is an initial slow change from -9 to 20 °C, and then a sharp change in

absorption between 20 °C and 40 °C followed by a slower change at temperatures greater than 40 °C. The colour change of blue to pink colour change of the TSL can be seen in fig.4.3.

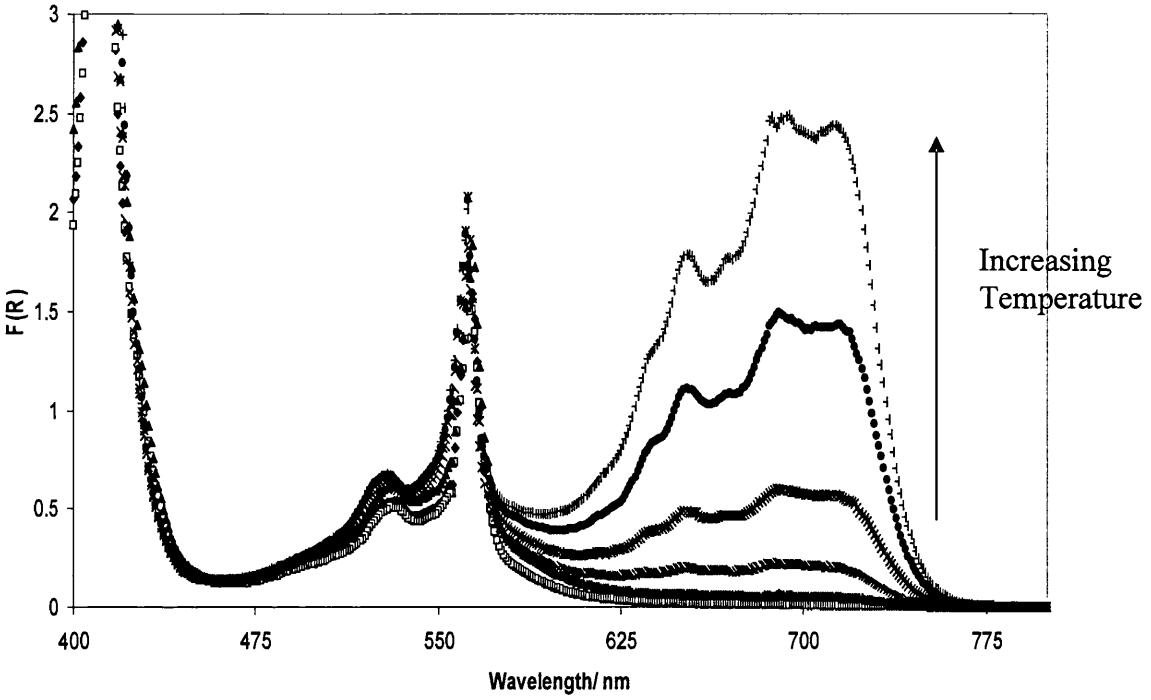

Fig. 4.8. Changes in the diffuse reflectance spectra of the TSL with temperature at: -9 °C, 16 °C, 25 °C, 22 °C, 34 °C, 42 °C and 50 °C, from which the CIE coordinates in table 4.1 were calculated

Temperature °C	CIE Coordinates
-9	x = 0.35, y = 0.31
16	x = 0.34, y = 0.31
25	x = 0.33, y = 0.30
29	x = 0.32, y = 0.30
34	x = 0.31, y = 0.29
42	x = 0.29, y = 0.29
50	x = 0.28, y = 0.29

Table 4.1. CIE Coordinates for the spectra shown in fig 5.8 for the temperature dependence of the sensor under the standard illuminant D^{65}

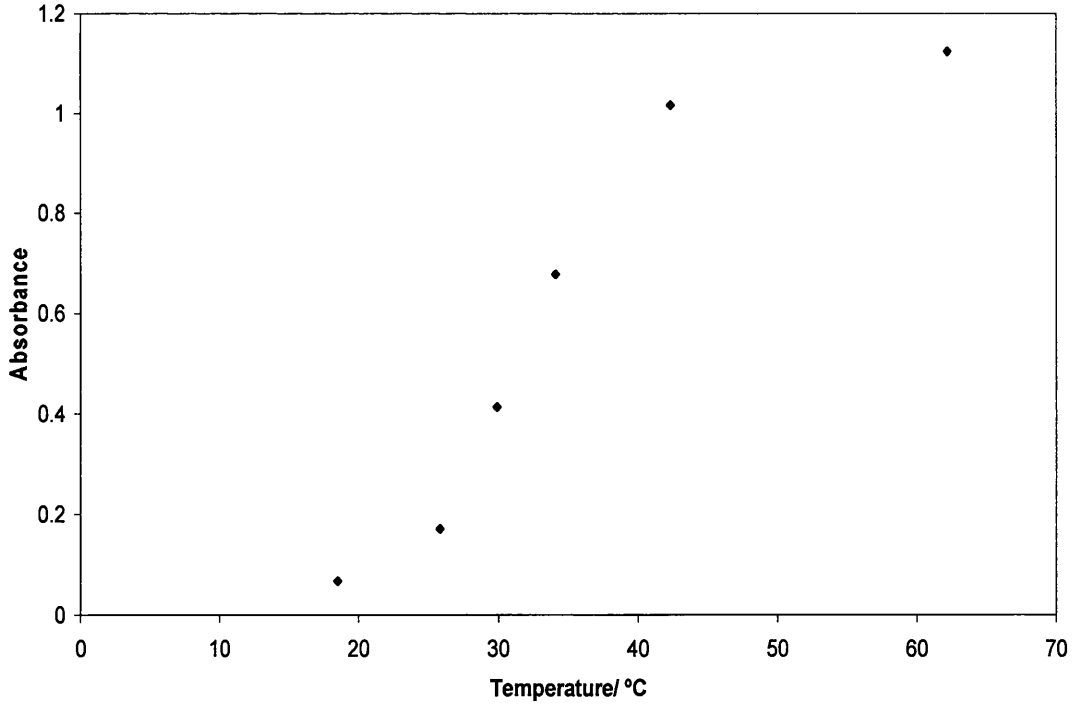

Fig.4.9. Changes in the absorption spectra of a TSL at 655 nm, which is the wavelength of maximum emission from PtOEP

4.5.4 Colorimetric pressure sensitive paint

The colorimetric pressure sensitive paint is based on a dual lumophore oxygen sensor similar to those sensors previously described in chapter 3. Two lumophores are used which have different sensitivities to oxygen. One lumophore is selectively quenched over the other, resulting in a change in emission colour.[29]

As previous discussed in chapter 3 the ideal colour change is a "traffic light" red to green colour change.[19] The first lumophore combination used was the green emitting coumarin 153 with PtOEP, in order to have a green to red colour change, however the visible absorption of coumarin 153 was shown to alter the apparent colour of the TSL at room temperature from pink to a brownish yellow, (fig.4.10) Therefore it was decided to use a combination of coumarin 110 and PtOEP to produce a red to blue colour change on increasing oxygen partial pressure (fig.4.11). This had the advantage that it did not affect the colour change of the TSL (fig.4.10), because even in at the high concentrations used to make the CPSP coumarin 110 only weakly absorbs in the visible region.

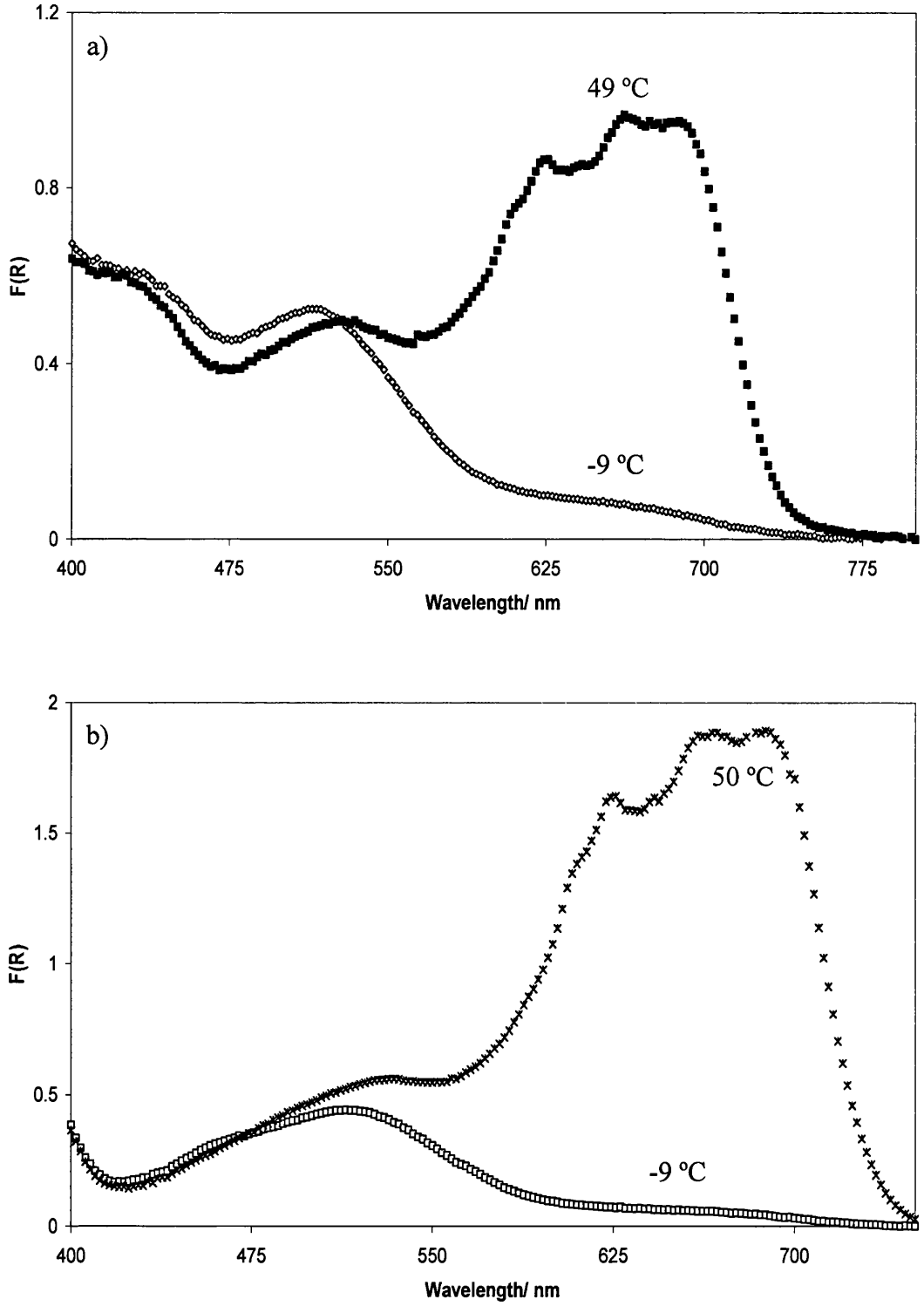

Fig. 4.10. Diffuse reflectance spectra of; a) a TSL with a coumarin 153 layer spin coated above it at -9 °C and 49 °C, b) a TSL with a coumarin 110 spin coated above it at -9 °C and 50 °C

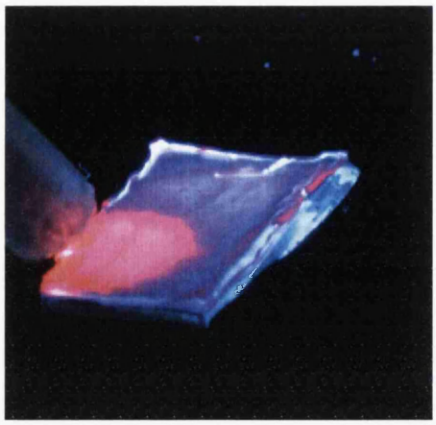

Fig.4.11. PSPSENS excited with UV light under air (blue emission) and nitrogen (red emission). The tip of the micropipette used to deliver nitrogen can be seen in the mid left of the image

4.5.5 Effect of temperature on the response of the CPSP

It is well known that the response of oxygen sensing optodes is sensitive to temperature, becoming more sensitive as the temperature increases.[1-5] This is shown for PtOEP in fig.4.12, whereby K_{SV} is shown to increase with temperature. If the emission from coumarin 110 were temperature dependent in the same way then this effect would not be so important. However, from figs.4.13 and 4.14, it can be seen that the emission from a single coumarin 110 layer in EC on a glass substrate is not affected by either oxygen concentration or temperature, and therefore the colour change of the CPSP will be both oxygen and temperature sensitive and this can be seen in fig. 4.15. It is therefore necessary to compensate the emission from the CPSP, by using the TSL as a reference.

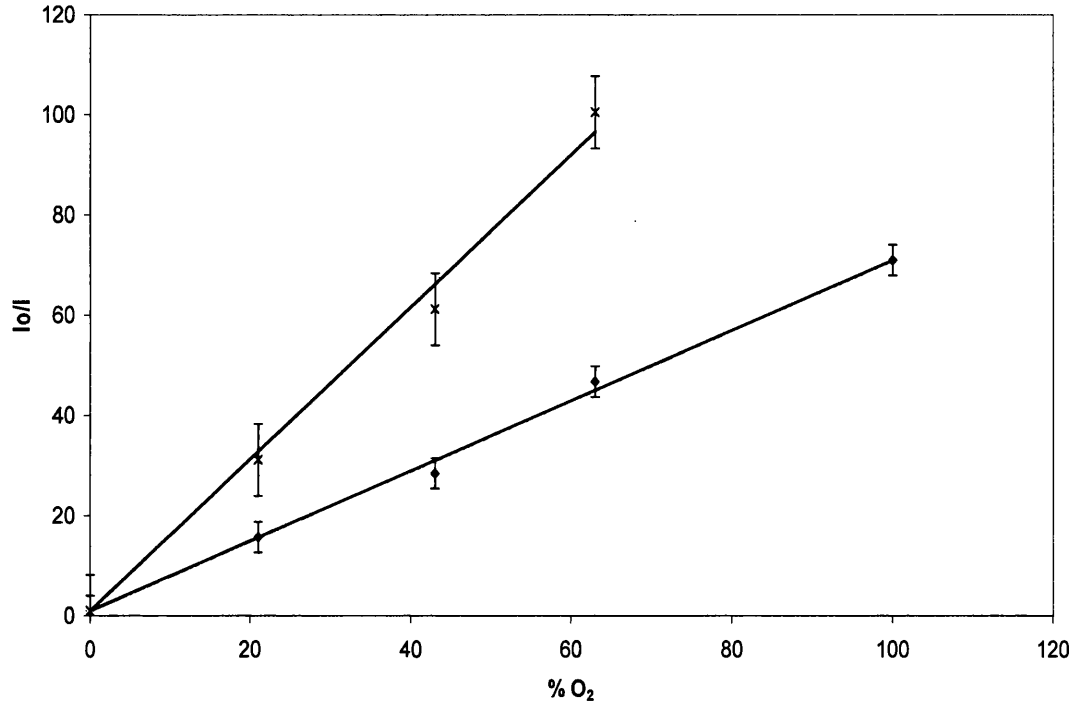

Fig.4.12. The changes in the Stern-Volmer constants with temperature for PtOEP in EC at: 18°C, $K_{SV} = 0.6995$ $R^2 = 0.9919$, and 51°C $K_{SV} = 1.5164$ $R^2 = 0.9967$

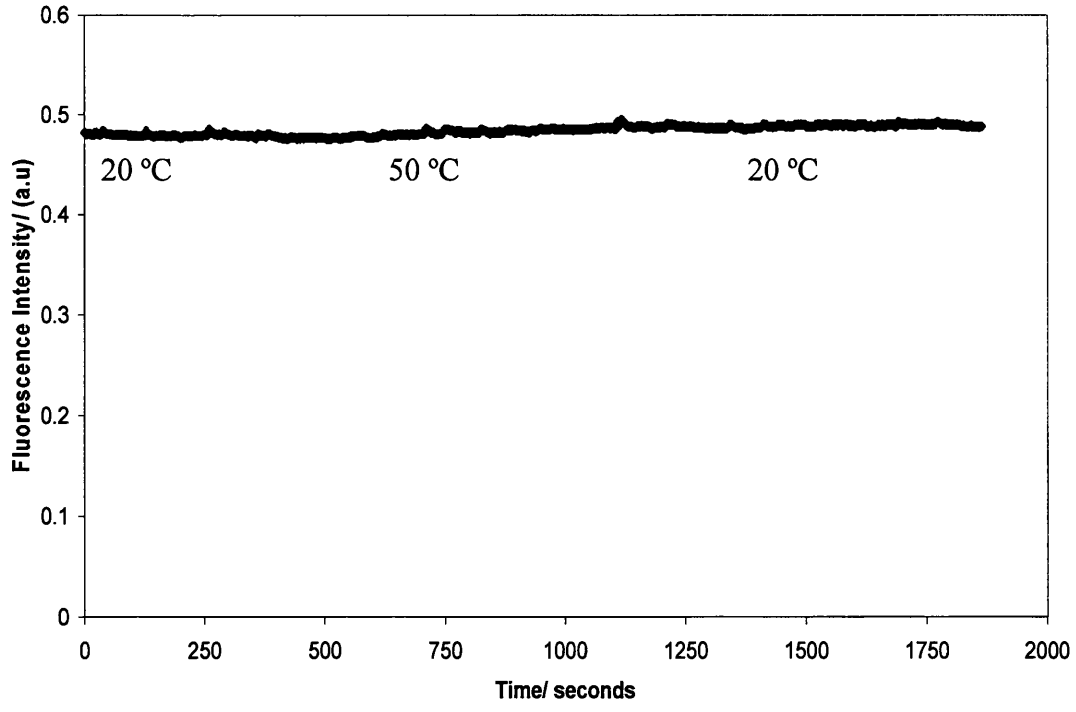

Fig.4.13. Changes in the coumarin 110 absorption peak recorded at 356 nm with temperature cycled between 20 and 50 °C

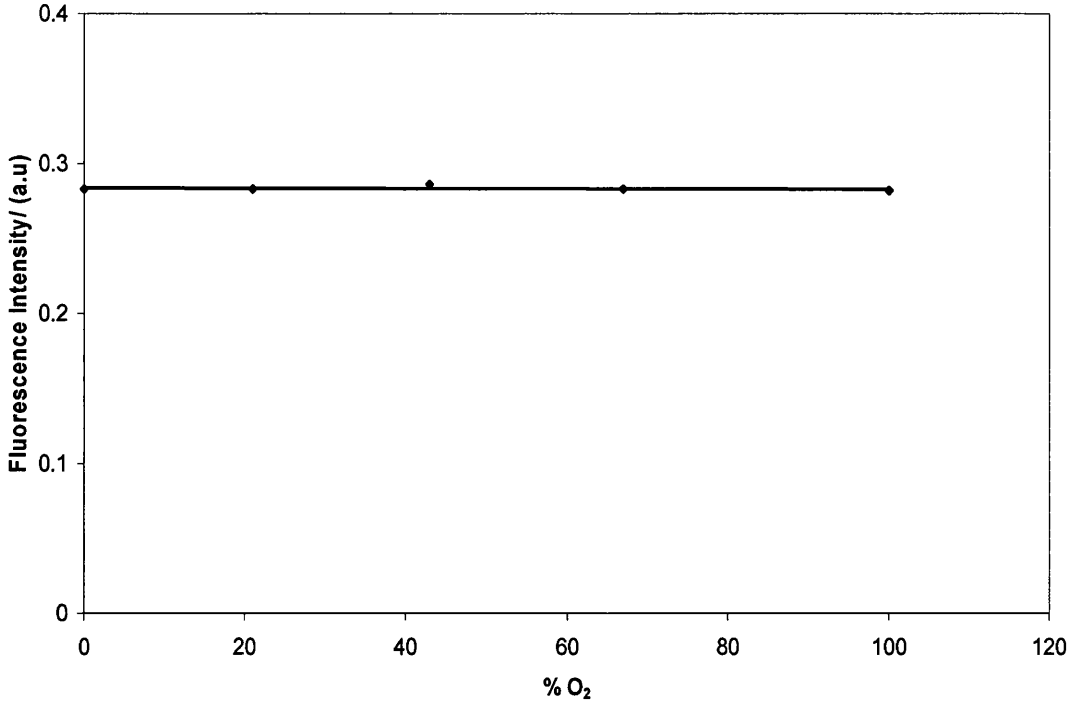

Fig.4.14. Changes in the coumarin peak at 421 nm at 33 °C with changing oxygen percentage

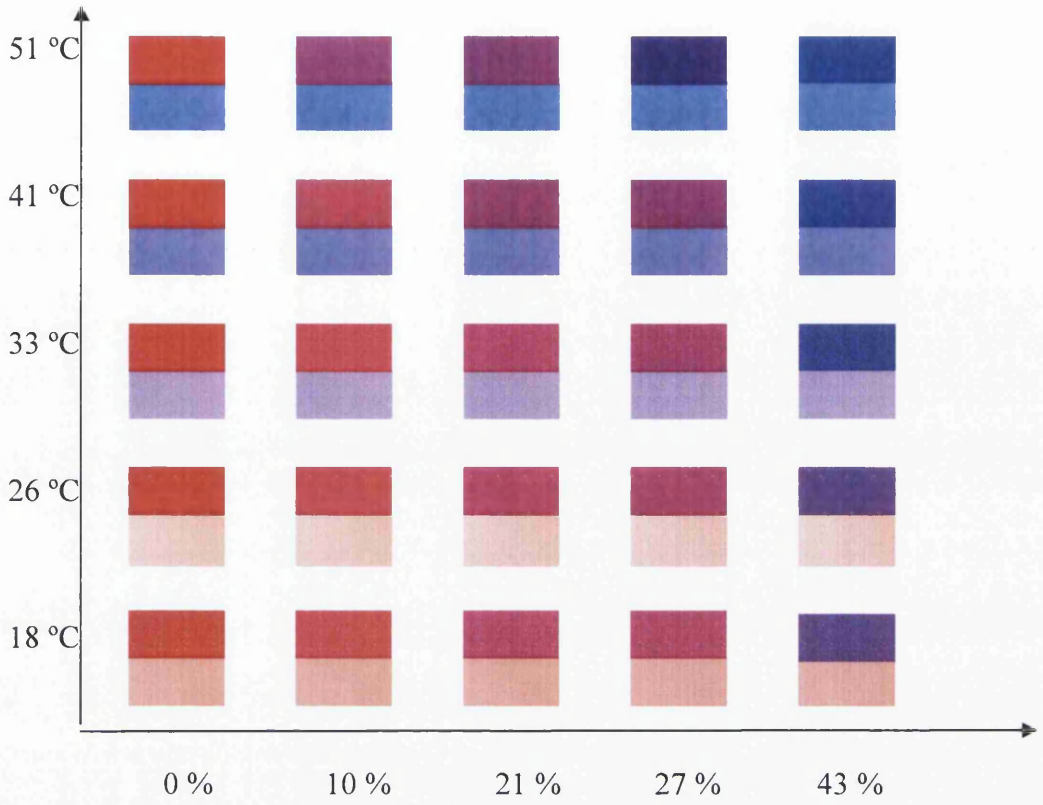

Fig.4.15. The observed colour scale for PSPSENS. The bottom half of each of the cells is the colour of the TSL and the upper half the colour for the CPSP, the temperature and colour ranges have been chosen to demonstrate the complete colour change of the sensor

4.5.6 Correcting the emission from CPSP

To correct the CPSP response the emission peaks for the CPSP (coumarin 110 λ_{max} = 421 nm, and PtOEP λ_{max} = 645 nm) were both treated separately. The PtOEP peak at 645 nm was modelled using the simple model of Yu-Lung *et al.*.[30] From equation 4.3 a temperature dependent correction factor C(T) can be obtained (fig 4.16). In practice C(T) varies slightly over the different partial pressures for a specific temperature so an average value is taken.

$$C(T) = \frac{I_0(T)}{I(T)} - \frac{I_0(T_{ref})\, Ksv(T_{ref})[\%O_2(T)]}{I(T)[1 + K_{SV}(T_{ref})[\%O_2(T)]} \qquad [4.3]$$

$$I_m(T) = I(T)\, C(T) \qquad [4.4]$$

C(T) is the temperature compensation coefficient; $I_0(T)$ is the luminescence intensity in the absence of oxygen at the reference temperature (18 °C); I(T) the luminescence intensity at the temperature of interest; $K_{SV1}(T_{ref})$ is the Stern Volmer constant at the reference temperature. By multiplying I(T) by C(T) $I_m(T)$ the modified intensity can be obtained which should be the same as $I_0(T)$ (eq. 4.4).

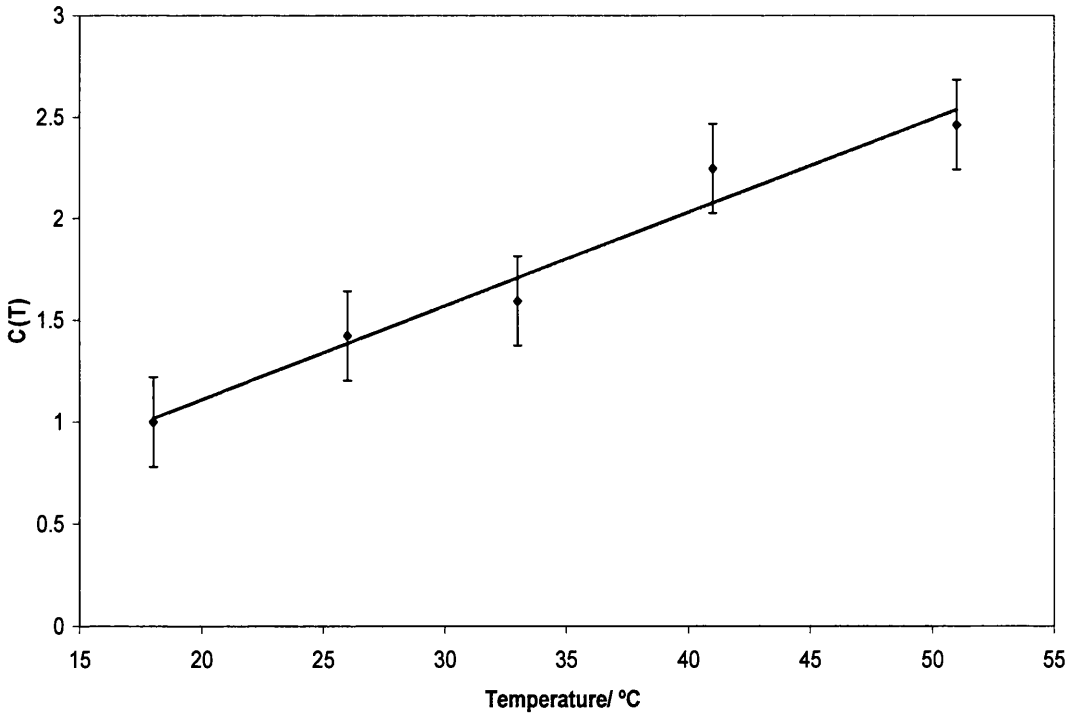

Fig.4.16. Average values for C(T) for the different temperatures $R^2 = 0.9661$

From fig.4.14 it was assumed that the emission from the coumarin 110 component would not change with temperature in the complete sensor, however, it was

discovered that the coumarin 110 emission intensity does change when incorporated into a full sensor with all layers present. This can be attributed to two factors, the first is that the absorption of the PtOEP layer above the coumarin layer can be shown to be decreasing with temperature (fig.4.17), therefore the coumarin layer receives more photons from the excitation source with increasing temperature, and this results in an increased emission from the coumarin layer. The decrease in absorption of the PtOEP layer may be the result of the changing refractive index of the polymer[14] with temperature although this is not known with any certainty and would require further work. The second factor is the absorption of the TSL (figs.4.8 and 4.9) which increases rapidly with temperature. While this is in a layer below that containing coumarin 110 the effect on the reflected excitation light, and emission from the coumarin, is still enough to have an effect, particularly at low temperatures (fig. 4.18). This is clearly undesirable behaviour, but it can be compensated for using a calibration curve, as shown in Fig 4.19. For the temperature range examined the data can be shown to fit to a cubic expression. The correction factor obtained from this analysis is denoted X in the subsequent discussion.

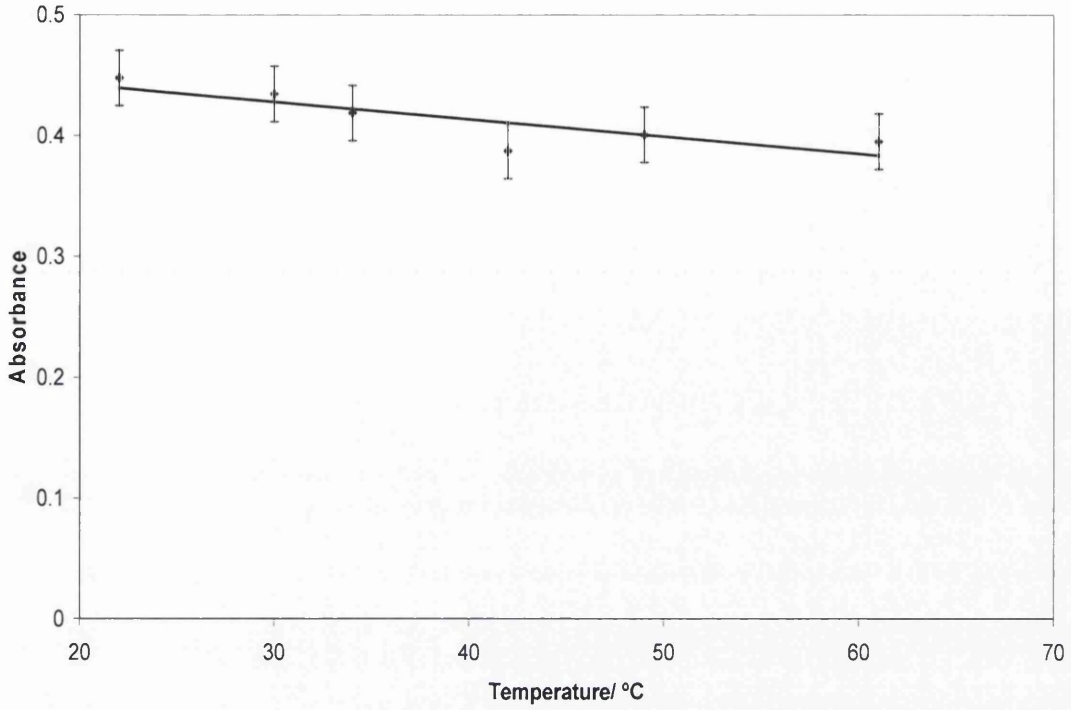

Fig.4.17. Decrease in PtOEP absorbance at 382 nm with increasing temperature.

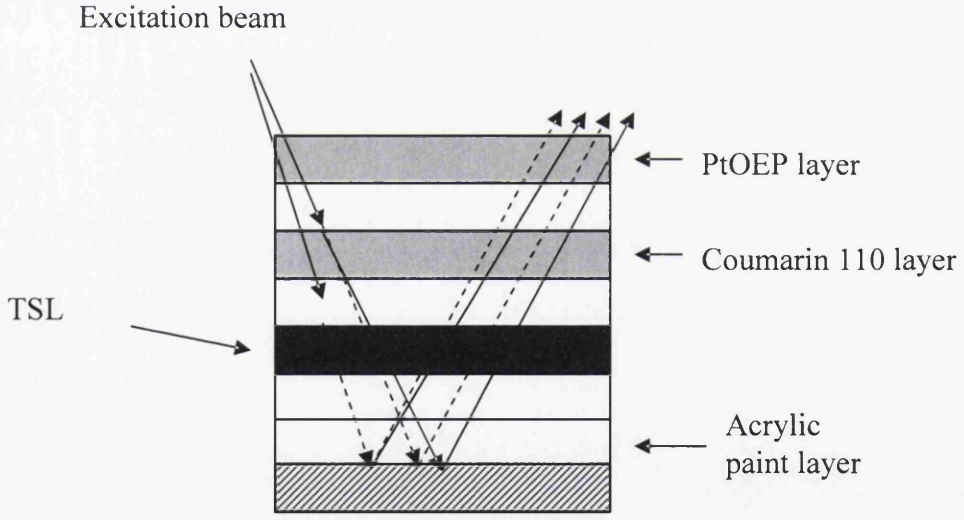

Fig.4.18. Light path (dashed line) for the emission reflected by the acrylic paint layer through the TSL from the PtOEP and coumarin 110 layers, the emission must pass through the TSL layer and the amount of light passing through the TSL is dependent on the absorption of the TSL.

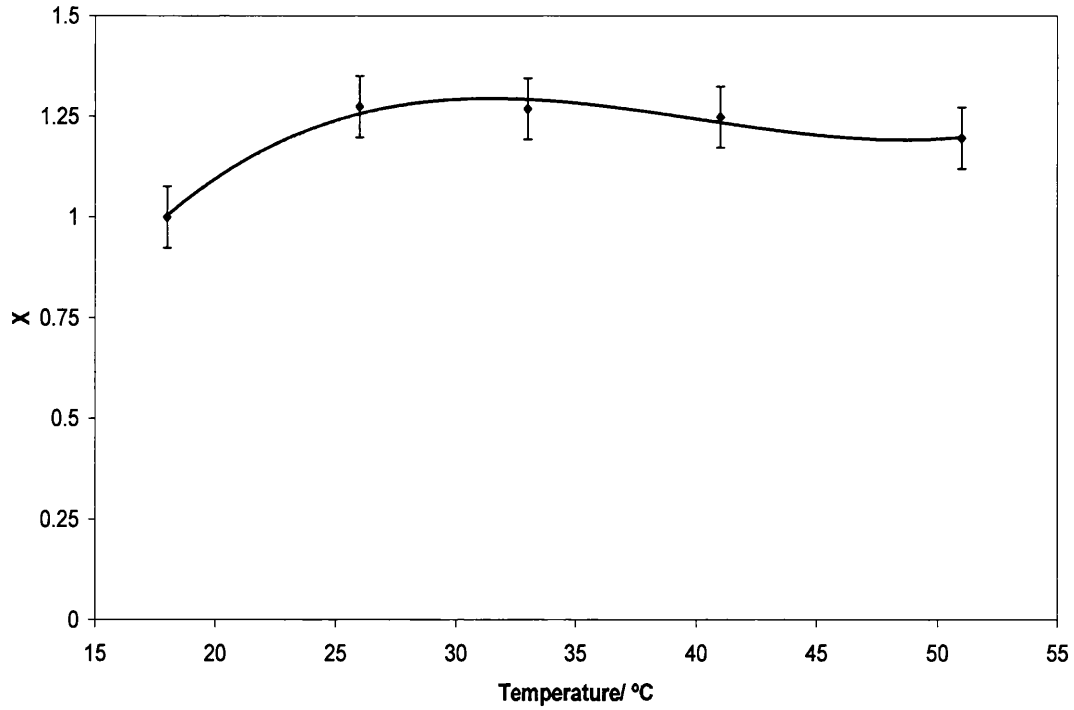

Fig.4.19. The calibration curve for the coumarin peak in the CPSP

$y = 4 \times 10^{-5} X^3 - 0.0049 X^2 + 0.1877 X - 1.0218$, $R^2 = 0.9798$

The colorimetric response of the TSL via changes in absorption gives the temperature of the surface and allows the calibration data to be applied as follows. The emission intensity at all wavelengths up to 600 nm, i.e. only the coumarin 110 emission, are multiplied by the correction factor (X) for the temperature, (as obtained from fig.4.19), thus correcting the coumarin 110 emission. Then all wavelengths from 600 nm onwards, i.e. only the PtOEP emission, are multiplied by the correction factor C(T) obtained from fig.4.16. This generates corrected spectra to which the colour matching functions can be applied and from which the CIE co-ordinates can be calculated (fig.4.20).

The results of the modelling can be seen in the table 4.2. At all the temperatures and partial pressures examined the modelling of the spectra can be seen to be in good

agreement with the reference spectra obtained at 18 °C. The effect of the model on a spectrum can be seen in fig.4.20. It is possible to gain an almost perfect match to the original spectra. It can therefore be seen that this simple model can be used to give an accurate picture of the air flow over a surface.

	18°C (Reference values)		**26°C**		**33°C**		**41°C**		**51°C**	
	x	y	X	y	X	y	x	y	X	y
0 %	0.67	0.28	0.67	0.29	0.67	0.28	0.67	0.28	0.66	0.27
0 %	-	-	**0.68**	**0.29**	**0.68**	**0.29**	**0.68**	**0.29**	**0.69**	**0.28**
21 %	0.42	0.16	0.42	0.16	0.40	0.15	0.35	0.10	0.32	0.11
21 %	-	-	**0.43**	**0.16**	**0.43**	**0.16**	**0.43**	**0.16**	**0.43**	**0.16**
43 %	0.34	0.12	0.34	0.12	0.29	0.10	0.27	0.09	0.25	0.08
43 %	-	-	**0.35**	**0.12**	**0.34**	**0.12**	**0.34**	**0.12**	**0.34**	**0.12**
67 %	0.29	0.09	0.29	0.10	0.27	0.08	0.22	0.06	0.21	0.05
67 %	-	-	**0.30**	**0.10**	**0.30**	**0.10**	**0.27**	**0.09**	**0.29**	**0.11**
100 %	0.24	0.07	0.22	0.06	-		-		-	
100 %	-	-	**0.24**	**0.07**	-		-		-	

Table.4.2. Table of CIE co-ordinates obtained from the uncorrected spectra (normal font) and the CIE co-ordinates obtained from the spectra corrected by the model (bold font)

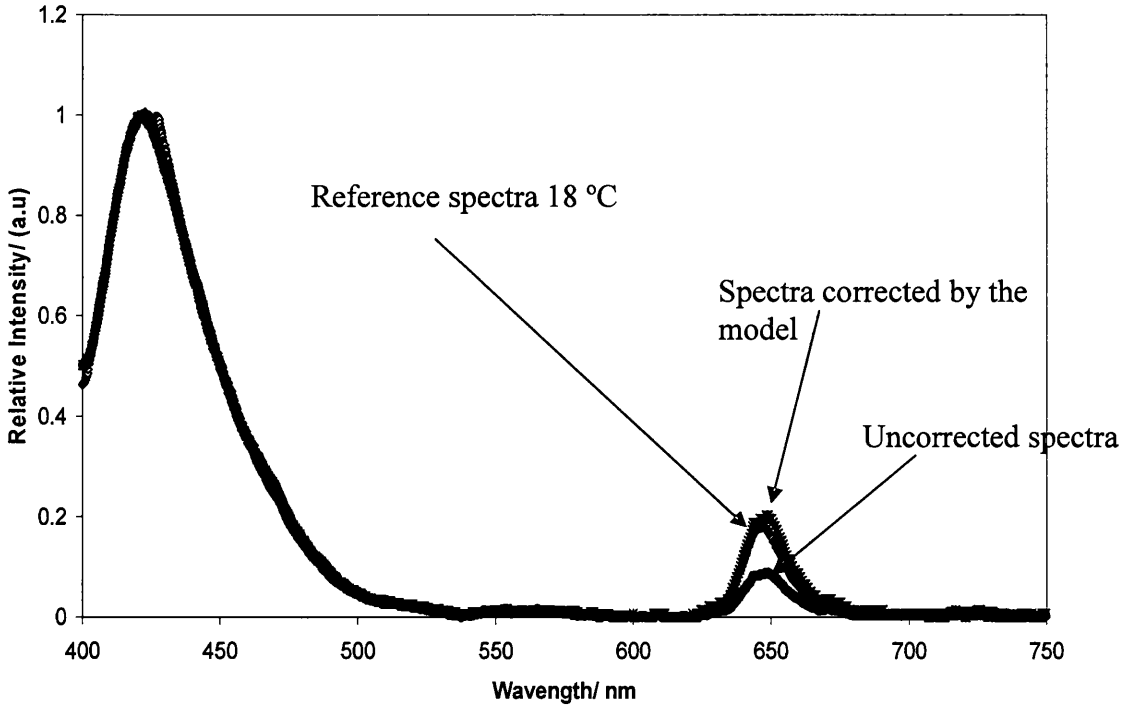

Fig.4.20. Comparison of emission spectra for CPSP at room temperature and 51 °C (corrected by the model), compared with the uncorrected spectra at 51 °C, all values are for 21 % oxygen

An attempt was made in order to reduce the effects caused by the increased absorption of TSL. A spiropyran (section 4.2) was encapsulated in an EC matrix. Under visible light this was colourless and so the TSL could be observed easily. Under UV light a ring opening reaction occurred (fig.4.21) from the spiropyran form which was colourless to the merocyanine form which was a purple colour.[32,33] It was hoped this would create a constant coloured background negating most of the effects of the temperature dependent TSL absorption. However this approach was flawed, because at high temperatures the thermal reverse reaction of the spiropyran photochromic reaction becomes much faster and the coloured form is converted back to the colourless form so fast that the equilibrium mixture is not highly coloured. Therefore this approach was abandoned.

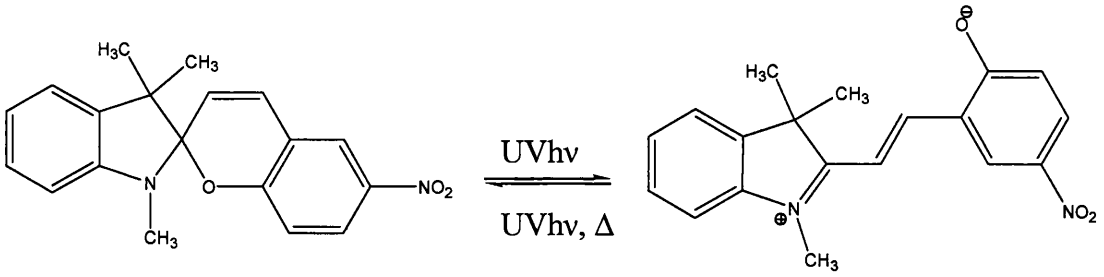

Fig.4.21. The photochemical reaction of the spiropyran[34] conversion from the spiropyran form (colourless) to the merocyanine form (purple)

The changes in PtOEP emission with temperature in oxygenated conditions can be attributed to a combination of the decrease in oxygen solubility and the increase in the oxygen diffusion rate with temperature, equations 4.5 and 4.6.[37] In general it is the latter diffusion term which dominates, however it is not possible to assign the loss of emission intensity from the PtOEP layer that occurs under nitrogen to these factors because no oxygen is present (fig.4.22).

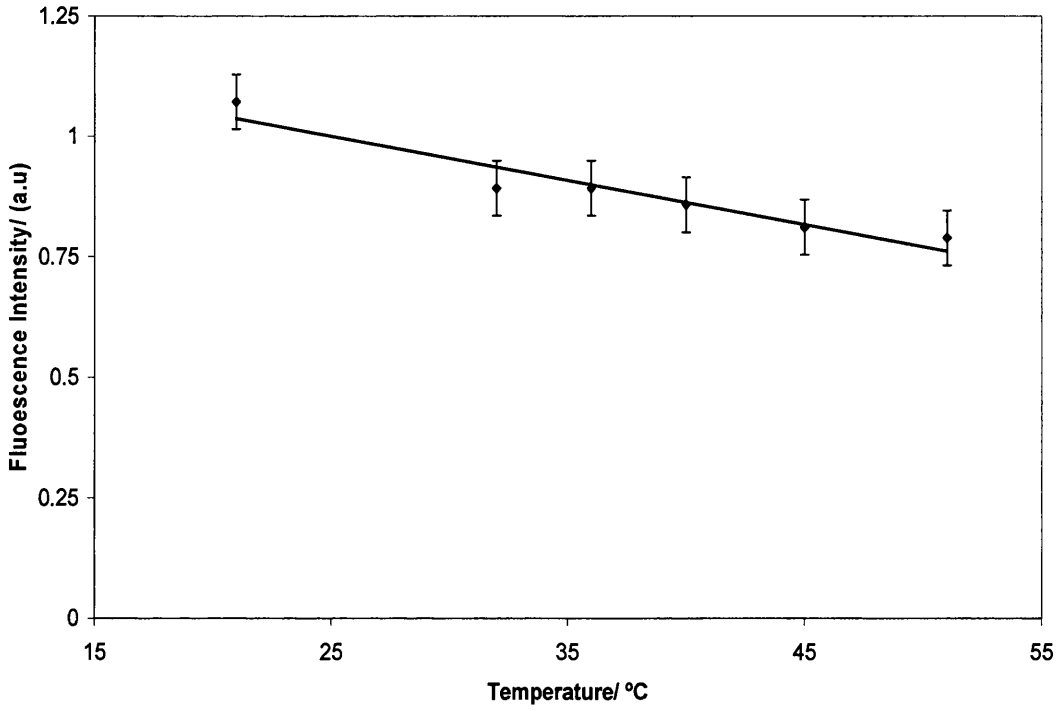

Fig.4.22. The change in emission from a single layer of PtOEP in EC on a glass substrate at 645 nm under nitrogen at different temperatures, $R^2 = 0.920$

These can be attributed in part to a decrease in the absorption of the PtOEP layer (fig. 4.17). However this does not account for all of the emission decrease observed under nitrogen. Therefore the possibility of temperature dependent reverse intersystem crossing, which has been shown to occur in some luminescent compounds,[35] must be considered. In some compounds this can lead to delayed fluorescence,[36] however PtOEP is not fluorescent, and therefore we can consider the loss of emission as the result of an intrinsic temperature dependent non radiative decay channel, (possibly via the thermally populated singlet state), as reported by Schanze and Carroll.[14]

$$P = P_0 \text{ x } \exp(-E_p/RT)$$

$$D = D_0 \text{ x } \exp(-E_D/RT)$$

$$S = S_0 \text{ x } \exp(-E_s/RT) \qquad [4.5]$$

$$S = P/D \qquad [4.6]$$

Here P is the permeability coefficient, D is the diffusion coefficient, S is the solubility coefficient, E_p is the activation energy of permeation, E_D is the activation energy of diffusion, E_s the heat of solution, R is the gas constant, T equals the temperature, and P_0, D_0 and S_0 are the relevant pre exponential factors.[37]

One area that was not studied in this work was sensor stability. Coumarin 110 and PtOEP both degrade under UV irradiation, however from the work on photodegradation discussed in chapter 3 it seems likely that by stabilising the upper PtOEP layer with DABCO both layers could be protected. No photodegradation was observed in the TSL.

4.6 Versatility of PSPSENS

This type of pressure sensitive paint has the advantage that it is very versatile, and can be used in a variety of ways. In its most simple form a picture taken with a camera of the paint under visible light and under UV light will produce a colorimetric picture of the temperature and air flow without any further calculation. Using a camera in which the RGB response for each picture area is automatically converted into CIE colour coordinates would allow a direct determination of oxygen

pressure across the whole image area. In a more complicated approach lifetime data could be collected from the coumarin and the PtOEP and ratiometric calculations could be used which give accurate information at specific points; this approach would probably remove any problems in calibration associated with changes in absorption of the TSL.

Although this sensor has primarily been designed for use as a PSP is could be easily used for other applications such as: the medical applications like those described in chapter 6 where temperature correction would extremely valuable; in preserving artefacts particularly if low temperatures are going to be used in conjunction with low oxygen partial pressures;[38] and in areas such as modified atmosphere packaging.[39]

4.7 Future work

The most important future work to be carried out here is the use of different TSLs that will work over a larger temperature range, thus extending the working range of the sensor, or perhaps the addition of a second TSL that is colourless up to 50 °C, and then changes colour. Changing the colour change of the CPSP, from the current red to blue colour change, to a green to red colour change would also be desirable, however this would require a different TSL or a new green lumophore. Polymer matrices that are more oxygen permeable maybe more desirable, because they may be affected less by changes in temperature. If a spiropyran or similar compound can be obtained whereby the forward reaction is stimulated by UV light and back reaction stimulated by and visible light, or vice versa, this may still be an area which

is very profitable and remove the current problems with the non linear calibration data, one possibility maybe the use of diarylethenes which are known to be thermally irreversible.[40]

4.8 Conclusions

In this chapter it has been shown that a colorimetric pressure sensitive paint can be developed in which an emissive colorimetric oxygen sensor is combined with a colorimetric absorption based temperature sensitive layer such that the absorption change of the temperature sensitive layer provides data for calibration of the colorimetric oxygen sensor.

Cobalt chloride was used as the TSL. This gives a visible colour change that allowed temperature correction over the range from 0 °C to 50 °C which is a perfectly adequate range for packaging and environmental applications.[41] It is suitable for the temperature range from 0 °C to 100 °C but may not be suitable for higher temperatures which maybe required for aerospace applications. It was shown that the colour change of the TSL influenced the response of the CPSP, although this undesirable effect any be minimised by incorporation of an additional UV absorbing or photochromic layer on top of the TSL.

Future work would be to extend the operational range of the TSL by utilising other compounds which do not effect the colour change of the CPSP. The slow response of the TSL is a consequence of the thermal properties of the whole sensors slide, glass substrate included.

The CPSP was made up of coumarin 110 and PtOEP. It was demonstrated that the colour change of the sensor was temperature dependent. However by applying the correction factors obtained (X and Cm), this could be corrected for successfully.

The most important future work would be to extend the operational range of the TSL by utilising other temperature sensitive materials which operate at higher temperatures or over a wider temperature range. If these could be developed then, along with the tuning of pO_2 response range available by choice of polymer matrix, it may be possible to fine tune the design of these types of sensors for specific applications.

In conclusion, the sensor described in this chapter shows proof of concept. They demonstrate the potential of a very promising concept that with development may provide solutions to some of the problems found with current pressure sensitive paint formulations, such as temperature compensation and problems of variation in excitation intensity. Furthermore the use of a colorimetric visible light absorption temperature sensor coupled with a colorimetric oxygen sensor suggests the possibility of very simple imaging of variation in gas pressure across surfaces.

4.9 References

1) Grenoble, S.; Gouterman, M.; Khalil, G.; Callis, J.; Dalton, L. *J. Lumin.,* 113, **2005,** 33-44.

2) Syed Azim, S.; Solaiyan, C.; Venkatachari, G. J. P. *Org. Coat.,* 62, **2008,** 28-31.

3) Ogurtsov, V.I.; Papkovsy, D.B. *Sens. Actuators B,* 113, **2006**, 917-929.

4) Lupton, J.M. *Appl. Phys. Lett.,* 81, **2002,** 2478-2480.

5) Basu, B. *Sens. Actuators B,* 123, **2007,** 568-577.

6) Castaldo, A; Massera, E.; Quercia, G.; Di Francia, G, *Sens. Actuators B,* 118, **2006**, 328-332.

7) Boristov, S.M.; Mayr, T.; Klimant, I., *Anal. Chem.,* 80, **2008,** 573-582.

8) Lui. Q.; Sleti, A.K.; Kapat, J.S., *I. J. Thermal. Sci.,* 47, **2008,** 749-757.

9) McLachlan, B.G.; Bell, J.H. *Exp. Therm. Fluid Sci.,*10, **1995,** 470-485.

10) Zelelow, B.; Khalil, G.E.; Phelan, G.; Carlon, B.; Gouterman, M.; Callis, J.B.; Dalton, L.R., *Sens. Actuators B,* 96, **2003,** 304-314.

11) Douglas, P; Eaton, K. *Sens. Actuators B,* 82, **2002,** 200-208.

12) Mills, A. *Platinum Metals Rev.,* 41, **1997,** 115-127.

13) Hradil, J.; Davis, C.; Mongey, K.; McDonagh, C.; MacCraith, B.D. *Meas. Sci. Technol.,* 13, **2002,** 1552-1557.

14) Schanze, K.S.; Carroll, B.F.; Korotkevitch, S.; Morris, M.J. *A.I.A.A. Journal,* 35, **1997,** 306-310.

15) Coyle, L.M.; Gouterman, M. *Sens. Actuators B,* 61, **1999,** 92-99.

16) Kahil, G.E.; Costin, C.; Crafton, J.; Jones, G.; Grenoble, S.; Gouterman, M.; Callis, J.B.; Dalton, L.R. *Sens. Actuators B,* 97, **2004,** 13-21.

17) Kose, M.E.; Omar, A.; Virgin, C.A.; Carroll, B.F.; Schanze, K.S. *Langmuir,* 21, **2005,** 9110-9120.

18) Demas, J.N; Crosby, G.A.; *J. Phys Chem.,* 75, **1971,** 991-1024.

19) Hunt, R.W.G, 3rd ed., Measuring Colour, Fountain Press, (1998)

20) Mills, A.; Lepre, A. *Analyst,* 124, **1999,** 685-689.

21) Day, J.H. *Chem. Rev.,* 63, **1963,** 65-80.

22) Zhu, C.F.; Wu, A.B. *Thermochim. Acta,* 425, **2005,** 7-12.

23) Day, J.H. *Chem. Rev.,* 68, **1968**, 649-657.

24) Manning, T.D.; Parkin, I.P.; Pemble, M.E.; Sheel, D.; Vernardou, D. *Chem. Mater.,* 16, **2004,** 744-749.

25) Dybko, A.; Wroblewski, W.; Rozniecka, E.; Maciejewski, J.; Brozka, Z. *Sens. Actuators A,* 76, **1999,** 203-207.

26) Greenwood, N.N.; Earnshaw, A., *Chemistry of the Elements, 2nd ed.*, Butterworth Heinemann, 2001, p1129.

27) Srivastava, J.; Srivastava, J.N.; Alam, S.; Mathur, G.N., *App. Poly. Sci.,* 100, **2006,** 4832-4834.

28) Lazareva, T.G.; Kabisheva, I.V.; Il'yushchenko, I.A., *Proc. S. P. I. E.,* 3324, **1998**, 308-317.

29) Xu-Dong, W.; Chen, X.; Zhao-xiong, X.; Xioa-ru, W., *Angew.,* 120, **2008**, 7560-7563.

30) Yu-Long, L.; Chen-Shane, C., Jiahn-Piring, Y., Yuan-Che, C. *Sens. Actuators B,* 131, **2008**, 479-488.

31) Hartmann, P.; Leiner, M.J.P.; Lippitsch, M.E. *Sens. Actuators B,* 29, **1995,** 251-257.

32) Ren, J.; Tian, H. *Sensors,* 7, **2007,** 3166-3178.

33) Suzuki, M.; Asahi, T.; Masuhara, H. *Phys. Chem. Chem. Phys.,* 4, **2002,** 185-192.

34) Querol, M.; Bozic, B.; Salluce, N.; Belser, P. *Polyhedron,* 22, **2003,** 655-664.

35) Turro, N.J. *Modern Molecular photochemistry, 1st ed.,* University Science books, (1989), pp 187-189.

36) Baleixao, C.; Nagl, S.; Scharfering, M.; Berberan-Santos, M.N.; Wolfbeis, O.S. *Anal. Chem.,* 80, **2008,** 6449-6457.

37) Bandrup, J.; Immergut, E.H.; Grulke, E.A. *Polymer Handbook, 4th ed.*, Wiley, (1999).

38) Maekawa, S., *Oxygen-Free Museum Cases, 1st ed.*, The Getty Conservation Institute, (1998), pp 1-15.

39) Mills, A. *Chem. Soc. Rev.,* 34, **2005,** 1003-1001.

40) Lucas, L.N.; Esch, J.V.; Kellog, M.; Feringa, B.L. *Chem. Comm.,* **1998,** 2313-2314.

41) Ogurtsov, V.I.; Papkovsky, D.B. *Sens. Actuators B,* 113, **2006,** 917-929.

A simple colorimetric luminescent oxygen sensor using a green LED with Pt octaethylporphyrin in ethyl cellulose as the oxygen responsive element

5.1 Summary

The aim of the work described in this chapter was to produce a simple colorimetric oxygen sensor using a coloured LED and only one luminescent oxygen sensitive emissive layer. In this sensor a green LED acts as both a green emission source and excitation source for a film of the oxygen sensitive Pt octaethylporphyrin (PtOEP) in ethyl cellulose (EC) containing TiO_2 or ZnO as a scattering agent[1]. This gives a sensor with a "traffic light", red-yellow-green response to increasing oxygen concentration. The addition of the singlet oxygen stabiliser diazobicyclo[2.2.2]octane increased the sensor stability significantly. Because of the relatively thick sensor layer used response times are long, with 90 % response times of ca. 1000 s for the switch from nitrogen to oxygen, and ca. 300 s for oxygen to nitrogen.

5.2 Introduction

In the work described in this chapter an LED was used as a source for excitation, and also as a source of emission in the visible region, in a colorimetric sensor. A single oxygen sensitive lumophore layer is excited by the LED emission to provide a colorimetric oxygen sensor. The emission from the oxygen sensitive layer is quenched while emission from the LED is unaffected creating a sensor with the desired red-green "traffic light" response.[2] In previous traffic light sensors two lumophores which have different sensitivities to oxygen partial pressures were used, and to observe the colour of the sensor it was illuminated using a UV light source such as a lamp or a UV LED.[3-6] The single lumophore sensor described here does not require UV excitation, since the LED acts as both an excitation source for the lumophore and a source of visible emission which is independent of the oxygen concentration.

The starting optical arrangement for the sensor was to use a green LED with a red lumophore in a polymer matrix. Of the available room temperature lumophores the red emitting platinum and palladium porphyrins are unusually long lived, and therefore very sensitive to oxygen. At present there are no other lumophores of comparable oxygen sensitivity.[7,8] Furthermore, due to the relative photon energies it is not possible to excite a green lumophore directly with a red LED.

LEDs are cheap, intense, relatively stable and although they generally emit across a range of wavelengths the bandwidth can be relatively narrow, in the order of 10 nm[9,10], They are attractive alternatives to other more expensive light sources such as

arc lamps or "black ray" lamps commonly used in photochemical research. There are a number of examples in the literature in which LED's[11,12] and OLED's[13,14] have been used to excite luminescent sensors, however to the best of our knowledge no sensors have been made that use a green LED to provide both lumophore excitation and emission colour.

5.3 Materials

Ethyl cellulose (46 % ethyloxy content), ZnO, diazobicyclo [2.2.2]octane (DABCO), tris (2-ethylhexyl)phosphate (EHP) and Degussa TiO_2 p25 were purchased from Aldrich. PtOEP was obtained from Frontier Scientific. Silicon rubber RTV118 was purchased from Techsil Ltd. "Superbright" 5mm LEDs (catalogue number: N62AX) were bought from Maplin Electronics, Valley Road, Wombwell, Barnsley, S73 0BS. "Clear green" 5mm LED's , (catalogue number: 5410Q-S) were bought from RS Components, Birchington Road, Corby, Northants, NN17 9RS. Emission spectra for the two LEDs are shown in fig.5.3 Dupont tripure TiO_2 was a gift from Dr. E. Jewell, The Welsh Centre for Printing and Coating, School of Engineering, Swansea University.

5.4 Experimental

Oxygen sensors were made by adding 1.2 ml of a solution of lumophore, PtOEP or PdOEP, in tetrahydrofuran (13.5 mg PtOEP or 10.4 mg PdOEP in 10 ml tetrahydrofuran) to 6 g of a solution of ethyl cellulose in a toluene/ethanol mix (10% w/v in 80:20 toluene:ethanol v/v), in a 2 cm diameter flat bottomed sample tube.

Other additives such as scattering agents and stabilisers were then added to the solution and, after mixing, the resulting suspension was placed in an oven to dry at 100 °C. Once dry, the tube was smashed and the rough film was removed. The block of polymer was then shaped to produce a flat disc approximately 0.5 mm in thickness. To make the bottom of sample tube flat the apparatus shown in fig. 5.1 was used. Film thicknesses were measured using a micrometer.

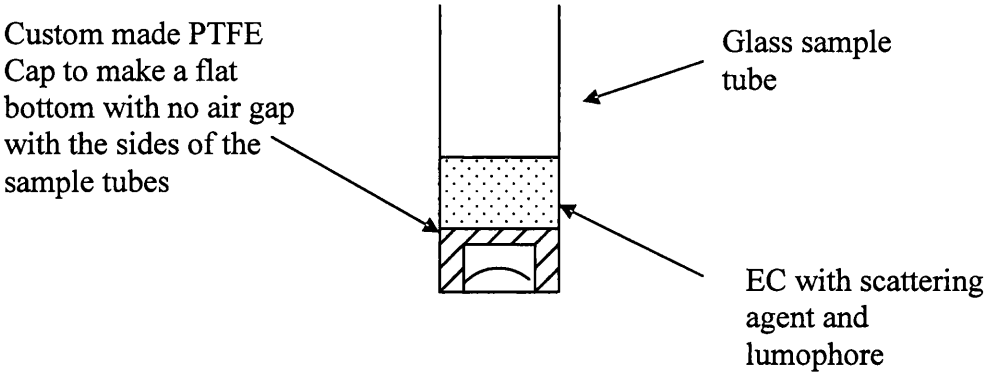

Fig.5.1. Apparatus for making thick films; a PTFE cap is placed over the bottom of the sample tube to make a flat surface

Emission spectra were obtained using the detection side of a Perkin Elmer MPF 44-E fluorimeter operated in DC mode and without an excitation beam. The film was placed over the LED (fig 5.2) and the sensor placed in a modified solid state holder (describe in chapter 2) with detection at ca. 25° to the LED. Emission correction factors for the fluorimeter were obtained as described in the experimental section.[16] CIE colour coordinates were calculated using the spectral response factors given in reference 2. Gas mixing was carried out using a model no. 852 V1-B gas blender from Signal Instruments Co. UK. 90% response times are given as the time for the

sensor to reach 90 % of its total response when switching from nitrogen to oxygen (oxygen response time) or oxygen to nitrogen (nitrogen response time).

For the Stern-Volmer plot in Figs.5.14 and 5.15, samples were equilibrated with the gas mixture for 20 minutes before measurement.

LEDs were operated using mains a 5 V DC power supply with a variable resistor.

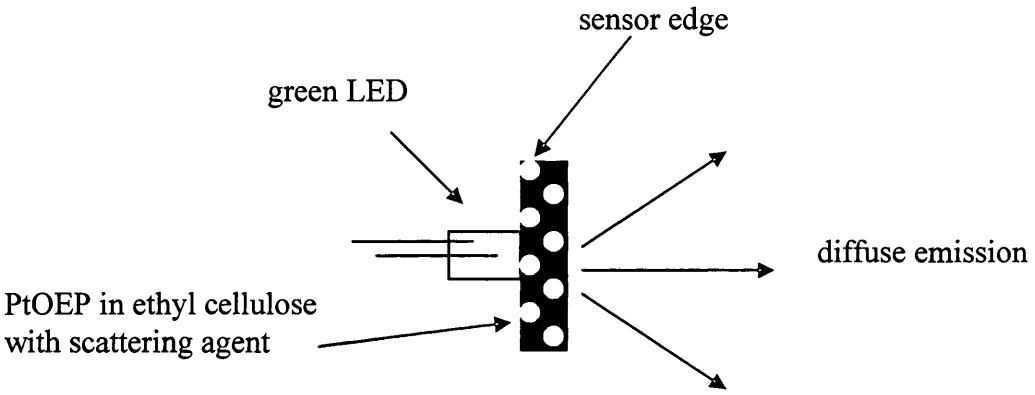

Fig.5.2. A schematic of the sensor design

5.5 Optical Arrangement

5.5.1 Choice of lumophore and polymer

The choice of red lumophore used in this work has generally centred on using PtOEP in an ethyl cellulose matrix, because this has an intense red colour, a high emission quantum yield and it is readily quenched by oxygen. It has also previously been demonstrated that PtOEP can be excited by a green LED (fig. 5.3) .[17] The palladium

analogue was also briefly investigated because of it higher sensitivity to oxygen quenching.

The polymer matrix used is almost exclusively EC, chosen because of its high permeability to oxygen high stability and excellent optical properties[18]. Silicone rubber RTV 118 was also investigated but this proved a poor choice, because when cured the silicone rubber film was slightly cloudy because of a white pigment in the film, and therefore the optical properties of the film were not as good as EC.

5.52 LEDs used for excitation

Two LEDs were chosen as the source of illumination for the sensor. They both have their peak emission at around 535 nm, chosen to overlap and excite the Q-band of Pt and PdOEP (fig 5.3). The first problem associated with LEDs is the focussing of the lens, which produces a small area of very intense emission whereas what is required for best detection is a diffuse light throughout the polymer layer. To reduce the emission and make it more uniform and less directional, a diffuser was placed over the LED.

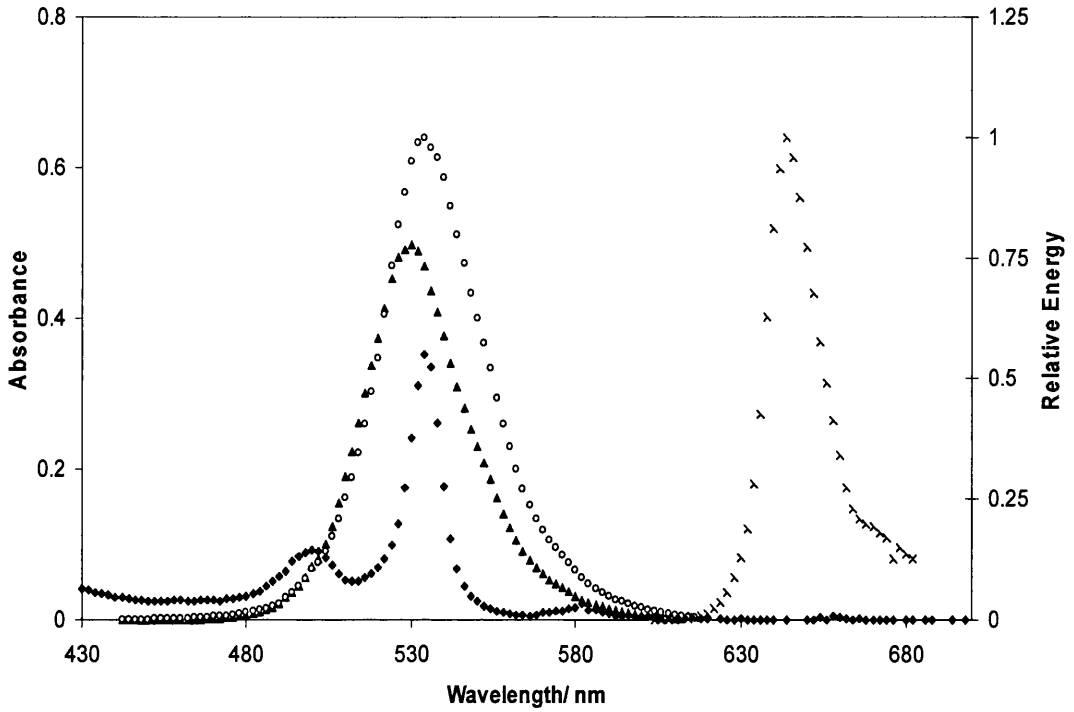

Fig. 5.3. Overlap of emission from green LEDs with the absorption of PtOEP. Absorption spectrum of Pt-OEP in THF (diamonds); emission spectra of Superbright LED (triangles) and Clear Green LED (circles). Also shown is the emission spectrum of Pt-OEP in THF (crosses). Emission spectra are in relative energy corrected for instrument response.

5.5.3 Scattering agents

The first approach we tried was to make a thin film containing a high concentration of PtOEP by spin coating and illuminate it with a green LED. However no emission could be seen from the thin film. The next attempt involved making a much thicker film, in the region of 0.5 mm in thickness using the method shown in fig. 5.1. When this was illuminated with a "superbright LED" no lumophore emission could be seen from the front of the film, only green light from the LED. However red lumophore emission could be clearly seen at the edge of the film.

It was thought this could be attributed to two effects. Firstly the pathlength of the excitation may be insufficient, therefore not enough of the light from the LED was absorbed by the lumophore. Secondly the light from the LED is still quite directional despite the addition of the diffuser, whereas emission from the lumophore in the polymer film is non directional. The observation of lumophore emission at the edge of the sensor can be understood since at the edges a longer pathlength can be obtained, and also total internal reflection will collect the diffuse lumophore emission and make it visible at the sensor edges.

Although emission could not be seen from the film it was clear that there was some absorption of the LED emission from the sensor film due to a change in the emission colour of the LED when viewed through the sensor film. We tried using a bandpass filter on the LED (fig. 5.4) to minimise transmission of non absorbed light, however a low transmission led to a large decrease in the emission from the LED and from the sensor film, and this approach was abandoned.

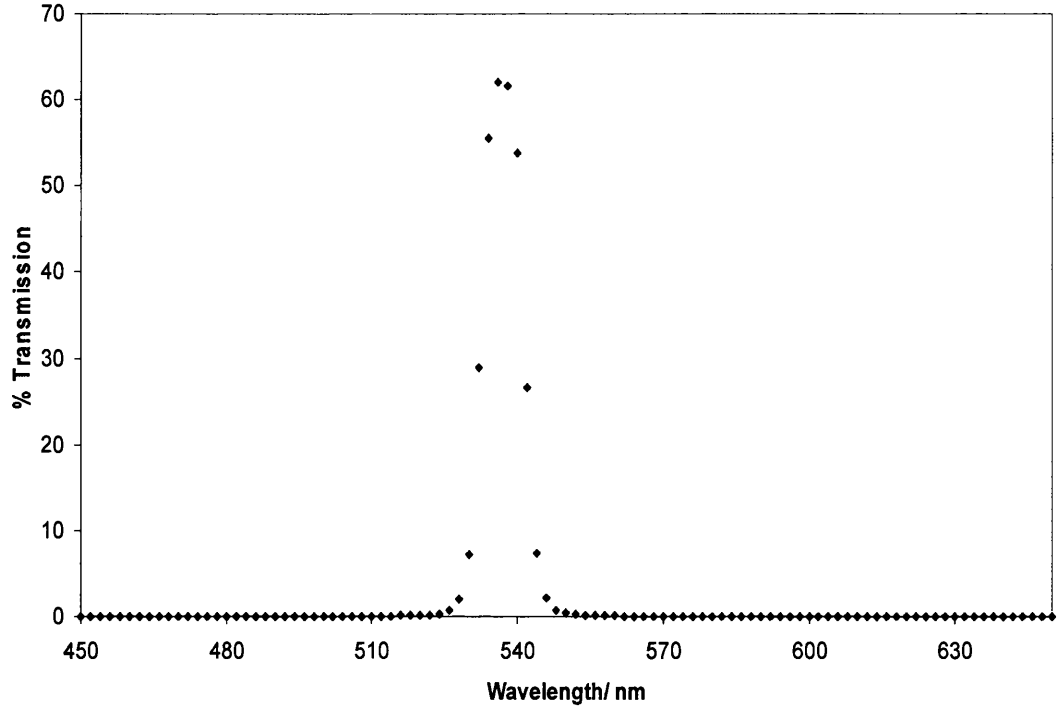

Fig.5.4. Transmission spectrum of the green bandpass filter used to limit the LED emission

The final approach to overcoming this problem of too dominant an LED emission from the sensor was the incorporation of a scattering agent into the polymer film. The scattering agent takes the form of a white solid which is not soluble in any of the components used to make the sensor, and which scatters excitation light from the LED and the emission from PtOEP. For the initial experiments this was Degussa TiO_2, which was later changed to ZnO[19] for reasons of stability. Once the scattering agent was added to the sensor film at a suitable concentration, red emission could be seen at the front of the sensor and the colour could be seen to change with changing pO_2. The effect of the scattering agent is believed to relieve the two problems of pathlength and directionality by making the emission from the LED take a more random path through the sensor film, and also making the LED emission less directional so that it can be viewed in the desired direction (fig 5.5).

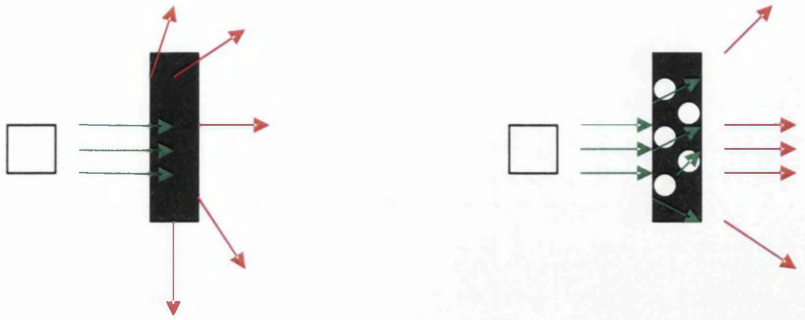

Fig.5.5. The effect of the addition of the scattering agent leads to relatively more emission at the front of the film (no scattering agent (left), scattering agent (right))

5.6 Emission Characteristics of sensors of varying formulation

5.6.1 Sensors with Degussa TiO_2 as a scattering agent

The first scattering agent used was Degussa TiO_2 p25 and it was found that the sensor colour change could be shifted by varying the amount of scattering agent used in the sensor film (figs.5.6a and b). Sensors B, C and E have differing amounts of Degussa TiO_2 present (table 5.1). The more scattering agent present in a sensor the further the emission is red shifted under both oxygen and nitrogen. Sensor C can be said to have the most desirable colour change of the three sensors with a colour change closest to the desired green to red colour change. Sensor B has the lowest concentration of scattering agent, which is not enough to produce a large shift in emission. Sensor E produces a larger colour change but is the most red shifted producing a yellow to red colour change. The variation in colour changes with amount of scattering agent can be attributed the changes in pathlength and directionality of emission, as previously discussed.

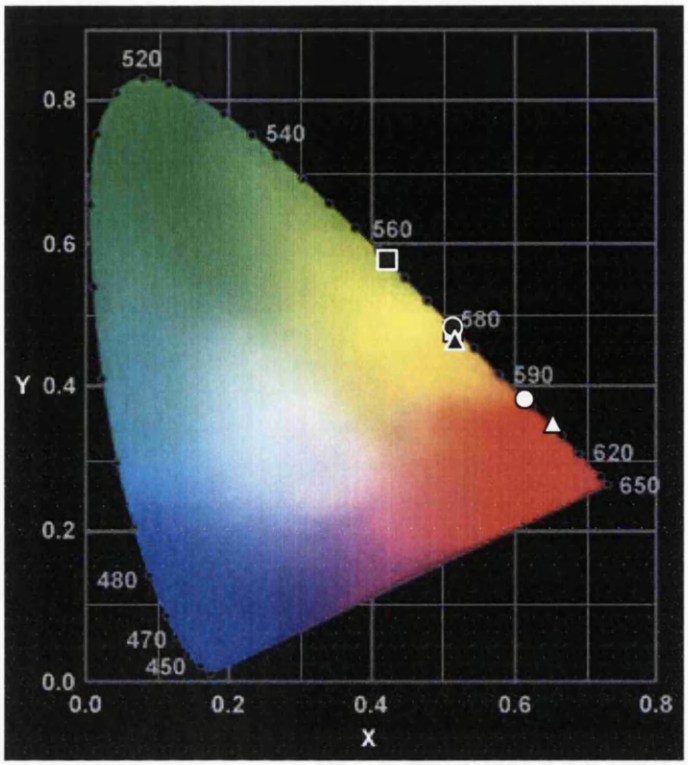

Fig.5.6.a. CIE colour coordinates under oxygen (black shapes) and nitrogen (white shapes) for sensors **B** (squares), **C** (circles) and **E** (triangles) with the corresponding shown in fig.5.6.b

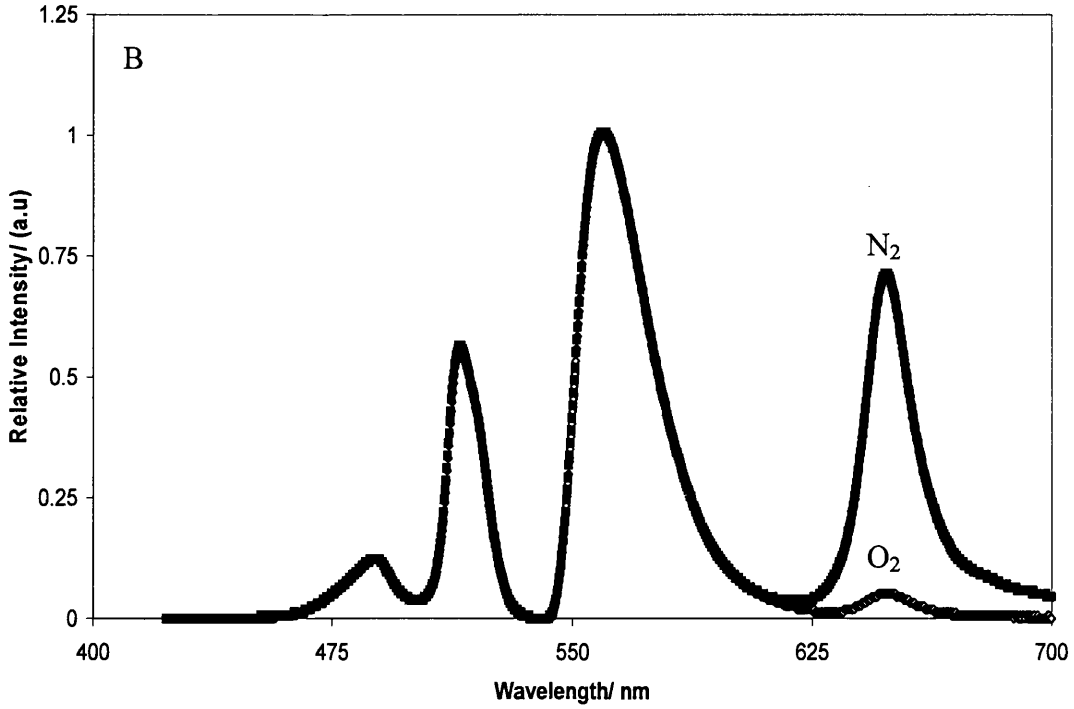
B
1.25
1
0.75
0.5
0.25
0
Relative Intensity/ (a.u)
400
475
550
625
700
Wavelength/ nm
N2
O2

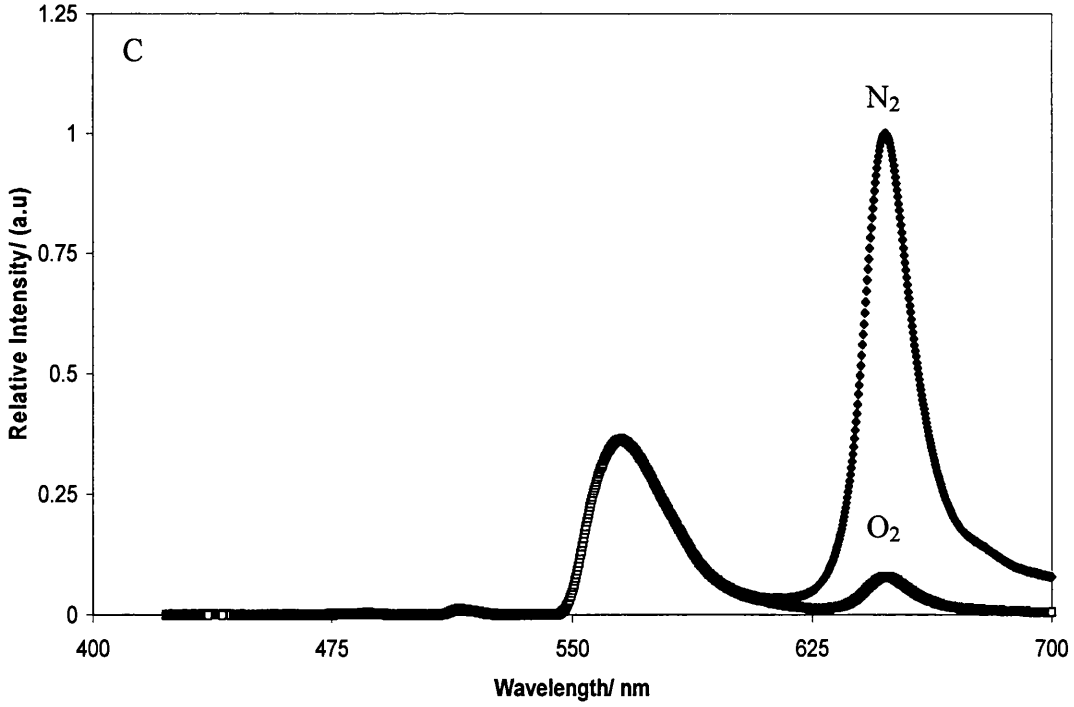
C
1.25
1
0.75
0.5
0.25
0
Relative Intensity/ (a.u)
400
475
550
625
700
Wavelength/ nm
N2
O2

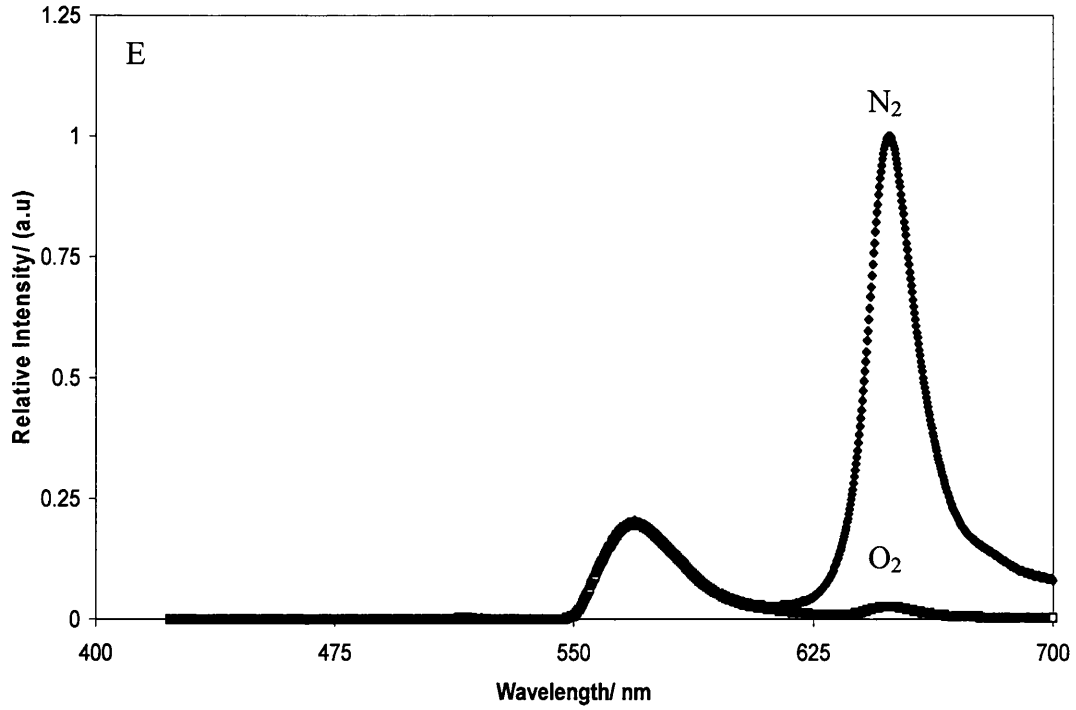

Fig.5.6.b. The spectra for the CIE coordinates in fig.5.6.a, for sensors **B**, **C** and **E** under nitrogen and oxygen

5.7 Stability

As shown in fig.5.7 sensors with Degussa TiO_2 p25 as the scattering agent sensors undergo significant photodegradation which can probably be attributed to the use of this particular grade of TiO_2 as this is the grade commonly used for research into photodegradation of pollutants etc.[20] This rapid degradation is clearly undesirable. Because emission from the LED is stable, photodegradation of PtOEP ultimately destroys the colour change of the sensor, in a similar way to the effect of different rates of degradation for PtOEP and PtPYR described in chapter 3.

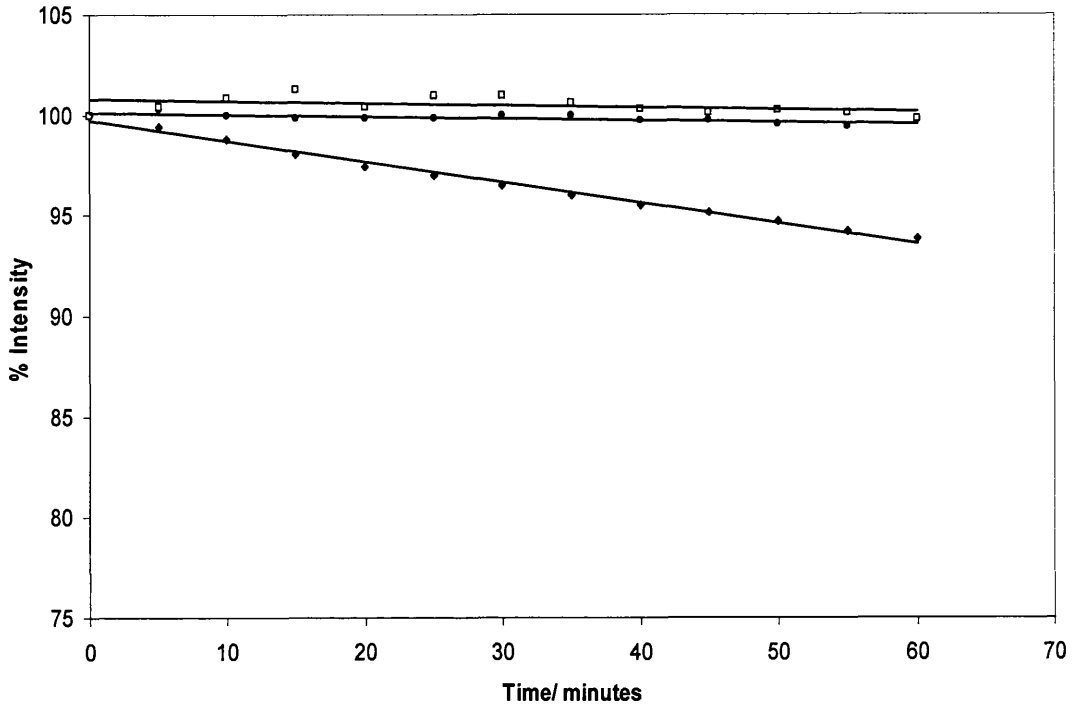

Fig.5.7. Stability of superbright LED (circles), and of sensors **C** (diamonds), **F** (squares), under nitrogen. The vertical axis is the emission intensity at 655 nm (corresponding to emission from PtOEP) referenced to 100% at t = 0

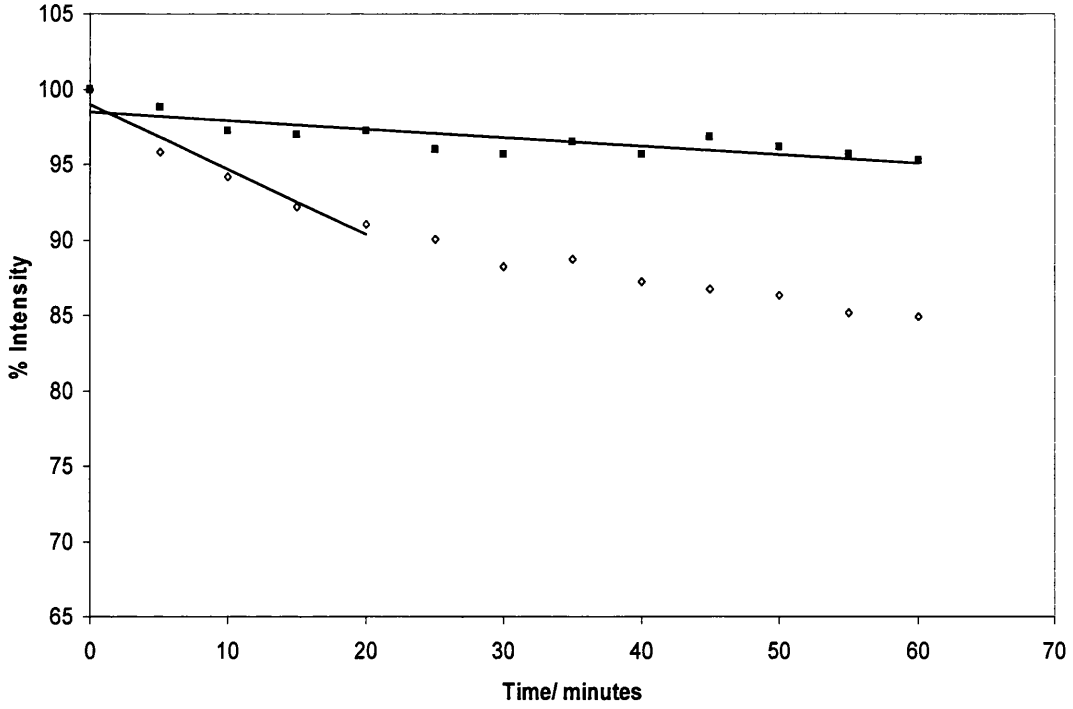

Fig.5.8. Stability of sensors **C** (diamonds) and **F** (squares), under oxygen. The vertical axis is the emission intensity at 655 nm referenced to 100% at t=0 (note that even under pure oxygen there is still some PtOEP emission detectable)

It therefore becomes necessary to prevent degradation of these sensors to maintain the initial colour change and calibration of the sensor. In sensor G the scattering agent was changed to Dupont tripure TiO_2 (a paint pigment where the TiO_2 is coated with silica which reduces the amount of TiO_2 present and also disrupts the conduction band in the TiO_2 reducing its activity,[21]) and in sensor H it was changed to ZnO. The substitution of these for Degussa TiO_2 reduces the degradation rate (table 5.1), but not as much as maybe expected.

In earlier work (chapter 3) it was shown that the degradation of the sensor probably arises from the self sensitised production of singlet oxygen by the PtOEP. In the work described in this chapter the fact that it is an oxidative fade is also supported by

the much faster degradation rate under oxygen than nitrogen (figs 5.7 and 5.8). It was therefore decided to use a singlet oxygen quencher as stabiliser. DABCO was chosen because it has been used in similar devices before.[22,23] DABCO is known as a quencher of PtOEP luminescence[22,23], however, this does not seem to have any effect on the colour change of the sensor, at least at the concentrations of DABCO used (compare sensor F to H in table 5.1).

The addition of DABCO in sensor F stabilises the sensor (figs.5.7 and 5.8). Under nitrogen, virtually no degradation is observed, while under oxygen some degradation is observed. This behaviour is replicated in all the sensors, and the increased degradation under oxygen suggests that degradation is the result of a reactive oxygen species, most likely singlet oxygen.

Film	Scattering agent weight per hundred grams of resin (phr)	LED	Thickness (mm)	Additives (phr)	CIE Co-ordinates oxygen	CIE Co-ordinates nitrogen	Degradation rates under oxygen(% loss per min)	Degradation rates under nitrogen(% loss per min)	Response times (s) O_2 to N_2 N_2 to O_2
A	0	Super bright	0.57	0	-	-	-	-	-
B	TiO_2 degussa 0.40	Super bright	0.38	0	x = 0.41, y = 0.57	x = 0.49, y = 0.50	-	-	1002 178
C	TiO_2 degussa 0.74	Super bright	0.48	0	x = 0.49, y = 0.51	x = 0.61, y = 0.39	1.767 ± 0.102	2.276 ± 0.007	-
D	TiO_2 degussa 0.74	Clear Green	0.48	0	x = 0.47, y = 0.53	x = 0.64, y = 0.36	-	-	-
E	TiO_2 degussa 1.12	Super bright	0.48	0	x = 0.50, y = 0.50	x = 0.65, y = 0.35	-	-	-
F	ZnO 0.81	Super bright	0.42	DABCO 0.62	x = 0.43, y = 0.55	x = 0.62, y = 0.38	0.046 ± 0.021	0.010 ± 0.008	972 204
G	TiO_2 dupont tripure 1.77	Super bright	0.83	0	-	-	0.239 ± 0.015	0.078 ± 0.001	-
H	ZnO 0.81	Super bright	0.44	0	x= 0.50, y= 0.50	x = 0.59, y = 0.40	0.116 ± 0.046	0.093 ± 0.019	-
I	ZnO 0.74	Super bright	0.59	VITE 2.79 EHP 1.79	-	-	-	-	707 25

Table 5.1. Data for all sensors used in this chapter * Parts per hundred resin

5.7.1 Response times

Response times were monitored by changing the gas around the sensor from 100 % oxygen to 100 % nitrogen using the gas blender. The response time was taken as the time for the sensor to reach 90 % of its maximum value.[24] Response times for the sensors were slow for all sensors (figs.5.9, 5.10 and 5.11) with the response for oxygen to nitrogen in the order of 1000s, and the response time from nitrogen to oxygen of the order 200s (table.5.1)

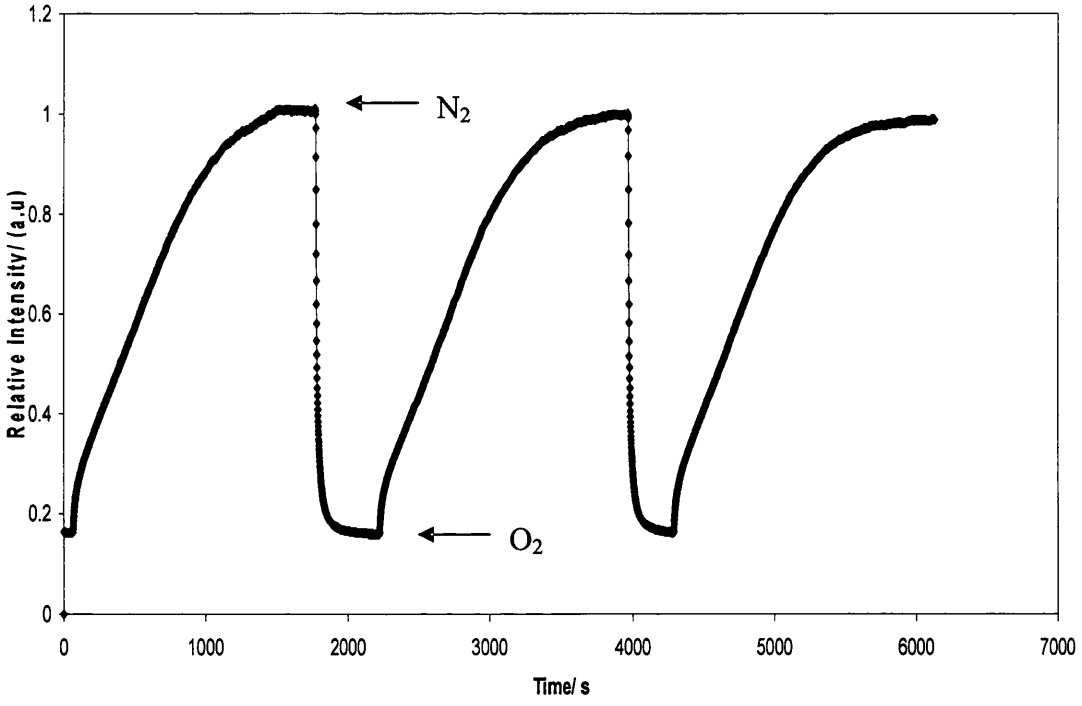

Fig 5.9. Response curves for sensor F to changing oxygen and nitrogen atmospheres

The sensor response is much slower than analogous thin film sensors, for which typical response times would be of the order of 5 s for oxygen to nitrogen, and approximately 1s for oxygen to nitrogen.[25] This can be understood in terms of the much greater thickness of the film in comparison to those previously used in the

group and by other workers. For example sensor F is 0.42 mm compared to a film thickness of around 10 microns for a spin coated sensor.

The asymmetric shape of the response is typical for almost all oxygen sensors, because the forward and backwards processes are different, i.e. from nitrogen to oxygen it is the diffusion into a layer from a plane of constant concentration, while for oxygen to nitrogen it is the diffusion out from the layer into a plane of constant zero concentration.[26] Fig.5.9 also demonstrates that the sensors demonstrate hysteresis.

Addition of plasticizer results in a moderate reduction in response time, as shown by the response curve for sensor I which contains the plasticiser tris(2-ethylhexyl) phosphate (see fig.5.10). The addition of a plasticizer leads to a change in the structure of the polymer increasing the permeability of the polymer to oxygen, and therefore increasing the response of the sensor.[27]

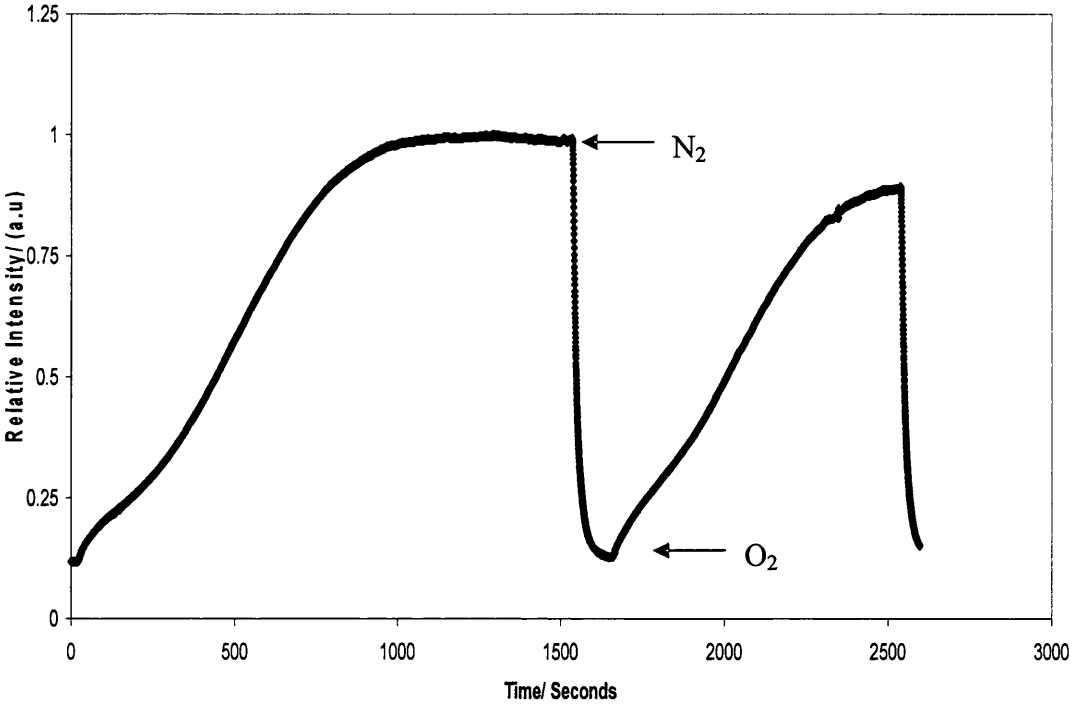

Fig.5.10. Response times of sensor I containing the plasticizer EHP and stabiliser VITE. It has a more rapid response than sensor C or F, but undergoes quite rapid photodegradation, showing VITE to be an unsuitable stabiliser (only the first change from oxygen to nitrogen and then nitrogen to oxygen was used to determine the response time)

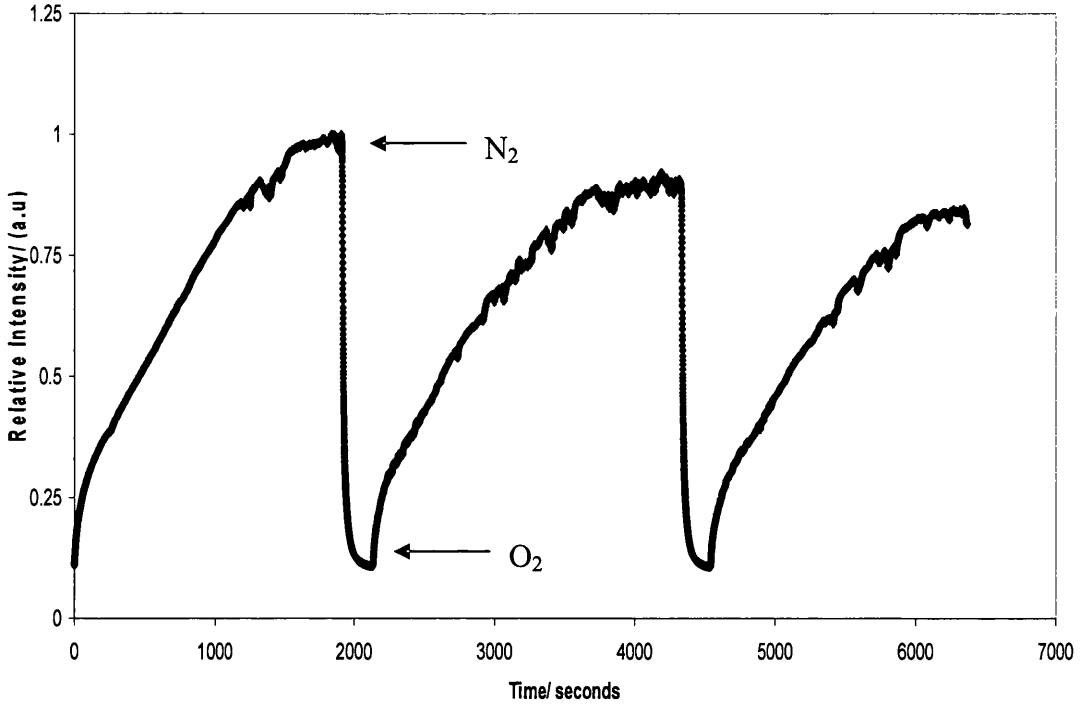

Fig.5.11. Response curves for sensor C to changing atmosphere from oxygen and nitrogen.

5.7.2 Emission from sensors with different LEDS and scattering agents

Figs.5.12.a and b demonstrate the effect of altering the LED from the superbright to a clear green LED. This red shifts the emission of the film due to increased excitation of the PtOEP, and illustrates the tuning in response colour that can be obtained by using different LEDs.

Using ZnO as the scattering agent instead of TiO_2 degussa still produces a traffic light response. However because ZnO is believed to be a less effective scattering agent the sensor response under the oxygen is closer to the green region on the CIE diagram. sensors F and H both contain ZnO as a scattering agent and both demonstrate traffic light responses. (table 5.1)

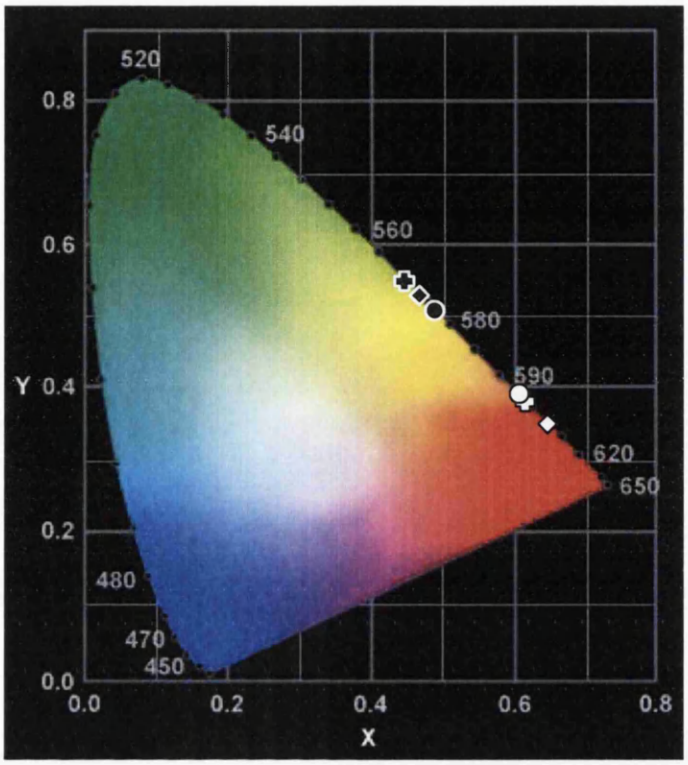

Fig. 5.12.a The CIE co-ordinates for sensors under oxygen (black shapes), and nitrogen (white shapes); **C** (which uses a clear green LED) (circles), **D** (diamonds) and **F** (crosses), with the corresponding spectra shown in fig.5.12.b

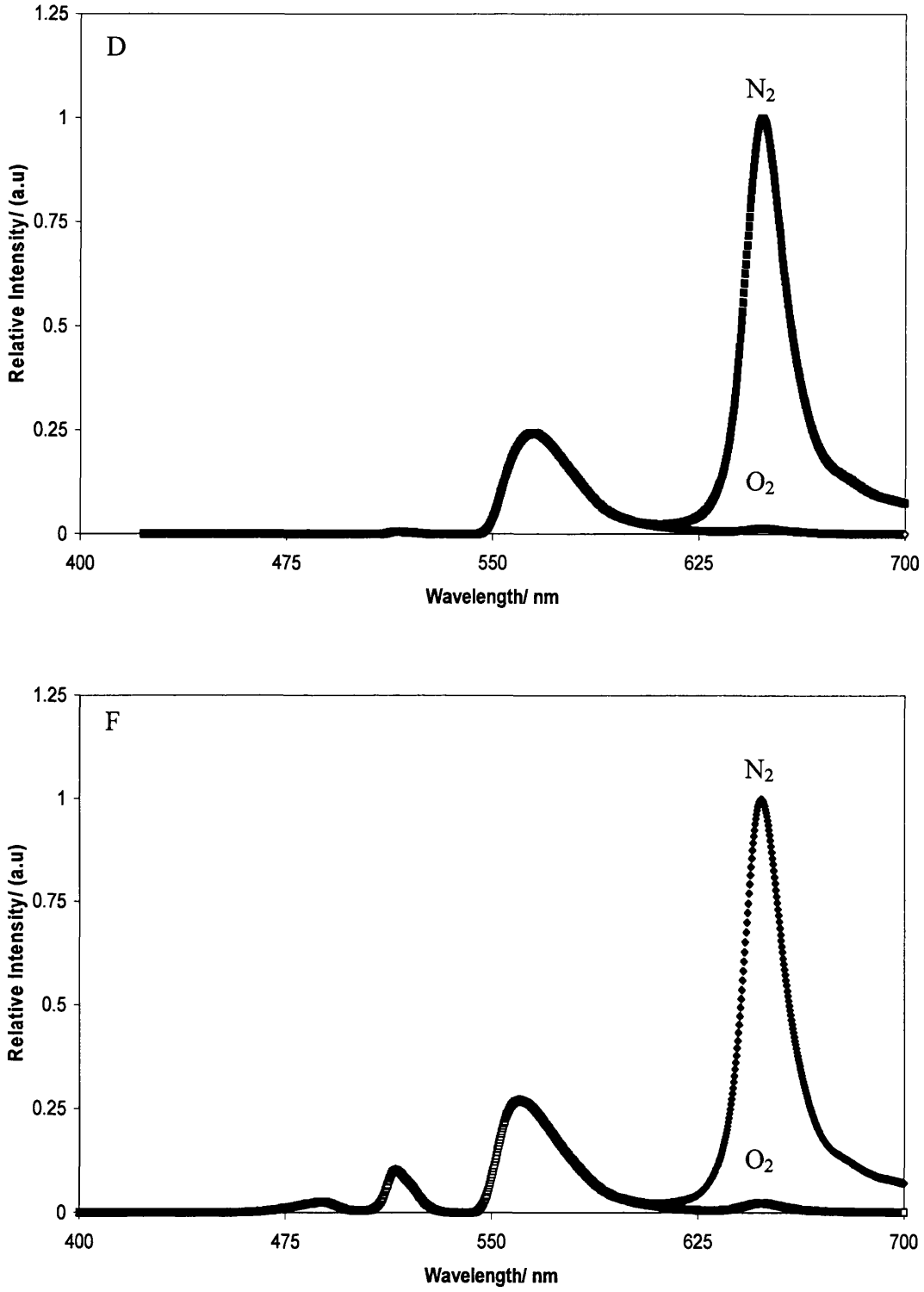

Fig.5.12.b. The spectra for the CIE coordinates in fig 5.12.a, for sensors **D** and **F** under oxygen and nitrogen **C** is shown in fig.5.6.b

5.7.2 Sensors using PdOEP as the oxygen sensitive lumophore

One PdOEP film was prepared, using TiO_2 as a scattering agent. However, with either the clear green or superbright LED's only a small change in colour was observed when changing the atmosphere between oxygen and nitrogen, as can be seen in fig. 5.13, because emission is still dominated by the green LED emission.

The major reason for the lack of response in this sensor is probably the lower quantum yield of PdOEP (Φ =0.2), compared to PtOEP (Φ =0.5)[8]. Therefore PdOEP does not appear to be a viable lumophore for this type of sensor.

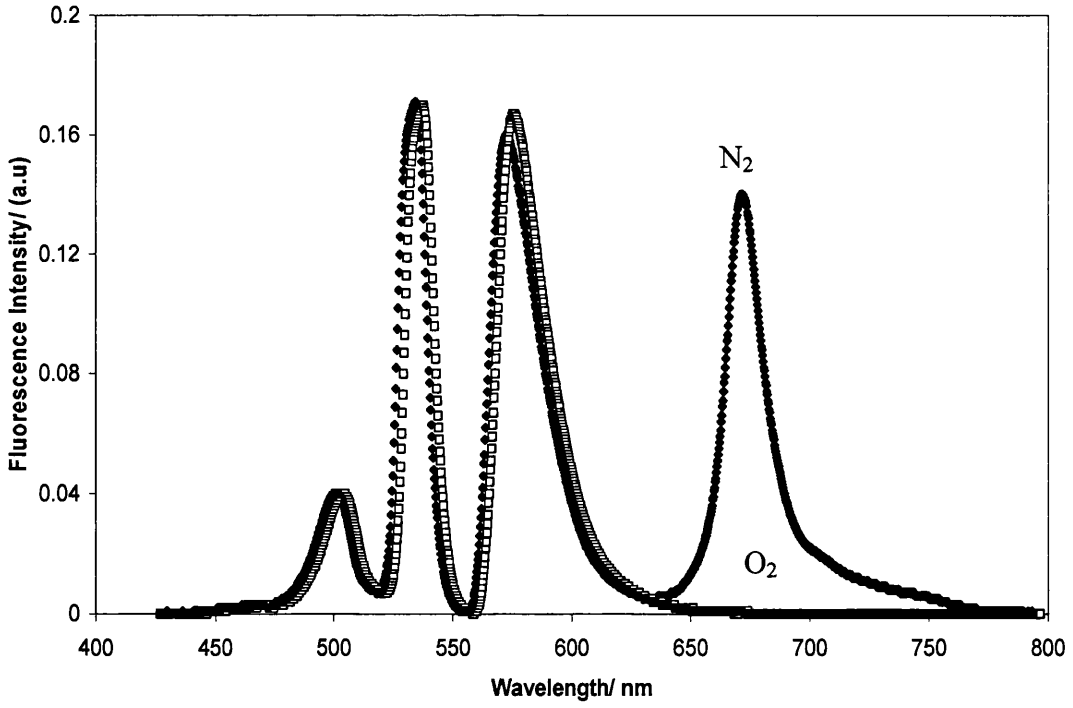

Fig.5.13. A PdOEP sensor under nitrogen (open squares) and oxygen (closed shapes) with a clear green LED used as a source of emission

5.7.3 Emission from sensor F

Sensor F was chosen for further analysis of its emission characteristics because it gave a good colour change and had the highest light stability.

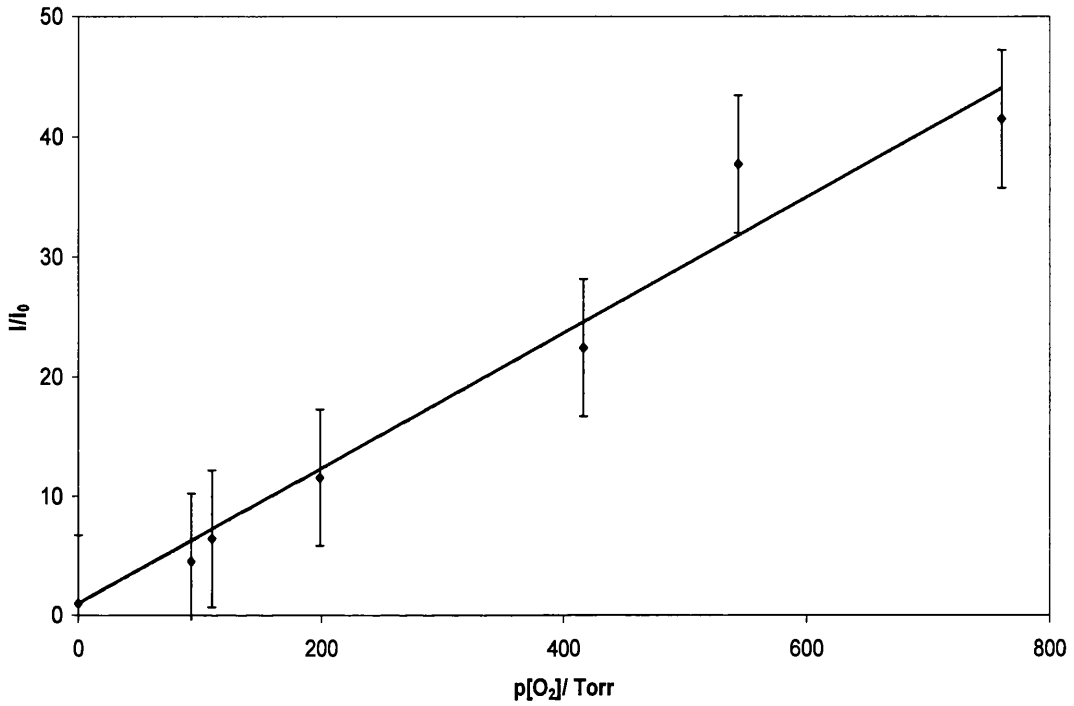

Fig.5.14. Stern-Volmer plot for sensor **F**, $K_{sv} = 0.058 \pm 0.00461$ Torr^{-1}, $R^2 = 0.9685$

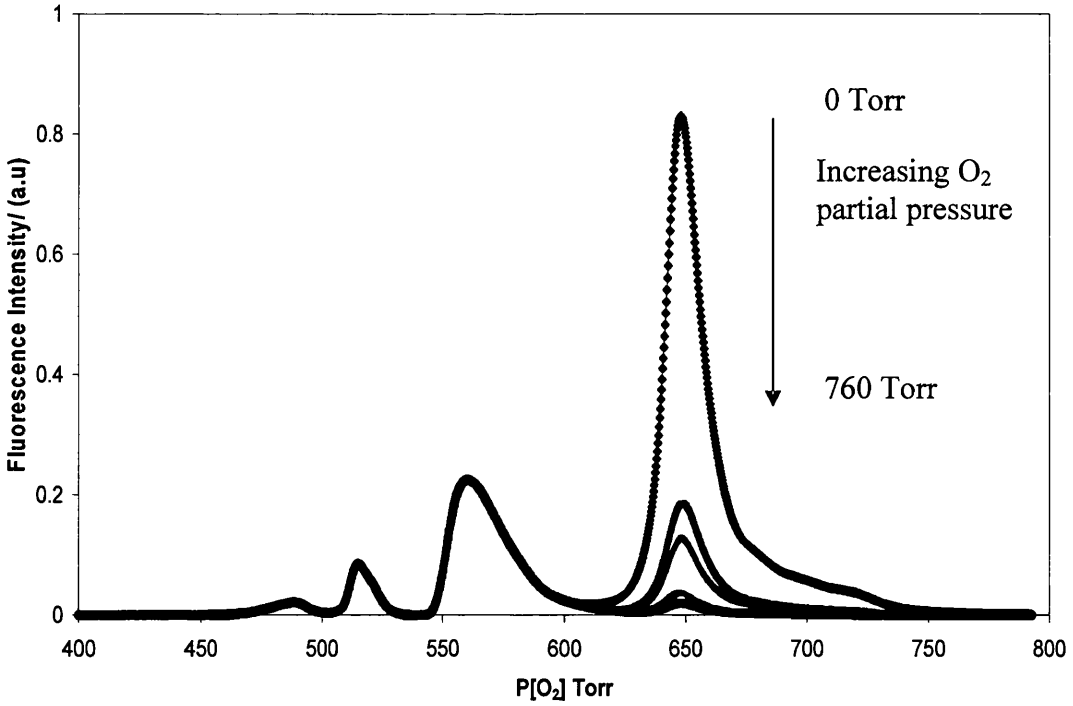

Fig.5.15. Uncorrected emission spectra for sensor **F** under different partial pressures of oxygen

Analysis of Stern-Volmer plots for sensor F gave a Stern-Volmer constant of 0.058 ± 0.00461 $Torr^{-1}$ which is much less than found with thin film sensors (figs. 5.14 and 5.15). We are not sure of the reason for this but film thickness, adsorption onto the scattering agent and possibly a higher level of heterogeneity[28] may be factors influencing the response.

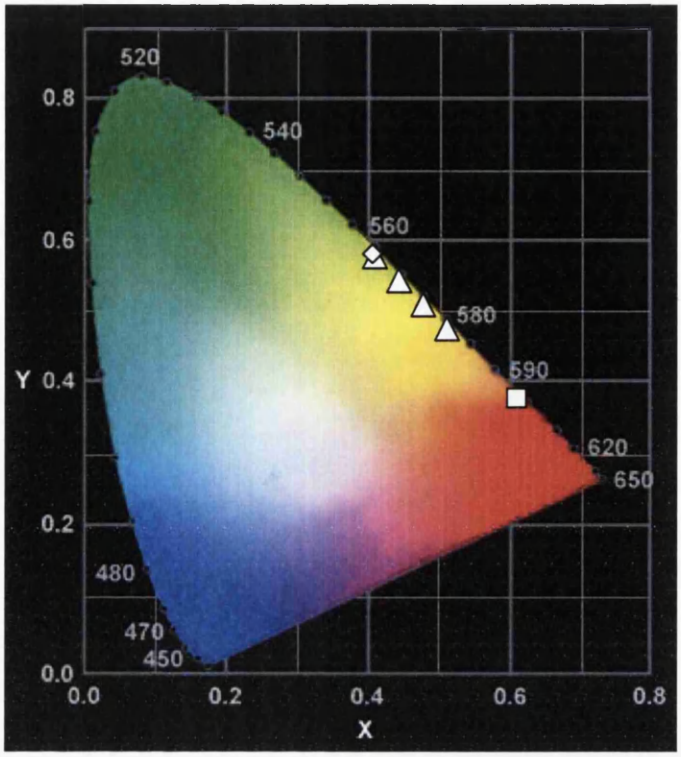

Fig.5.16. The response for sensor F under different partial pressures oxygen from pure oxygen (diamond) to nitrogen (square), The following partial pressures are shown, 0, 93, 110, 198, 416, 544, 760 Torr

The CIE coordinates reveals that, for this sensor, the most significant colour change occurs at a low pO_2 (figs.5.14, 5.15, and 5.16). This is to be expected because the green emission is not affected by changes in pO_2, and therefore this is a similar arrangement to the BM sensor in chapter. Fig. 5.17 shows the colour change observed for sensor F under oxygen and nitrogen, and demonstrates that the colour change is a definite green to red colour change, which may not be obvious to from the CIE chromaticity diagrams.

Partial pressure of oxygen (Torr)	CIE co-ordinates
0	x = 0.62, y = 0.38
93	x = 0.51, y = 0.48
110	x = 0.49, y = 0.50
198	x = 0.46, y = 0.52
416	x = 0.44, y = 0.54
544	x = 0.44, y = 0.55
760	x = 0.43, y = 0.55

Table.5.2. CIE co-ordinates for sensor F, plotted in Fig.4.14.

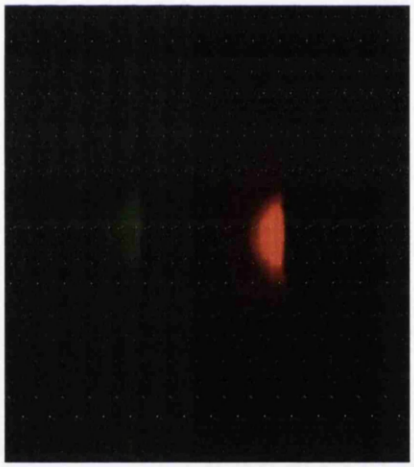

Fig.5.17. Photograph of sensor F under 100% oxygen (left) and 100% nitrogen (right)

5.8 Conclusion

From the work presented in this chapter it can be seen that an oxygen sensor can be fabricated that can give a "traffic light" response to changing oxygen partial pressures, using an LED as a green emission source and also as an excitation source exciting the Q-band of PtOEP in an ethyl cellulose matrix.

Various optical arrangements were tried in order to gain the necessary colour change, and it was ultimately found necessary to add a scattering agent. Two effects are believed to be important as a result of the addition of a scattering agent: firstly the pathlength is dramatically increased by producing a more random path through the sensor film, and therefore the absorption of the LED light and resultant lumophore emission are enhanced; secondly the scattering agent has the effect of moderating the LED light at the front of the film by decreasing the directionality of the emission from the LED. Both effects enhance the relative emission seen from the oxygen sensitive lumophore to give a better ratio of LED light and lumophore emission for sensor operation.

Three different scattering agents were used: Degussa TiO_2 p25, TiO_2 Dupont tripure and ZnO. While good visible colour changes could be observed in the sensors made using TiO_2 Degussa, use of this scattering agent led to sensor degradation under both oxygen and nitrogen. Both the other scattering agents gave improved sensor stability. Further stabilisation was obtained, as in previous investigations (see chapter 3), by incorporation of the singlet oxygen stabiliser DABCO.

Two different oxygen sensitive lumophores were immobilised in ethyl cellulose and assessed for their suitability for use in these sensors. It was discovered that although PdOEP absorbed light from both the clear green and the superbright LEDs the resulting sensor did not give a colour change as the atmosphere was changed between oxygen and nitrogen. This can be attributed to the difference in the emission quantum yields of PdOEP (Φ =0.5) and PtOEP (Φ =0.2)[8].

One disappointing feature of the sensor characteristics is their slow response times which are around ten minutes from oxygen to nitrogen in sensor F. Use of a plasticizer was shown to speed up the response time of the sensor, but this was still not particularly rapid. The thickness of the films is the major barrier for improving the response times, and future work might involve using a more soluble Pt porphyrin, such as those described by Papkovsky and co workers,[29] which would allow a thinner film to be made, and hopefully faster response times.

The resulting colour change is very clear and occurs at quite low oxygen partial pressures, under nitrogen the colour of the sensor is red, but at 93 Torr pO_2 a significant colour change is observed and the sensor is already changing to yellow (table 5.2). This gives them possible application in areas where detecting changes in oxygen concentration in this sort of range are important, such as the preservation of artefacts previously described when discussing the development of sensors for museum applications (see chapter 3).

5.9 References

1) Ricketts, S.R.; Douglas, P.; *Sensors and Actuators B*, 135, **2008**, 46-51.

2) Hunt, R.W.G., *Measuring Colour, 3rd ed.,* Fountain Press, (1998), 48.

3) Evans, R.C.; Douglas, P. *Anal. Chem.*, 78, **2006**, 5645-5652.

4) Evans, R.C.; Douglas, D.;Williams, J.A.G.; Rochester, D.L. *J. Fluores.,*15, **2006**, 201-206.

5) Wang, X.; Chen, X.; Zhao-xiong; X.; Wang, X., *Angew. Chem. Int. Ed.,* 47, **2008**, 7450-7453.

6) Katoh, R.; Nakamura, M.; Sasaki, Y.; Furube, A.; Yokoyama, T.; Nanjo, H., *Chem. Lett.,*36, **2007**, 1310-1311.

7) Farley, S.J.; Rochester, D.L.; Thompson, A.L.; Howard, J.A.K.; Williams, J.A.G. *Inorg. Chem.,* 44, **2005**, 9690-9703.

8) Mills, A.; Lepre, A., *Anal. Chem.,* 69, **1997,** 4653-4659.

9) Seuntiens, P.J.H.; Vogels, I.M.L.C.; Kraaijenbrink, E.B. *Proc. SPIE,* 6492, **2007**, 64920U-1-64920U-12.

10) Standish, B. *Biophotonics Int., 14,* **2007**, 37-40.

11) Chodavarapu, V.P.; Bukowski, R.M.; Kim, S.J.; Titus, A.H.; Cartwright, A.N.; Bright, F.V. *Electronics Letts.,* 41, **2005**, 1031-1033.

12) Malins, C.; Niggemann, M.; MacCraith, B.D. *Meas. Sci. Technol.,*11, **2000**, 1105-1110.

13) Savvate'ev, V; Chen-Esterlit, Z; Aylott, J.W; Choudhury, B; Zou, K.L; Shinar, F.R; Shinar, J; Kopelman, R., *Appl. Phys. Lett.,*18, **2002,** 4652-4654.

14) Ghosh, D; Shinar, R; Yuankun, C; Zhou, Z; Dalal, V.L; Shinar, J., *Proc of SPIE,* 6559, **2007**, 66590E-1-66590E-7.

15) Crowley, K; Pacquit, A; Hayes, J; King, T.L; Diamond, D., *Sensors 2008 IEEE,* **2008,** 754-757.

16) Demas, J.N.; Crosby, G.A. *J. Phys. Chem.*, 75, **1971,** 991-1024.

17) Shinar, R.; Zhou. Z.; Choudhury, B.; Shinar, J. *Anal. Chim. Acta,* 568, **2006**, 190-199.

18) Bandrup, J.; Immergut, E.H.; Grulke, E.A. *Polymer Handbook, 4th ed.,* Wiley. 1991.

19) Nasu, A.; Otsubo, Y. J. *Colloid Interface Sci.,* 310, **2007,** 617-623.

21) Dongdong, Z.; Rongliang, Q.; Song, L.; Brewer, E.; Mo, Y.; Xiongfei, H. *J. Haz. Mat.,* 163, **2009,** 843-847.

20) Mahvi, A.H.; Ghanbarian, M.; Nasseri, S.; Khariri, A. *Desline.,* 239, **2009,** 309-311.

22) Captitan-Vallvey, L.F; Asensio, L.J; Lopez-Gonzalez, J; M.D. Fernandez-Ramos, M.D; Palma, A.J, *Anal. Chim. Acta.,*583, **2007,** 166-173.

23) Palma, A.J; Lopez-Gonzalez, J; Asensio, L.J; Fernandez-Ramos, M.D; Captan-Vallvey, L.J., *Sens. Actuators B,* 121, **2007,** 629-638.

24) Herne, R.; Brocas, E.; Vander Donckt, V. *Anal. Chim. Acta.,* 364, **1998,** 131-141.

25) Eaton, K.; Douglas, P. *Sens. Actuators B,* 82, **2002,** 94-104.

26) Crank.J, *The Mathematics of diffusion, 2nd ed.,* Oxford: Claredon Press, 1975.

27) Hughes, V.A.; Douglas, P. *J. Fluoresc.*, 16, **2006,** 403-409.

28) Douglas, P.; Eaton, K. *Sens. Actuators B*, 41, **2002**, 1-9.

29) Papkovski, D.B.; Ponomarev, G.V; Trettnak, W.; O'Leary, P. *Anal. Chem.,* 67, **1995,** 4112-4117.

Sensors for detecting partial pressures of oxygen and carbon dioxide in blood

6.1 Summary

The aim of the work presented in this chapter was to develop a working optical sensor device for the insitu measurement of dissolved carbon dioxide and oxygen in blood. This was achieved by the design and manufacture of two flow cells, one of which contains a carbon dioxide sensitive membrane consisting of 8-hydoxypyrene-1, 3, 6, trisulfonic acid (HPTS) encapsulated in a sol gel matrix, while the other contains an oxygen sensitive film consisting of PtOEP in an EC matrix stabilised by DABCO. Both sensor membranes (SM) are kept out of contact with the blood by a thin diffusion membrane (DM) of either polyethersulfone or polypropylene through which the analytes diffuses out of the blood, and into the SM. Detection was by optical means and both films were excited by LEDs. Detection is via phototransistors with bandpass filters to improve the signal to noise ratio. This sensor is compact, accurate, and stable, and has a fast response time. It can be used with any solution which does not destroy the DM or the flow cell.

6.2 Introduction

Detecting the concentration of carbon dioxide and oxygen in the blood is of great interest in medical applications.[1] The concentration of these gases gives a key indication as to the health of an individual.[2-4] Individuals with poor respiration have relatively low concentrations of oxygen and relatively high partial pressures of carbon dioxide as the result of poor gas exchange in the alveoli, therefore starving the tissues of oxygen. Furthermore the levels of carbon dioxide increase because it is not effectively removed from the body and this leads to a decrease in blood pH because carbon dioxide reacts with water to form carbonic acid. A sustained increase in carbon dioxide results in a condition known as acidosis, which in turn leads to hyperkalemia, whereby potassium is leached out of the cells producing paralysis and cardiac arrhythmia.[5-8] Typical partial pressure for carbon dioxide, in blood, in a man breathing air in a room is 6.1 kPa, and sensors are generally required to measured a range between 2 kPa and 8 kPa.[9] The typical value for oxygen is approximately 16.6 kPa,[10] with the range of clinical interest from 0 kPa up to 21 kPa.[9] (Throughout this chapter partial pressures are given in kPa rather than Torr because this was the units that was used by Haemair and so were adopted to comply with their needs.)

The traditional treatment for patients with poor respiration is to give them pure oxygen.[11] While this helps to solve the problem of low oxygen levels it does not reduce the amount of carbon dioxide, which is very dangerous and not sustainable for long periods;[12] and ultimately the only current long term option is a transplant.

Traditional transplants from donors are not widely available, and have the additional problems associated with the use of immunosuppressants which can lead to complications and rejection by the patient.[13,14] However Professor Bill Johns' company Haemair (Haemair Ltd., Unit 212, Technium Digital, UW Swansea, SA2 8PP.) are current working on an artificial lung which will exchange both gases in the blood with those in the atmosphere, thus both increasing oxygen concentration and reducing carbon dioxide concentration to help provide patients with a better quality of life.

In order to produce an artificial lung and measure and optimise its performance it is necessary to measure the concentrations of oxygen and carbon dioxide in the blood, preferably in real time. A number of different techniques are available for this. The traditional method is that of pulse oximetry, whereby two beams of "light" are passed through the blood (one red and one in the IR) and the changed in absorbance and ratio of the two beams is measured by a photodiode giving an indication of the concentration. However this technique is susceptible to changes in metabolite concentrations in the blood, and can be inaccurate because of interference from haemoglobin content and plasma composition.[15-16]

The current method used by Haemair is a commercially available system based on electrochemical cells. [17,18] This method is accurate, however it requires taking 1 cm^3 samples of the blood that then have to be disposed of after measurement. This limits the number of measurements that can be made, because the maximum amount of blood that can be used at any one time is 20 cm^3 due to ethical approval. A second problem associated with taking samples is that mixing can taken place with

oxygenated and non oxygenated blood in the sampling vessel and thus a false value can be obtained.

As a possible alternative to these sensors we have developed a sensor based on optical methods for the measurement of dissolved carbon dioxide and oxygen in blood. There are a number of problems with using luminescent sensors for the measurement of blood gases: it is best if the sensor is not in contact with the blood for both medical and analytical reasons, and blood is not very transparent across the UV-Vis spectral wavelengths.[19,20] Despite these technological challenges the potential is there to provide a sensor which is cheaper and faster than the traditional electrochemical method, which has a higher degree of accuracy and repeatability than pulse oximetry, and which also provides real time measurement. [21-24]

6.3 Materials and Methods

8-hydoxypyrene-1, 3, 6, trisulfonic acid trisodium salt (HPTS), methyltriethyloxysilane (MTEOS), HCl, ethyl cellulose (EC) (46 % ethyloxy content), toluene, ethanol, THF, polystyrene, silver oxide, methanol and DABCO were all purchased from Aldrich, cetyltrimethyl ammonium bromide and PtOEP were purchased from Fischer scientific. Phototransistors are ambient light phototransistors from RS components cat no. 654-7808. Blue LEDs for the carbon dioxide sensor are 465 nm hyper 5 mm blue LEDs obtained from RS. UV LEDs were obtained from Roitner-lasertechnik, http://www.roithner-laser.com/LED_diverse.htm and are 385 nm 16 ° epoxy UV LEDs. OSRAM opto

semiconductor photodiodes were also purchased from RS components cat. no. 652-0207.

Two types of carbon dioxide SMs were made, both based on HPTS. The first used an EC matrix and was prepared by ion pairing. 0.085 g of HPTS was dissolved in 30 ml of distilled water containing 1 % sodium carbonate, to this 0.02 g of tetraoctyl ammonium bromide was added to form an ion paired species.[25] On adding the tetraoctyl ammonium bromide the ion pair began to precipitate out of solution, and was then extracted into 30 ml of CH_2Cl_2. The aqueous layer was washed with portions of a 1 % NaOH solution in water to aid precipitation. The ion pair was recovered by evaporation of CH_2Cl_2.

A separate solution of tetraoctyl ammonium hydroxide was made by dissolving 1.4 mg of tetraoctyl ammonium bromide in 10 ml of methanol and adding a suspension of 0.6 g Ag_2O. The resulting suspension was stirred for 4 hrs and then allowed to settle; the tetraoctyl ammonium hydroxide was decanted and kept in a stoppered flask. EC sensors were made by dissolving 60 mg of the ion pair in 1 g of 10 % EC in 80:20 toluene: ethanol (w:v), to this 0.6 ml of the base was added, and the resulting solution spin coated onto a glass substrate at 1000 rpm.

The second carbon dioxide sensor membrane that was made, and the one that was chosen for used in the blood sensor was based on a sol gel matrix. The sol-gel was prepared by taking 4.0 ml of MTEOS, adding 1.5 ml of 0.1 M HCl, and stirring vigorously for 2 hours.[26] To this was added 5 ml of a solution of 80 mg HPTS dissolved in 5.4 ml cetyltrimethyl ammonium hydroxide solution. A second

cetyltrimethyl ammonium hydroxide solution was prepared for use with the sol gel sensor, by dissolving 1.8 g of cetyltrimethyl ammonium bromide in 10 ml of methanol, 1.2 g of Ag_2O was then added and the solution stirred for four hours before being allowed to settle. The resulting solution was decanted and kept in a sealed vessel to allow the solid to settle out.

Measurements of emission spectra were performed using a Perkin-Elmer MPF 44E fluorimeter. Absorption measurements were performed on a Hewlett-Packard 825A diode array spectrophotometer.

All sensor measurements were carried out at 25 °C.

To test the oxygen sensor in water, the partial pressures of the water was changed by bubbling in mixed gases of oxygen and nitrogen from a V1-B gas blender from Signal Instruments Co. UK into a reservoir. This was then pumped through the sensor by a peristaltic pump at 10 ml/min. Oxygen partial pressures were measured using a Handy Polaris dissolved oxygen probe.

For testing the carbon dioxide sensor in water two peristaltic pumps were used. The first pumped water from a reservoir with distilled water which was virtually free from carbon dioxide (under ambient conditions approximately 0.03 %).[27] The second was saturated with carbon dioxide. By varying the pumping rates it was possible to get solutions of different concentrations of carbon dioxide. A pH meter was used to determine the concentration of carbon dioxide; the equilibrium partial pressure of which is given by eqs. 6.1 and 6.2.

$$pH = -\log[H^+] \qquad [6.1]$$

$$[H^+] = (10^{-14} + (k_h k_{a1}/k_H)pCO_2)^{1/2} \qquad [6.2]$$

k_H is the Henry's law constant, (29.76 atm mol^{-1} L), k_{a1} the equilibrium constant for the dissociation of the first proton from methanoic acid, (2.5×10^{-4}), k_h the hydration equilibrium between dissolved CO_2 and methanoic acid (2.6×10^{-3}). [28-29]

Carbon dioxide reacts with water, therefore is not possible to simply use Henry's law to calculate the concentration of carbon dioxide in water. Carbon dioxide dissolves into the water and most of the carbon dioxide is in an aqueous neutral species which can not be detected by a pH meter (see section 1.9 in the introduction), but the concentration of this species can be calculated using the Henry's law constant kH. A small portion of carbon dioxide reacts with water to form methanoic acid, and this will dissociate to produce protons in line with its dissociation constant ka_1. Therefore by measuring the pH it is possible to calculate concentration of protons present using equation 6.1, and correspondingly the partial pressure of the carbon dioxide can be calculated by substituting the proton concentration into equation 6.2.

Experiments to test repeatability were performed by passing water through the sensors from a reservoir equilibrated with gas of known composition via a peristaltic pump. The analyte gas, either oxygen or carbon dioxide was passed into the reservoir until a steady reading was obtained and then the bubbling gas was changed to nitrogen. The process was then repeated.

Carboxylation and oxygenation of the blood was accomplished by passing the analyte gases through custom made gas exchangers provided by Heamair, where the partial pressures of gases in the exchanging atmosphere were obtained using an Irma Trupoint gas analysis system.

6.4 Sensor Design

Each of the sensors for carbon dioxide and oxygen can be separated into three constituent parts; the first is the luminescent sensor itself that produces a measurable response to the analyte concentration and is referred to as the sensor membrane (SM), the second part is the flow cell which houses the luminescent sensor and allows the blood to flow through it so that the gases can diffuse out of the blood and into the SM, the final part of the sensor is the sensor optics that comprise an LED to excite the SM and a detector that measures the change of an optical parameter from the SM.

6.4.1 Choice of sensor membrane

The sensor membrane (SM) is a critical choice for the sensor as this is the part of the sensor that senses the analyte. The mechanism for the blood oxygen sensor involves the quenching of a luminescent dye in a polymer matrix in the already familiar Stern-Volmer relationship discussed in detail in chapters 1, 3, 4 and 5.

The mechanism of a carbon dioxide sensor has not yet been described. The mechanism is based on the protonation and deprotonation of a dye fig.6.1, which is encapsulated in a polymeric matrix with a bicarbonate buffer or an ion pair.[25] As the

carbon dioxide enters the sol gel a small portion of the carbon dioxide reacts with water that is trapped in the sol gel matrix generating methanoic acid which is the source of protonation of the encapsulated dye producing an optical change which can be measured (fig.6.2). Initial work centred on absorption based dyes[30,31], while later examples are based on luminescence dyes.[32,33]

$$COA^+ / Dye^- + xH_2O + CO_2 \rightleftharpoons COA^+/ HCO_3^- + (x-1)\, H_2O + H\text{-}Dye$$

Fig.6.1. The mechanism of a carbon dioxide sensor, COA^+ is the ion pair bound to the dye, Dye^- is the unprotonated form of the dye and H-Dye the protonated form

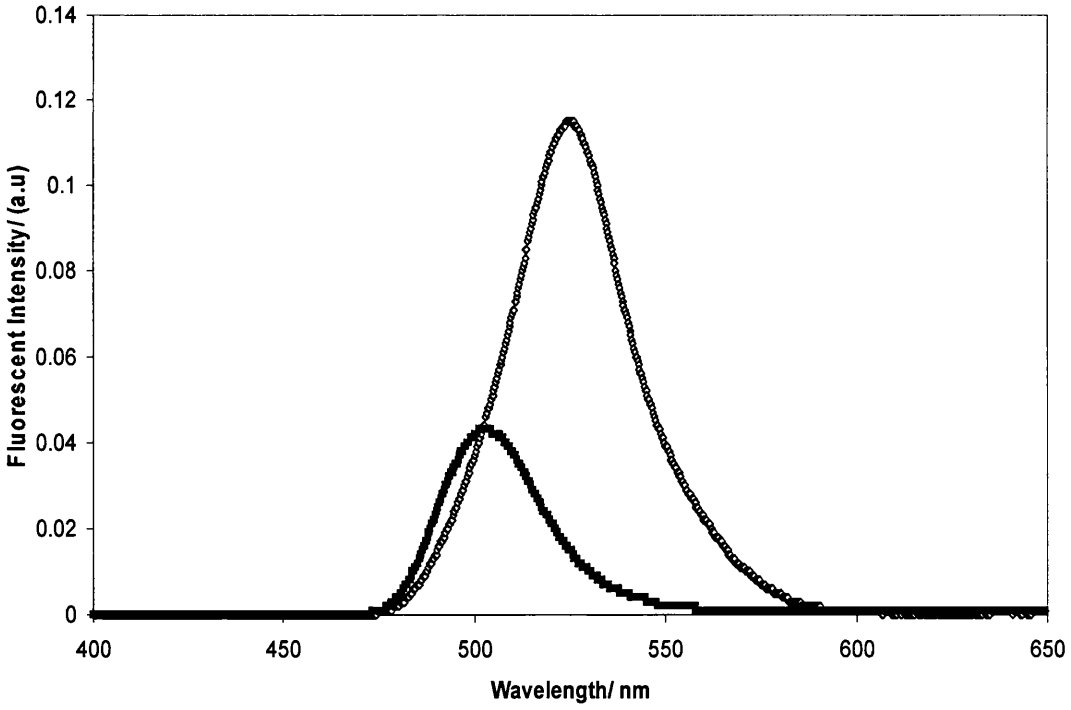

Fig.6.2. Change in emission of HPTS with a cetyltrimethyl ammonium hydroxide ion pair in a sol gel polymer matrix under carbon dioxide (open symbols) and nitrogen (filled symbols)

The choice made for the oxygen sensor was PtOEP in an ethyl cellulose matrix. This has already been demonstrated to be readily quenched by oxygen, possess a high quantum yield, have good optical properties, and is very stable with the addition of DABCO.[34,35] Fig. 6.3 demonstrates the photostability of such a sensor film.

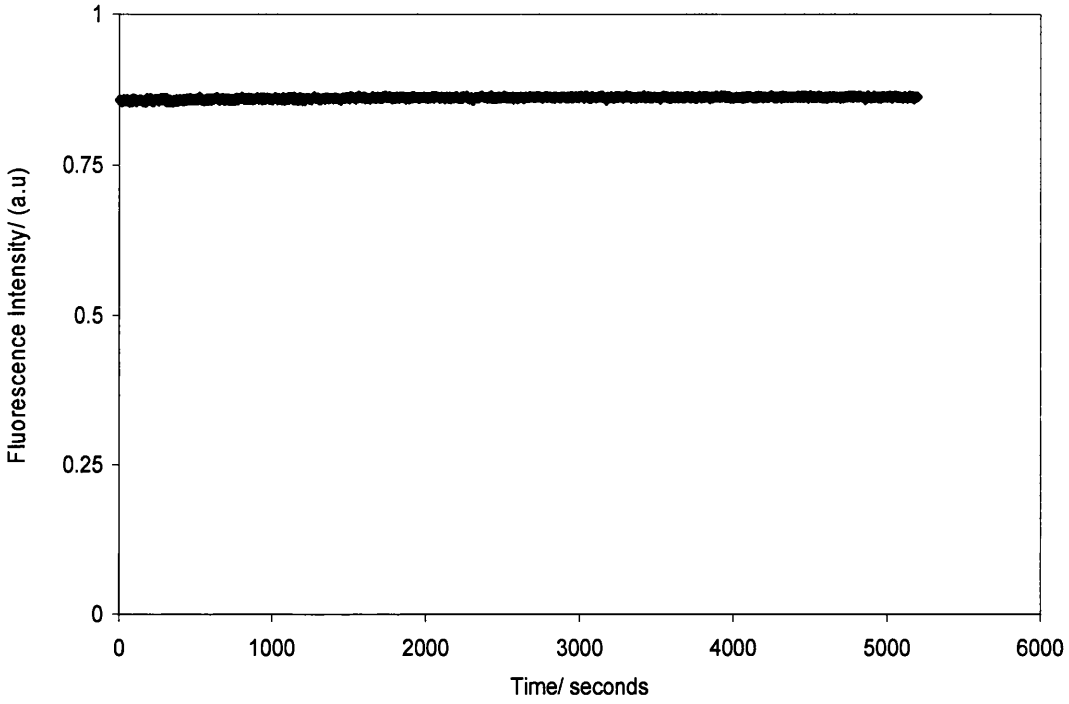

Fig.6.3. Stability with of a carbon dioxide SM in EC, with a blue LED A under air

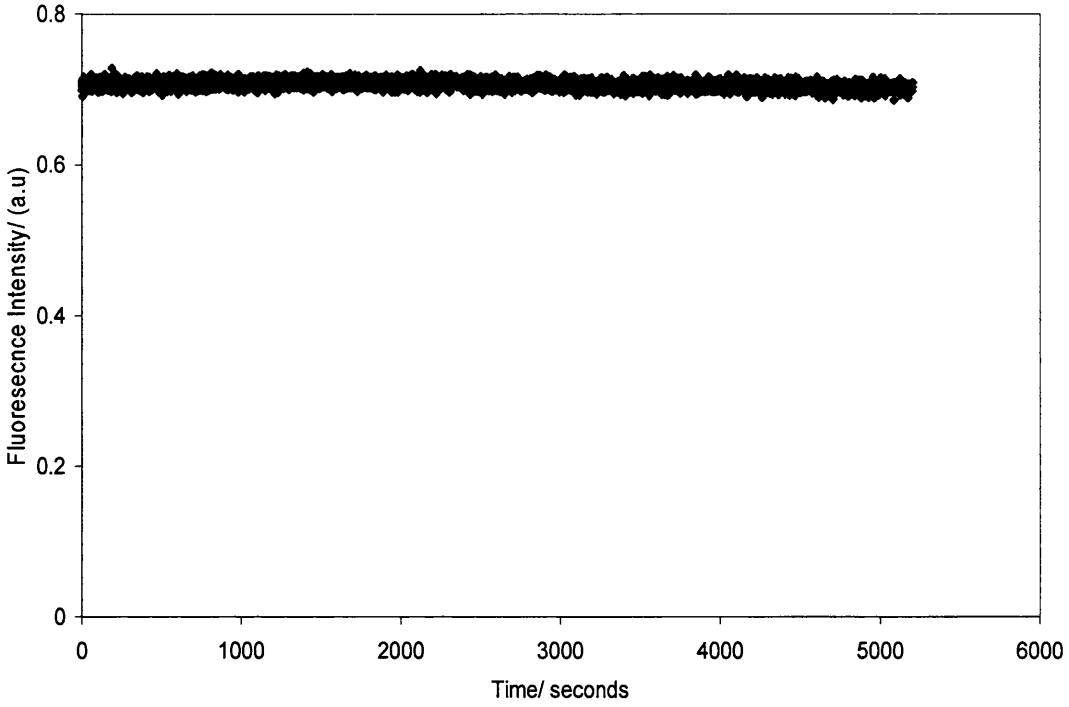

Fig.6.4. Stability plot of PtOEP in a EC with DABCO, under air, excited with a UV LED

For the carbon dioxide sensor HPTS was chosen as the luminescent dye because it has a high quantum yield, and demonstrates excellent photostability (fig 6.4)[36] Carbon dioxide sensors are tuneable, the sensitivity of the sensor depends on the ion pair or buffer used.[26] The earlier examples of carbon dioxide optodes used bicarbonate buffers, however this was later superseded by using ion pairs. Ion pairing uses tertiary ammonium hydroxides which can bind to the indicator dye (fig. 6.5). The major advantage of this is that it makes the dyes more soluble in hydrophobic polymers such as EC and the sol gel used in this chapter. The earliest examples of ion pairing used tetraoctylammonium hydroxide to form the ion pair and this produced sensors with high sensitivity. However at high carbon dioxide concentrations such a high sensitivity sensor shows very little change, therefore for most applications a less sensitive sensor made using cetylammonium hydroxide is

preferred. If less sensitivity is required it is also possible to use tetrabutylammonium hydroxide. This control of sensitivity is related to the way that the ion pair shields the positive charge from the HPTS [26,37] Further changes in sensitivity can be obtained by adding more ion pair to the matrix, generally the more ion pair used the lower the sensitivity.[38]

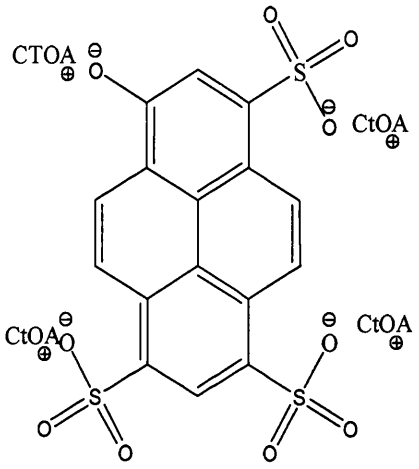

Fig.6.5. Ion pairing between HPTS and the cetylammonium hydroxide (CtOA)

The use of cetylammonium hydroxide is also beneficial because the sensor shows a faster recovery time from 90 % carbon dioxide to 100 % nitrogen (figs. 6.6 and 6.7).

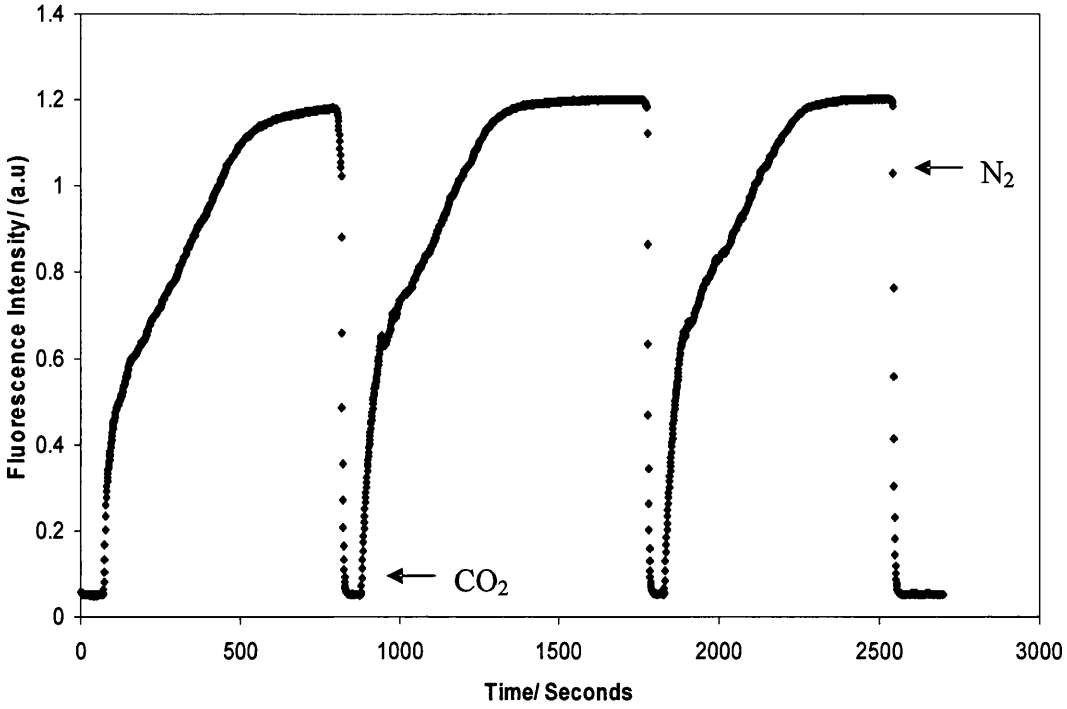

Fig.6.6. Responses of a carbon dioxide sensor in EC, excited with a blue LED A, the time for the response from 100 % carbon dioxide to 90 % nitrogen is 353 s, the corresponding time for the change from nitrogen to carbon dioxide is 59 s

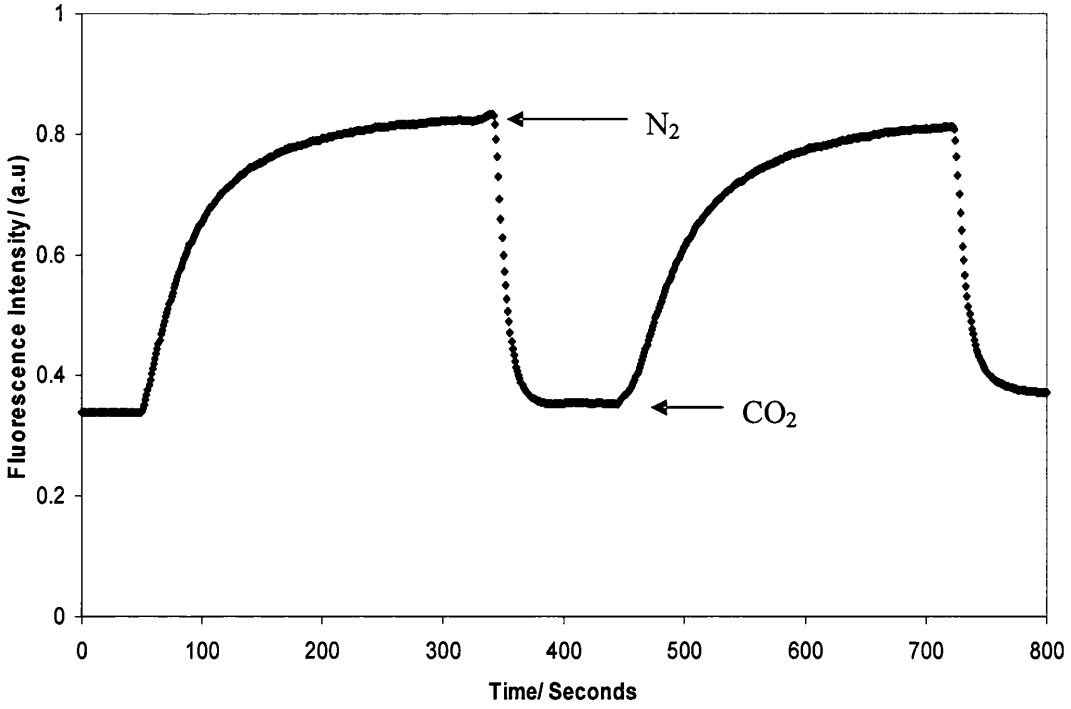

Fig.6.7. Response of a sol gel SM containing HPTS with cetylammonium hydroxide as the ion pair under oxygen and nitrogen, (90%) CO_2 to N_2 response is 92 s, nitrogen to carbon dioxide response is 54 s

Initially the polymer matrix used for the carbon dioxide sensor was EC. However considerable degradation can be seen over time, this is thought to arise because of a number phenomena such as leaching of the ion pair out of the polymer, and also gases such a SO_2 and NO_2 entering the polymer and forming much stronger acids that permanently protonate the dye. It has also been suggested that the ion pair is thermally unstable, however some sensors have been kept for many hundreds of days without degradation so this would seem unlikely.[30,39] When HPTS was encapsulated in a sol gel[40] it was much more resistant to dye leaching. However, it was discovered that the sol gel did not adhere well to a glass substrate, and that in the carbon dioxide sensor the sol gel film could be damaged easily due to the SM becoming damp in the

sensor. The presence of water was confusing, however it seems most likely to be due to water vapour passing through the membrane. When blood was used no evidence was found of the blood passing through the diffusion membrane. To prevent this, an EC film was first spin coated over the glass substrate to provide an anchor for the sol gel. Two layers of the sol gel were spin coated over each other. It was necessary to spin coat two layers of the sol gel to produce a high enough absorption of the LED emission. These were then allowed to dry for 45 minutes. It is normal for sol gel films to be dried in an oven at 70 °C, however this produced poor quality slides probably due to rapid solvent evaporation of the methanol so the layers were dried in air at room temperature. Once dry a protective layer of a 2 % solution of polystyrene in toluene was spin coated over it. All layers in the sensor were spin coated at 1000 rpm.

The resulting sensor composition of the four layers (EC, sol gel, sol gel, polystyrene) produces a much more resistant, but still sensitive, sensor which is not easily damaged. From fig 6.8 it can be seen that none of the layers are affected by the spin coating of subsequent layers and so no further barrier layers are required. Once fabricated the carbon dioxide sensor needs to be activated with water. In the sensor the SM becomes wet during operation so the SM can be stored in dry conditions as long as water is run through the flow cell before use to activate the sensor.

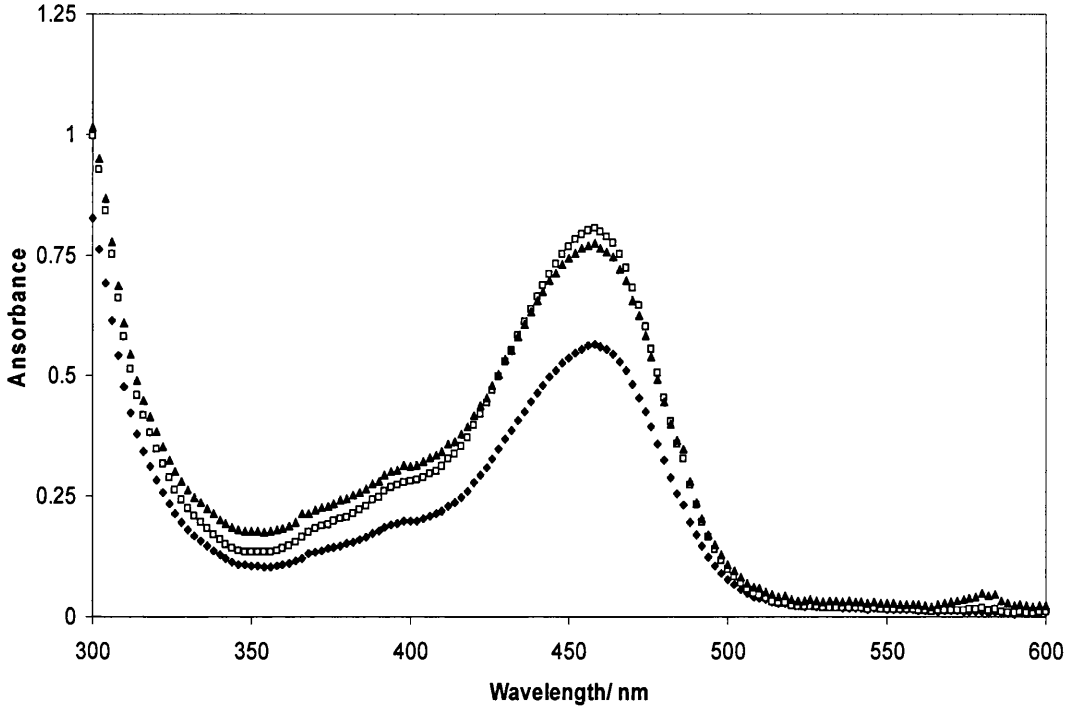

Fig.6.8. Absorption spectra of the layers of a carbon dioxide sensor membrane after each is spin coated, 1st layer of HPTS in the sol gel polymer (diamonds), 2nd layer of HPTS in the sol gel polymer (triangles), 2 % polystyrene layer (squares open)

6.4.2 Design of the flow cell

It was initially decided that the sensor should be made to fit into a fluorimeter in order to analyse the sensors. Therefore the flow cells (fig.6.9) were designed to fit to a brass plate which sat securely in the fluorimeter.

It was decided also that the sensor should not come into contact with the blood as this was likely to provide false readings especially with the pH sensor and would also mean that the sensors would have to be replaced every time for reasons of hygiene.

Therefore a membrane was required between the SM and the blood flowing through the sensor which would allow diffusion of gases out of the blood into the SM. Two different types of membrane were investigated: polyethersulfone and polypropylene. These can be both manufactured to be permeable to oxygen and carbon dioxide. The degree of permeability of the SMs is dependent on the size of the pores in the membrane.[41,42] Both of the diffusion membranes investigated were white in colour and therefore reflective. This property was used in the sensor design since it allowed reflection of emission from the SMs.

The oxygen sensor was slightly smaller internally because this was designed first, a larger volume was used on the carbon dioxide sensor to promote a more laminar flow. (Laminar flow is thought to slow down the clotting of blood, however, on testing the flow cells there was no noticeable difference in the rate of clotting in the oxygen or carbon dioxide sensors.) The general structure of the flow cells is shown in fig.6.9.

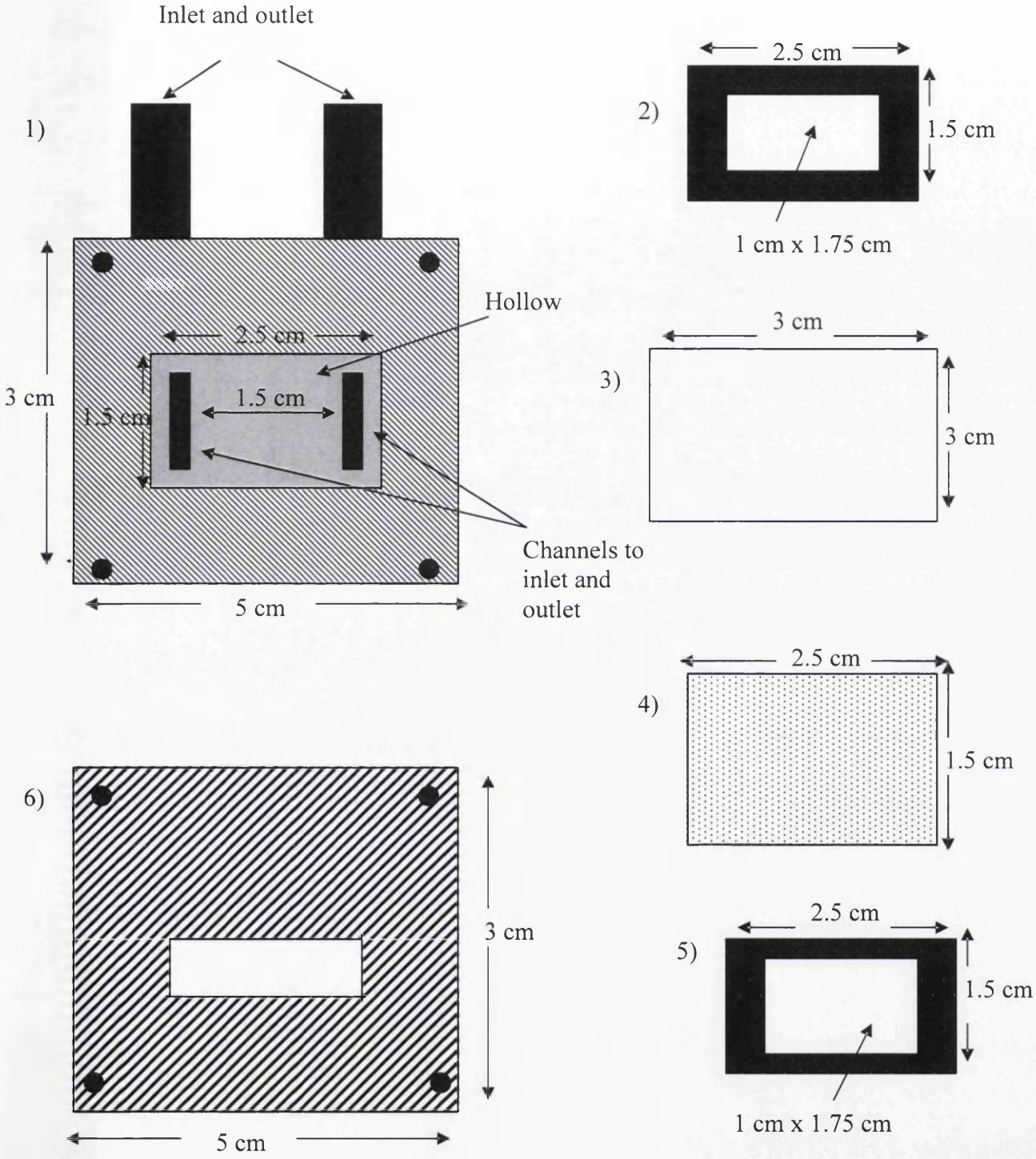

Fig.6.9. The parts of the flow cell (sizes refer to the blood oxygen flow cell)

Each of the parts is numbered in the order that they are set into the flow cell (fig. 6.9).

Part 1 - The flow cell has channels set into it so that the blood can flow through the cell and out again.

Part 2 - A piece of PTFE which is cut so that is acts as a washer by sitting in the channel cut out of flow cell and allows blood to flow through it. It is 3.5 mm and sits slightly proud of the channel enabling a better seal to be made.

Part 3 - The diffusion membrane.

Part 4 - The SM set so that the sensing side is in contact with the diffusion membrane.

Part 5 - A second piece of PTFE which is used to create the seal and pushes down on the SM.

Part 6 - A stainless seal plate which screws into part 1 and holds all of the parts together.

6.4.3 Optical arrangements

Originally the sensors were designed to be placed in the fluorimeter since this was the initial method of excitation and detection for "proof of principle" work. However a different arrangement was required for the working sensors, which were required to be small and compact.

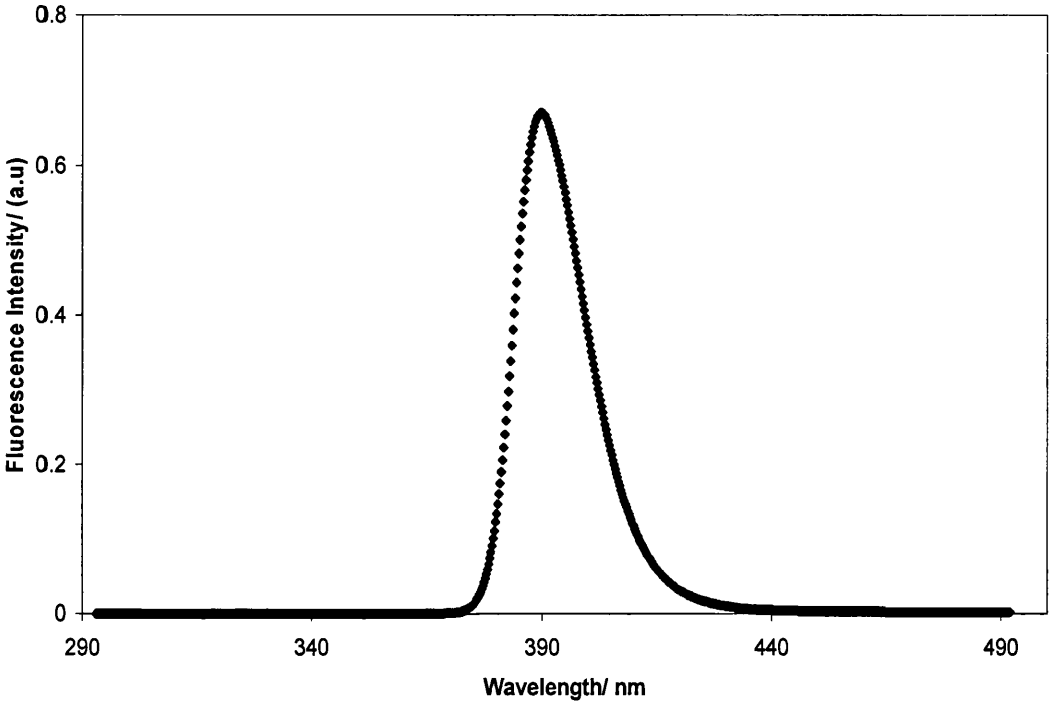

Fig.6.10. Emission spectra of the UV LED used for excitation in the blood oxygen sensor

By experiment it was found possible to excite both of the sensor membranes using LEDs (figs.6.10 and 6.14). The LED selected for the oxygen sensor was the UV LED (fig.6.10) used in the torch for the "British Museum" sensor described in chapter 3. From the absorption spectra of an EC carbon dioxide sensor membrane it was established that there were three main absorption peaks (fig. 6.21) which could be excited at 464 nm, 408 nm and 376 nm (figs.6.11-6.13). It was discovered that

exciting the carbon dioxide sensor membrane at 464 nm produced the biggest sensor response, therefore two LEDs (fig.6.14) were used to excite the carbon dioxide sensitive membrane at around 464 nm. LED A is the most intense but this was later replaced by LED B because LED A was found to be so intense it was drowning out the emission from the SM.

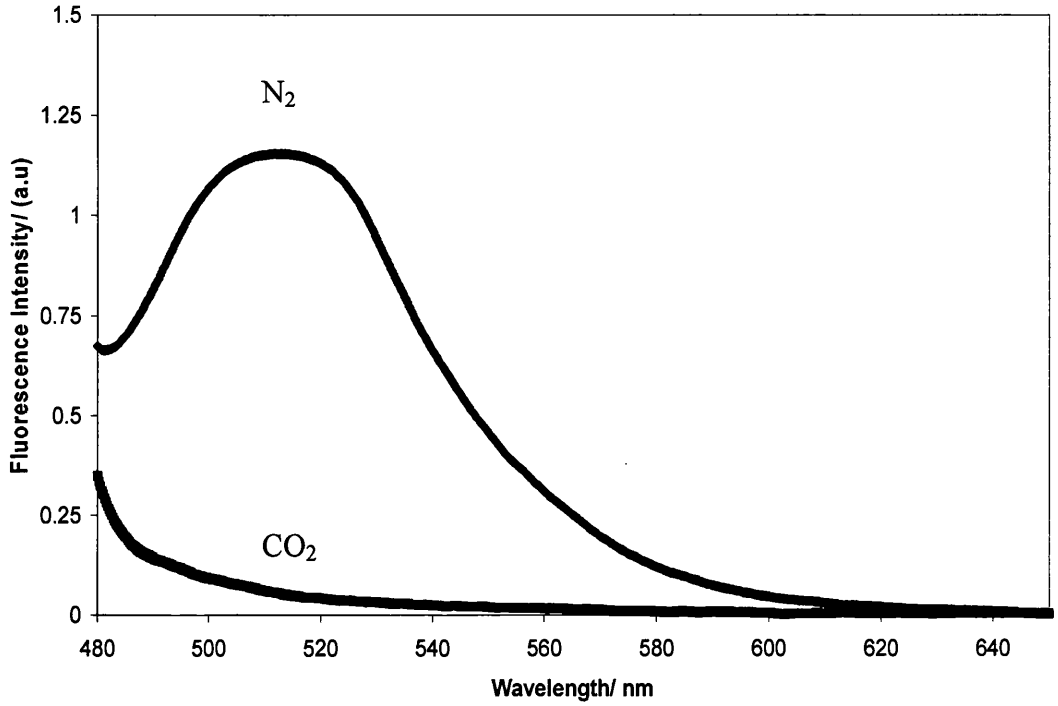

Fig.6.11. The emission spectrum of a carbon dioxide SM excited at 464 nm under carbon dioxide and nitrogen shown from 480 nm onwards to avoid the excitation peak

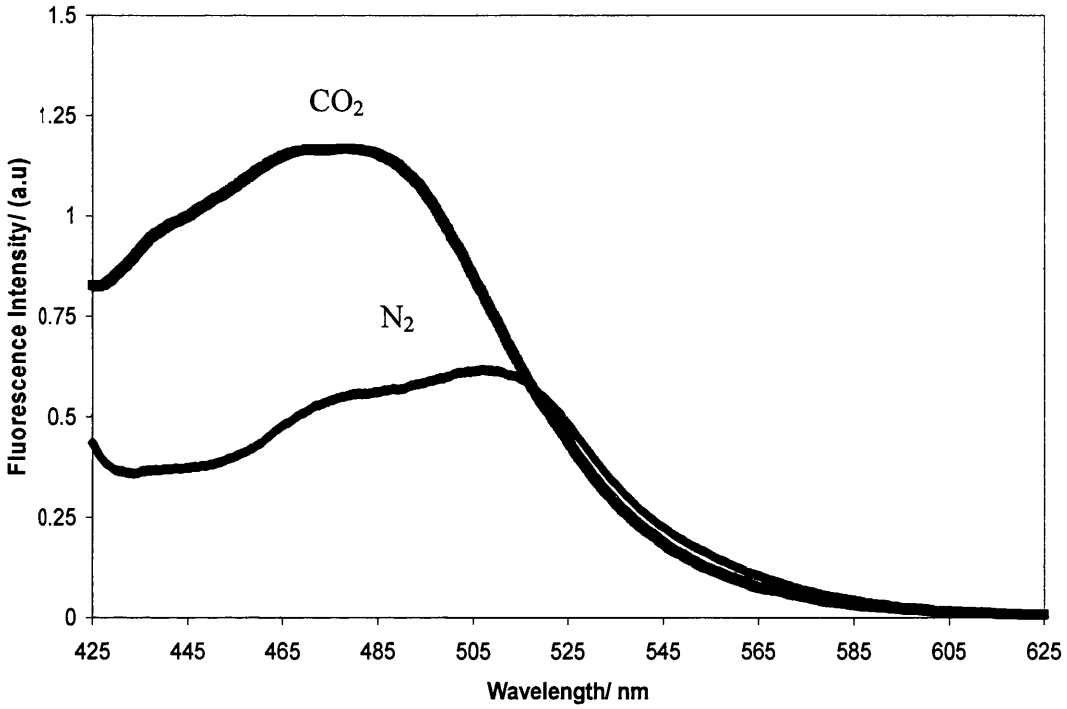

Fig.6.12. The emission spectrum of a carbon dioxide SM excited at 408 nm under carbon dioxide and nitrogen, emission shown from 425 nm onwards to avoid the excitation peak

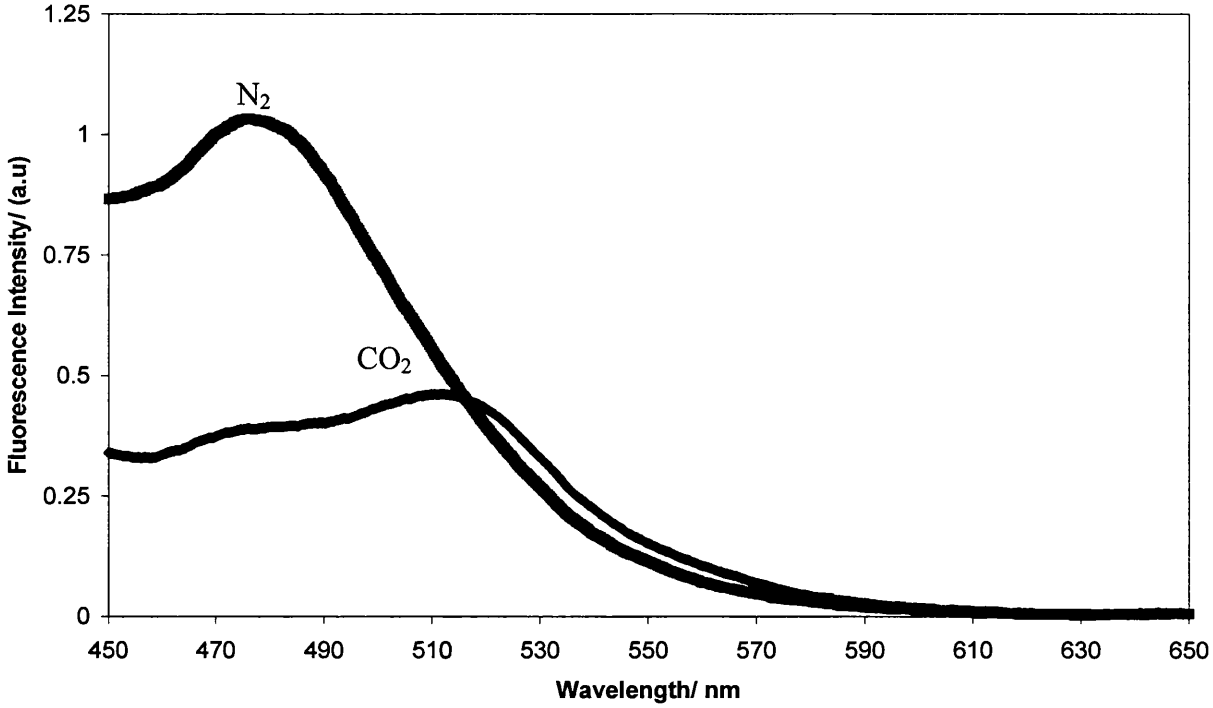

Fig.6.13. The emission spectrum of a carbon dioxide SM excited at 408 nm under carbon dioxide and nitrogen, shown from 450 nm onwards to avoid the excitation peak

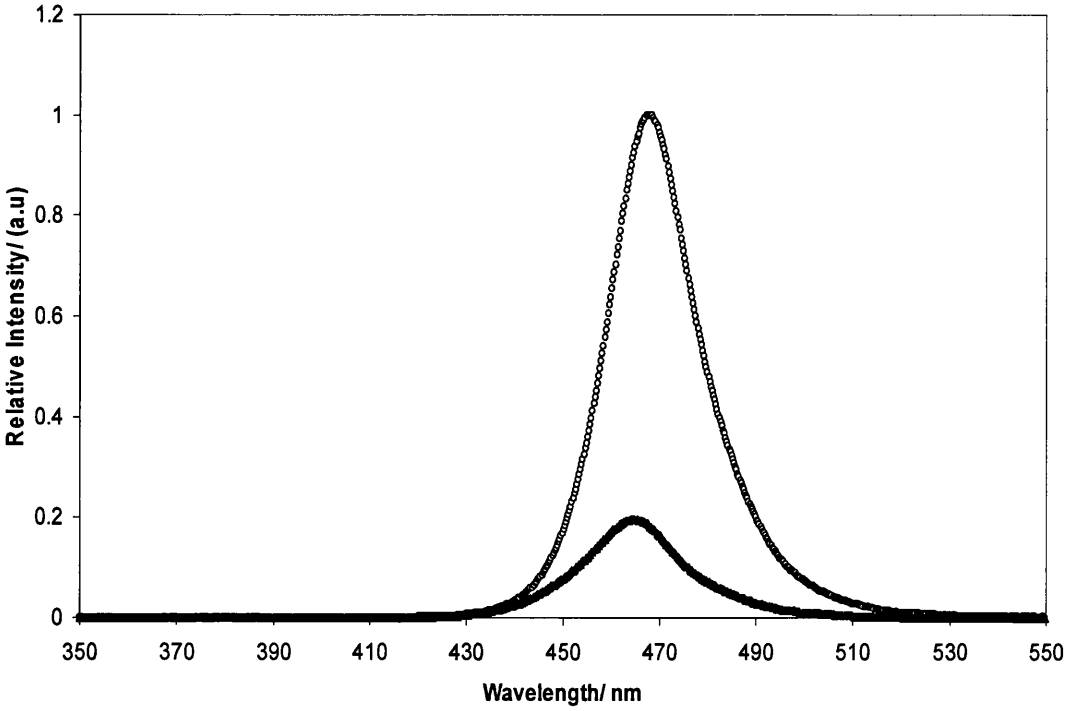

Fig.6.14. LED's used for excitation of CO_2 sensor membrane: LED A (open shapes), LED B (closed shapes)

The first detector used was a "human eye response" photodiode connected to a picolog Pico scope, (replacing the photomultiplier of the fluorimeter). In a fluorimeter the emission is detected at 90 ° to the excitation beam so that as little as possible of the excitation beam is seen by the detector. In the blood gas sensor 90 ° angles were not possible and the emission from the LED's was very intense. It was therefore necessary to stop the emission from the SM's being drowned out by the much larger excitation peak. Bandpass filters were used for this purpose.

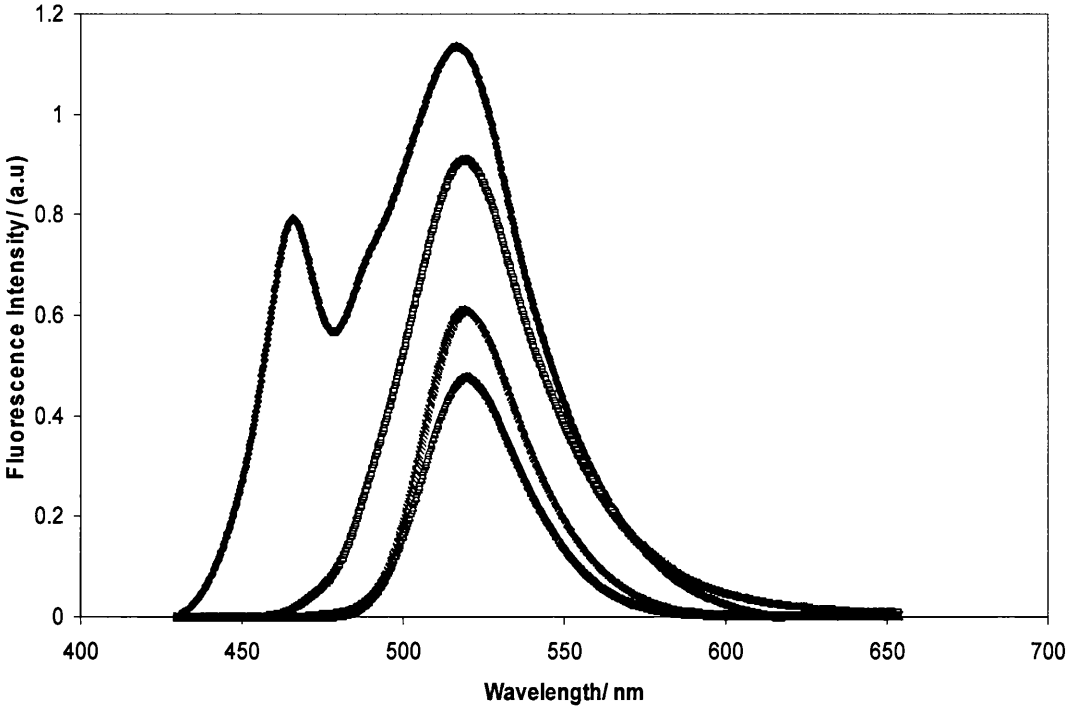

Fig.6.15. The effect of the possible bandpass filters on emission from a the carbon dioxide SM, starting with the highest emission to the lowest, the 1st peak is the emission from the carbon dioxide sensor with no bandpass filter present, the 2nd peak is the emission with a yellow filter, the 3rd peak is with the emission with a green filter G19, and the 4th is with a green filter G95

For the oxygen sensor the simple optical arrangement shown in fig.6.19 was used. A red bandpass filter (fig.6.16) was placed over the photodiode and a UV LED was used for excitation. For the first test these were simply suspended on a piece of cardboard and this was taped to the sensor. For detection the photodiode was linked to a picolog oscilloscope, and the changed in oxygen concentration could be monitored as a change in voltage with time. This gave a change from oxygenated to deoxygenated distilled water of around 25 mV proving that the technique was viable; but this is a small voltage change, and a much larger change would be preferred.

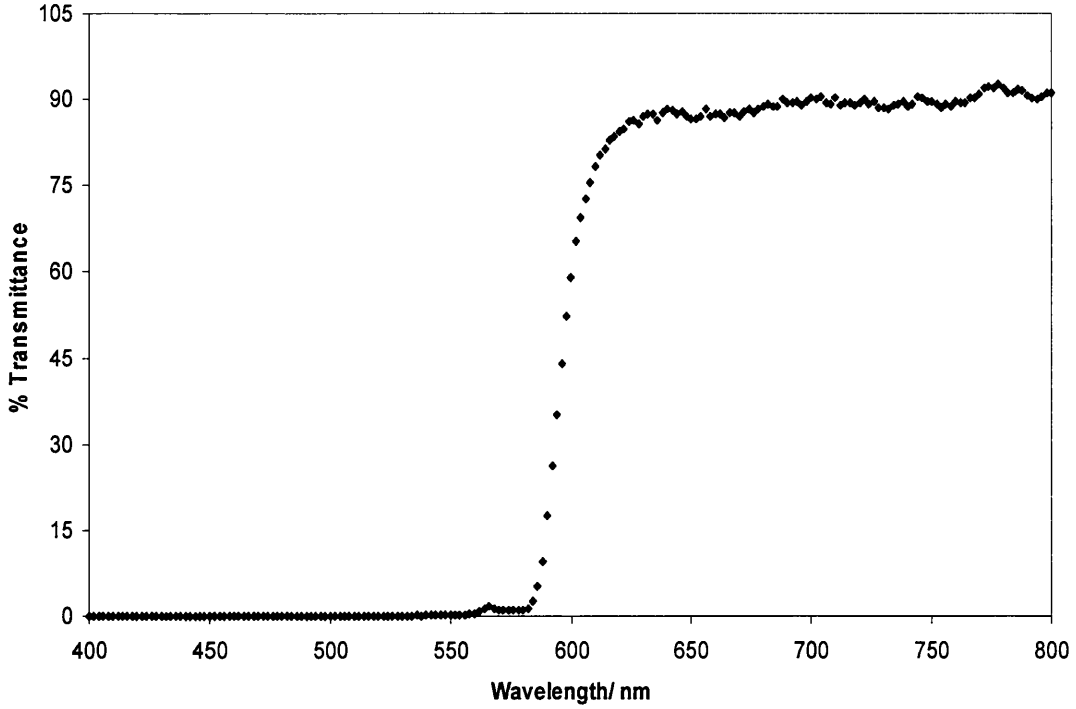

Fig.6.16. Band pass filter for emission photodetector of the blood O_2 sensor

Traditionally the best way to increase the signal size is to use a preamplifier circuit which is a simple circuit containing a transistor that amplifies the current. It is however possible to buy a phototransistor which already has a preamplifier integrated into it. The phototransistors required a separate 1.5 V source, and battery power supply and this was added to the system (fig.6.19). This produced a much improved signal size. In the blood oxygen sensor it was possible to get signal changes of around 900 mV.

To compensate for any changes in LED emission intensity it was necessary to make ratiometric measurements. In the oxygen sensor this was simply made by using a second phototransistor with a blue band pass filter (fig.6.17), which monitored the emission from the UV LED after it has passed through the SM. The first band pass used led to a weak signal for the reference (fig.6.17). Changing this to the filter with

higher transmittance and aligning the optics properly led to a much improved signal and this filter was used in all subsequent experiments. In practice very little change in reference signal is observed during oxygenation and deoxygenation of the blood, making this is an ideal reference.

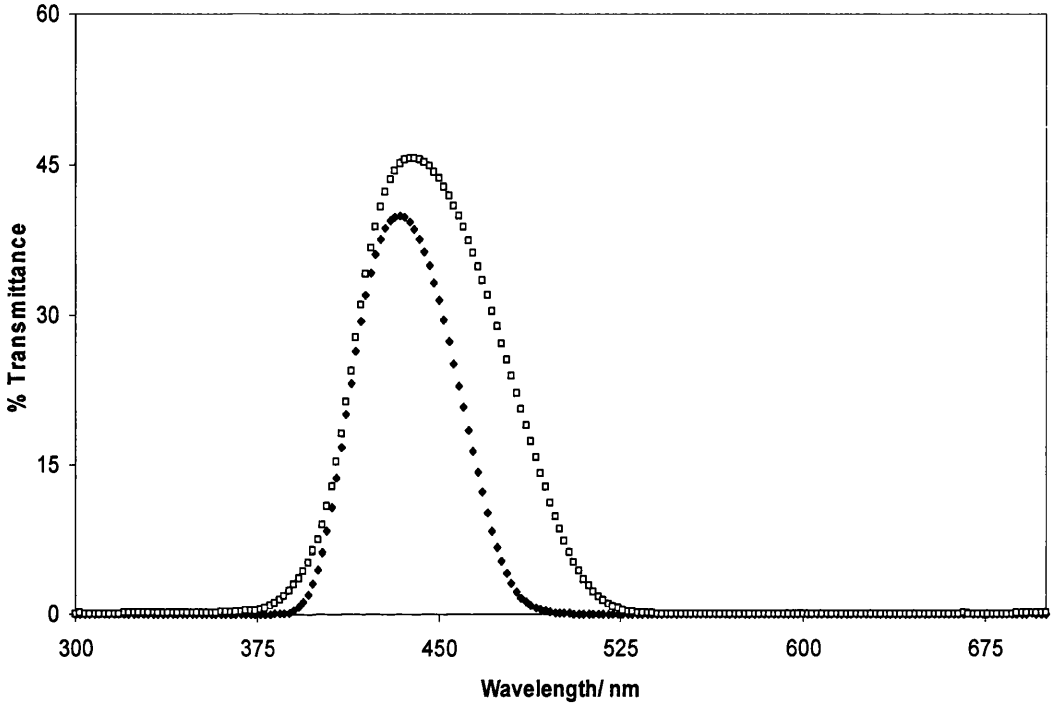

Fig.6.17. Choice of blue filters: blue 1 (closed), blue 2 (open). Blue 2 was used to cover the reference phototransistor in both sensors, blue 2 was also used to cover the transmittance phototransistor in the carbon dioxide sensor, as well as cover the blue LED used for excitation in the carbon dioxide sensor

The carbon dioxide sensor has the optical arrangement shown in fig.6.18, Sensor design for carbon dioxide measurement was more problematic than that for the oxygen sensor. The first problem was that while PtOEP has a large Stokes shift, this is not the case for HPTS which has a Stokes shift of only around 60 nm. The blue LED used in the carbon dioxide sensor was also much more intense than the UV

LED on the oxygen sensor, and the blue LED intensity had to be reduced. Because of this LED B was used rather than LED A, and a blue filter (fig.6.17) was placed over the LED. Initially two phototransistors were used with a blue filter for the reference and a green filter for the emission. The green filter G19 in fig.6.15 was chosen because this had the maximum transmittance at 521 nm, and therefore allows the maximum emission from the LED through, eventually this was changed to the yellow filter in fig.6.15, producing the maximum signal.

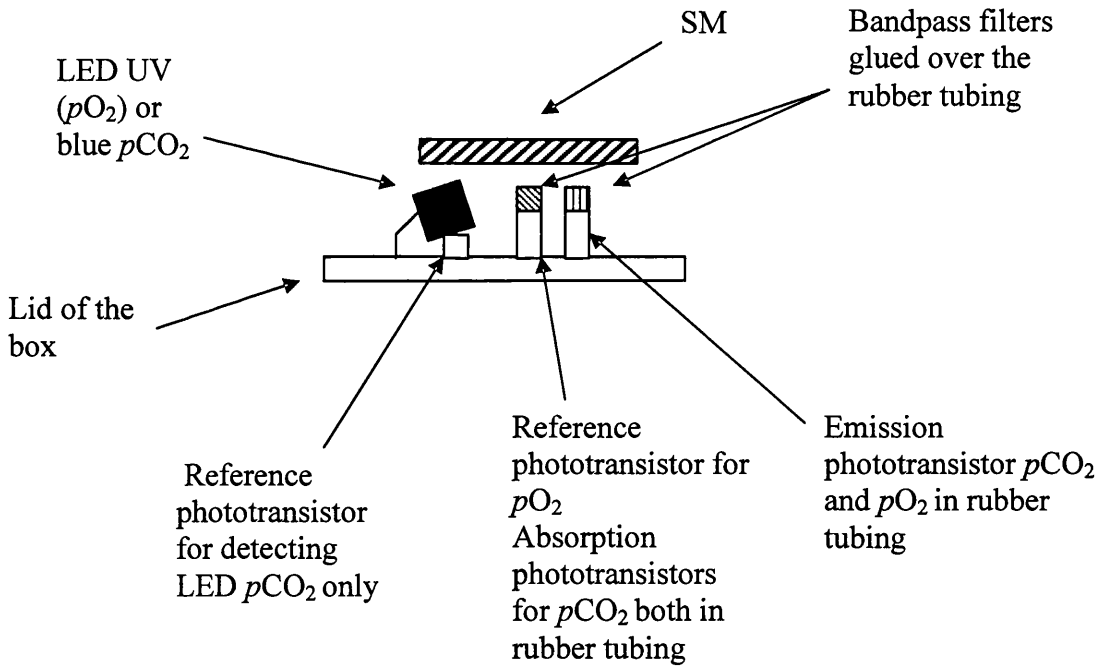

Fig.6.18. Optical arrangements for the two sensors

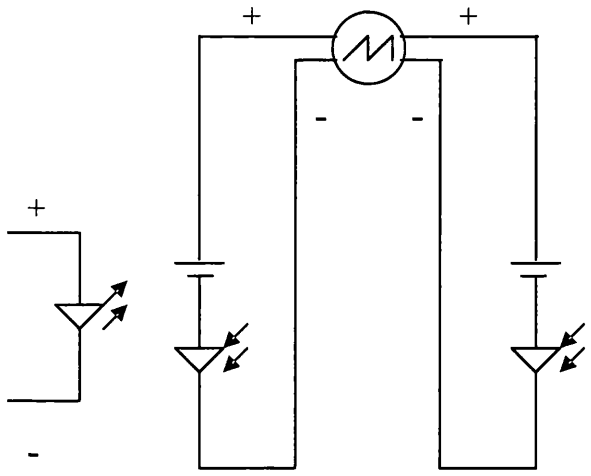

Fig.6.19. A schematic diagram of the electronic arrangement in the sensors. The phototransistors have been shown as photodiodes because they are integrated into the circuit and only have a negative and positive terminal, the picolog is shown as an oscilloscope for convenience.

When the carbon dioxide sensor was tested and the partial pressure of the carbon dioxide was increased a corresponding increase was observed in the reference phototransistor fig.6.20. The emission phototransistor covered with the yellow band pass filter was found to give the opposite response (fig.6.15). This was attributed to the fact that, unlike PtOEP the absorption of the carbon dioxide sensor also changes as a result of partial pressure changes (figs.6.21 and 6.22). Therefore the transmission of the LED emission through the SM was increasing, and this was detected by the reference phototransistor. While this meant that two parameters could be measured, potentially improving the precision of the sensor, there was no reference for the emission of the LED. This was solved by putting in a third detector, which only took emission directly from the LED (fig.6.18).

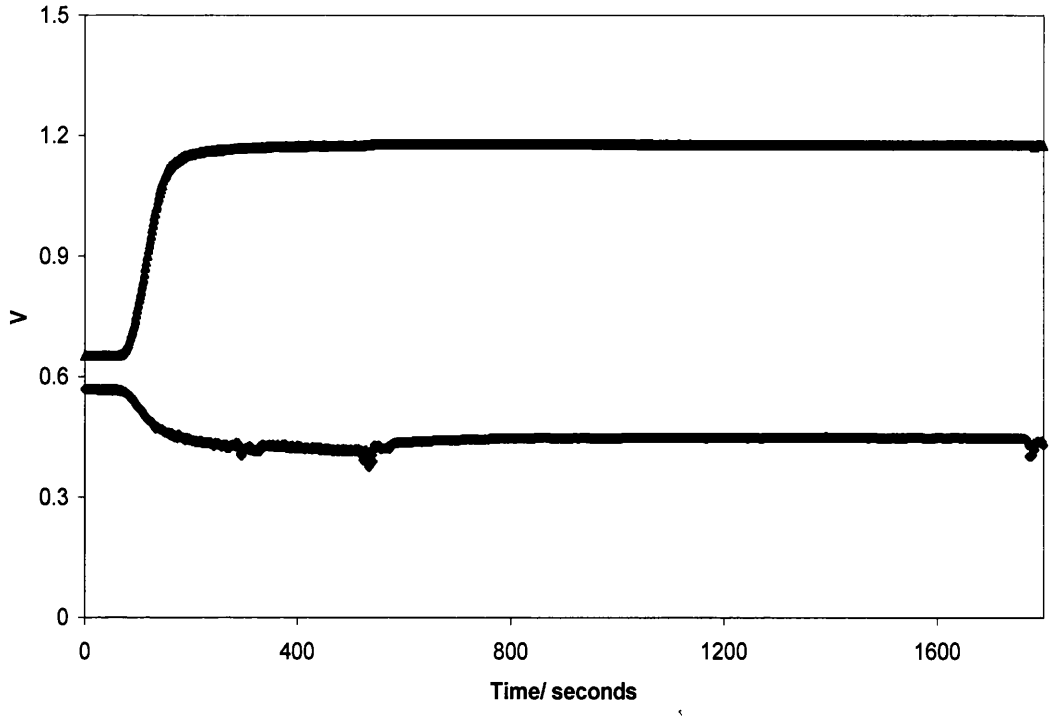

Fig.6.20. Changes observed for the emission (bottom) and transmission (top) phototransistors in the carbon dioxide sensor with increasing carbon dioxide partial pressure

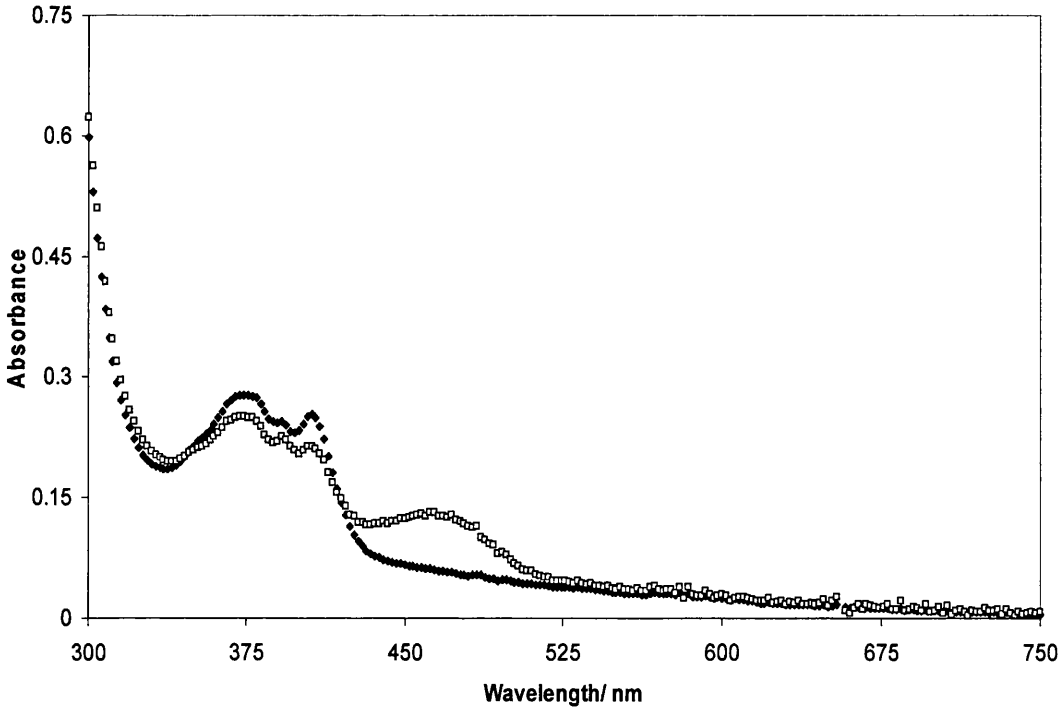

Fig.6.21. Change in absorption of HPTS in EC with a tetraoctyl ammonium hydroxide ion pair under air (closed shapes) and nitrogen open (shapes).

Therefore three different signals can be produced by the carbon dioxide sensor, so a second picoscope was employed in order to monitor all the signals. Finally all of the sensors were placed inside sealed black boxes reducing the amount of noise and background light substantially, as can be seen in the later experiments with water. The box also acts as a housing to which all the components are securely fastened.

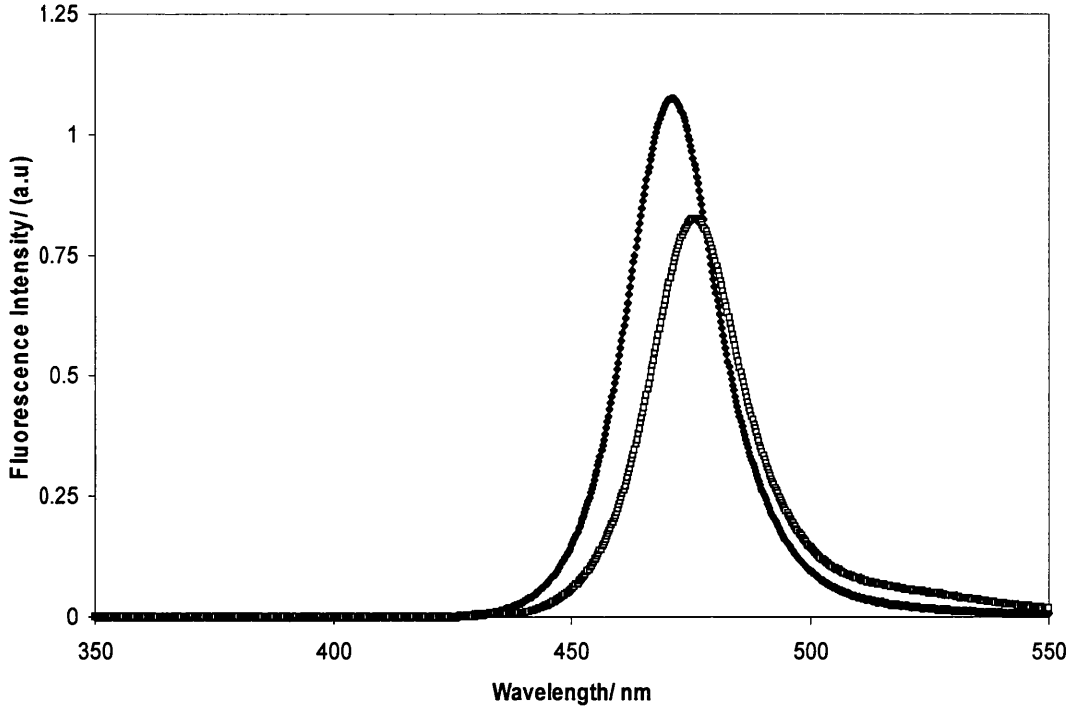

Fig.6.22. The change in emission of the LED through blue filter 1 after it has passed through a the carbon dioxide SM under carbon dioxide (closed shapes) and nitrogen (open shapes) the change in emission is produced by the change in transmission of the carbon dioxide SM

6.4.4 Choice of Membrane and response times

Two different membranes were used for the sensors: polypropylene and polyethersulfone, both provided by Haemair. Polypropylene was found to be the more permeable of the two. It can be seen from the different response times in figs. 6.23 and 6.24 that the addition of the different DM's leads to substantial increases in the response times for the sensor. There is also an additional problem caused by using polypropylene as the DM, instead of polyethersulfone particularly for the oxygen sensor; it can be observed that there is a substantial loss of signal size when polypropylene is used as the DM which ultimately affects the signal to noise ratio

and the detection range of the sensor. This was attributed to the fact that when polypropylene is wetted it becomes translucent and once translucent some of the excitation and emission is lost into the analyte, and not reflected. It was therefore also possible that changing the colour of the analyte solution from colourless to red would alter the signal observed, however tests involving the addition of a blood coloured substance, hemin, did not lead to any change in the signal. For the oxygen sensor the best DM was found to be polyethersulfone.

For the carbon dioxide sensor the DM chosen was polypropylene, because a sizeable signal and faster response could be obtained using polypropylene. In both cases the sensors demonstrated hysteresis, and demonstrate good repeatability. (figs.6.23 and 6.24).

The DM can be supposed to be the key component in determining the response time of the sensor. The change from polyethersulfone to polypropylene led to faster responses of the sensor, and even when gas was used instead of gases dissolved in water the response was similar to that observed for water.

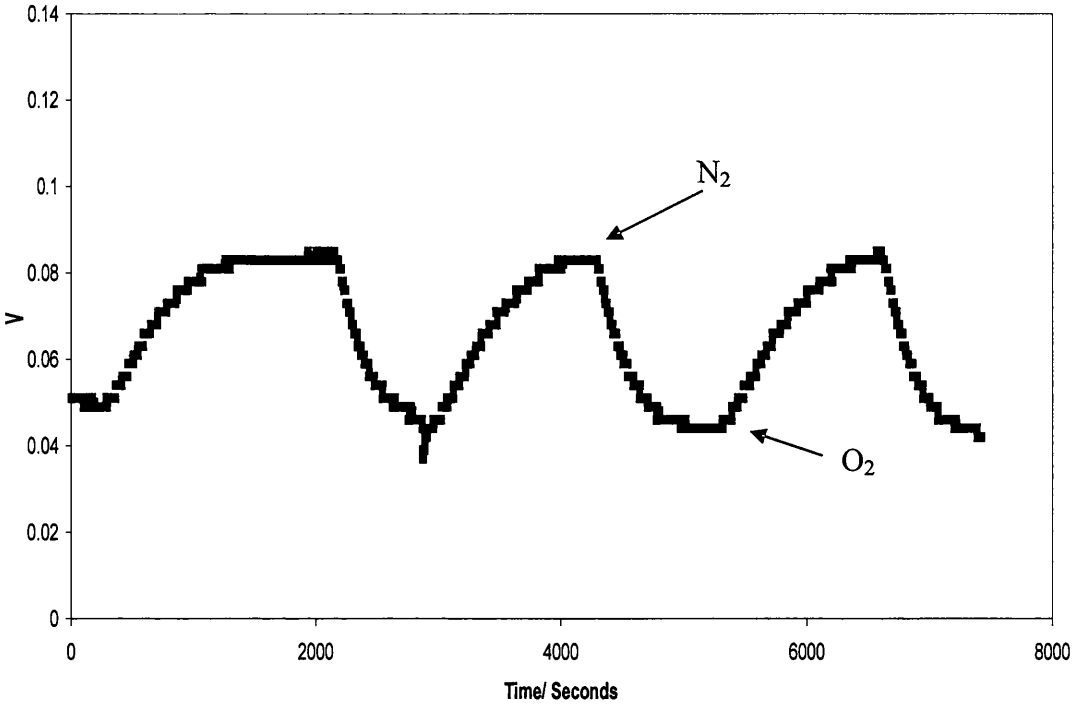

Fig.6.23. Responses of the oxygen sensor with a polypropylene DM with water saturated with oxygen and nitrogen, shows the decrease in signal observed when using a different DM compared to the change observed in fig.6.27, The response time for 90 % O_2 to N_2 is 838 s and from N_2 to O_2 is 730 s

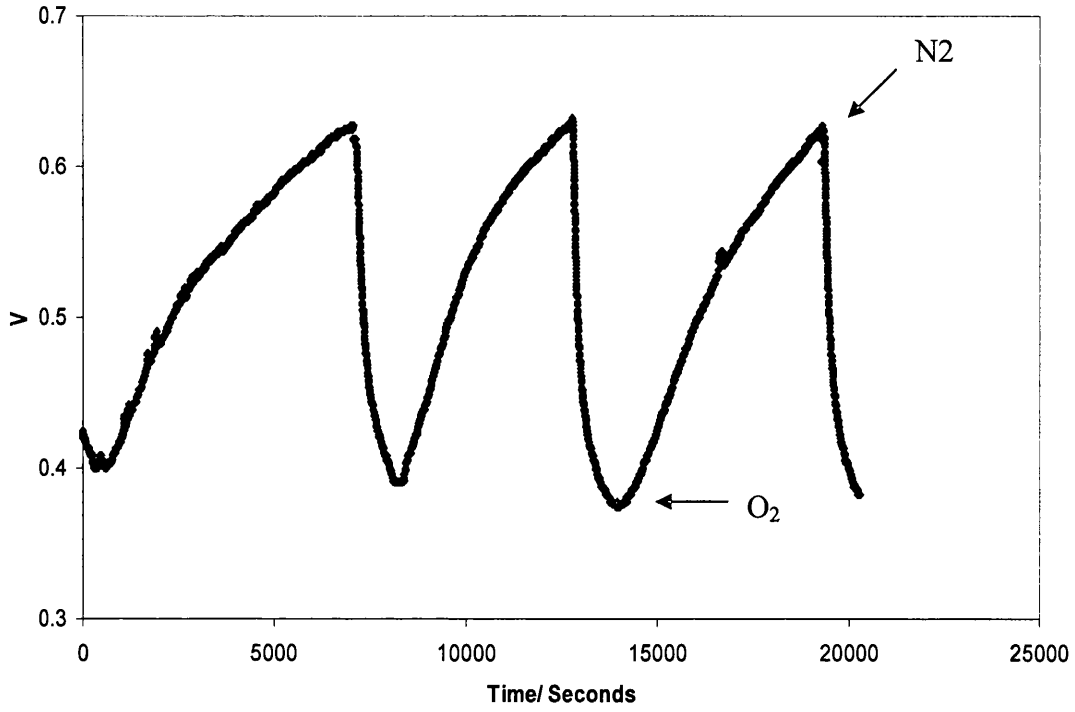

Fig.6.24. Responses of a carbon dioxide sensor with water saturated with carbon dioxide and then nitrogen with a polyethersulfone DM, from carbon dioxide to 90 % nitrogen the response time was 4037 s, from 90 % nitrogen to oxygen the response time was 1130 s

6.4.5 Flow rates

The effect of flow rate was looked at, because when the tests were done to begin with, the flow rates seemed to lead to a change in the peak heights. Later this was attributed to low flow rates not filling up the hollow in the flow cell. This can be overcome by priming the flow cell with the solution of interest first. Fig.6.25 demonstrates that no change is seen with the variation of flow rate. Slow flow rates lead to low response times as it takes a long time for the solution to fully displace the liquid in the channel. This slow flow also allows for mixing to take place and therefore an even longer response time.

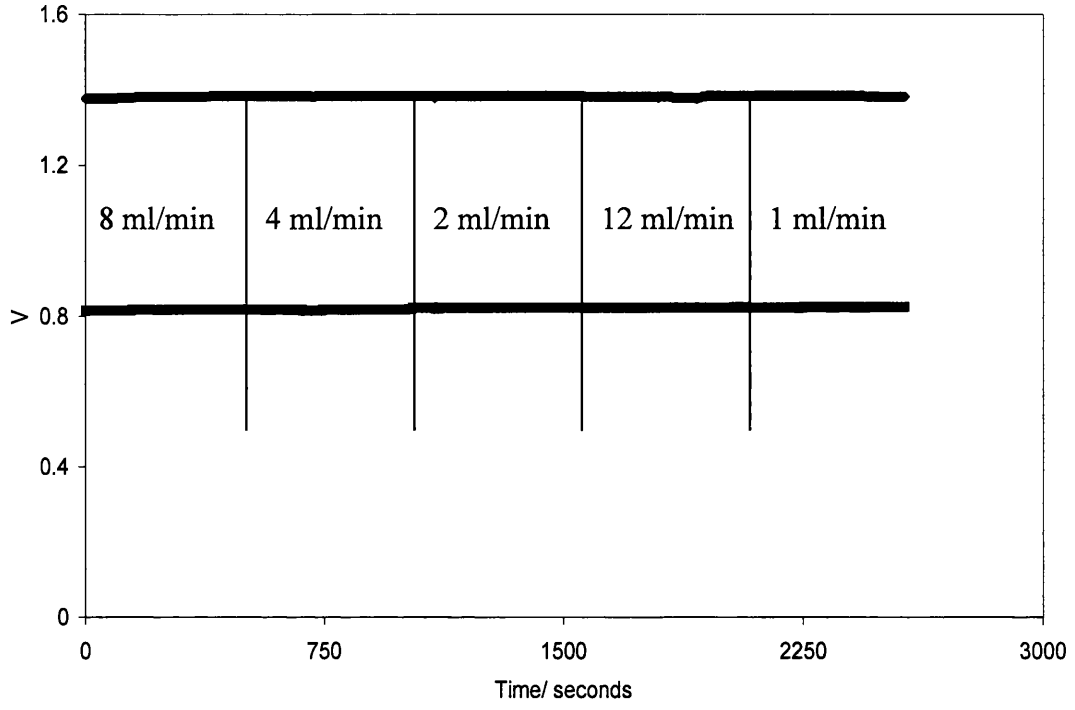

Fig.6.25. The blood oxygen sensor with deoxygenated water at different flow rates 8 ml/min, 4 ml/min, 2 ml/min, 12 ml/ min and finally 1ml/ min applied, with no change being observed

6.5 Responses in blood and water

Both of the sensors were first tested in water rather than blood (figs.6.26 and 6.28). Fig.6.26 shows the responses for the oxygen sensor over the range from 0 to 100 KPa with water and a polyethersulfone membrane. This shows an excellent response over a wide range, with good stability and signal to noise ratio.

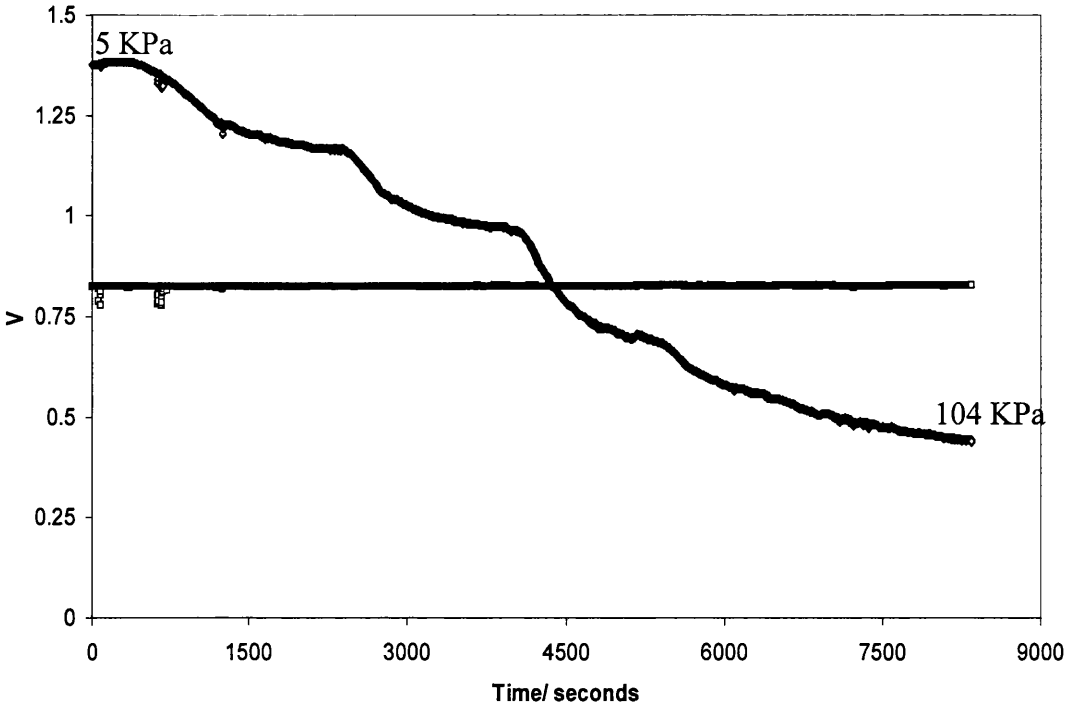

Fig.6.26. Changes recorded in the emission (changing line) and reference phototransistors (flat line) of the blood sensor with stepwise increasing oxygen partial pressure in water, the ratio of the two lines are plotted in fig.6.28

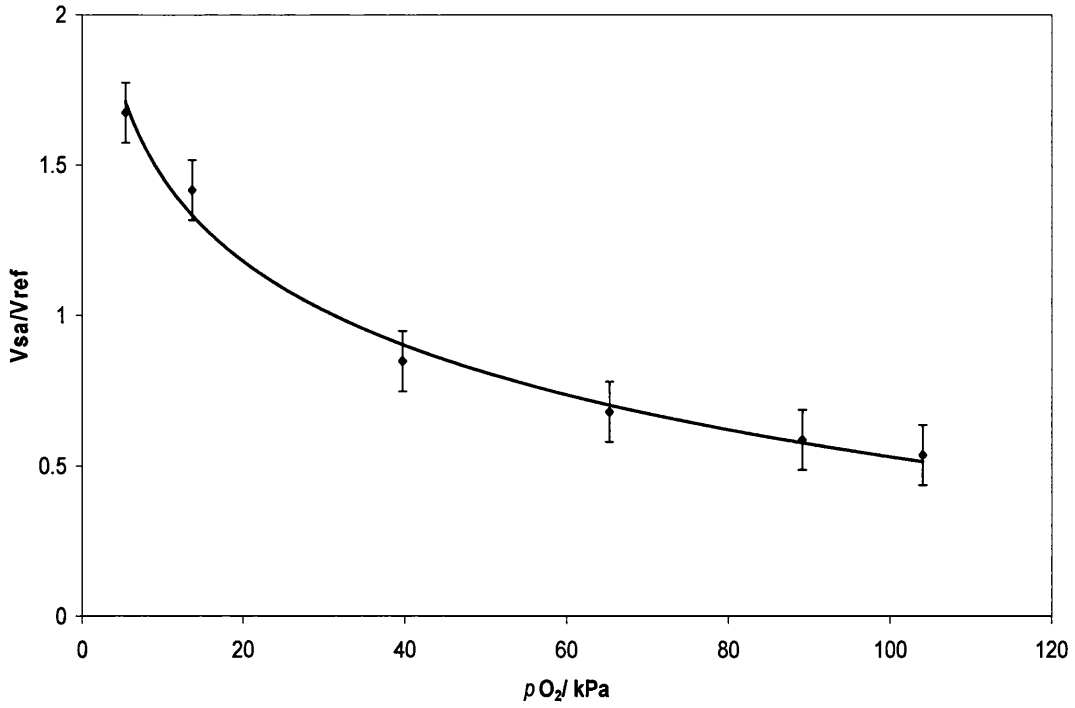

Fig.6.27. Plot of Vsa/ Vref for the blood oxygen sensor in water from fig. 6.27, equation of the trend line is (Vsa\Vref) = $-0.403\ln(pO_2) + 2.39$, $R^2 = 0.989$

Fig.6.27. shows a plot of the ratio of the emission phototransistor voltage (Vsa) over the reference transistor voltage (Vref), against the dissolved oxygen partial pressure. The result is a plot that fits a power function, which can be used for calibration. This non linear response has the effect that the sensor is most sensitive at pressures between 0- 40 kPa.

The carbon dioxide sensor can be seen to have a good response with high S/N ratios (fig. 6.28). The carbon dioxide sensor also produces a power function trendline that makes it more sensitive at lower partial pressures (fig.6.29). From fig. 6.30 the sensor is seen to respond well to changing partial pressures of the blood.

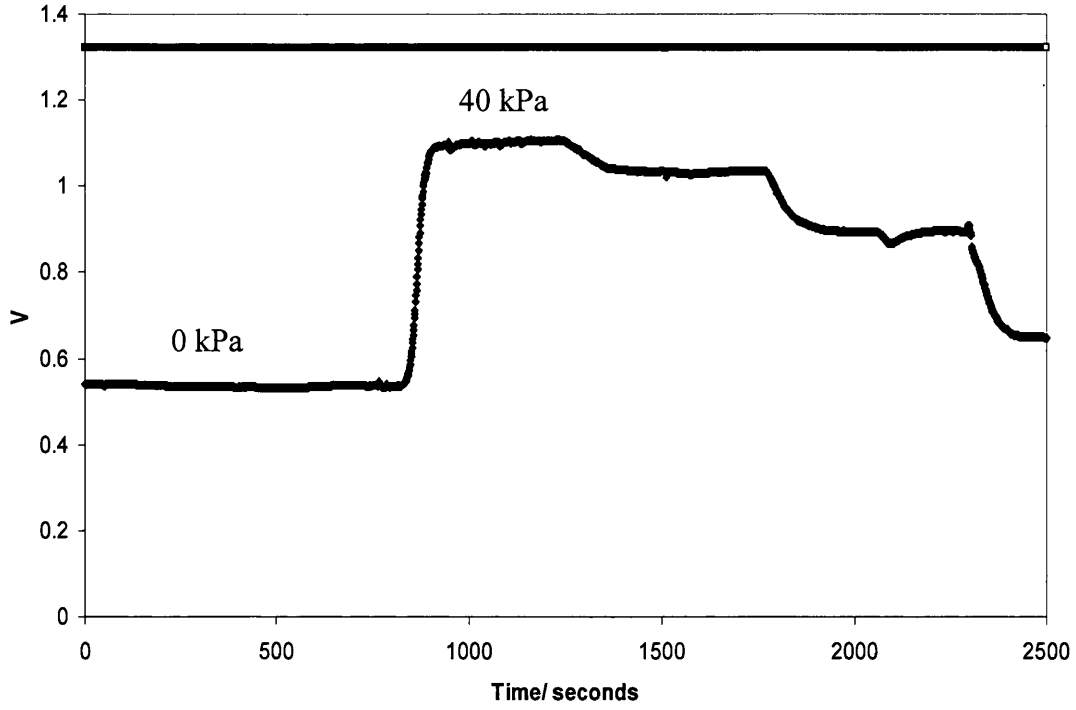

Fig.6.28. Changes observed in the absorption and reference phototransistors for the carbon dioxide sensor in water

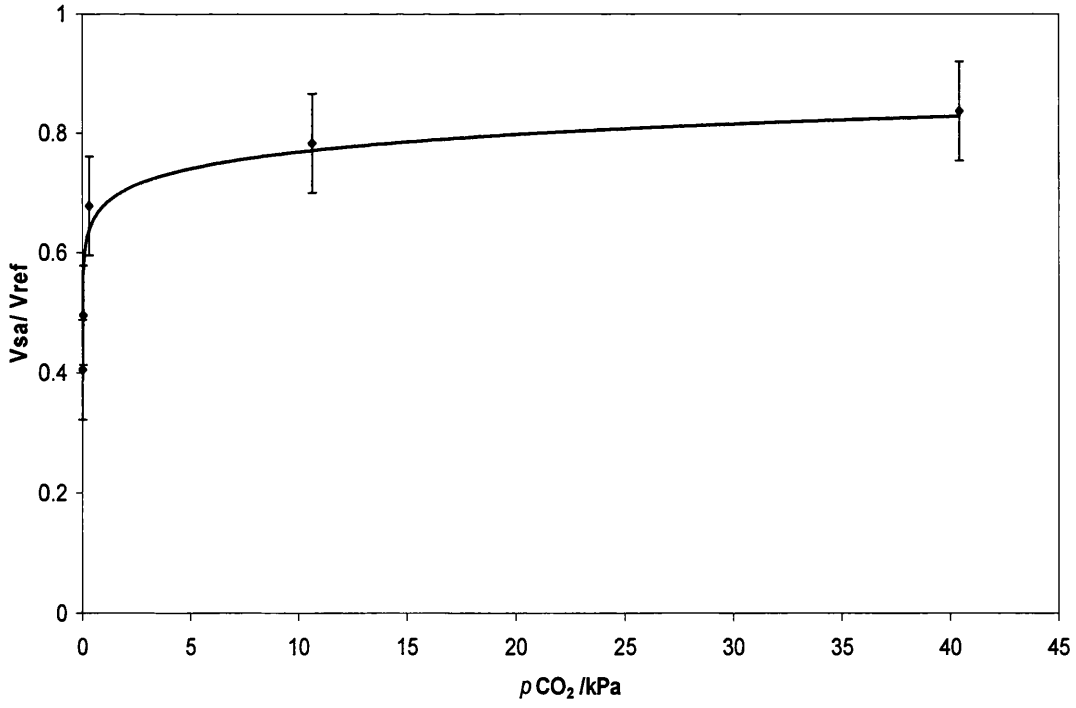

Fig.6.29. A plot of the values in fig. 6.25 against partial pressure equation of the trend line is Vsa/Vref = 0.6795 x $(pCO_2)^{0.0537}$ $R^2 = 0.940$

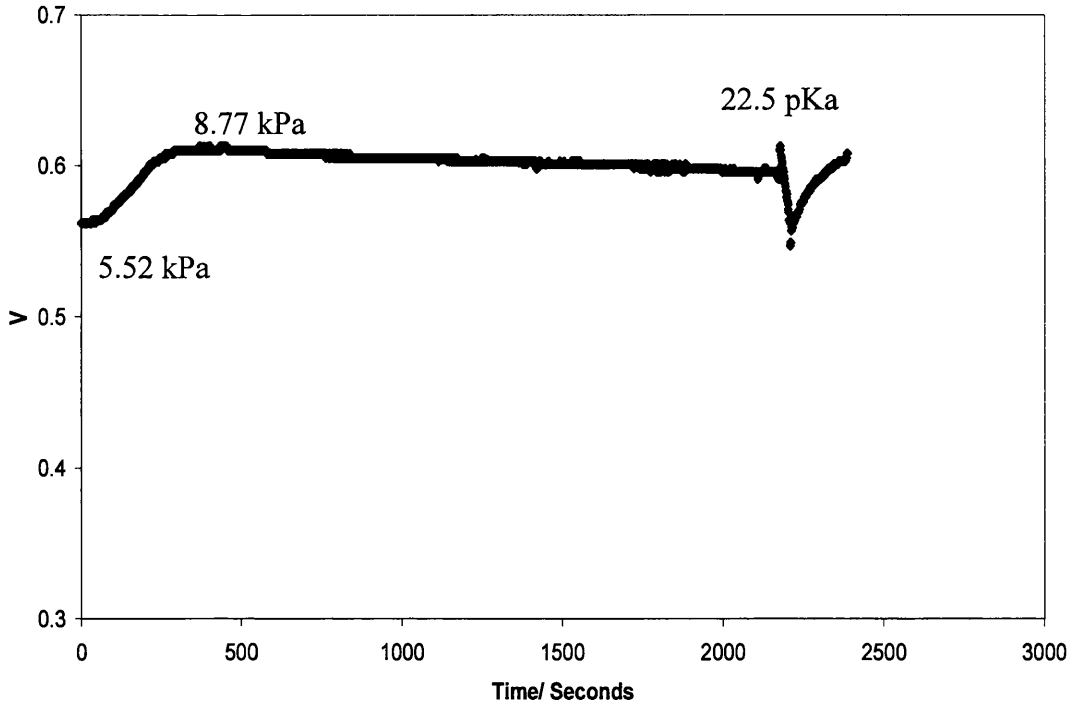

Fig.6.30. Response of the carbon dioxide sensor to changes in the concentration of carbon dioxide in the blood (The response of the reference phototransistor is not shown but was found to not be influenced by changes in concentration)

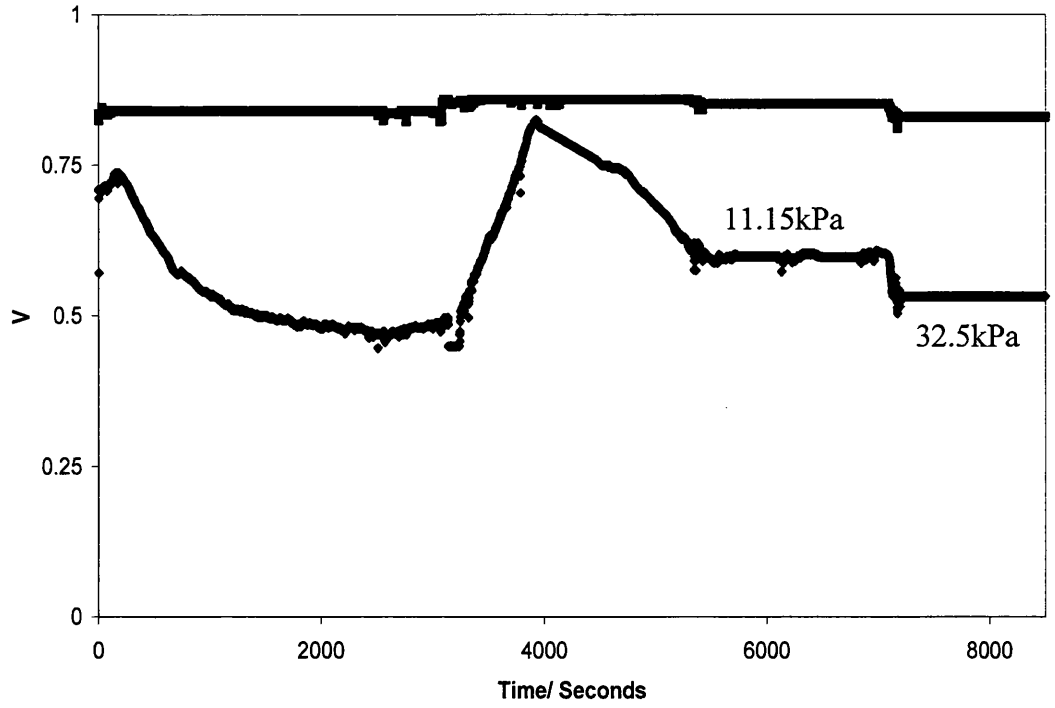

Fig.6.31. (lower plot) Changes in response of the blood oxygen sensor with changes in oxygen concentration in the blood, (top plot) response of the reference photomultiplier

From fig.6.31 the oxygen sensor response can be seen for the sensor with blood. (The noisy signal is the result of damage to the optical arrangement caused moving the sensor in order to obtain a sample to run through the blood gas analyser)

6.6 Conclusions

It has been possible to make two sensors which measure dissolved oxygen and carbon dioxide in blood and water and which give an inline response to changing concentrations of these gases from partial pressures of 0 kPa to 100 kPa in water for the oxygen sensor and 0 kPa to 40 kPa for the carbon dioxide sensor. They are

therefore capable of measurement over concentrations of interest for the development of an artificial lung, while also possessing a high enough range to cover the values obtained for patients with breathing difficulties.

Both sensors used a SM supported on a glass slide. By putting these in contact with the diffusion membrane it was possible to use the DMs to: provide diffuse reflectance for the optical arrangement; protect the SMs from the blood: protect the blood from the SMs; and facilitate diffusion. The choice of DM membrane influenced the signal size because of variation in diffuse reflectance especially when they are wet. This is most obvious in the oxygen sensor where a total signal change of around 900 mV could be obtained using polyethersulfone, but this was reduced to only around 60 mV using polypropylene.

Both of the gas sensors gave non linear responses, with the oxygen sensor being most sensitive between 0 kPa and 60 kPa, and the carbon dioxide sensor most sensitive between 0 kPa and 20 kPa. Both of which lie within the range of clinical interest.

Both of the SMs could be excited by LEDs and this made choice of excitation source relatively straightforward. Detection via phototransistors was preferred to photodiodes because this maximised signal size and removed the need for a preamplification circuit. The use of bandpass filters help to remove any problems with interference from the LED.

This device offers definite advantages compared to the conventional methods: samples do not have to be taken from system, thus allowing for constant monitoring of the system; the response is quite fast especially in the case of the carbon dioxide sensor; a large signal can be obtained giving a good signal to noise ratio, and therefore a high degree of precision; and, with most of the sensor components being made from cheap readily available materials, there is the possibility to mass produce these sensors at low cost.

6.7 Future work

The work for this thesis came to an end with this work, and therefore no further development of the sensors for use in the real world application involving blood samples, beyond that shown in figs.6.30 and 6.31 was possible. Perhaps surprisingly the first improvement we suggest is to improve the connections. This is quite a simple step, and it would help remove the noise that occurs when the sensors are moved for sampling. The second improvement would be to remove the batteries that are currently being used in the sensors to provide power for the phototransistors, and build a circuit such as the one shown in fig.6.32 which uses a mains power source. This would remove any problems of change in battery voltage with time which might affect calibration.

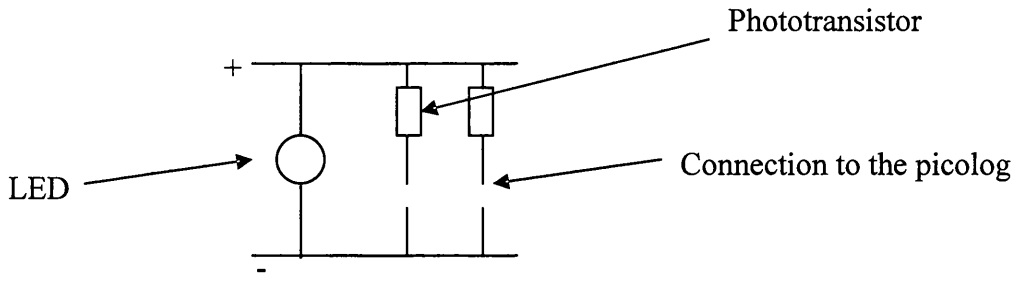

Fig.6.32. Possible circuit for the sensors which only uses one power source.

Further developments would be to integrate both sensors into the same device, and then add a temperature sensor, which could be used to correct for any temperature variation in calibration. Finally the suitability of different ion pair systems may be assessed. These may give a carbon dioxide sensor which is less sensitive and thus more suitable for the measurement of higher carbon dioxide concentrations.

6.8 References

1) Leiner, M.J.P. *Anal. Chim. Acta,* 225, **1991,** 209-222.

2) Nickol, A.H.; Dunroy, H.; Polkey, M.I.; Simonds, A.; Cordingley, J.; Corfield, D.R.; Morrell, M.J. *J. R. Med.,* 103, **2009,** 258-267.

3) Rich, K. *J. Vasc. Nurs.,* 26, **2008,** 6-14.

4) Sorenson, L.T.; Jorgensten, S.; Petersen, L.J.; Hemmingsen, U.; Bulow, J.; Loft, S.; Gottrup, F. *J. S. Re.,* **2008,** doi: 10.1016/j.jss.2008.02.066.

5) Sood, M.M.; Pauly, R.P, *Crit. Care,* 23, **2008,** 431-433.

6) William, D.T.; Smith, R.S.; Mallon, W.K. *J. Emer. Med.,* doi: 10.1016/j.jemermed.2008.05.001.

7) Cheng, H.; Smith, G.L.; Orchard, C.H.; Hancox, J.C. *J. Mol. Cardiol.,* 46, **2009,** 75-78.

8) Meinke, M.; Ott, E.; Gersonde, I.; Helfmann, J.; Albrecht, H.; Muller, G.; Hahn, A.; Kopitz, M.; Hetzer, R. *Med. Laser. App.,* 22, **2007,** 248-255.

9) Hahn, C.E.W. *Analyst,* 123, **1998,** 57R-86R.

10) Schedler, O.; Kalske, P.; Handschank, H. *Air Med. J.,* 23, **2004,** 36-39.

11) Ouellette, D.R. *Chest,* 128, **2005,** 575S-582S

12) Chuan, P.S. *Singapore, Med. J.,* 10, **1989,** 178-181.

13) Zivkovic, S.A.; Jumaa, M.; Barisic, N.; McCurray, K. *J. Neurol. Sci.,* doi:10.1016/j.jns.2009.02.308.

14) Susa, D.; Engel, S.; Damme, L.; Roset, H.P.; Krams, R.; Ijzermans, J.N.M.; de Bruin, R.W.F. *Pharmacol. Res.,* 59, **2009,** 273-278.

15) Jubran, A. *Crit. Care,* 3, **1999,** 11-17.

16) Weiwei, Y.; Aiyu, Z.; Baoshan, H.; Xinxia, C, *Sens. Actuators B,* 130, **2008,** 21-24.

17) Lauks, I.R, *Acc. Chem. Res.,* 31, **1999,** 317-324.

18) Anjos, T.G.; Hahn, C.E.W, *Sens. Actuators B,* 135, **2005,** 224-229.

19) Horecker, B.L. *J. Biol. Chem.,* 148, **1943,** 173-174.

20) Stenstrom, W.; Reinhard, M. *J. Biol. Chem.,* 66, **1925,** 819-827.

21) Cooney, C.G.; Towe, B.C.; Eyster, C.R. *Sens. Actuators B,* 69, **2000,** 183-188.

22) Leiner, M.J.P, *Anal. Chim. Acta,* 255, **1991,** 209-222.

23) Peterson, J.I.; Fitzgerald, R.V.; Buckhold, D.K. *Anal. Chem.,* 56, **1985,** 62-67.

24) Babilas, P.; Lamby, P.; Prantil, L.; Schreml, S.; Jung, E.; Leibsch, G.; Wolfbeis, O.S.; Landthaler, M.; Szeimies, R-M.; Abels, C. *Skin Research Technol.,* 14, **2008,** 304-311.

25) Ertkin, K.; Klimant, I.; Neurauter, G.; Wolfbeis, O.S. *Talanta,* 59, **2003,** 261-267.

26) Bultzinglowen, C.; McEnvoy, A.K.; McDonagh, C.; MacCrath, B.D.; Klimant, I.; Krause, C.; Wolfbeis, O.S, *Analyst,* 127, **2002,** 1478-1483.

27) Jones, L.; Atkins, P. *Molecules Matter and Change, 4th 2ed.,* Freeman, (2000), pp 177-197.

28) Mills, A.; Chang, Q.; McMurray, N. *Anal. Chem.,* 54, **1992,** 1383-1389.

29) Soli, A.L.; Byrne, R.H. *Mar. Chem.,* 78, **2002,** 65-73.

30) McMurray, N.H, *J. Mater. Chem.,* 2, **1992,** 401-406.

31) Burke, C.S.; Markey, A.; Nooney, R.I.; Byrene, P.; McDonagh, C. *Sens. Actuators B,* 119, **2006,** 288-294.

32) Kocincova, A.S.; Borisov, S.M.; Krause, C.; Wolfbeis, O.S. *Anal. Chem.,* 79, **2007,** 8486-8493.

33) Captitan-Vallvey, L.F.; Asensio, L.J.; Lopez-Gonzalez, J.; Fernandez-Ramos, M.D.; Palma, A.J. *Anal. Chim. Acta.,* 583, **2007,** 166-173.

34) Lopez-Gonzalez, A.J.; Asensio, L.J.; Fernandez-Ramos, M.D.; Captan-Vallvey, L.J. *Sens. Actuators B,* 121, **2007,** 629-638.

35) Mills, A.; Lepre, A.; Wild, L. *Sens. Actuators B,* 38-39, **1997,** 419-425.

36) Chen-Shane, C.; Yu-Lung, L. *Sens. Actuators B,* 129, **2008,** 120-125.

37) Chang, Q.; Randers-Eichorn, L.; Lakowicz, J.R.; Rao, G. *Biotechnol. Prog.,* 14, **1998,** 326-331.

38) Rao, A.; Pajonk, G.M.; Haranath, D.; Wagh, P.B, *J. Mat. Synth. Proc.,* 6, **1998,** 37-48.

39) Oter, O.; Ertekin, K.; Topkaya, D.; Alp, S. *Sens. Actuators B,* 117, **2006,** 295-301.

40) Weig, B.H.; Wofbeis, O.S. *Sens. Actuators B,* 28, **1995,** 151-156.

41) Ismail, A.F.; Kusworo, T.D.; Mustafa, A, *J. Membr. Sci.,* 319, **2008,** 306-317

42) Dias, P.; Lin, Y.J.; Hiltner, A.; Baer, E.; Chen, H.Y.; Chum, S.P, *J. App. Polym. Sci.,* 107, **2007,** 1730-1736.

7.1 Conclusions

The main conclusions that can be drawn from this thesis are that optical oxygen and carbon dioxide sensors are potentially extremely versatile and can be used to measure these analytes in both gas and solution phases with accuracy and precision, and that they offer many advantages over currently available sensors.

Lumophores and complexes

The preferred lumophore for oxygen sensing in the applications discussed in this thesis was found to be PtOEP. PtOEP emits a "cherry red" phosphorescence from a long lived triplet state which is therefore very susceptible to quenching by oxygen However, it was not quite the perfect lumophore because it has been shown to be unstable with respect to photodegradation, and also the emission intensity is dependent to some degree on temperature. For carbon dioxide sensing the preferred lumophore was found to be HPTS which demonstrates a high sensitivity, a high quantum yield and excellent photostability. Coumarin 110 and rhodamine 110 were used as oxygen insensitive lumophores as anchor colours in dual lumophore colorimetric oxygen sensors. They fluoresce with high quantum yields, and showed no temperature dependence of emission.

For the temperature sensitive layer in the pressure sensitive paint described in chapter 4 a Co(II) complex was used, and this was shown to be stable and sensitive over a reasonable temperature range.

Matrices

A number of different polymer matrices were investigated for encapsulating the lumophores. The most commonly used polymer matrix was EC. This proved to be an excellent choice because it is very permeable to oxygen thus providing sensors which have high sensitivity, and was easy to spin coat as uniform layers. Sensors made from EC, such as the BM sensor described in chapter 3, generally give a fast response. The other polymer matrices that were investigated were: polystyrene, which was used to protect the sol gel sensing membrane in the carbon dioxide blood sensor; gelatin, which proved to be an excellent barrier layers, and was not permeable to oxygen; sol gels which proved to have high permeability to carbon dioxide, but were shown to have problems adhering to the glass substrate; and polyvinyl alcohol, which was used for the temperature sensing layer because it complexed Co(II) ,although it produced a film of lower optical transmission than the other polymers which caused problems when being over coated, and had to be heated to prevent stripping out.

Coating methods

Chapter 3 investigated methods for the manufacture of dual lumophore sensors. It was determined that spin coating is one of the better methods for the production of sensors. Attempts made to use inkjet printing proved to be unsatisfactory because it took many layers to produce sensors with the required emission intensity, and it ultimately took far too long to produce sensors. Meyer bar coating was also investigated and was shown to be a viable alternative to spin coating.

Barrier layers and substrates

Barrier layers were also investigated and turned out to be very important in the production of sensors. Lumophores, which were incorporated in EC in particular, seemed to be stripped out by the application of a second organic layer above this. It was therefore necessary to add an interlayer, which was normally gelatin. In general it seems that placing a hydrophobic layer over a another hydrophobic layer lead to the stripping out of the lumophore, while the application of a hydrophilic layer above a hydrophobic layer will generally not strip out the lower layer.

Chapter 3 also investigated the use of substrates, which turned out to be a critical choice for the construction of optical sensors since a substrate which scatters light will amplify the emission from a lumophore layer which is applied directly above it. Therefore all dual lumophores sensors used scattering substrates.

Colorimetric response

Chapters 3, 4 and 5 were concerned with the development of colorimetric oxygen sensors. Different colour changes could be produced by using different lumophores with different sensitivities. Chapter 3 described the production of "traffic light" sensors using a green lumophore and a red lumophore in the same sensor in which emission from one lumophore is quenched selectively thus leading to the colour change occurs.

Chapter 5 was concerned with the development of a colorimetric oxygen sensor that contained only one lumophore and utilised the green emission from the LED to produce a "traffic light" colour change. While the required colour change response

could be obtained these sensors were found to have a very slow response time, almost certainly because of the thickness of the polymer layer used. This slow response can be compared to the sensors described in Chapters 3 and 4 which were made using thin, spin coated, films, and which were found to have very fast response times, of around 1 s.

In chapter 4 different lumophores were utilised to produce a different colour change of red to blue. The intermediate colour is purple which was found to be difficult to differentiate from blue. Using one lumophore which is essentially insensitive to changes in oxygen partial pressure gives a sensor which produces a colour change at a lower partial pressure than one made using two lumophores both of which are quenched to some degree.

Photodegradation

While there are clear advantages in using luminescent sensors a few problems persist which were outlined in the introduction. One of these is photodegradation, which is discussed in detail in chapter 3. Degradation of a colorimetric sensor alters the colour change response if the lumophores degrade at separate rates. Work described in chapters 3 and 5 suggests that the mechanism of degradation is by a reactive oxygen species, probably singlet oxygen generated as a consequence of lumophore quenching by oxygen. It was found that addition of the singlet oxygen quencher DABCO to the PtOEP layer significantly increased sensor photostability.

Temperature response

In chapter 4 a dual lumophore sensor made to be used in a pressure sensitive paint is described. Problems of changes in emission due to temperature had to be addressed. This was done by adding a second absorption based temperature sensor, which was constructed using cobalt chloride in a PVA matrix with phosphoric acid. Altering the phosphoric acid concentration was found to alter the response of the sensor, the more phosphoric acid added the more gradual the temperature response. When combined with a colorimetric oxygen sensors this gave a sensor that could be used to measure the air flow under UV light and the temperature of the surface under visible light, creating a new type of pressure sensitive paint, whereby the UV excited colorimetric oxygen response could be corrected for temperature using the visible excited colorimetric temperature response.

.

Specific applications

The advantage of colorimetric sensors is that they are very simple to use, and therefore they can be used with very little training. In chapter 3 the sensors were designed with the requirements of monitoring museum storage in mind. However chapter 4 used a similar sensor as pressure sensitive paint to measure the flow of air over the surface of a vehicle. Thus demonstrating that these sensors can be used for a variety of very different applications, and although it was not investigated further this technology could be used easily for modified atmosphere packaging with little alteration.

Chapter 6 describes the development of sensors for measuring dissolved oxygen and carbon dioxide in blood. These sensors were developed to be small hand held units

containing excitation source, sensor elements, and detector. Excitation was by means of LEDs and the detection was accomplished by using a using phototransistor. To maximise the signal to noise ratios bandpass filters had to be used. Ratiometric sensing was used in these sensors so as to stop any problems that occurred due to changes in the intensity of excitation light. The sensor elements were shielded from the blood by gas permeable membranes, which were white in colour and therefore also acted as diffuse reflectors of the signals from the sensing membranes.

Chapter 6 also sees the use of both luminescent and absorption based sensors for carbon dioxide, based on an ion paired pH sensitive dye. The initial sensors used an EC polymer matrix which was sensitive but not very stable, and this was therefore changed to a sol gel matrix which substantially improved the stability of the system. The first ion pair that was used was tetraoctyl ammonium hydroxide which gave a very sensitive sensor but a slow response time; changing this to cetyltrimethyl ammonium hydroxide resulted in a lower sensitivity but a greater range and a faster response time.

The use of these types of sensor allowed the measurement of the gaseous content of the blood over the range from 0 to 100 kPa for oxygen and 0 to 40 kPa for dissolved carbon dioxide, which cover the useful clinical ranges. They also demonstrated good stability and repeatability. They are potentially a very exciting prospect because they have many advantages over the current methods which are available. They have the advantage that they sense the gases inline and therefore blood does not need to be removed from the system as in the current method used by the collaborating

company Haemair. We are currently examining the patenting possibilities arising from this work.

7.2 Future Work

Some work still remains that could not be finished in the time allowed for the completion of the project. It would be interesting to know whether singlet oxygen was migrating from the PtOEP layer into other layers in a dual lumophore colorimetric layer. It would also be interesting to try other methods of production of the sensors such as screen printing. Further future work would be to try some trials of the museum sensors with the British Museum to move on from the proof of concept stage towards a practical sensor.

Chapter 4 saw the development of a proof of concept pressure sensitive paint. Future work for this chapter would be the development of new sensors using different temperature sensitive layers to extend the range at which the PSP could operate over. Other possible work would look at the addition of thermally stable photochromic compounds that could provide a constant colour background layer between the colorimetric pressure sensitive paint and the temperature sensing layer.

Chapter 5 saw the development of a new type of colorimetric oxygen sensor that utilised an LED as a source of both excitation and emission. The major barrier to any further use of this sensor was the slow response times. Further work would be to try and improve these response times, probably by using a more soluble porphyrin in a thinner sensor layer.

Chapter 6 saw the development of two prototype sensors for the measurement of dissolved oxygen and carbon dioxide. Both were developed to a proof of concept stage, however there are a number of further experiments and improvements that would be worth making. It would be valuable to evaluate the sensors more rigorously using blood rather than water as the analyte medium. And it may be useful to consider powering the LEDs and detectors from a mains supply rather than using batteries.